REAL-TIME INVESTIGATION OF FOULING PHENOMENA IN MEMBRANE FILTRATIONS BY A NON-INVASIVE ULTRASONIC TECHNIQUE

by

JIANXIN LI

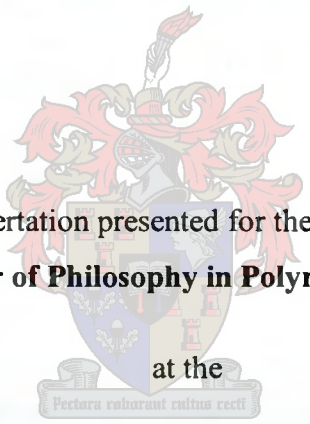

Dissertation presented for the degree of

Doctor of Philosophy in Polymer Science

at the

University of Stellenbosch

Supervisor:

Professor R.D. Sanderson

Stellenbosch

December 2002

DECLARATION

I, the undersigned hereby declare that the work contained in this dissertation is my own original work and has not previously in its entirely or in part been submitted at any university for a degree.

Signature **Date**

ABSTRACT

Membrane fouling is universally accepted as one of the most critical problems limiting the wider application of membranes in liquid separations. The development and utilization of a suitable non-invasive technique for the on-line monitoring of fouling in industrial and laboratory applications may enable the effectiveness of fouling remediation and cleaning strategies to be quantified.

The overall objective of this research is to develop ultrasonic time-domain reflectometry (UTDR) and its use as an analytical tool for the real-time study of inorganic-, organic- and protein- fouling of various types of membranes including nylon, polysulfone (PSU) and polyethersulfone (PESU) and modules, including flat-sheet and tubular types. Different separation systems including microfiltration (MF) and ultrafiltration (UF), flat-sheet and tubular modules, and suitable ultrasonic probes were used in this study.

Results of this study show a good correlation between the UTDR signal response and the development of a fouling layer on a membrane surface. UTDR effectively detected the appearance, growth and movement of a fouling layer echo as fouling proceeded. Cake (fouling)-layer compressibility was observed by UTDR. The structure and compaction of an asymmetric PSU membrane could be detected by UTDR. UTDR was also successfully used for monitoring membrane cleaning and evaluating the cleaning effectiveness of various cleaning methods. UTDR results corroborated the flux measurements and SEM analyses.

The ultrasonic unit is a programmed microprocessor, and can be used to compare reference and test signals to produce a differential signal (a fouling layer echo). A differential signal indicates the state and progress of a fouling layer on the membrane surface in actual operations. Both amplitude and arrival time of differential signals as a function of operation time provide useful quantitative information, i.e. changes in thickness and density of a fouling layer, on the fouling processes.

A predictive modelling program, ultrasonic reflection modelling (URM), was developed to describe the processes of ultrasonic testing related to the deposition of fouling layers on membrane surfaces. The mathematical model could substantiate changes in the densities of the fouling layer as well as the thickness. This is important as deposit resistance to flow is related to both thickness and density (compressibility). The predicted results of cake layer deposition are in good agreement with the actual UTDR measurements obtained in MF and UF.

Furthermore, protein fouling was successfully detected in tubular UF by UTDR. Ultrasonic frequency spectra could be used as an additional tool for fouling detection.

OPSOMMING

Membraan-aanvuiling of –verstopping is die grootste struikelblok wat die meer algemene aanwending van membrane vir verskillende watersuiweringsprosesse beinvloed. Die ontwikkeling en gebruik van 'n geskikte nie-inmengende tegniek vir die in-lyn meting van aanvuiling van membrane in laboratorium-en nywerheidstoepassings mag 'n geleentheid bied vir die kwantifisering van die verwydering van aanvuiling en skoonmaakstrategieë.

Die hoofdoel van hierdie studie was die ontwikkeling van ultrasoniese tyd-gebiedsweerkaatsing (Eng: ultrasonic time-domain reflectometry, UTDR) en die gebruik daarvan as 'n analitiese metode vir die studie van anorganiese-, organiese- en bio-besoedeling op verskeie tips membrane, insluitend nylon, polisufoon (PSU) en polietersulfoon (PESU), in beide platvel- en buismodules. Verskeie skeidingsisteme, insluitend mikrofiltrasie (MF) en ultrafiltrasie (UF) is ontwerp en gebruik in hierdie studie.

Eksperimentele resultate het goeie ooreenstemming tussen die UTDR seinrespons en die ontwikkeling van 'n aanvuilingslaag op die membraanoppervlakte bewys. Die ultrasoniese tegniek kon die vorming, groei en beweging van 'n bevuilingslaagterugkaartsing waarneem namate bevuiling vorder. Aanvuilingslaagsamepersing is deur UTDR waargeneem. Die struktuur en samepersing van 'n asimmetriese PSU membraan is ook deur UTDR gesien. UTDR is verder suksesvol gebruik om die skoonmaak van membrane te monitor en om die skoonmaakgeskiktheid (cleaning effectiveness) van verskeie skoonmaakmetodes te bepaal. UTDR resultate het permeaatvloeimetings en SEM analyses bevestig,.

Die ultrasoniese eenheid is 'n geprogrameerde mikroverwerker, en kan gebruik word om verwysings- en toetsseine te vergelyk, en dan 'n differensiaalsein te gee ('n aanvuilingslaagweerklank). 'n Differensiaalsein dui die toestand en vordering van 'n aanvuilingslaag op die membraanoppervlakte gedurende gebruik aan. Beide amplitude asook aankomstyd van differensiaalseine as funksies van gebruikstyd verskaf

bruikbare kwantatiewe inligting, dws. Veranderings in die dikte en digtheid van 'n aanvuilingslaag, op die aanvuilingsproses.

'n Voorspellingsmodelleringprogram – ultrasonieseweerkaatsingsmodellering (Eng: ultrasonic reflection modeling, URM) is ontwikkel om die proses van ultrasoniese toetsing by die deponering van aanvuilingslae op membraanoppervlaktes beter te beskryf. Veranderings in die digtheid en dikte van die aanvuilingslaag teenvloei is verwant aan dikte en digtheid (saampersbaarheid). Die voorspelde resultate van anvuilingslaagdeponering stem goed ooreen met die werklike UTDR-metings wat in MF en UF gemaak is.

Bio-aanvuiling is suksesvol waargeneem deur UTDR in buisvormige UF membrane. Ultrasoniese frekwensiespektra kan dus as 'n bykomende metode gebruik word vir die waarneming van aanvuiling op skeidingsmembrane.

ACKNOWLEDGEMENTS

I wish to express my very sincere thanks to:

Professor R.D. Sanderson, Director of the UNESCO assoc. Center for Macromolecules and Materials, Dept. of Chemistry, University of Stellenbosch, my supervisor, for his enthusiasm, encouragement and help throughout this study.

The Water Research Commission for financial support for this research.

Dr M.J. Hurndall for her generous and patient assistance, for the many helpful suggestions in the technical writing and for the proofreading of this thesis.

Dr E.P. Jacobs for his generous assistance and useful advice, especially in the early days of my research in this field.

Professor D.K. Hallbauer and **Dr. V.Y. Hallbauer-Zadorozhnaya** for sharing their knowledge of ultrasound with me.

Professor G. Chai, Central Research Institute of China Chemical Science and Technology, for her assistance and helpful advice, especially during her visiting to Stellenbosch (Jan. – April 2002).

Professors A.G. Fane, School of Chemical Engineering and Industrial Chemistry, University of New South Wales, **E. Drioli**, Department of Engineering Chemical and Material, Università della Calabtia and **C. Aldrich**, Department of Chemical Engineering, University of Stellenbosch for examining this thesis.

Mrs Miranda Waldron, Department of Physics, University of Cape Town, for her patient recording of many SEM images.

Dr W. Michaels for the friendly and patient manner in which she offered me generous assistance, especially at the beginning of this study.

Mr L.J. Koen for his initial work on ultrasonic measurements in our group.

The paper coating group – **Valeska**, **Angelo**, **Sheriff** and **Carmen**, who give me very good memories.

All the staff and fellow students at the Institute for Polymer Science. A special word of thanks goes to **Mrs Erinda Cooper**, **Mrs Aneli Forrie**, **Mr John Bonthuys** and **Mr Deon J. Keon** for their assistance.

Dr H. Wan, Fine Chemicals Corporation, my friend, for his generous and kind assistance in numerous ways.

My parents, my wife – **Weiping** and my daughter – **Ziyue**, for their love, understanding and support throughout this study.

LIST OF ABBREVIATIONS

BSA	Bovine serum albumin
CP	Concentration polarization
C_r	Coefficient/amplitude of reflected wave
C_t	Coefficient/amplitude of transmitted wave
E_c	Clean efficiency (%)
ED	Electrodialysis
MF	Microfiltration
NF	Nanofiltration
Nylon	Dupont trade name for polyamide 6, 6
J	Permeate flux
I	Intensity of sound wave (W/m^2)
ΔP	Transmembrane pressure difference (kPa)
P_0	Amplitude of pulse (N/m^2)
PA	Polyamide
PESU	Polyethersulfone
P_i	The sound pressures of the incident wave (N/m^2)
P_r	The sound pressures of the reflected wave (N/m^2)
P_t	The sound pressures of the transmitted wave (N/m^2)
PSU	Polysulfone
P_t	The sound pressures of the transmitted wave (N/m^2)
R	Distance between the sources (transducer) in Eq. 4.1 (m)
R_c	The resistance of residual fouling layer (m^{-1})
R_f	Fouling resistance (m^{-1})
R_g	Gel resistance (m^{-1})
R_m	Membrane resistance (m^{-1})
R_r	Reversible resistance (m^{-1})
R_t	Total resistance (m^{-1})
r_0	Unit of the vector, directed to the radius
RO	Reverse osmosis
dt	Difference in arrival times (s)
dS	Thickness of material (m)

SEM	Scanning electronic microscope
u	Particle velocity in sound wave (m/s)
UF	Ultrafiltration
URM	Ultrasonic reflection modeling
UTDR	Ultrasonic time-domain reflectometry
V	Velocity of sound wave in a medium (m/s)
W_1	The acoustic impedance of material 1 (kg/m^2s)
W_2	The acoustic impedance of material 2 (kg/m^2s)

Greek letters

a_p	Coefficient of the attenuation of the source (transducer)
ρ	Density of the material (kg/m^3)
t_1	Time of wave's arriving (s)
μ	Viscosity of solution (Pa.s)
ω	Frequency (Hz)
ω_0	$2\pi/T$
ω_{0p}	Frequency of the self-oscillation of source (transducer) (radian per second)

LIST OF TABLES

LIST OF FIGURES

CHAPTER 6

CHAPTER 7

CHAPTER 8

CHAPTER 9

LIST OF CONTENTS

CHAPTER 1

INTRODUCTION

This investigation forms part of a research project carried out to develop a noninvasive ultrasonic technique to study fouling in membrane processes.

1.1 MEMBRANE DEVELOPMENT

A membrane may be defined as a permeable or semi-permeable phase forming a selective barrier between two fluids or gases, which restricts the movement of one or more of the components of one or both fluids across the barrier [Mulder, 1996; Howell et al., 1993]. Membranes are often polymeric materials. While the term filtration conventionally refers to the separation of solid, immiscible particles from liquid or gaseous streams, the application of membrane filtration includes the separation of dissolved solutes from liquid streams and the separation of gas mixtures [Cheryan, 1998].

Historically, the first recorded study of membrane phenomena was conducted by Abbe' Jean Antoine Nollet in 1748 [Lonsdale, 1982]. He immersed wine contained in an animal bladder in pure water and observed that water permeated through the bladder into the wine.

Although the membrane phenomenon has been observed and studied for over 200 years, it was not until the early twentieth century that the first commercial membranes for practical applications (bacteriological laboratory use) were developed by Zsigmondy [Lonsdale, 1982] and manufactured by Sartorius in Germany. These were symmetric microfiltration (MF) membranes. A major breakthrough in industrial membrane applications was achieved for reverse osmosis (RO) desalination of seawater by the development of asymmetric cellulose acetate (CA) membranes, by the phase inversion process, in the early 1960s [Loeb and Sourirajan, 1962]. Shortly thereafter, Michaels made an asymmetric polyionic membrane for ultrafiltration (UF) [Michaels, 1968]. These membranes consisted of a very thin and dense top layer (<

0.5 μm), supported by a porous sublayer (50-200 μm). These asymmetric membranes exhibited high permeation and perm-selectivity.

In the 1950-80s, many original membrane technologies such as gas separation, haemodialysis, electrodialysis (ED), membrane distillation, nanofiltration (NF) and pervaporation, and liquid membranes, were developed for commercial applications [Jönsson, 1990; Mulder, 1996; Noble and Stern, 1995]. Sales of membrane systems in the worldwide membrane market increased from about US$3.2 Billion in 1999 to US$4.2 Billion in 2001 [Offringa, 2002]. Experts have predicted healthy annual growth rates of between 5 and 20 % for various membrane processes in the next decade. Meantime, the cost of membranes continuously declines. For example, the cost of RO membrane materials declined from about US$580 in 1987 to about US$420 in 1998 [Offringa, 2002].

Today, almost 50% of all brackish and sea water desalination occurs through membrane processes, producing more than 10 million cubic metres of fresh, potable water every day. Of equal importance is the ability of membrane filters to remove harmful organisms from drinking water. As a result, utilities in Paris, France; Kenosha, Wisconsin; and many cities are replacing sand filter systems with membranes [Offringa, 2002].

Membrane technology for separations is a rapidly emerging technology due to its continuous operation, low energy consumption, easy adaptability, versatility and the requirement for only relatively mild operating conditions in comparison with conventional separation processes such as distillation, evaporation and crystallization. Membranes are now being used for a variety of separations: particles from solution, salts from water, toxins from blood, one gas from a gas mixture, and so on. Two other technologically important applications of membranes are membrane electrodes and controlled release [Lonsdale, 1982].

1.2 MEMBRANE FOULING

Fouling is the most critical problem associated with membrane separations in liquid media. Fouling is generally defined as the deposition of retained particles, colloids, emulsions, suspensions, macromolecules, salts, etc. on or in a membrane [Mulder, 1991]. Fouling manifests itself as a decline in permeate flux with time of operation. It significantly affects operational efficiency and economics in numerous membrane separations, including microfiltration (MF), ultrafiltration (UF), nanofiltration (NF), reverse osmosis (RO) and electrodialysis (ED).

It is known that the pretreatment of feed water can be helpful in minimizing this fouling [Maartens, et al., 1999; Abdel-Jawad et al., 1997; Chakravorty et al., 1997; Dudley and Darton, 1997]. At the same time, membrane fouling can be minimized by the membrane geometry and stacking structure [Schwinge and Fane, 2001], surface feed flow velocities, turbulent pulses, sponge balls [Burch, 2001], backwashes [Redkar et al., 1996], air splurges [Laorie et al., 1997], ultrasound [Chai et al., 1999], electro and electromagnetic influences (certain effluents) [Huotari, 1999, Baker et al., 1997], chemical and biological cleaning protocols. However, these efforts to develop a means of fouling mitigation have been only partially successful. Fouling problems are still severe in some major membrane processes because synthetic membrane fouling is a very complicated phenomenon, compounded by the wide variety of foulants encountered in practice.

1.3 MOTIVATION

The extent of fouling and the success of cleaning protocols are currently measured by flux or pressure changes across a membrane. The nature and thickness of fouling layers on membranes in operating plants are currently determined by expensive and destructive tests, such as autopsies [Butt et al., 1995 and 1997; van Hoof et al., 2002]. The progression and mechanism of fouling are difficult to investigate with destructive or interfering techniques.

Monitoring of the fouling process is important for two reasons. First, fouling has a detrimental effect on the filtration process. Second, when a membrane is being cleaned, it is most desirable to know the state of cleaning. Hence, the development of a non-invasive visualization technique that is sensitive to changes in the condition of a membrane surface is of considerable interest. With the development of high-frequency digital and computer techniques, good progress has been made in investigating fouling using a non-destructive ultrasonic technique [Mairal et al. 1999 and 2000, Koen, 2000].

Mairal et al. [1999 & 2000] described a systematic attempt to adapt and employ ultrasonic-time-domain-reflectometry (UTDR) for the non-invasive measurement of RO membrane fouling and cleaning in real-time. They used three 5 MHz and three 10 MHz transducers in this study. Results showed a decline in the membrane signal amplitude as a fouling layer started to develop and grow on the membrane. UTDR thus appears to be well suited for the real-time monitoring of membrane fouling, as well as other phenomena of interest such as membrane compaction.

Koen [2000] reported results describing the use of UTDR for the investigation of membrane fouling and cleaning in flat-sheet RO membrane modules. These results showed that an echo of a fouling layer appeared and grew on the membrane surface, and disappeared as fouling and cleaning proceeded.

The above studies on the UTDR technique provided valuable information on the presence and development of a fouling layer on a membrane surface. However, different separation systems use different membranes and operating pressures, and different foulants are present. These factors all influence the capabilities of UTDR measurements. Further understanding of the process of ultrasonic testing, relative to the deposition and development of a fouling layer on a membrane surface in different membrane separation processes, is still required. The successful application of UTDR in the field can potentially save hundreds of millions of dollars annually.

1.4 OBJECTIVES

The overall objective of this study is to describe the development of ultrasonic time-domain and amplitude-domain reflectometry and their use as a real-time visualization technique for monitoring inorganic, organic and protein fouling in various membranes and modules (including flat-sheet and tubular). These results were to be compared with those obtained from the traditional methods of fouling indicators, such as permeate flux changes and visualization of the membrane surface covered by the fouling layer. The specific objectives of this study were to:

1. Develop and understand ultrasonic time-domain reflectometry (UTDR) as a possible non-destructive technique for monitoring of particle deposition in MF.
2. Design an ultrasonic cleaning system and develop an improved cleaning method.
3. Apply UTDR to the detection of cake-layer formation, growth and compressibility in MF.
4. Evaluate the efficiency of various cleaning techniques by UTDR.
5. Further develop UTDR to detect organic fouling as well as the structure and compaction of an asymmetric polysulfone (PSU) membrane in UF.
6. Correlate the ultrasonic signal response with membrane performance and corroborate the results via morphological characterization of the fouling layer.
7. Quantify and interpret the reflection signals obtained in MF and UF experiments.
8. Model and understand the processes of ultrasonic testing relative to the deposition of fouling layers on the membrane surface.
9. Investigate fouling mechanisms by experimental and modeling studies
10. Construct a tubular test cell and design suitable ultrasonic probes for advancing the focal ultrasonic technique for use in tubular membrane modules.

These results obtained were to be subsequently used to construct an ultrasonic fouling index meter for use as a process parameter to quantify fouling in actual operations in the membrane separation industry (this was to be done later, in conjunction with an overseas company).

1.5 LAYOUT OF THIS THESIS

This thesis is presented in 10 chapters. Chapter 2 presents an overview of pressure-driven membrane process and prior research carried out in the field of membrane fouling, detection and control, and includes all relevant non-invasive visualization techniques investigated to date. The experimental and modeling studies of the various fouling phenomena encountered in practice are also presented in this chapter. In the overview of fouling literature, the limitations of existing fouling-characterization methods are discussed. The ultrasonic technique developed in this study seeks to overcome these limitations. Hence, a brief overview of the working and application of ultrasonic waves is provided.

Chapter 3 explains the experimental approach for this research, including the principle of ultrasonic measurement of fouling, the design of separation systems related to test cells. Chapter 3 provides a thorough overview on the ultrasonic techniques relevant to the ultrasonic equipment used. In Chapter 4, a mathematical model – Ultrasonic Reflection Model (URM) was developed to understand the relationship between ultrasonic reflections and the growth of a fouling layer on a membrane surface. Simulation results of its use are presented in Chapters 7 and 8. Chapter 5 describes the development of UTDR for monitoring particle deposition, growth of cake and its removal in MF. Chapter 6 investigates three kinds of cleaning methods and compares their cleaning efficiencies in different operations. A new ultrasonic cleaning method was obtained. In Chapter 7, further investigation of deposition and growth of a compressible cake in MF was done by UTDR to as certain the capabilities of UTDR for different foulants. The compressibility (density) of cake could be determined by ultrasonic measurement and URM.

In order to further evaluate the capabilities of the ultrasonic testing technique in different membrane separation systems, an investigation into UF membrane fouling and cleaning by UTDR was carried out. Results are presented in Chapter 8. In chapter 9, a focal ultrasonic technique was developed to monitor protein fouling in tubular UF. Major conclusions of this research are summarized in Chapter 10, followed by recommendations for future research. A list of references used and publications that have emanated from this research to date are also listed.

CHAPTER 2

HISTORICAL AND THEORETICAL BACKGROUND

2.1 SCOPE OF THIS CHAPTER

The literature pertinent to the four major fields relevant to this research is covered, namely: pressure-driven membrane processes, concentration polarization, membrane fouling and ultrasonic techniques.

In the first part (Section 2.2), the main pressure-driven membrane processes: microfiltration (MF), ultrafiltration (UF), nanofiltration (NF) and reverse osmosis (RO), their characteristic and applications are mentioned.

In the second part (Section 2.3), a description of studies on membrane fouling including experimental and theoretical investigations is presented. It is followed by consideration of the various methods and techniques used for the prediction and measurement of fouling, to date, and strategies for fouling control. It is observed that a large portion of operating costs in membrane costs in separation processes can be attributed to the prevention and removal of fouling. To date, efforts to mitigate fouling have been only partially successful due to the lack of direct real-time information about fouling layer build-up. Recently some progress has been made in the real-time measurement of fouling phenomena by using various methods and techniques. Such research attempts have been to elucidate the process involved in the deposition and growth of a fouling layer on a membrane surface and its effect on membrane performance. In the past ten years, the literature has shown that ultrasonic testing, as a non-destructive, real-time visualization technique may be useful to monitor fouling phenomena in actual operations in membrane processes.

The third part of this chapter (Section 2.4) focuses on the above ultrasonic techniques; a description of the working of ultrasonics and various applications of ultrasonic techniques is given. Some theoretical formulations that describe the ultrasonic

response from some interfaces and aid interpretation the data generated by the experimental measurements are discussed.

2.2 MEMBRANE PROCESSES

All membrane processes have the common feature that separation is achieved via a membrane. A membrane can be considered to be a perm-selective barrier existing between two homogenous phases. Transport through the membrane takes place when a driving force is applied to the components in one of the phases. In most membrane processes the driving force is a pressure difference, a concentration (or activity) difference or a temperature difference. Membrane processes may be classified according to their driving force. Such a classification is given in Table 2.1 [Mulder, 1996].

Table 2.1: Classification of membrane processes according to their driving forces [Mulder, 1996]

Pressure difference	Concentration (activity) difference	Temperature difference	Electrical potential difference
Microfiltration	Pervaporation	Thermo-osmosis	Electro-dialysis
Ultrafiltration	Gas separation	Membrane distillation	Electro-osmosis
Nanofiltration	Vapour permeation		
Reverse osmosis	Dialysis		
Piezodialysis	Diffusion dialysis		

2.2.1 PRESSURE-DRIVEN MEMBRANE PROCESSES

Various pressure-driven membrane processes can be used to concentrate or purify a dilute (aqueous) solution. Various separation processes can be distinguished, related to the particle size of the solute and consequently to the membrane structure. These processes are microfiltration (MF), ultrafiltration, nanofiltration (NF) and reverse osmosis (RO). Figure 2.1 shows their application range [Scott and Hughes, 1996].

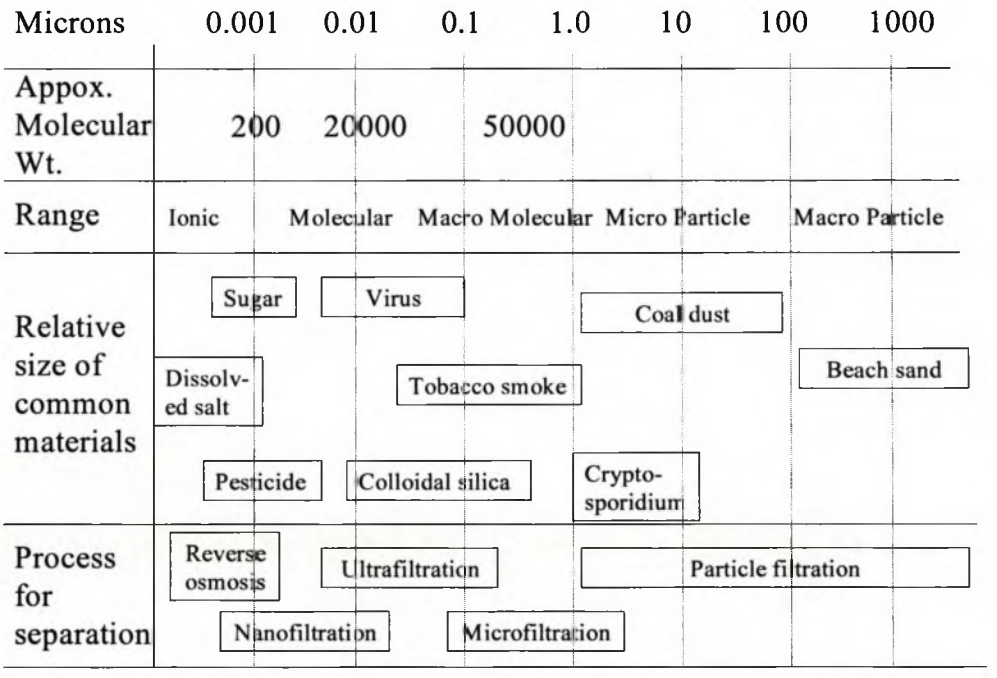

Figure 2.1: Useful ranges of various separation processes [Scott & Hughes, 1996].

The various processes can be distinguished in terms of membrane structure. In the case of MF, the entire membrane thickness contributes towards transport resistance, especially when a symmetrical porous structure is involved. The membrane thickness can extend from 10 μm to more than 150 μm. With UF, NF and RO, on the other hand, asymmetric membranes are used. Those have a thin, relatively dense top layer (thickness 0.1-1.0 μm), supported by a porous substructure (thickness 50-150 μm).

The hydraulic resistance is almost completely located in the top layer, the sublayer having only a supporting function. The flux through these membrane is inversely proportional to the (effective) thickness. A comparison of the various processes is given in Table 2.2 [Mulder, 1996].

Table 2.2: Comparison of various pressure driven membrane processes [Mulder, 1996]

Microfiltration	Ultrafiltration	Reverse osmosis
Separation of particles (bacteria, yeasts)	Separation of macromolecules (proteins)	Separation of low MW solutes (salt, glucose, lactose)
Osmotic pressure low - negligible	Osmotic pressure low - negligible	Osmotic pressure high (1-25 bar)
Applied pressure low (< 0.2 MPa)	Applied pressure low (0.1 – 1.0 MPa)	Applied pressure high (1.0 – 6.0 MPa)
Symmetric structure	Asymmetric structure	Asymmetric structure
Thickness of separating layer: 10–150 μm	Thickness of actual separating layer (1-10 μm)	Thickness of actual separating layer (0.1-1 μm)
Separation based on particle size	Separation based on particle size	Separation based on differences in solubility and diffusivity of solutes

2.2.2 MICROFILTRATION

Microfiltration (MF) is the membrane process that most closely resembles conventional coarse filtration. The pore sizes of MF membranes range from 10 to 0.05 μm. MF membranes are made from a number of organic and inorganic materials, for example:

- polymeric membranes: polyamide (PA)/polyamide 6,6 (nylon), cellulose esters, polysulfone/poly(ether sulfone) (PSU/PESU), polypropylene (PP), poly (vinylidene fluoride) (PVDF), polycarbonate (PC),
- ceramic membranes: alumina (Al_2O_3), zirconia (ZrO_2).

MF typically operates at low transmembrane pressures to minimise build-up of the suspended solids at the membrane surface. Pressures of 0.03-0.3 MPa and cross-flow velocities of up to 3-6 m/s in tubular modules are common. On an industrial scale, MF is usually implemented as a multistage (stages-in-series) operation in a feed-and-bleed mode of operation. The volume flow through these MF membranes can be described by Darcy's law, the flux J through the membrane being directly proportional to the applied pressure (ΔP):

$$J = k \Delta P \tag{2.1}$$

Where the permeability constant k contains structural factors such as the porosity and pore size (pore size distribution).

MF can separate 0.1 to 10 μm-sized particles from a liquid or gaseous feed stream. As a consequence of the large pore size of MF membranes, MF is used primarily for particle and microbial removal. MF separates macro-materials and suspended solids like starch, bacteria, moulds, yeast and emulsified oils. It is finding increased applications as a pre-treatment to other membrane processes, in bioreactors for sludge concentration, recovery of backwash waters and for the replacement of conventional clarification and filtration technologies [Porter, 1986; Eykamp, 1995; Cheryan, 1998].

2.2.3 ULTRAFILTRATION

Ultrafiltration (UF) is a membrane process whose nature lies between that of NF and MF. The pore sizes of UF membranes range from 0.05 μm to 1 nm. UF separates dissolved solutes of 0.005 to 0.1 microns. This corresponds to a molecular weight cut-off of about 1,000 to 500,000 [Cheryan, 1998]. Depending on the molecular weight cut-off selected, the membrane will concentrate high molecular weight species while allowing dissolved salts and lower molecular weight materials to pass through the membrane. Most UF membranes used commercially these days are prepared from polymeric materials by a phase inversion process. Some of these materials are listed below:

- polysulfone/poly (ether sulfone) (PSU/PESU)
- poly (vinylidene fluoride) (PVDF)
- polyacrylonitrile (PAN)
- cellulosics (e.g. cellulose acetate)
- polyimide/poly(ether imide) (PI/PEI).

UF membranes are used in numerous industries, for the concentration and clarification of large process streams such as in the food and dairy industry, pharmaceutical industry, textile industry, metallurgy, paper industry and leather industry [Jönsson and Trägårdh, 1990; Cheryan, 1998;]. It is also widely used as a pre-treatment process for downstream membrane systems.

2.2.4 NANOFILTRATION

Nanofiltration (NF) is similar to RO and is applied in the area between the separation capabilities of RO and UF. NF is a relatively new process that uses charged membranes with pores that are larger than RO membranes, but too small to allow permeation of some organic compounds such as sugars [Wadley et al. 1995]. The NF membrane displays excellent rejection of divalent ions while allowing the majority of mono-valent ions to pass. Organic molecules in the 200-300 molecular weight range are also highly rejected. NF systems typically operate at lower pressures than required

for RO (e.g. 1.0 - 1.5 MPa), but yield higher flow-rates of water, albeit of a different quality to RO permeate.

The unique separation capability of NF provides the opportunity to selectively concentrate either valuable or undesirable substance from a process stream with great effectiveness, consistency, reliability and economy. In most water sources, there will be single-charged ions, such as sodium ions (Na^+) and chloride ions (Cl^-), and double charged ions, such as calcium ions (Ca^{2+}) and sulphate ions (SO_4^{2-}). The single-charged, positive ions do not generally participate in scale formation, so they may be considered as soft ions. The double-charged positive ions such as calcium and magnesium, in conjunction with certain negatively charged ions, can form hard scale within water treatment equipment and piping and are called hard ions. Depending upon the membrane, water chemistry, and operating conditions, NF membranes can remove more than 90% of feed water's hardness ions. NF membranes also remove large colour molecules and many of the trihalomethane (THM) precursors. Nanofiltration can treat the same amount of water, or more, than RO at half the pressure. Since NF membranes can remove the double-charged scaling ions like calcium and magnesium ions, another term for NF is membrane softening. The largest users of NF technology are municipal drinking water plants. A future trend is for NF to replace lime softening, to achieve an industry standard of 50 parts per million (ppm) of alkalinity and meet the USA federal THM limits. NF is well established in the dairy industry for cheese-whey desalting [Yacubowicz, 1995; van der Horst et al., 1995; Dresch et al., 2001]. Other growing markets are in RO pre-treatment; pharmaceutical concentration; kidney dialysis units; and maple sugar concentration.

2.2.5 REVERSE OSMOSIS

Reverse osmosis (RO) is the most complex technique in membrane separation. RO membranes concentrate low molecular weight organic materials and salts while allowing water and solvents to pass. High pressures of about 3.5-10 MPa are required in order to overcome the high osmotic pressures across the membrane. This permits water to flow from the concentrated feed stream to the dilute permeate - a direction

that is just the reverse of what occurs naturally during osmosis. The pore sizes of RO membranes are < 2 nm. Most RO membranes are prepared from polymeric materials such as cellulose triacetate, aromatic polyamides, poly (ether urea) [Mulder, 1996].

RO has been the most widely used technology for desalinating seawater and reclaiming brackish well water [Porter, 1986; Eykamp, 1995; Mulder, 1996]. A RO membrane will typically reject all of the organic molecules over 150 molecular weight and a percentage of those between 25 and 150 MW. It is generally used for the production of very high purity water used in boilers, microelectronics processing and pharmaceutical formulation.

Membrane separations are in competition with physical methods of separation such as selective adsorption, absorption, solvent extraction, distillation, crystallisation, cryogenic gas separation etc. Table 2.3 summarises the various membrane treatment processes, their application(s), as well as comparable traditional treatment methods [Koen, 2000].

Table 2.3: Various membrane processes, their applications and comparable traditional treatment methods [Koen, 2000]

Membrane separation technology	Substances removed	Comparable traditional water treatment methods
Microfiltration	Bacteria and larger colloids; separation of precipitates and coagulates	Ozonation-ultraviolet radiation, chlorination, sand filters, bioreactors and coagulation-settling tanks
Ultrafiltration	All of the above, plus viruses, high-molecular weight proteins, organics and pyrogen	Sand filters, bioreactors and activated carbon
Nanofiltration	All of the above, plus divalent ions, larger monovalent ions, colour and odour	Lime-soda softening and ion exchange
Reverse osmosis	All of the above, plus monovalent ions	Distillation, evaporation, ion exchange, ED, EDR
Electrodialyses (ED) and Electrodialyses reversal (EDR)	Dissolved ionic salts	Ion exchange, Reverse osmosis

2.3 CONCENTRATION POLARIZATION AND FOULING

In order to achieve a particular separation via a membrane process, the first step is to develop a suitable membrane. However, during an actual separation, the membrane performance can vary greatly over time; often a typical flux-time behaviour is observed: the flux through the membrane decreases over time. Especially in MF and UF, the flux decline is very severe; the process flux is often less than 5% that of pure water. This is mainly due to concentration polarization (CP) and fouling, although membrane compaction and physical transformation of the membrane structure also occur during operation [Anderson et al., 1981; Fane and Fell, 1987; Eisold et al., 1990; Brinkert et al., 1993].

2.3.1 CONCENTRATION POLARIZATION

In membrane-based liquid separation processes, one or more components in the feed solution are preferentially retained on the membrane surface. Generally, the convective transport of these components to the surface is greater than the diffusive and convective transport away from the membrane [Mulder, 1999]. CP is caused by the accumulation of retained solutes or particles on the membrane or in the boundary layer adjacent to the membrane surface. This concentration is highest at the membrane surface, and decreases exponentially toward the solution. In the case of higher molecular weight (or inorganic) substances, the solubility limit is often reached at the membrane surface. The precipitated layer then acts as a secondary membrane, referred to as the 'gel layer'. Formation of the gel layer decreases the flux considerably. The gel layer may also have a higher retention than the membrane itself, which increases the actual retention of the membrane as the filtration process proceeds.

The effects of CP include: a decline in permeate flux as a result of a reduced driving force for separation, a decline in product quality due to the increased diffusion of undesirable components through the membrane, and the increased risk of deposition of these components on the membrane surface. CP is considered to be reversible and can be reduced by diluting the process solution, stirring, tangential flow of the solution across the membrane surface or by means of pulsation, ultrasound and an

electric or magnetic fields [Gupta et al, 1992; Howell et al., 1993; Lin and Nadiv, 1988; Wakeman and Tarleton, 1991].

2.3.2 FOULING

Fouling may be defined as the irreversible deposition of retained particles, colloids, macromolecules, salts, etc., at the membrane surface or inside the membrane at the pore wall, which causes a continuous flux decline. Membrane fouling is complicated in that it is considered as a group of physical, chemical, and biological effects leading to irreversible loss of membrane permeability. Attempts to analyse the fouling phenomenon, for example, have shown that the main factors are: adsorption of feed components, clogging of pores, deposition of solids on the membrane surface accompanied by crystallization and compaction of the membrane structure, chemical interaction between membrane material and components of the solution, gel coacervation, and bacterial growth [Potts et al. 1981; Fane and Fell 1987; Belfort et al. 1994; Mulder, 1996].

Membrane fouling is universally accepted as the most critical problem in several membrane processes including microfiltration (MF), ultrafiltration (UF), nanofiltration (NF), reverse osmosis (RO), and electrodialysis (ED) [Belfort, 1984; Rautenbach and Albrecht, 1989; Mulder, 1996; Davis, 1992]. An extensive body of literature exists on the various aspects of membrane fouling due to the importance of this problem. Some excellent reviews on various aspects of membrane fouling are given by Potts et al. [1981], Belfort and Altena [1983], Fane and Fell [1987], Belfort [1989], Nilsson [1990], Marshall et al. [1993], Belfort et al. [1994], and Mulder [1998].

2.3.3 MEMBRANE FOULING STUDIES

2.3.3.1 Experimental Investigations

Since the pig-bladder experiments of Abbe Jean Antoine Nollet in 1784, membranes have been utilized in numerous liquid separation applications. Membrane fouling has been observed in nearly all of these applications [Strathmann, 1981; Lonsdale, 1982]. The experimental investigations of membrane fouling can be classified into three broad categories – inorganic fouling, colloidal fouling, and fouling due to dissolved organics and biological constituents in the feed.

Inorganic fouling occurs in separations where the solubility of a dissolved salt is exceeded. It is typically encountered in RO and ED but has also been observed in MF and UF. Colloidal fouling is a very common phenomenon in almost all membrane processes, and occurs when colloidal organic constituents in the feed are deposited on the membrane surface due to hydrodynamic and physical-chemical characteristics of the separation system. Biological and organic fouling is observed in separations where the feed solution exhibits substantial biological growth and dissolved organic content.

2.3.3.2 Theoretical Investigations

Membrane fouling is widely acknowledged to be the most important economic determinant of most membrane processes. A number of mathematical models of CP and fouling have been developed to understand this complicated phenomenon. The following mathematical models are available:

1. Empirical models [Sheppard et al., 1972]
2. Gel polarization models [Michaels, 1968; Belfort and Altena, 1983; Kimura and Nakao, 1975]
3. Osmotic pressure models [Vilker et al., 1981; Jonsson, 1984; Wijmans et al, 1985]
4. Particle trajectory models [Hung and Tien, 1976; Bacchin et al., 1995]
5. Differential rate models [Carter and Hoyland, 1976]

6. Resistance models [Belfort and Marx, 1979; Schippers et al., 1981; Fane and Fell, 1987]
7. Surface reaction models [Gilron and Hasson, 1987; Borden et al., 1987]
8. Compressible cake filtration models [Shirato et al., 1969, Tiller, 1975; Murase et al., 1995; Tiller and Kwon, 1998; Tiller and Li, 2001].

Gel polarization model

The gel polarization model [Michaels, 1968] was proposed to explain the effects of concentration polarization in UF. The solute concentration at the membrane surface reaches a very high value and a maximum concentration, the gel concentration (c_g), may be reached for a number of macromolecular solutes. The two phenomena, concentration polarization and gel formation, are shown in Fig. 2.2.

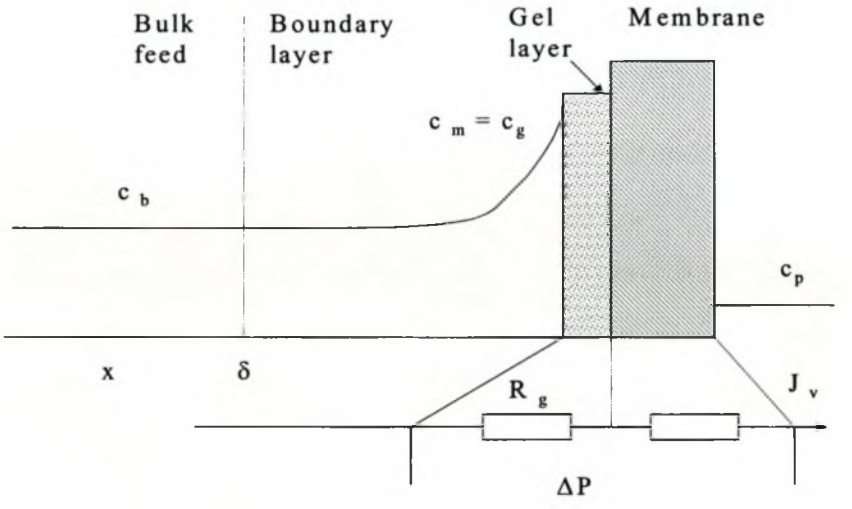

Figure 2.2: Concentration polarization and gel layer formation [Mulder, 1996].

The gel polarization (GP) model is capable of describing the occurrence of limiting flux by assuming that $c_m \rightarrow c_g$. The limiting flux J_∞ can now be described by

$$J_\infty = \frac{\Delta P}{\eta(R_m + R_g)} = k \ln(\frac{c_g}{c_b}) \qquad (2.2)$$

where ΔP is the applied pressure (Pa); η is the viscosity of solution (Pa.s); R_m is the membrane resistance (m^{-1}); R_g is the gel layer resistance (m^{-1}); c_g is the gel concentration (kg/m^3); c_b is the concentration of the bulk feed (kg/m^3).

If J_∞ is plotted as a function of ln (c_b), the result must be a straight line of slope $-k$. The intercept on the abscissa ($J_\infty = 0$) will give the value of ln (c_g) (see Fig. 2.3).

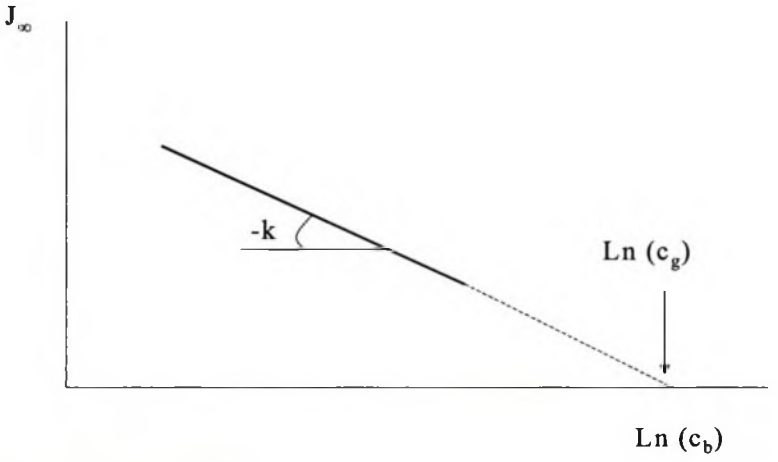

Figure 2.3: Limiting flux (J_∞) plotted as a function of the logarithm of the bulk concentration [Mulder, 1996].

Although this model may be considered to be a significant contribution to the theory of CP and limiting flux behaviour in UF, some drawbacks should be mentioned. Belfort et al [Belfort et al., 1983] modified the GP model for application in RO. In the literature, data have indicated that the gel concentration c_g is not a constant but depends on the bulk concentration and the cross-flaw velocity [Wijmans et al., 1984]. In addition, different authors have reported widely varying values for c_g for a given solute [Dejmek, 1975]. Furthermore, k is assumed to be constant whereas the diffusivity of the macromolecular solute is often concentration-dependent. Despite

these physical limitations the GP model can still be considered as a very convenient and simple model.

Osmotic pressure model

The limiting flux in the osmotic pressure model is regarded as being due to the increased osmotic counter-pressure produced by the high concentration of the rejected solute near the membrane surface [Denisov, 1994]. If the osmotic pressure at the membrane surface is taken into account, the flux (J) is the given by:

$$J = \frac{\Delta P - \Delta \pi}{\eta R_m} \tag{2.3}$$

Here, ΔP is the hydraulic pressure difference and $\Delta\pi$ the osmotic pressure difference across the membrane. The value of $\Delta\pi$ is determined by the concentration at the membrane surface c. It can be described by:

$$\Delta \pi = a\, c^n \tag{2.4}$$

where a is a constant and n is an exponential factor with a value greater than 1.
Applying this osmotic pressure effect to the concentration at the membrane interface (c_m), and combing Equations. 2.2 and 2.3, is possible to calculate the flux assuming that the solutes are retained completely:

$$J = \frac{\Delta P - a c_b^n \exp(\frac{nJ}{k})}{\eta R_m} \tag{2.5}$$

From Eq. 2.5 the following relationship can be derived:

$$\frac{\partial J}{\partial \ln(c_b)} = -k(1 + \frac{R_m k \eta}{\Delta \pi n})^{-1} \tag{2.6}$$

which shows that $\partial J/\partial \ln(c_b) \rightarrow -k$ for $(\Delta\pi \cdot n)/(\eta \cdot R_m \cdot k) >> 1$. Hence, the osmotic pressure model predicts a slope equal to $-k$, similar to that obtained from the GP model.

Resistance model

By analogy to the standard Darcy's-law filtration model, flux can be considered to be controlled by several resistances:

$$J = \frac{\Delta P}{\eta R_t} \tag{2.7}$$

The resistance models constitute one of the most common approaches for analyzing flux-decline behavior via visualization of the system as resistances-in-series [Belfort and Marx, 1979; Schippers et al., 1981; Fane and Fell, 1987]. These phenomenological models allow for the evaluation of the resistance due to individual components and factors such as membrane compaction, internal and external fouling, osmotic effects, and the back-diffusion of the solute using the experimental data. A more general equation would be

$$J = \frac{\Delta P - \Delta\pi}{\eta R_t} = \frac{\Delta P - \Delta\pi}{\eta(R_m + R_a + R_p + R_g + R_{cp})} \tag{2.8}$$

Here, R_t is the total resistance; R_m is the membrane resistance; R_a is the adsorption resistance; R_p is the pore-blocking resistance; R_g is the gel layer resistance; R_{cp} is the concentration polarization.

The resistance due to pore constriction is modelled by the Standard Blocking Law, that assumes that the pore volume decrease is directly proportional to the filtered volume [Viswanathan and Aim, 1989]. The Complete Blocking Law is used to model pore blockage by external fouling. This model assumes that each particle reaching the surface participates in sealing the pores and no superposition of the particles takes place [Gésan et al., 1993].

The contribution due to the cake layer is usually modelled by the cake filtration theory, wherein the cake resistance is expressed by the Carman-Kozeny equation [Nilsson, 1990]

$$R_c = \alpha m \tag{2.9}$$

where m is the mass of the cake layer. The specific resistance, α, is given by

$$\alpha = \frac{180(1-\varepsilon)^2 \delta_c}{d_c^2 \varepsilon^3} \tag{2.10}$$

where ε is the porosity of the cake layer, δ_c is the thickness of the cake, and d_c is the pore diameter of the porous cake.

2.3.4 PREDICTION AND MEASUREMENT OF FOULING

The phenomenon of fouling is very complex and difficult to describe theoretically. A number of studies have been carried out to understand fouling before the start of the separation process, during the process, or after the process. The ability to accurately measure fouling is essential for the development of fouling control strategies, which is the ultimate goal of membrane fouling research.

2.3.4.1 Prediction Fouling

For the design of RO facilities, it would be most desirable to have an analytical procedure available to quantitatively predict how rapidly or severely a given feed will foul a membrane. Many parameters such as the plugging index (PI), the fouling index (FI) [Lipp et al., 1990] or silt-density index (SDI) [Potts et al., 1981], the modified fouling index or the membrane filtration index (MFI) [Schippers and Verdouw, 1980] et al. and Langelier saturation index [Du Pont, 1977] have been used to describe fouling.

The silt density index [Potts et al., 1981] is, to date, the only widely accepted test for fouling prediction in the RO industry. The silt density index test is performed in the following manner. RO feed is pumped through a 0.45μm cellulose acetate Millipore filter at a constant pressure. The time required to collect the first 500-ml of filtrate is noted and recorded as t_i. Fifteen minutes after the start of the test, another 500 ml is collected and the time is recorded as t_f. The plugging factor (%P) is computed as follows:

$$\%P = 100\,(1 - \frac{t_i}{t_f}) \tag{2.11}$$

The silt density index is computed by dividing %P by the time of the test, i.e., 15-min in this case.

Shippers and Verdouw [1980] applied a filtration theory to the SDI test and derived a formula for a modified fouling index (MFI). With the SDI no linear relationship exists between the index and the colloid or suspended matter concentration, while the MFI is directly proportional to colloidal concentration. The relation has the form:

$$MFI = \frac{\eta_{20}}{\eta}\frac{\Delta P}{210}\tan\alpha \tag{2.12}$$

where η_{20} = viscosity at 20 °C

η = viscosity at water temperature

ΔP = applied pressure difference in kPa

$\tan\alpha$ = slope of the straight-line portion of a plot of reciprocal volumetric flow rate (t/V_{tot}) vs. accumulated volume of filtrate.

The MFI is directly proportional to the colloidal concentration in the feed as confirmed by experiments [Schippers et al. 1981]. Thus, the MFI can be used to predict the fouling tendency of one feed solution relative to another. Fouling is, however, too complex to be described by a single parameter.

2.3.4.2 Membrane Autopsy

The term autopsy is used to describe a series of observations made of and scientific tests carried out on, a used membrane element. Chemical, physical and microbiological analyses determine the type of foulant present and its effect on membrane performance. Other techniques used to investigate membrane fouling are scanning electron microscopy (SEM), x-ray fluorescence (XRF), x-ray diffractometry (XRD), inductively coupled plasma (ICP) spectrometry, ion chromatography (IC), energy-dispersive x-ray spectroscopy (EDS), atomic absorption spectroscopy (AAS), prompt ion x-ray excitation (PIXE) and biocide sensitivity tests [Butt et al, 1995; Dudley and Darton, 1996; van Hoof et al., 2002].

Van Hoof et al. [2002] investigated 150 eight-inch (200 mm) polyamide elements, received within the last two years from around the world, by various autopsy methods. Results from so many systems have been helpful in developing improved anti-scalants and anti-foulants, more effective cleaners and improved cleaning programmes. A better understanding of membrane fouling has also helped many equipment manufactures predict problem areas and take remedial actions at the system design stage. Although these analytical methods can supply some information on the fouling mechanism, they have provided little information regarding the actual and dynamic build-up of foulant on a membrane surface. Furthermore, an autopsy is a destructive procedure and the membrane cannot be returned to service once the autopsy is completed.

2.3.4.3 *In situ* Measurements

Numerous indirect and direct real-time measurements have been conducted to study membrane fouling. Traditionally, real-time fouling investigations have involved the analysis of flux-decline data for inference of fouling [Mashiko et al., 1983; Bhattacharjee and Bhattacharya, 1992; Herrero et al., 1997]. Other methods of fouling analysis include the monitoring of permeate concentration change, increase in the pressure drop along the membrane, and sudden change in retentate concentration

[Fárkorá, 1991; Karode and Kumar, 2001]. These indirect methods however provide little information regarding direct observation of the fouling deposition process.

Non-invasive techniques have been developed to overcome the limitations of the above-mentioned methods in providing direct information about CP and fouling. Hendricks and Williams [1971] developed sensitive electrical conductivity microprobes for the direct measurement of concentration profile in unstirred batch and parallel plate channel RO cells. The measurement method involved the placement of these microprobes within the feed solution, very close to the membrane surface, to measure the solution conductivity, which was then converted into a concentration value using calibration charts. The probes used in the flow cells were very small (5-20 μm) and gave measurements of thin concentration boundary layers.

Johnson [1974] developed laser interferometry for the non-invasive measurement of concentration profiles in RO systems. He utilized an interferometer with a helium-neon laser as a light source. The increased concentration near the membrane surface caused a change in the refractive index, leading to a shift in the interference fringes. The concentration profiles calculated from the interferograms were found to be within 5% of the theoretical predictions after correcting for the deflection of the beam due to large concentration gradients.

Over the last ten years there have been a number of non-invasive techniques used to study membrane fouling. Mackley and Sherman [1992] conducted an *in situ*, direct observation of particle deposition during filtration of sub-millimetre particles (size range 120-180 μm) using a 15-times magnification video camera. They were able to record the growth of cake and particle motions on the cake surface. Their crossflow velocity increased, indicting that the particles in the cake at higher crossflow velocity were smaller than that those at low velocity. These interesting observations were made for particles significantly larger than those typical of microfiltration.

Wandelt et al [1992] set up an NMR micro-imaging technique, with a resolution of 10-20 μm, to measure cake thickness in a hollow-fibre module during crossflow microfiltraion of bentonite slurry. Tiller et al [1995] developed a CATSCAN method

that can be applied to measure the variation in slurry concentration as well as sediment height in a sedimentation process.

Chung *et al.* [1993] used nuclear magnetic resonance (NMR) flow imaging to measure fluid-flow characteristics in a curved channel membrane system. They also conducted dye-streaking experiments to verify the fluid-flow patterns observed by the NMR technique. Fane and co-workers [Yao et al., 1995] later applied NMR micro-imaging to visualize the growth of oil layers in MF of oil/water emulsions, using hollow-fiber modules. By combining chemical-shift imaging with flow-velocity imaging, they concluded that the oil layers on the fiber surfaces were not moving, thereby supporting the stationery cake model for MF.

Wakeman [1994] employed a high-speed camera and a high-magnification zoom lens to record the development of the cake layer at the centre axis of a membrane. It was observed that the cake thickness along the membrane length was uniform, with a slight dip at both ends of the membrane, and that the particle layer was thinner at higher velocity. The process of particle deposition on the membrane surface and the particle-particle interactions at or near the membrane surface could not be observed.

McDonogh et al. [1995] reported two non-invasive techniques for the study of concentration polarisation during filtration of bovine serum albumen (BSA) and dextran blue. The first technique, which measures overall layer build up, is a radioisotope technique. The second technique uses a micro-array of semiconductor photosites to measure infrared absorption of species in the polarised layer. The development of the polarised region is observed as a function of distance, perpendicular to the membrane surface.

Altman and Ripperger [1997] used a laser triangulometer in situ to measure the cake layer height under various filtration conditions. For filtration under constant transmembrane pressure they observed that the layer height reached steady state very quickly (<5 min), while the flux had a longer transient (~30 min). The non-stationary period is influenced by the particle size distribution, while the stationary state

especially depends on the fine material of the particle system. Simultaneously the layer showed an asymmetric structure.

The above studies provided valuable information on polarisation profiles and cake thickness, but little information on the phenomenon occurring at the membrane-solution interface as particles deposit. Oppenheim et al. [1994] employed electron paramagnetic response (EPR) spectroscopy as a method for exploring the transient development of fouling in single protein ultrafiltration and as a potential method to determine protein-membrane interaction. The results showed that the proteins on the membrane surface might have a different conformation than the proteins trapped and lodged in the membrane pores. The proteins within the pores may be more compressed than those on the surface. Preliminary research showed that EPR is an ideal method for analysing short-time solute uptakes in UF.

Fane and co-workers [Li et al., 1998] reported observations of particle deposition on membrane surfaces using non-invasive, continuous, direct observation through a membrane (DOTM). The image observed by the microscope was recorded and viewed via a video camera attached to a super-VHS video recorder and monitor. The filtration tests were conducted in the imposed flux mode, so that the flux could be controlled at below, or above, the "critical flux." The "critical flux" is the flux rate (dependant on the crossflow velocity), which controls particle deposition on the membrane surface. Below the critical flux, particle deposition is negligible and above the critical flux, particle layers form rather quickly on the membrane surface. The results demonstrated that DOTM is a powerful technique with which the fundamentals of particle deposition and the interaction between particles and the membrane can be studied.

Lu et al [2002] applied the infrared reflection method to measure filter cake thickness in situ and verify the theoretical results in crossflow microfiltration. Crossflow microfiltration of mono-dispersed deformable particles of Saccharomyces cerevisiae and Ca-alginate, and rigid PMMA particles with an average size 4 - 6 μm, were added to the MF feed in order to compare the structure of the flux-limiting layer. Results of this study showed that the cake formed by deformable particles exhibited a rapid increase in flow resistance, or a decrease in local porosity, and a highly resistant

limiting layer was formed next to the filter medium during filtration. This was stated to be due to the deformation of particles (caused by frictional drag and mass of the cake). Although this method can measure changes in the cake thickness and compressibility under crossflow filtration, the intrinsic local cake properties can only be estimated by the dynamic analysis of constant pressure filtration developed by Lu and Hwang [1995].

Using micro-video photography, Mores and Davis [2001] explored the direct visual observation (DVO) of yeast deposition on a MF membrane and its subsequent removal via backwashing and single backpulses. Although their results showed the relationship between the membrane flux and the fraction of membrane surface covered, information on cake thickness was not available.

Ultrasonic techniques have been shown to be an excellent tool for the non-destructive testing or imaging [Lynnworth, 1989; Mason and Lorimer, 1988; Ensminger, 1998]. With the development of a high-frequency digital and computer technique it was possible to apply ultrasonic methods for monitoring processing or material characterization. Ultrasonic methods have been successfully applied to the monitoring of cake thickness during a ceramics slip-casting process [Hutchins and Mair, 1989; Haerle and Haber, 1993], chemical reactions [Parthun and Johari, 1995], film formation [Alig et al. 1998; Kools et al 1998], glue processes or crystallization in polymers [Alig and Tadjbakhsch, 1998] and membrane fouling in water treatment [Mairal, 1998; Koen, 2000].

Hutchins and Mair [1989] developed an ultrasound imaging technique to monitor cake thickness during a ceramics slip-casting process. This was done by utilizing transducers configured in a pulse-echo mode. Haerle and Haber [1993] further expanded the work of Hutchins and Mair to determine the effect of frequency on the peak resolution. The frequency of 1 MHz was found to give the best peak resolution.

Kools et al. [1998] had some success in employing ultrasound for real-time visualisation of thickness changes during the evaporative casting of polymeric films, while Reinsch et al. [1998] employed the ultrasound for real-time measurement of membrane compaction and performance during exposure to high-pressure gas.

Peterson et al. [1998] used real-time noninvasive ultrasonic TDR to measure compressive strain during membrane compaction.

Mairal et al. [1999 and 2000] described the first, and so far the only, systematic attempt to adapt and employ ultrasonic-time-domain-reflectometry (UTDR) for the non-invasive measurement of membrane fouling and cleaning in real-time. Results showed a decline in the membrane signal amplitude as a fouling layer started to develop and grow on the membrane. UTDR thus appears to be ideally suited for the real-time monitoring of membrane fouling, as well as other phenomena of interest such as membrane compaction.

Koen [2000] reported results describing the use of UTDR for the investigation of calcium carbonate deposition and removal in flat-sheet RO membrane modules. These results showed that an echo of a fouling layer appeared and grew on the membrane surface, and disappeared as fouling and cleaning proceeded.

2.3.5 FOULING: PREVENTION AND REDUCTION

The ultimate objective of the numerous fouling studies is the prevention and reduction of fouling. The methods used to date to mitigate fouling include: pre-treatment of the feed solution, modification of membrane properties, optimisation of the module and process conditions, and frequent cleaning of the fouled membranes by chemical, biological and physical (electric, magnetic, ultrasonic) methods [Mulder, 1991]. These methods have been discussed in great detail by Mathiasson and Sivik [1980], Potts et al. [1981], Belfort and Altena [1983], Fane and Fell [1987], Howell et al., 1993; Belfort et al. 1994; Cheryan, 1998; and Wakeman and Williams [2002]. A brief discussion and some illustrative examples are presented here for each of these approaches.

2.3.5.1 Pretreatment of Feed Solution

Fouling effects can be reduced by pretreating the feed. Feed pretreatment is commonly used either to remove foulants that may cause clogging in the module or to prevent foulants from reaching and depositing on the membrane surface, or to reduce the total contaminant load in downstream membrane modules. Pretreatment can involve either physical or chemical processes.

Physical processes usually include prefiltration or centrifugation to remove suspended solids that may plug the module or blind the membrane. Baker et al. [1997] employed magnetic pre-treatment of RO feed water to prevent inorganic scaling. Tsujimoto et al. [1998] used granular activated carbon (GAC) to pretreat feed solution prior to UF. Results demonstrated that GAC filtering is considered to play a role in preventing irreversible fouling and minimize chemical cleaning frequency and to realize lower pressure operation.

Chemical processes include feed pH adjustment, precipitation, coagulation or flocculation, ion exchange and antiscalants. Applegate and Sackinger [1987] emphasized the need for coagulation-flocculation-filtration pre-treatment of feed water containing iron in RO desalination. Lahoussine-Tucaud et al. [1990] reported that coagulation of model dispersions containing tannic acid, humic acid and kaolin was very effective in reducing fouling of hollow-fiber UF modules. Maartens et al. [1999] reported that membrane fouling by natural organic matter was reduced by changing the pH of the feed solution and coagulation with metal-ions prior to filtration.

Amjad [1985] ranked various antiscalants for controlling calcium sulfate scaling in the following order: formulated polyelectrolytes > polyacrylates > hexametaphosphates. Saad [1992] and Rowley [1992] recommended the use of biocides for preventing biofouling in RO systems. Protein fouling can be minimized in MF and UF by adjusting the pH of the feed to a value corresponding to the isoelectric point of the protein [Mulder, 1996].

2.3.5.2 Modification of Membrane Properties

Membrane fouling can also be minimized by changing the membrane characteristics. Utilization of charged membranes, immobilization of enzymes on the membrane surface, chemical modification of the membrane to render it hydrophilic, use of fixed and dynamic protective layers, and membrane casting with physical protrusions have been reported in the literature [Matthiasson and Sivik, 1980; Potts et al., 1981; Belfort and Altena, 1983; Maartens et al., 1998 and 1999].

Belfort and coworkers [Belfort and Marx, 1980] developed the protective cover method in which fixed and dynamic precoats were employed to provide better fouling resistance and improved flux behavior during RO separations.

Polysulfone UF membranes used for the purification of natural brown water were pretreated by commercial non-ionic surfactants Triton X-100 and Pluronic F108 [Jucker and Clarke, 1994; Maartens et al., 1998 and 1999]. Specific characterisation techniques were used to determine and compare the effects induced by the adsorption of natural organic matter on the permeability of untreated as well as surfactant treated capillary UF membranes. Results showed that this method was able to reduce fouling by natural organic matter.

2.3.5.3 Optimisation of Module Design - Flow Manipulation

Concentration polarization and fouling in commercial membrane modules is controlled by either increased shear at the membrane surface or the use of turbulence inducers [Belfort et al., 1994; Wakeman and Williams, 2002]. Increased shear is obtained by pumping the feed at higher flow rates or by using thin flow channels above the membrane surface. Turbulence is encouraged by appropriately designed feed spacers or static mixers. These methods of optimisation of module design include:

(1) Turbulence promoters - local vortex promotion [Gupta et al., 1992; Holdich and Zhang, 1992; Bellhouse, 1994; Millward et al., 1995].

(2) Backflushing, pulsing and shocking [Milisic and Bersillon, 1986; Redkar and Davis, 1995 and 1996; Wenten, 1995; Cheryan, 1998; Kennedy et al., 1998].
(3) Pulsatile flow [Finnigan and Howell, 1989; Howell et al., 1993; Gupta et al., 1992 and 1993].
(4) Rotating membranes - high shear (dynamic) filtration [Gravas and Martin, 1978; Hildebrandt and Saxton, 1987; Min and Lueptow, 1994].
(5) Gas sparging and using sponge balls [Cui and Wright, 1994; Laborie et al. 1997; Burch, 2001].

2.3.5.4 Application of External Fields

In principle, a number of alternative force fields (electric, magnetic, sonic) can be used to enhance the performance of membranes.

Magnetic fields

The first known patent on this subject was issued to France and Cabell in 1890 [France, 1890]. Although the method has been used worldwide since the pioneering work of Vermeiren, a Belgian engineer who founded the EURO company in the early 1940's [Vermeiren, 1953], commercial units using magnets to treat water were only introduced in the early 1950's.

The use of magnetic pre-treatment can prevent crystalline scale formation [Lin and Nadiv, 1988; Baker et al., 1997]. In this case a commercially available magnetic treatment device was used on the high pressure feed line to the reverse osmosis cell in a fully recycled system of hard tap water at a pH of 10.5.

Blokhra (1994) applied a strong magnetic field perpendicular to the direction of flow across a cellulose acetate membrane. The result was an increase in repulsive forces between structural elements of the membrane, which were balanced by their mechanical strength. A South African company [Cooray, 1998] recently applied magnetic fields to membrane processes and they seem to be very successful.

Electric fields

In the crossflow filtration processes the bulk flow is tangential to the membrane, which causes solutes or particles to be transported laterally towards the membrane. The convective flow of the solutes or particles can be counterbalanced to a greater or lesser extent by giving an electrophoretic velocity to the particles through the application of a D.C. electric field gradient. The contribution of fine particles and colloids to membrane fouling can be reduced by this means, thereby enhancing the filtrate flux [Wakeman and Tarleton, 1987; Huotari et al., 1999; Wakeman and Willianms, 2002].

Power consumption and other problems associated with continuously applied electric fields can be reduced by pulsing the electric field. The pulsing may be achieved by switching the applied potential on and off at regular (or irregular) intervals [Bowen et al., 1989; Wakeman and Sabri, 1995].

Membrane permeability to both charged and uncharged solutes has also been changed under the influence of an applied electric field. This behaviour, exhibited by 'deformable' membranes, has been attributed to electric field control of membrane pore size. Grodzinsky and Weiss [1985] favour the mechanism of 'electro-diffusion' in which the intra-membrane pH or ionic strength is modified. The result is an increase in repulsive forces between structural elements of the membrane, which are balanced by their mechanical strength.

Ultrasonic fields

Several articles [Hurvey, 1965; Wakeman and Tarleton, 1991; Schimichi, 1995; Li et al. 1995; Band, 1997; Kobayashi et al. 1999] deal with the application of ultrasound in water treatment. Hurvey [1965] used an acoustic liquid whistle or transducer to produce cavitation on membranes. It is believed that the formation of air bubbles during cavitation suppresses fouling. When a cavitating air bubble is oscillating near a solid surface, it generates micro-jets of very high velocities that can effectively decrease the boundary layer thickness. In effect, mass transfer is enhanced.

Lenart and Auslander [1980] studied the effect of ultrasound on the diffusion of some electrolytes – sodium, potassium and calcium chlorides – through cellophane

membranes. The intensity of the ultrasound field in their experiment varied from 1.2 to 6 Wcm^{-2} at 1 MHz frequency. The results obtained demonstrated intensification of the diffusion process by the ultrasound. The authors considered the main cause of acceleration of diffusion with ultrasound to be the appearance of acoustic microcurrents on the liquid. Radiation pressure, gravitation, cavitation and acoustic pressure also play a role.

Schimichi [1995] proposed the application of ultrasound in a purification process where water was passed through an ion-exchange resin bed.

Li et al [1995] describe the results of investigations of the influence of ultrasound on the diffusion of electrolytes through a cellophane membrane. It was found that the diffusion velocity of electrolyte through the membrane with ultrasound irradiation is higher than that without ultrasonic and the amount of solvent permeated increases with acoustic pressure.

Band [1997] studied the influence of specially mounted ultrasound signals on water desalination through special polymeric ion-exchange hollow fibres. Both Na^+ and H^+ ion exchange were enhanced under ultrasound.

Wakeman and Tarleton [1987] reported that the filtrate flux could be markedly increased by the simultaneous addition of electric and ultrasound fields. Kobayashi et al. [1999] used on-line ultrasound to enhance permeation in UF. Ultrasound effects at frequencies of 28, 45 and 100 kHz and at a power intensity in the range of 2.5-3.3 W/cm^2 on a permeate flux of dextran solution through polyacrylonitrile UF membranes were examined. Although ultrasound with a low frequency (28 kHz) and a high intensity (3.3 W/cm^2) was beneficial to permeation through the membrane, ultrasonic waves have to be used with care, as the polymeric material itself is sensitive to the ultrasonic waves at the chosen frequency and intensity [Masselin et al., 2001].

2.3.5.5 Membrane Cleaning

Although all the above methods reduce fouling to some extent, cleaning methods will always be required in practice. Cleaning is the removal of foreign material from the surface and body of a membrane. Cleaning methods include chemical and biological cleaning, and physical cleaning.

Chemical and biological cleaning

Chemical and biological cleaning involves the introduction of a chemical or biological solution that is capable of dissolving or removing the fouling layer from a membrane. Chemical and biological cleaning are two of the most important methods by which to reduce fouling. Some important chemicals used are [Trägrädh, 1989; Mulder, 1996]:

- Acids (alkyl sulfates, alkyl sulfonates, quaternary ammonium compounds et al.) for improving wet-ability and rinse-ability of the fouling layer
- Alkalis (hydroxides, carbonates, phosphates etc.) for removing fats and proteins
- Enzymes for removing bio-fouling (micro-organisms)
- Sequestering agents (EDTA) and disinfectants (sodium bisulfite, hydrogen peroxide, hypochloride etc.)

Harding et al. [1978] developed a chemical descaling technique, using an EDTA solution, to remove calcium sulfate in desalination plants. The EDTA solution was found to remove the scales almost completely.

Buckley et al. [1983] reported on a number of cleaning techniques that were employed to remove polyvinyl alcohol fouling from spiral-wound UF modules during the treatment of textile effluent. Sodium peroxide and cold water rinses were the two most effective cleaning strategies. Jaffer [1994] also reported the application of a chemical treatment method to mitigate scaling and fouling in RO.

Kim et al. [1993] investigated the relationship between membrane fouling and cleaning in terms of flow conditions, transmembrane pressures, pH, membrane (UF) properties and cleaning agents (hydrochloric acid, sodium hydroxide, sodium dodecyl sulfate and cetyl-tri-methyl-ammonium bromide) using a stirred batch cell and

aqueous albumin solution. Cleaning efficiency was affected by protein charge during UF, the nature of the fouled layer and electrostatic interactions between this layer and the cleaner. It appears important to select cleaning agents with due consideration to solute properties.

Maartens et al. [1996] applied an enzymatic approach to the cleaning of UF membranes fouled with abattoir effluent. The enzymes and enzyme detergent mixtures were effective cleaning agents and the pure-water flux of statically fouled membranes could be restored by treatment with these agents.

Physical cleaning

The physical removal of a fouling layer utilizes hydraulic cleaning and mechanical cleaning. Hydraulic cleaning methods include backflushing, backshock treatment, alternate pressurising and depressurising and by reversing the flow direction at a given frequency [Potts et al., 1981; Strathmann, 1981; Leger and Hawker, 1987; Redkar and Davis, 1995; Pontie et al., 1997; Kennedy et al., 1998]. Mechanical cleaning includes sponge-ball cleaning in tubular membranes [Burch, 2001], electrically-induced vibrations [Bowen et al., 1989], and ultrasonically-induced vibrations [Wakeman and Tarleton, 1991; Ebrahim, 1994; Chai et al., 1999; Czekaj et al., 2000].

Kost and Langer's patent [1988] proposes a method for enhancing or controlling the permeability of small and large molecular weight molecules in a membrane system which is exposed to ultrasound of selected intensity of 0.05 to 30 Wcm^{-2} and frequency between 10 kHz and 20 MHz for most polymeric membranes and an intensity of 0.05-3 Wcm^{-2} and a frequency of 1-3 MHz for biological membranes.

Leger and Hawker [1987] investigated turbulent flushing, flow reversal, sponge-ball cleaning, and alkali cleaning for the removal of complex fouling layers containing organics, colloid clays, quartz, and iron and zinc compounds. Their results suggested that a combination of the tested techniques was necessary to completely clean the RO membranes.

Bowen et al. [1989] developed the electrically enhanced cleaning of yeast and titanium dioxide fouling layers in crossflow MF. They observed that mild chemical

cleaning, when used in conjunction with a forced electrical current, significantly improved the cleaning efficiency. Ebrahim [1994] presented a comprehensive review of various cleaning strategies employed in RO desalination and wastewater applications. He cited ultrasonic cavitation as an effective physical cleaning method for RO and UF membranes.

Chai et al [1999] used an ultrasonic technique to clean polymeric UF and MF membranes fouled by peptone. Ultrasound generated by a sonicator bath was employed to examine the effect of ultrasound on the cleaning of fouled membranes in a crossflow cell under various filtration operating conditions. It is suggested that the cleaning of fouled membranes by ultrasound in association with water cleaning is an effective method.

Czekaj et al. [2000] used an infrasonic pulsing technique to remove foulant cake and improve flux through MF membranes. The technique consists of applying pressure pulses with frequencies on the order of 1-10 Hz on the permeate side. It is proposed that the infrasonic pulses cause rapid vibrations of the membrane, which lift a portion of the foulant cake off its surface.

Note: ultrasound with low frequencies (kHz) and high power outputs was used as a cleaning method [Mason and Lorimer, 1989]. Frequencies in the order of 20 - 100 kHz showed the best cleaning abilities. In contrast to this, the visualisation technique needs good spatial resolution, and thus a shorter wavelength is required. Ultrasound with higher frequencies (> 1 MHz) is therefore needed. At this high frequency it has no cleaning ability (ultrasound of frequency 5 – 7.5 MHz is used for visualisation in the human body) and is therefore suitable to study membrane fouling.

2.3.6 OVERVIEW OF FOULING LITERATURE

Numerous fouling studies have been carried out worldwide to better understand the complexity of fouling. The efforts to develop means of fouling mitigation have been only partially successful. Fouling remains problematic in most membrane processes because of an incomplete understanding of the dynamics of fouling and its relationship to membrane performance decline.

Although membrane autopsy or destructive analytical methods can supply some information on the fouling mechanism [Butt et al, 1995; Dudley and Darton, 1996; van Hoof et al., 2002], they have provided little information regarding the actual and dynamic build-up of foulant on a membrane surface. Furthermore, an autopsy is a destructive procedure and the membrane cannot be returned to service once it is completed.

A number of non-invasive observations using microelectrode measurements, laser interferometry and light reflectometry have been applied to the measurement of CP [Hendricks and Williams, 1971; Mahlab et al., 1978; Ethier and Lin, 1992]. Although these measurements were limited by the spatial resolution of the various techniques very close to the membrane surface, they have provided significant insights into CP development in membrane systems.

Over the last ten years, other non-invasive techniques such as radioisotope, micro-array of semiconductor photosets, optical methods and photography have been developed to study CP and fouling on a membrane surface in real time [McDonogh et al., 1990 and 1995; Mores and Davis, 2001; Lu et al., 2002; Macklay and Shereman, 1992; Wakeman, 1994 et al.]. Although these studies have provided valuable information on polarization profiles and fouling layer, these measurements are limited, as shown in Table 2.4.

Table 2.4: Various non-invasive fouling measurement techniques

Methods	Measuring	Limits
Radio isotope & micro-array of semiconductor photoset [McDonogh, 1990 & 1995]	Layer build up; Concentration polarization	The small range of flow conditions and no information closer (<20 μm) to the membrane
15× video camera [Macklay and Shereman, 1992]	The growth of cake and the particle motions	Particles used are larger than those of MF
High-speed camera [Wakeman, 1994]	Development of the cake layer and its thickness	Particle deposition and interaction
Laser technique [Madsen, 1988; Altmann, 1997]	The cake layer height; Particle deposition	Steady state, no agreement with flux
DOTM by microscope and video camera [Li and Fane, 1998]	Interaction between particles and membrane	Further development of cake and fouling layers
Scintillation proximity assay and EPR spectroscopy [Diaz, 1992; Oppenheim, 1994]	Transient development of fouling and protein-membrane interaction	Requires radioactive or spin-labeling of the foulants
NMR micro- imaging technique [Yao and Fane, 1995; Bond, 1995]	Flow profiles and polarization layers	Too expensive and impractical
Ultrasonic technique [Mairal et al., 1999 and 2000; Koen, 2000]	Membrane compaction and fouling	Still being assessed

The scintillation proximity assay and EPR spectroscopy require radioactive or spin labelling of the foulants which is impractical in most fouling situations [Diaz et al., 1992; Oppenheim et al., 1994]. The streaming potential analysis method developed for protein fouling is of limited use in those membrane-fouling situations where the surface properties do not play a major role [Nystrom et al., 1994].

The laser reflectometry technique [Altmann and Ripperger, 1997] that allows installation of an optical window is useful for those systems. However, the ability to monitor the growth of a fouling layer that does not provide significant optical contrast makes such measurements very difficult.

NMR micro-imaging [Yao et al., 1995; Bond et al., 1995] is a sophisticated technique that can be used for visualizing the development of CP as well as the growth of fouling layer. However, the cost and size of the equipment make it impractical for industrial applications.

A non-invasive ultrasonic technique is a relatively inexpensive and versatile technique. It can successfully measure the membrane compaction, and growth of fouling layers. Additionally, it can be extended to visualize the fouling layer in real time under realistic operating conditions [Peterson et al. 1998; Mairal et al. 1999 and 2000; Koen, 2000].

In the light of this review, it is clear that membrane fouling continues to be a significant problem in membrane-based liquid separations. The development and utilization of a suitable non-invasive technique for the on-line monitoring of fouling in industrial and laboratory applications would enable the effectiveness of fouling remediation and cleaning strategies to be more quantified. Ultrasonic testing appears to be most useful for the on-line monitoring of fouling under realistic operating conditions (see Table 2.4). The focus of the present study is the development and application of this ultrasonic technique to provide quantitative information regarding deposition and growth of a fouling layer on a membrane surface in real-time. The following section discusses topics relevant to the further development of this technique.

2.4 ULTRASONIC TECHNIQUES

2.4.1 SOUND RANGES

Acoustics, the science of sound, describes the phenomenon of mechanical vibrations and their propagation in solid, liquid or gaseous materials. The sound is audible if it reaches the ear either through the air or through the body. The range of human hearing is from about 16 Hz to 16 kHz [hertz = cycles per second (c/s)] (with middle at 261 Hz and the meadow grasshopper at around 7 kHz), as shown Figure 2.4 [Mason and Lorimer, 1989]. Sound below 10 Hz and above 16,000 to 20,000 Hz is inaudible to the human ear. The sound waves below 10 Hz are called subsonics [Krautkrämer et al., 1969]. The sound waves above 20,000 Hz (20 kHz) are referred to as ultrasound or ultrasonics. The upper limit of ultrasonic frequency is not defined, but is usually taken to be 5 MHz for gases and 500 MHz for liquids and solids. Completely different demarcations apply in the case of their generating and detecting methods.

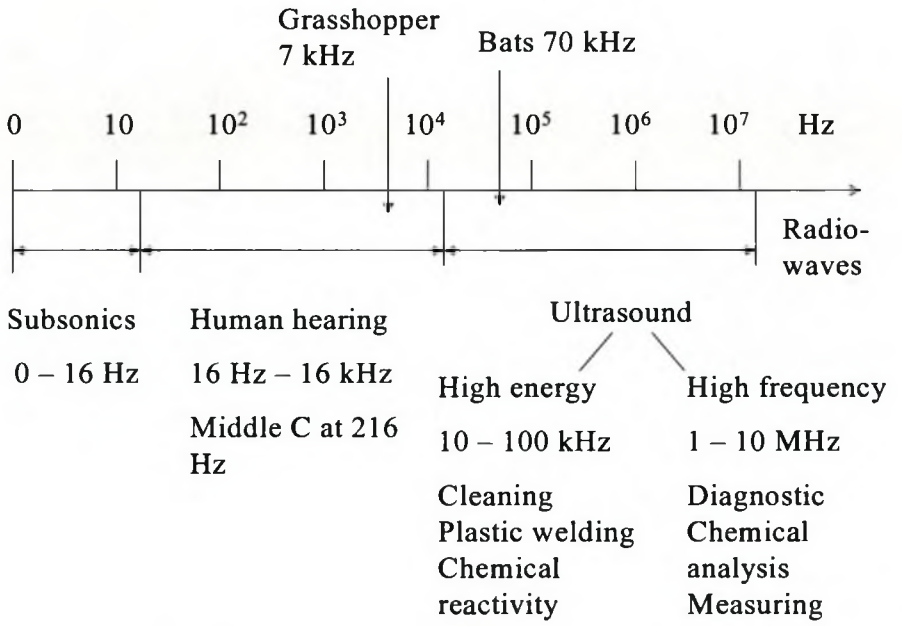

Figure 2.4: Sound frequencies (c/s) [Mason and Lorimer, 1989].

The uses of ultrasound within a large frequency range may be divided broadly into two areas. The first area involves high frequency (low amplitude), which is concerned with the effect of the medium on the wave, is commonly referred to as low power or high frequency ultrasound. Typically, high frequency waves are used to measure the velocity and absorption coefficient of the wave in a medium in the 2 to 10 MHz range. The high frequency waves are used in medical scanning, chemical analysis, testing materials for flaws and the study of relaxation phenomena. The second area involves high energy (low frequency) waves between 20 and 100 kHz, known as power ultrasound, which is used for cleaning, plastic welding and, more recently, to effect chemical reactivity [Mason and Lorimer, 1989].

2.4.2 ULTRASONICS

The whole study of ultrasonics is primarily concerned with the generation, transmission and reception of energy in the form of longitudinal waves in matter.

2.4.2.1 Generation of Ultrasonic Waves

The basis for the present-day generation of ultrasound was established as bar back as 1880 with the discovery of the piezoelectric effect and its inverse by the Curies [Cracknell, 1980]. Most modern ultrasonic devices rely on transducers, which use the inverse effect, i.e. the production of a change in dimension of certain materials by the application of an electrical potential across opposite faces. If the potential is alternated at high frequencies, the crystal converts the electrical energy to mechanical (sound) energy – rather like a loudspeaker.

Recently significant developments have been made in electronic circuitry and transducer design i.e. devices that convert electrical to mechanical signals and vice versa. The quartz crystal has the property of expanding and sending out an ultrasonic wave when a voltage, generated by a pulser-receiver, is applied to it. It can also produce an electrical signal when it is mechanically vibrated. The transducer sends out this high frequency signal into the medium that needs to be investigated.

2.4.2.2 Propagation of Ultrasonic Waves

Ultrasonic testing of materials makes use of mechanical waves, whereas, for instance, X-ray techniques use electromagnetic waves. Any mechanical wave is composed of oscillations of discrete particles of material. Any material that has elasticity can propagate ultrasonic waves. The propagation takes the form of a displacement of successive elements of the medium. If the substance is elastic, there is a restoring force that tends to bring each element of the material back to its original position. Since all such media also possess inertia, the particle continues to move after it returns to the position from which it started and finally reaches another different position, past the original one. From this second point it returns to its starting position, about which it continues to oscillate with constantly diminishing amplitude.

As the wave travels through the material, successive elements in the material experience these displacements, each such element in the wave path moving a little later than its neighbour. In other words, the phase of the wave or vibration changes along the path of wave transmission. This displacement can be plotted, and the graph is descriptive of the wave.

2.4.2.3 Types of Waves

An ultrasonic wave being transmitted through a medium may be of several types. Each type causes a specific movement in the elements of the medium and the paths that these elements follow as they move in response to the wave are called their orbits. These orbits may be essentially parallel to the line of propagation, in which case the wave is *longitudinal.* On the other hand, they may be executed normal to the direction of propagation. Such waves are called *transverse* or *shear.*

Longitudinal waves

Longitudinal waves exist when the motion of particles in a medium is parallel to the direction of wave propagation. This kind of wave, also called the L wave, will travel in liquids, solids and some gases, and is easily generated and detected. L waves have a high velocity of travel in most media, and the wavelengths in some materials are usually very short in comparison with the cross-sectional area of the transducer.

Shear waves

When shear waves, also called S waves, are used, the movement of the particles in the medium is at right angles to the direction of wave propagation. If the wave movement is in the x-direction, the particle displacement is in the y-direction. These waves may also exist in a limited area of, or entirely throughout, a body. Usually, due to this lower velocity, the wavelength of shear waves is much shorter that that of L waves.

Surface or Rayleigh Waves

These waves can be propagated over the surface of a part without penetrating below that surface to any extent. These waves are roughly analogous to water waves, which travel over a body of water. Their velocity depends upon the material itself and is about nine-tenths of S-wave velocity. The wavelength of a surface wave is always extremely short. Surface waves consist of both L and S types of particle motion. These types of waves can be used for exploration of materials for defects, for measuring thickness by resonance, or for measuring other characteristics of the material through which the wave travels.

2.4.2.4 Reflection and Transmission

The ultrasonic signal is reflected by a change in acoustic impedance, which happens when the ultrasonic signal reaches a layer with different acoustic impedance than the medium it is travelling through. When this happens, part of the energy travels forward as one wave through the second medium, while the rest of the signal is reflected back into the first medium, usually with a phase change. These reflections can be seen on an oscilloscope and be interpreted. Consider such an example where a plane acoustic wave is transmitted from one medium to another as in Figure 2.5 [Ford, 1970]. Assume a plane wave in material I travelling in the positive x direction at right angles to the plane of the boundary, the material acoustic impedance W can be described as:

$$W = V_p \rho \tag{2.13}$$

where V_p is the sound velocity (m/s); ρ is the material density (kg/m^3).

The incident waves can be represented by

$$P_i = A_1 e^{j(\omega t - k_1 x)} \tag{2.14}$$

where P_i = sound pressure of incident waves

$\omega = 2\pi f$ (with f – frequency in rad/s)

t = time (s)

k = wavelength constants

x = distance (m)

A_1 = constant

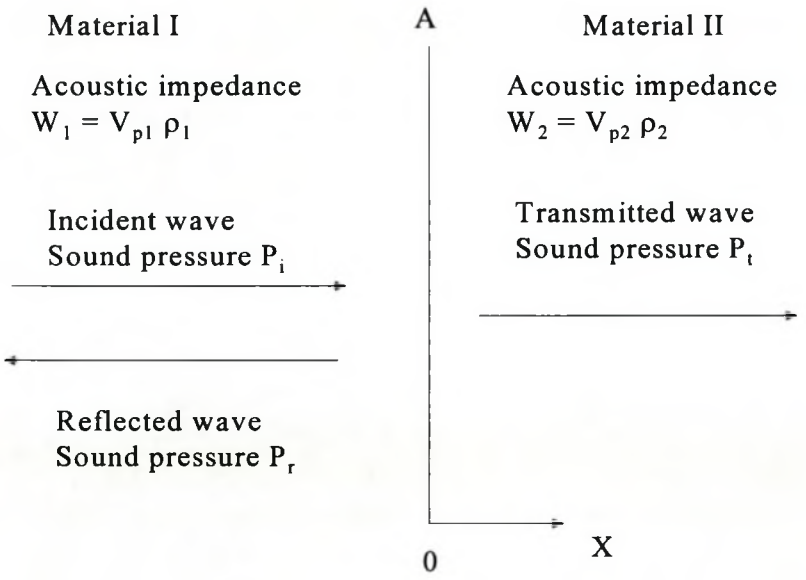

Figure 2.5: Reflection and transmission of plane waves at a boundary [Krautkrämer, 1969].

Upon striking the plane of the boundary between the two materials at x = 0, reflected waves are produced [Ford, 1970]

$$P_r = B_1 e^{j(\omega t - k_1 x)} \tag{2.15}$$

and transmitted waves are produced

$$P_t = A_2 e^{j(\omega t - k_2 x)} \tag{2.16}$$

A_1, B_1 and A_2 are complex in order to allow for phase differences between the three waves. The transmitted waves always have the same frequency as the incident wave, but as a result of the difference between the velocities V_{p1} and V_{p2} in the two materials, the values of the wavelength constants, $k_1 = \omega/V_{p1}$ in medium I, and $k_2 = \omega/V_{p2}$ in medium II, are different.

There are two boundary conditions that must be satisfied at all times and at all points on the plane surface separating the two media [Ford, 1970]:

1. The acoustic pressures on the two sides of the boundary are equal, and
2. The particle velocities normal to the interface are equal.

The first condition of continuity of pressure results from the fundamental law that pressure in a fluid is a continuous, single-value, scalar function, and the second condition is equivalent to the requirement that the two media remain in constant contact at the boundary. Since pressure is a scalar quantity, the pressure at a point in medium I is given by $P_i + P_r$. By setting this expression equal to P_t at the boundary, one obtains

$$A_1 e^{j(\omega t - k_1 x)} + B_1 e^{j(\omega t - k_1 x)} = A_2 e^{j(\omega t - k_2 x)} \tag{2.17}$$

so that

$$A_1 + B_1 = A_2 \tag{2.18}$$

If we consider each of the three waves separately, we can divide the pressure by the appropriate acoustic impedance to the particle velocities u_i (in the incident wave), u_r (in the reflected wave) and u_t (in transmitted wave), which can be represented by

$$u_i = \frac{P_i}{\rho_1 V_1} \tag{2.19}$$

$$u_r = -\frac{P_r}{\rho_1 V_1} \tag{2.20}$$

$$u_t = \frac{P_r}{\rho_2 V_2} \tag{2.21}$$

The velocity of a particle in medium I is $u_i + u_r$, which makes the second boundary condition

$$u_i + u_r = u_t \tag{2.22}$$

Substituting Equations 2.19-21 into Equation 2.22 gives

$$\frac{P_i}{\rho_1 V_1} - \frac{P_r}{\rho_1 V_1} = \frac{P_t}{\rho_2 V_2} \tag{2.23}$$

By introducing the respective expressions for the pressure at x=0, this equation can be reduced to

$$\rho_2 c_2 (A_1 - B_1) = \rho_1 c_1 \tag{2.24}$$

Further, Equation 2.17 and Equation 2.23 can be combined to eliminate A_2, which gives

$$B_1 = A_1 \frac{\rho_2 V_2 - \rho_1 V_1}{\rho_2 V_2 + \rho_1 V_1} \tag{2.25}$$

The amplitude of the reflected wave (C_r) is thus related to the incident one as [Ford, 1970]

$$C_r = \frac{B_1}{A_1} = \frac{\rho_2 V_2 - \rho_1 V_1}{\rho_2 V_2 + \rho_1 V_1} = \frac{W_2 - W_1}{W_2 + W_1} \tag{2.26}$$

Or B_1 may be eliminated to give the amplitude of the transmitted wave (C_t) related to the incident wave as

$$C_t = \frac{A_2}{A_1} = \frac{2\rho_2 V_2}{\rho_2 V_2 + \rho_1 V_1} = \frac{2W_2}{W_2 + W_1} \tag{2.27}$$

C_r and C_t are also called the coefficients of reflection and transmission, respectively, of the sound pressure (both are dimensionless numerical values). As an example, C_r

and C_t on the interface steel/water can be calculated as showed in Figure 2.6. Acoustic impedances of steel and water for longitudinal waves are [Krautkrämer, 1969]

$$W_1 \text{ (steel)} = 45 \times 10^6 \text{ kg/m}^2\text{s} \quad \text{and} \quad W_2 \text{ (water)} = 1.5 \times 10^6 \text{ kg/m}^2\text{s}$$

thus

$$C_{r1} = \frac{1.5-45}{1.5+45} = -0.935 \quad \text{and} \quad C_{t1} = \frac{2\times1.5}{1.5+45} = 0.065$$

Expressed as percentages, the reflected wave has – 93.5 % of the sound pressure of the incident wave and the transmitted wave 6.5 %. The negative sign indicates the reversal of the phase relative to the incident wave, that is, the incident wave passes from a material of higher velocity into a low-velocity layer [Krautkrämer, 1969].

If, in the reverse case, the wave coming from water strikes steel, an exchange of W_1 and W_2 furnishes

$$Cr_2 = +0.935 \quad \text{and} \quad C_{t2} = 1.935.$$

Since Cr_2 is positive, the incident and reflected waves are in phase. The transmitted wave has 193.5 % of the sound pressure (see Figure 2.7).

Note: At first glance a sound pressure exceeding 100% seems paradoxical and one suspects a contradiction of the energy law. However, according to Equation 2.28 the intensity is not calculated from the sound pressure only but also from the acoustic impedance of the material in which the wave travels. However, since this resistance in steel is very much greater than in water, the calculate shows that the intensity of the transmitted wave is very much smaller there than in water in spite of the higher sound pressure.

$$I = \frac{1}{2}\frac{P^2}{W} \text{ [W/m}^2\text{]} \qquad (2.28)$$

In the case of an air - solid boundary, practically 100 per cent of the energy is reflected. It should be remembered that in a reflection system, the energy passes through an interface twice, once going and once returning. All above calculations are entirely independent of attenuation and scattering. The amount of energy actually

reflected may differ vastly from that calculated theoretically. Energy may be dissipated at a boundary or in a material in several ways. The formulae above refer only to an absolutely perfect boundary between two infinite media. If there is any discontinuity, no matter how minute, these relationships no longer apply. It is accordingly difficult to obtain actual values of reflected energy except by experiment [Krautkrämer, 1969].

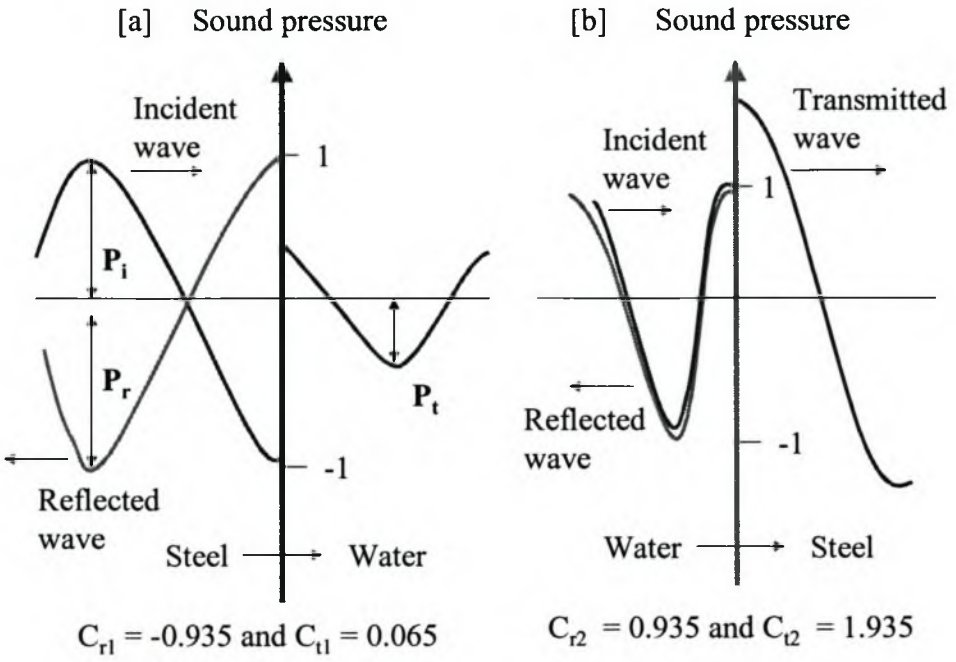

Figure 2.6: Sound wave values in the case of reflection on the interface steel/water , incident wave in steel (a) or in water (b) [Krautkrämer, 1969].

2.4.2.5 Power Ultrasound in Membrane Processes

Ultrasound with low frequencies (20 - 100 kHz) has high power outputs and shows the best cleaning abilities. Ultrasonic cleaning basically consists of immersing the article to be cleaned in a suitable solvent, which is then ultrasonically irradiated as follows. High-frequency electrical oscillations produced by an electronic generator are fed to a transducer, which converts them to mechanical vibrations. By suitably coupling the transducer to the cleaning solvent (or medium/water), the ultrasonic vibrations thus

produced are propagated in the solvent (or water). Provided the energy and frequency of the ultrasonic waves are suitable, their propagation through the liquid initiates cavitaion. Shock waves produced during cavitation impinge on any solid surfaces present in the liquid and very effectively scour the surface. The effect is similar to mechanical scrubbing but acts much more efficiently, rapidly penetrating to every hole and corner of an assembly immersed in the liquid.

The range of useful frequencies is from about 13 kHz to about 1 MHz and the type of transducer used varies with the frequency. The production of low-frequency (power) ultrasonic waves for cleaning purposes is accomplished by the use of various types of magneto-strictive and piezoelectric transducers made of quartz or barium titanate. The electronic generator is normally fairly simple in design supplying electrical oscillations at a fixed frequency and power output.

Power ultrasound has been widely used as a method for cleaning materials [Mason and Lorimer, 1989; Price, 1992]. Furthermore, this power ultrasound can enhance permeate flux and clean membranes in membrane processes [Hurvey, 1965; Lenart and Auslander 1980; Wakeman and Tarleton, 1991; Ebrahim, 1994; Shimichi ,1995; Chai et al., 1999].

2.4.3 SOME APPLICATIONS OF ULTRASOUND

Ultrasonic echo ranging (the basis of the pulse-echo technique) is used by bats for locating obstacles and prey. The first commercial application of ultrasound did not appear until 1917, with Langevin's echo-sounding technique for the estimation of depths of water. Langevin's discovery was the direct result of an idea, which arose as a suggestion generated by a competition organised in 1912 to find a method of detecting icebergs in the open sea and so avoid any repetition of the disaster which befell the Titanic [Mason and Lorimer, 1989].

The early 'echo sounder' simply sent a pulse of ultrasound from the keel of a boat to the bottom of the sea, from which it was reflected back to a detector also on the keel. For sound waves, since the distance travelled through a medium = ½ × time × velocity

(and the velocity of sound in seawater is accurately known) the distance to the bottom could be determined from the time taken for the signal to return to the boat. Later developments resulted in the system known as SONAR (Sound Navigation And Ranging), which allowed the surrounding sea to be scanned. The RADAR (Radio Detection And Ranging) system was developed 50 years ago. This method (the reflection of a short ultrasonic pulse) was used by Sokolov in 1929 for detecting the presence of defects in materials [Mason and Lorimer, 1989].

Essentially, all imaging, from medical ultrasound to non-destructive testing, relies upon the same pulse-echo type of approach, but with considerably refined electronic hardware. The refinements enable the equipment to not only detect reflections of the sound from the hard, metallic surface of a submarine in water, but also much more subtle changes in the media through which sound passes (e.g. those between different tissue structures in the body). These systems are known as A-scan (one-dimension ultrasonic scan), B-scan (two-dimension ultrasonic scan) and C-scan (three-dimension ultrasonic scan). It is possible to detect much smaller areas of phase by using high-frequency ultrasound (in the range 2 to 10 MHz) with much shorter wavelengths.

It is only since 1945, with the increased understanding of the phenomenon of cavitations, together with significant developments in the fields of electronic circuitry and transducer design, that rapid expansion in the application of power ultrasound to chemical processes (Sonochemistry) has taken place [Mason and Lorimer, 1989; Price, 1992]. Power ultrasound affects chemical reactivity through cavitation. The ultrasonic technique has since been utilized in a wide range of applications in industry, military and medicine [Frederick, 1965; Lynnworth, 1989; Mason and Lorimer, 1989]. Some of these have been in existence for many years and a range of such are shown in Table 2.5 [Mason and Lorimer, 1989].

Table 2.5: Some industrial uses of ultrasound [Mason and Lorimer, 1989]

Field	Application
Biology, biochemistry	Homogenisation and cell disruption: Power ultrasound is used to rupture cell walls in order to release contents for further studies.
Engineering	Ultrasound has been used in drilling, grinding and cutting. It is particularly useful for processing hard, brittle materials, e.g. glass, ceramics. Other uses of power ultrasound are welding (both plastics and metals) and metal tube drawing. High-frequency (MHz) ultrasound is used in the non-destructive testing of materials and flaw detection.
Dentistry	For both the cleaning and drilling of teeth
Geography, geology	Pulse/echo techniques are used in the location of mineral and oil deposits and in depth gauges for seas and oceans. Echo ranging at sea has been used for many years (SONAR).
Industrial	Pigments and solids can be easily dispersed in paints, inks and resins. Engineering articles are often cleaned and degreased by immersion in ultrasonic baths.
Medicine	Ultrasound imaging (2-10 MHz) is used, particularly in obstetrics, for observing the foetus and for guiding subcutaneous surgical implements. In physiotherapy, lower frequencies (20-50 kHz) are used in the treatment of muscle strains.
Plastics and polymers	The welding of thermoplastics is effectively achieved using power ultrasound, The initiation of polymerisation and polymer degradation is also affected. Cure rates of resins and their composition can be measured with high-frequency ultrasound. Recently the mechanical rheological parameters of polymers can be determined [Alig, 1997 and 1998].

CHAPTER 3

EXPERIMENTAL

3.1 SCOPE OF THIS CHAPTER

This chapter covers five sections. The various design considerations for the experimental development of the UTDR technique are discussed in Section 3.2. These considerations provide the rationale for choosing an appropriate membrane separation system. Section 3.3 presents the measurement principle of UTDR as it applies to the membrane separation system utilized in this work. An integrated experimental system is provided in the following chapters. The test cells that allow for simultaneous monitoring and separation were designed and employed in this study. The details of the test cells are presented in Section 3.5. An ultrasonic measurement system including all the hardware i.e. pulser-receiver, oscilloscope, transducers etc. was designed and implemented to monitor membrane compaction and fouling. These components are briefly discussed in Section 3.6.

3.2 DESIGN CONSIDERATION

The main objectives of this study were to develop UTDR for real-time measurement of fouling and subsequently provide a process parameter – fouling index meter to quantify fouling in actual membrane separation operations. In developing an experimental methodology for achieving these goals, important design considerations regarding the selection and development of a suitable membrane separation system and the ultrasonic measurement system had to be addressed.

The selection of an appropriate membrane separation system involves the choice of a separation process, a feed solution containing one or more potential foulants, a membrane, a separation module, and an associated flow system. The design of the ultrasonic measurement system involves selection of appropriate hardware including ultrasonic transducers, a pulser-receiver, and an oscilloscope, as well as the

development of suitable software for the generation and post-processing of the ultrasonic signals.

The separation process should be industrially relevant and should be significantly affected by fouling during operation. The feed solution is also predicated by the commercial importance; in particular, the potential foulant chosen should occur frequently in industry. The membrane chosen to effect the separation must also be readily available and widely employed. The module should allow a safe and continous operation under existing process conditions. The associated flow system should ensure constant operating conditions and permit automated, and quantitative monitoring and control of systemic parameters.

The ultrasonic measurement system should provide sensitive and continuous measurements of fouling. The ultrasonic transducers should have a frequency that allows for sufficiently sensitive detection of the fouling layer while providing a strong signal response. The pulser-receiver employed to generate and receive signals should have a wide range of signal modification capabilities including signal gain, attenuation and filtering. The oscilloscope should have a digitizing capability for real-time processing and display of the ultrasonic signals as well as appropriate time-domain and amplitude-domain resolution, and sensitivity for accurate measurement of fouling layer growth.

3.3 PRINCIPLE OF ULTRASONIC MEASUREMENT OF FOULING

Ultrasonic measurements are based upon the propagation of mechanical waves. The velocity of the waves is dictated by the medium through which they travel. When an ultrasonic wave encounters an interface between two media, energy will generally be partitioned such that a reflected wave occurs. The energy partition is controlled by the ultrasonic impedance contrast (W_1/W_2), where $W = \rho V$ (ρ is the mass density of the medium and V is the velocity of sound wave in the medium), as shown in Equation 2.13. When the angle of the incident wave is zero, the coefficient of the reflected wave relative to the incident wave, C_r, is given by Equation 2.25.

Figure. 3.1 is a cross-sectional view of the typical flat-sheet cell that was used in our UTDR experiments. A membrane was placed between two polymethyl methacrylate (Perspex) plates. A transducer was externally mounted, in contact with the top plate. The feed solution flowed over the top of the membrane. The permeate was withdrawn from the bottom side. Now, suppose a fouling layer with thickness dS is present on the membrane surface and the reflected echoes A, B and C are generated from the various interfaces within the cell. The corresponding time-domain response is shown in Figure 3.2. The top plate/feed solution interface is represented by echo A and the initial feed solution/membrane interface by echo B. Note: The transducer produces one pulse each time. The pulse is reflected when it encounters an interface, then continuously goes through the following mediums and interfaces

Generally, once fouling is initiated on the membrane surface, the acoustic impedance difference and the topographical characteristics at the feed solution/membrane interface will change, resulting in a change in the amplitude of echo B, this is echo B'. Further, if the fouling layer is thick enough to be measured by an ultrasonic signal, i.e., it falls within the spatial resolution capabilities of the system, a new echo C will be formed as a consequence of the new feed/fouling interface. If the difference in arrival times, dt, between echoes B and C is measured, the thickness of the fouling layer, dS, can be determined from the following equation [Birks, 1991]:

$$dS = 0.5\ V\ dt \qquad (3.1)$$

where V is the velocity of the ultrasonic wave in the medium.

Thus, the detection of the interface echoes allows fouling to be monitored in real-time. Two basic quantities are measured in ultrasonic testing: the time of flight, or the amount of time taken for the sound to travel through the sample, and the amplitude of the received signal.

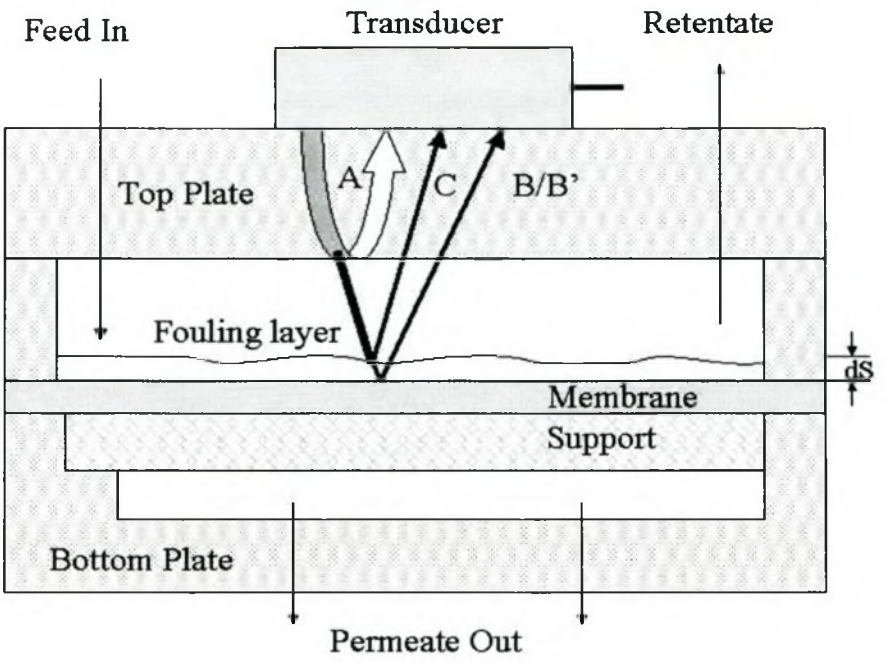

Figure 3.1: Schematic representation of the principle of UTDR measurement in a flat-sheet membrane module. Note: All the monitored incident and reflected acoustic waves (A, C, B/B') are all perpendicular to the transducer and the membrane surface. The cartoon uses the angle for clarity of explanation.

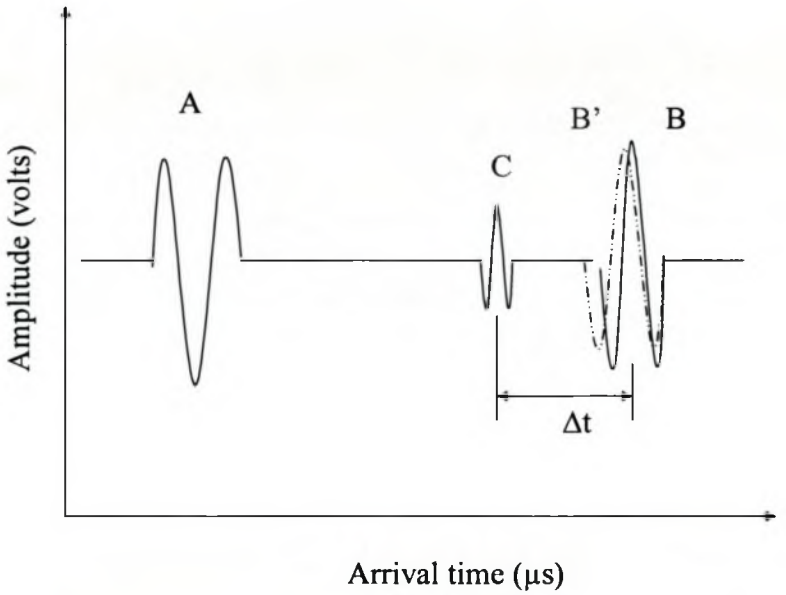

Figure 3.2: Corresponding time-domain response for the set-up in Fig.3.1.

3.4 EXPERIMENTAL SYSTEM

Different experiments were carried out with different foulants, membranes and flow systems (see Table 3.1), as will be described in the following Chapters 5 - 10.

Table 3.1: The use of UTDR in various types of membranes, foulants & modules

Foulant	Membrane	Test cell	Separation system	Chapter
Kaolin	Nylon	Flat-sheet	MF	5
Paper effluent	Nylon	Flat-sheet	MF	7
Paper effluent from MF products	PSU	Flat-sheet	UF	8
BSA	PESU	Tubular	UF	9

3.5 TEST CELLS

3.5.1 FLAT-SHEET CELL

The characteristic properties of the material selected for construction of the test cell are very important, as the ultrasonic signal must be able to penetrate the material. Figure 3.3 is a schematic representation of the test cell used in the MF and UF separation systems. The cell was made from polymethyl methacrylate (Perspex). All dimensions are shown in Figure 3.3.

The topside of the top part of the cell had a 90 mm × 45mm × 16mm flat recess. It was filled with a coupling agent, which connects the transducer with the cell. The membrane with a support-plate/spacer combination was positioned on the bottom plate (Figure 3.4) and the unit was sealed with a dual o-ring combination. The complete module assembly was clamped together with fourteen 6 mm-diameter bolts. A rectangular channel 100 mm × 20 mm × 2.5 mm formed the actual flow channel.

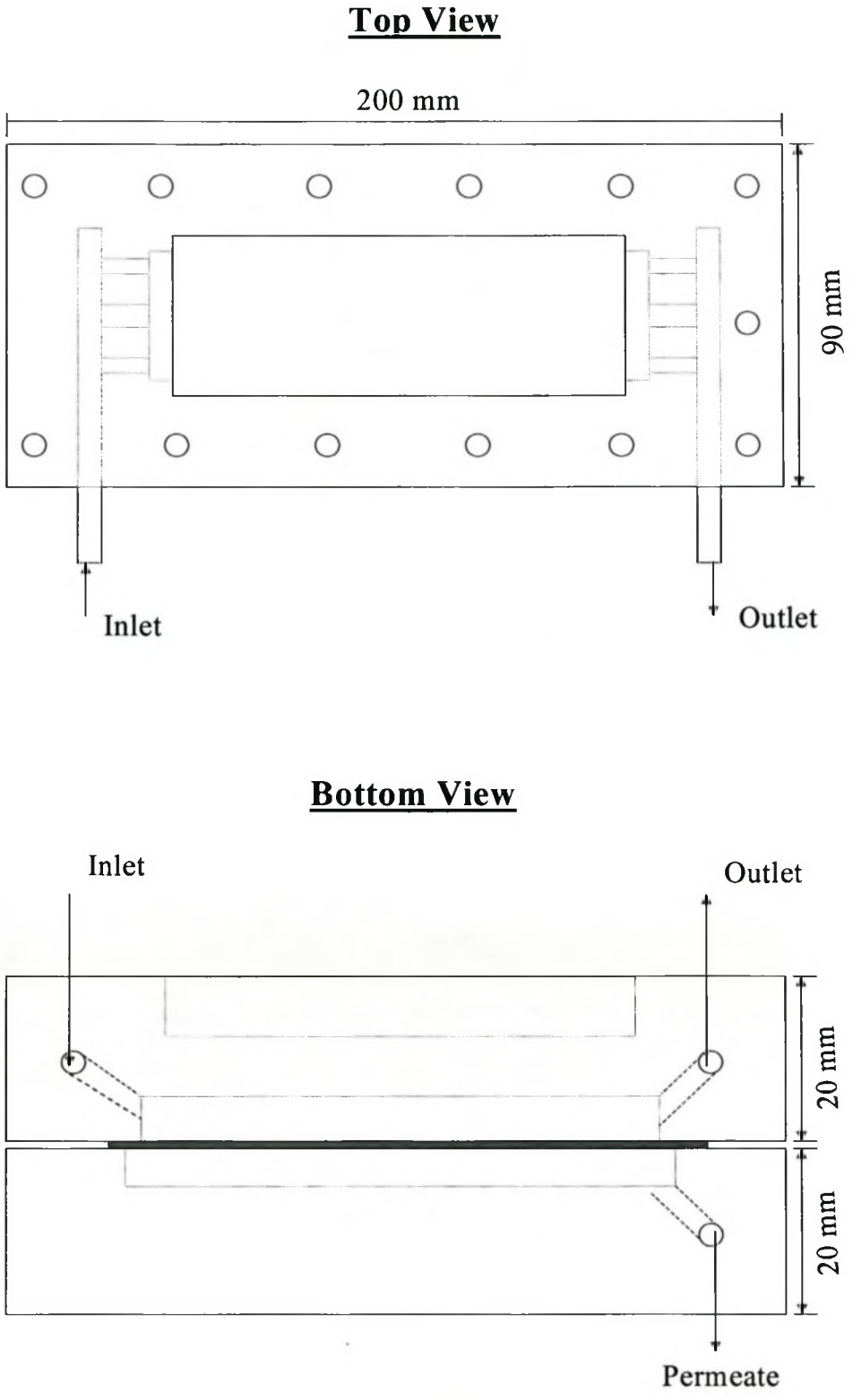

Figure 3.3: Drawings of flat test cell used in MF and UF separations.

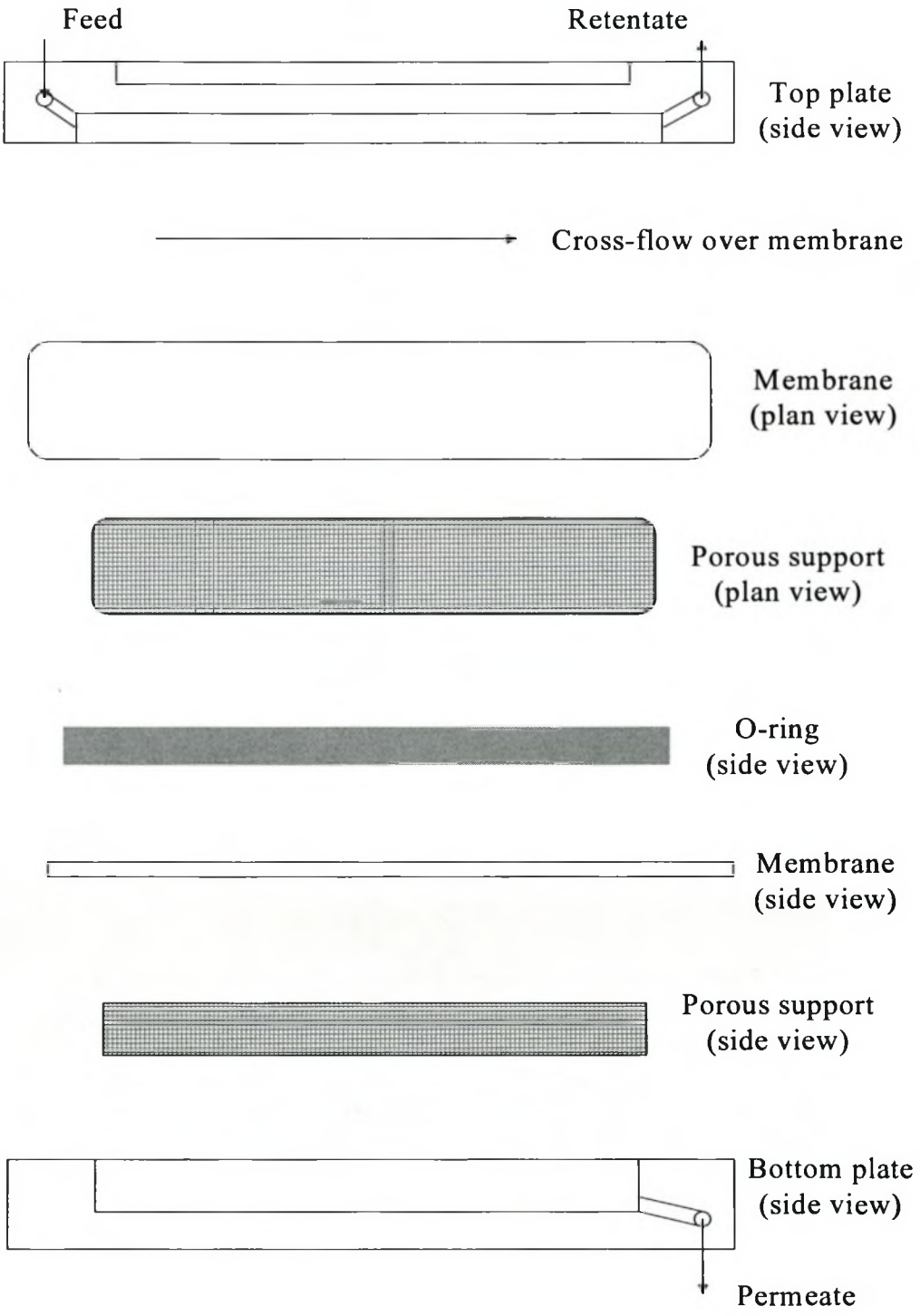

Figure 3.4: Placement of membrane in a flat-cell.

3.5.2 TUBULAR CELL

Figure 3.5 shows a drawing of the tubular test cell for UF. The shell was made of Perspex. The membrane, with a steel support was set up in the center of the cell. The dimensions of the membrane were Φ 14 × 180 mm. The unit was sealed with two O-rings at each side. Feed flows in the inside of the membrane. The permeate was drawn from the inside to the outside of the tubular membrane and entered the channel between the steel support and perspex shell.

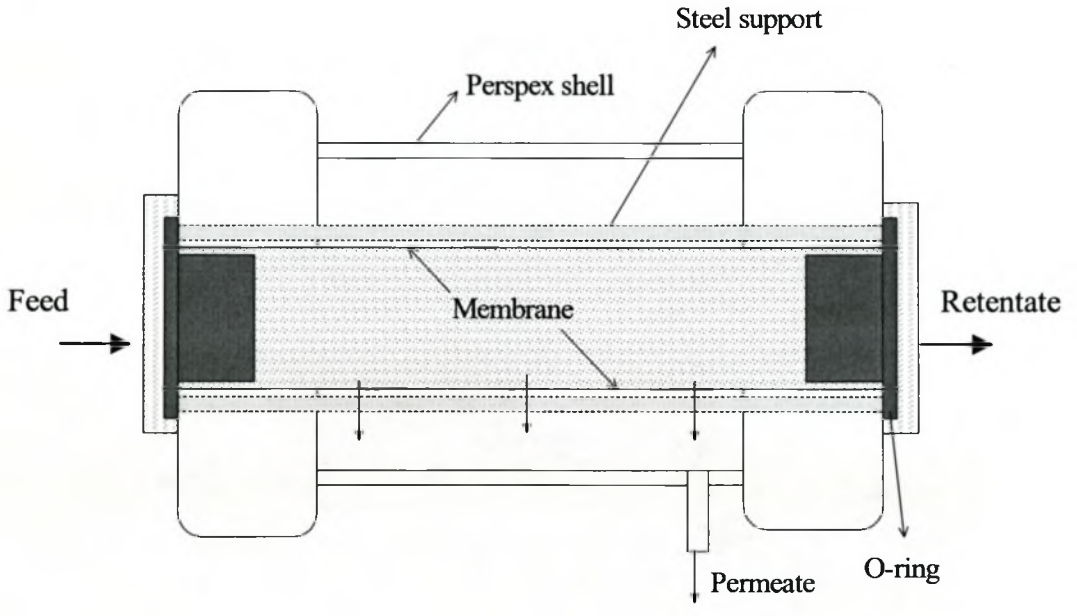

Figure 3.5: Drawings of tubular test cell used in UF.

3.6 ULTRASONIC TESTING SYSTEM

3.6.1 ULTRASONIC SET-UP

Figure 3.6 is a simplified drawing of all the hardware in a typical ultrasonic set-up. A pulser/receiver generates the voltage signal that triggers the transducer to send out an ultrasonic wave. The oscilloscope that is connected to the pulser/receiver captures and displays the data as amplitude changes on its front panel. These data can be stored on a computer's hard drive.

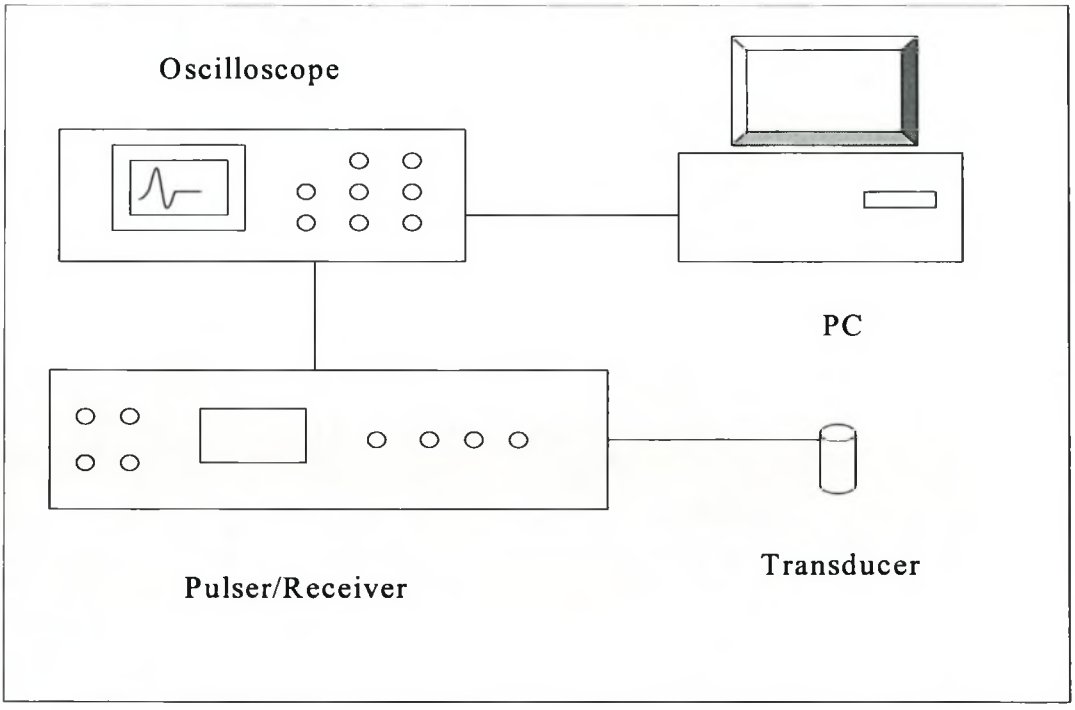

Figure 3.6: Ultrasonic set-up for UTDR pulse-echo operation.

3.6.2 PULSER/RECEIVER

A Panametrics Model 5058PR High Voltage Pulsar-Receiver was used. It was designed especially for ultrasonic testing and measurement applications that require a high material penetration capability. The pulser section of the Model 5058PR can deliver up to 900 volts in an impulse-type excitation pulse to appropriate low frequency transducers. The receiver section provides 60 dB RF gain, with an additional 30 dB available from an integral auxiliary preamplifier. A full range of front panel controls permits either discrete, calibrated settings or continuous adjustments for all important instrument functions. Pulse voltage is continuously adjustable by four values from 100 to 900 volts with a front panel meter displaying the available voltage to the transducer. Receiver gain is selectable as 40 or 60 dB, while receiver attenuation is adjustable from 0 to 80 dB in 1dB steps, with a ± 1 dB vernier for precise setting. The Model 5058PR includes an internal preamplifier that can be used to create an additional 30 dB gain. Echo pulses can be selected as either normal or inverted 180° for peak detection applications.

The 5058PR can be internally triggered at any of seven preamplifier radio-frequency (PRF) rates from 20 Hz to 2 kHz, or externally triggered at any frequency up to 2 kHz. Pulse damping is continuously adjustable over a range of 50 to 333 Ω, or in stepped values of 50, 100, 200, or 500 Ω. All transducer and radio-frequency (RF) output connectors are front-panel mounted for easy access.

FEATURES of Model 5058PR Pulser-Receiver

- High voltage pulsar, switched settings or continuously adjustable to 900 volts
- High gain, low noise broadband (10 MHz) receiver
- Pulse-echo and through transmission modes
- Additional 30dB gain available from integral auxiliary preamplifier
- ±1dB vernier for fine adjustment
- Switchable high pass and low pass filters
- PRF rate switch, selectable from 20 Hz to 2 kHz

- Compatible with Panametrics Step-less Gates, Gated Peak Detectors, and Gated Threshold Alarms

3.6.3 OSCILLOSCOPE

The choice of the correct oscilloscope is very important, as real-time signal changes are displayed on it. The oscilloscope should have a digitising capability for real-time processing and display of the ultrasonic signals as well as appropriate time-domain resolution and sensitivity for accurate measurement of fouling layer growth. A Hewlett Packard oscilloscope with the following characteristics was used.

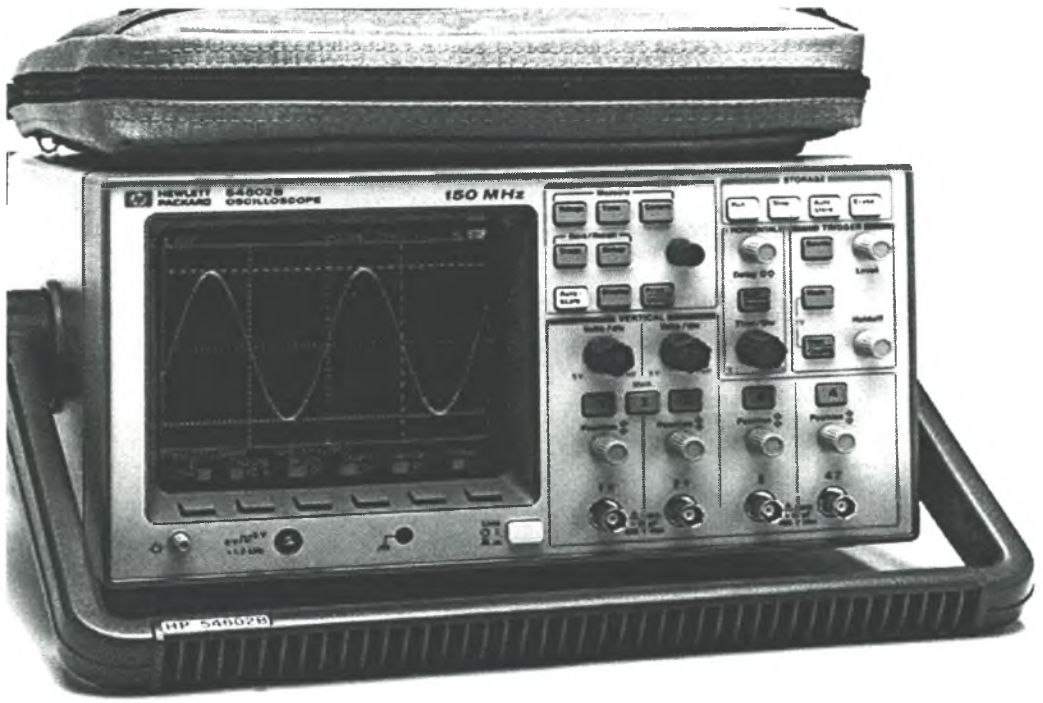

IP 54602B (2+2) Channel 150 MHz Oscilloscope

Figure 3.7: Hewlett Packard Oscilloscope Model 54602B

Hewlett Packard Oscilloscope Model 54602B

- 150 MHz bandwidth
- 2+2 Input channels
- Sweep speeds from 5 s/div to 2 ns/div
- Up to 1.5 million points per sec screen update rate
- I/O function
- 1 mV/div sensitivity

Figure 3.7 shows a schematic representation of Hewlett Packard Oscilloscope Model 54602B. Figure 3.8 shows the pulser/receiver – oscilloscope set-up for pulse-echo operation.

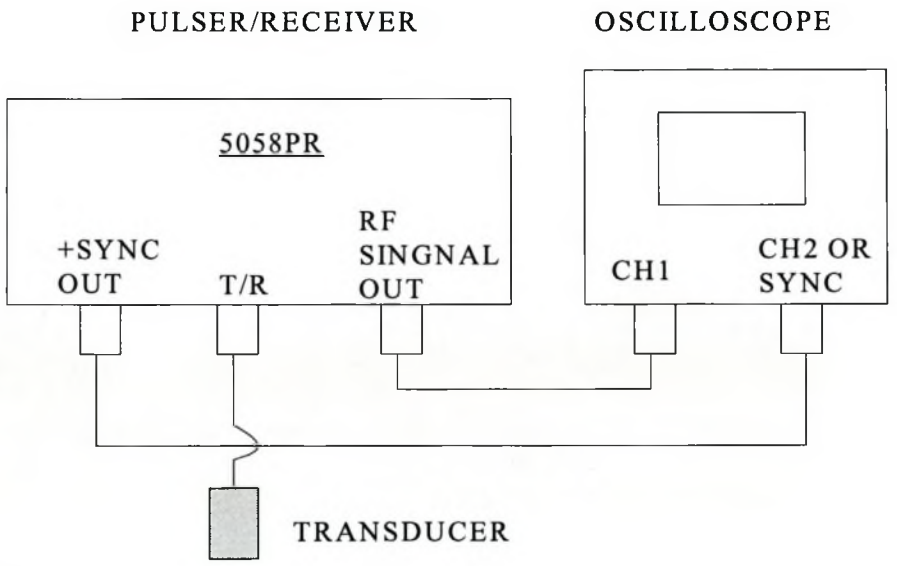

Figure 3.8: Pulser/Receiver – oscilloscope set-up for pulse-echo operation.

3.6.4 TRANSDUCER

The transducer is one of the most critical components of any ultrasonic test system. Careful attention should therefore be paid to selecting the most suitable transducer for the application. Variation in instrument characteristics and settings as well as material properties and coupling conditions play a major role in system performance.

Most often the transducer is chosen to enhance either the sensitivity or the resolution of the system. A system with good sensitivity has the ability to detect small variations at a given depth in the test material. A system with good resolution has the ability to produce simultaneous and distinct indications from reflectors lying at nearly the same depth and position with respect to the sound beam. In applications where good resolution is of primary importance it is common to select a highly dampened transducer. A high degree of damping will help to shorten interface ring-down or recovery time and allows the system to resolve closely positioned reflectors.

The specific transducer configuration also has an impact on system performance. Consideration should be given to the use of focused transducers with wear surfaces that are appropriate to the test material, and the choice of the appropriate frequency and element diameter.

In this study the following Panametrics Videoscan transducers were investigated: V106-RB, 2.25 MHz; V182-RB, 3.5 MHz; V109-RB, 5 MHz; V120-RB, 7.5 MHz and V111-RB, 10 MHz. Videoscan transducers are untuned transducers, which provide heavily damped broadband performance. They are the best choice in many applications where good axial or distance resolution is necessary or in tests that require improved signal-to-noise in attenuating or scattering materials.

Figure 3.9 is the typical signal waveform and frequency spectrum for a 5 MHz transducer (Panametrics V109-RB), employed in the current work, having a central frequency of 5 MHz [Panametrics, 2000]. It has a relatively broad frequency band and is thus useful in this context. Other transducers used have central frequencies of 7.5 and 10 MHz, respectively. After numerous experiments it was found that the 7.5 MHz

and 10 MHz transducers gave the best response for the system under investigation. In all the flat-sheet experiments that were chosen for data gathering 10 MHz transducers were thus used.

Another 7.5 MHz focal transducer was designed and used to measure of fouling in tubular UF.

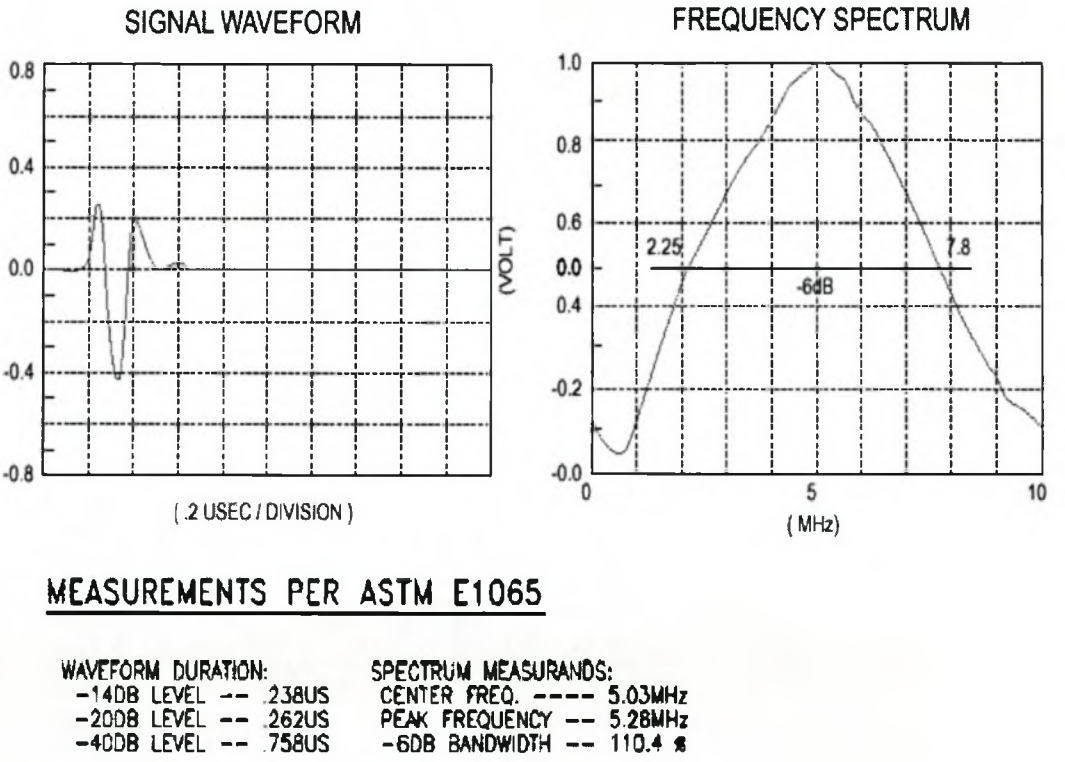

Figure 3.9: Typical signal waveform and frequency spectrum for a 5 MHz transducer [Panametrics, 2000].

3.6.5 THEORETICAL RESOLUTION

The theoretical resolution of a specific frequency transducer can be calculated if the speed of the sound wave in the medium that is under investigation is known. The wavelength can be calculated from Equation 3.2 [Koen, 2000]

$$\lambda = v/\omega \tag{3.2}$$

where λ - wavelength (m);

v - speed of sound wave (m/s);

ω - frequency (c/s or Hz)

The smallest detail that the transducer will pick up is that which is 0.25 of the sound wave's wavelength (explained in Figure 3.10). The theoretical resolution can thus be calculated with Equation 3.3 where

$$\text{Resolution} = 0.25\ \lambda \tag{3.3}$$

The possible theoretical resolution (in water) of the range of transducers that were used during this study is tabulated in Table 3.2.

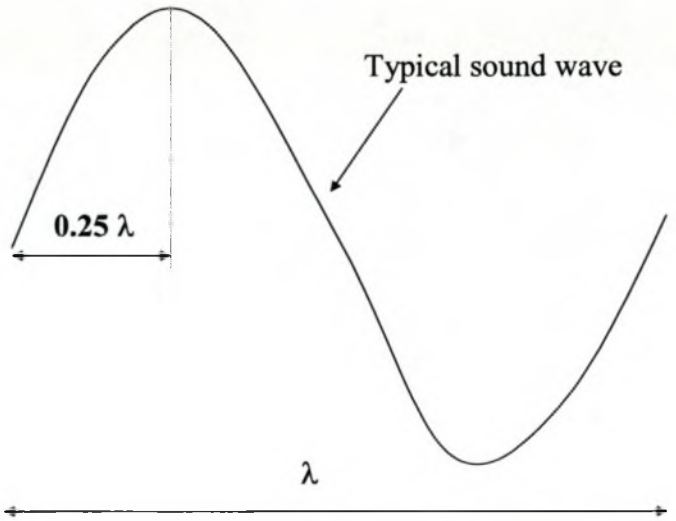

Figure 3.10: Typical sound wave.

Table 3.2: The theoretical resolution of the range of transducers used in this study [Koen, 2000]

Transducer	Frequency (MHz)	Resolution (μm)
V106-RB	2.25	159
V182-RB	3.5	102
V109-RB	5	72
V120-RB	7.45	48
V111-RB	10	36

3.7 MORPHOLOGICAL CHARACTERISATION OF THE FOULING LAYER

A morphological study of the fouled and cleaned membrane samples was carried out to establish a correlation between the measurement of UR and the coverage of the membranes. A LEO S440 scanning electron microscope (SEM) was used and samples were viewed at 10 kV and 20 mm working distance. Optical microscopy was also employed to investigate the membrane surfaces.

CHAPTER 4

ULTRASONIC REFLECTOMETRY MODELING

4.1 SCOPE OF THIS CHAPTER

The purpose of this chapter is to present a mathematical modeling that seeks to describe the process of ultrasonic testing related to the deposition of fouling, in even more complex membrane environments. Section 4.2 summarizes the program development of software for ultrasonic reflectometry. The program ultrasonic reflectometry modeling (URM) can handle an environment of 11 layers and uses as input parameters the sonic velocities, thicknesses and densities of these layers. The modeling is based on some actual ultrasonic records. The modeling procedure is followed by Section 4.3. The chapter is concluded with a few representative simulation results to demonstrate some actual ultrasonic records and the accuracy of this program. Section 4.4 enumerates examples of modelling applications.

4.2 PROGRAM DEVELOPMENT OF SOFTWARE FOR ULTRASONIC REFLECTOMETRY

Process simulation and modeling have become increasingly important approaches of the research and development environments as tools to improve the effectiveness of the research and development process. In order to gain more insight into the process of ultrasonic testing of membranes and membrane fouling, and to better understand the processes related to the deposition of fouling layers, a predictive program, ultrasonic reflection modeling (URM) was developed [Hallbauer-Zadorozhnaya, 2001].

It is a well-known principle that acoustic waves are generated if a spherical source of pressure D*(t)*, with a radius r_1, is applied to a medium at time t [Gurvich, 1960]. The acoustic waves thus generated propagate in the medium away from the source by displacing small volumes of the material they pass through. Such a displacement of material at each point of the model can be given as:

$$U_P(R,t) = \left[\frac{f_s(\tau_1)}{R^2} + \frac{f_s'(\tau_1)}{V_P R}\right]\frac{r_0}{\rho} r, \qquad (4.1)$$

where, r_0 - unit of the vector, directed to the radius,

V_P - compressional velocity of acoustic wave (m/s),

ρ - density of the material (kg/m^3),

R - distance between the sources (transducer) (m).

At the receiver, values of $f_s(\tau)$ can be given as a function of the pressure spectrum D(ω) as:

$$f_s(\tau_1) = \frac{1}{2\pi}\int_{-\infty}^{+\infty} \frac{D(\omega)\exp i\omega\tau d\omega}{\omega_{0P}{}^2 - \omega^2 + 2i\omega\alpha_P} \qquad (4.2)$$

where, $\tau_1 = t - (R\text{-}r_1)/V_1$ - time of wave's arriving (second),

$\omega_{0P} = 2V_S/r_1$ – frequency of the self-oscillation of source (transducer) (radian per second),

$a_p = 2V_S^2/RV_P$ – coefficient of the attenuation the source (transducer),

D *(ω)* represents the spectrum of the pressure and V_S is shear wave velocity (we assume $V_S \sim 2V_P/3$).

The systematic change of pressure or a sound wave is an oscillation and, for modelling purposes, we assume a $1\frac{1}{2}$ sine function. The spectrum of that pressure transmission can be given as:

$$D(\omega) = P_0 \cdot \frac{\omega_0\left[1+\exp\left(-i\omega\frac{3T}{2}\right)\right]}{\omega 2 - \omega_0^2} = D_S(\omega)\cdot P_0, \qquad (4.3)$$

where, P_0 – amplitude of pulse [N/m^2],

T - period of sinus function (i.e. $T/2 = \Delta T$- duration of the pulse),

$\omega_0 = 2\pi/T$,

ω– angular frequency (Hz).

For the analysis of sound waves in an assembly of membranes a number of material boundaries or free boundaries at which the propagation of a wave is disturbed have to be considered, i.e. at which a signal is reflected. We consider a case where the sound signal strikes planes and smooth boundaries at right angles. For reasons of symmetry only plane waves can then be propagated at right angles from the boundary. Reflected waves and transmitted waves are in opposite directions.

In order to apply the above formulae (Equations 4.1 – 4.3) and to calculate or predict the behaviour of a sound signal in the layered medium of a membrane assembly, the sound pressures and acoustic impedances of the materials contained in the assembly have to be considered. The acoustic impedances of two adjacent materials, W_1 and W_2, depend on their specific sound velocities and densities, as described by Equation 2.13

Considering the sound pressures of the incident wave, P_i, the reflected wave, P_r, and the transmitted wave, Pt, we can form two ratios; also known as the coefficient of reflection and the coefficient of transmission in Equations 2-26 and 2-27.

The program URM combines the above mathematical considerations and, from input parameters, produces a text file-type output, which can be used to produce a graphical presentation of the problem, using Microsoft EXCEL, Sigma Plot or similar commercially available software. In its present form, URM can handle an environment of 11 layers and uses as input parameters the sonic velocities, thicknesses and densities of these layers. The output contains data on the individual pulses as well as a combined signal, as would be observed on an oscilloscope screen.

At present the program is only available as a FORTRAN version. A WINDOWS version is currently being developed in collaboration with an overseas company.

4.3 MODELLING PROCEDURE

It is the aim of mathematical modelling to describe and/or predict processes from known or assumed parameters. A typical modelling cycle would be:

- begin with observations
- based on observation, construct a mental image or model
- use the model to make predictions and test those predictions by doing new experiments
- if necessary, revise the model
- repeat the last two steps above, as necessary, to obtain better models.

In the case of the layered structure of membrane assemblies a large number of observations are available. The current model of fouling predicts that during ultrasonic testing of a fouling process an extra echo or reflection would develop in front of the membrane echo and grow according to the progress of fouling. It is also known that the physical and elastic parameters of the system have an influence on the reflection pattern. Input parameters for modelling based on theoretical considerations would thus be:

- acoustic velocities in the participating components
- densities of the components
- thicknesses of individual layers.

4.4 EXAMPLES OF MODELING APPLICATION

A number of modelling exercises have been carried out and good agreement has been obtained with the above model. However, observations that depart from that model have also been made. The ultrasonic records of such an experiment are shown in Figure 4.1, where the individual records have been stacked according to the fouling progress. In this experiment a polysulfone (PSU) membrane was tested with paper mill effluent as feed in a flat-sheet test cell test.

Three principal echoes can be recognized for the clean membrane (bottom of Figure 4.1) i.e. from left to right: PSU membrane, polyester support and the porous metal support for the membrane. While the latter two echoes remain stationary during progressing fouling, the first echo moves forward and a stationary, additional echo develops in front of the polyester support. In a first hypothesis this behaviour was explained as:

- The PSU membrane consists of three physically different parts: top layer, intermediate layer and polyester backing;
- The fouling layer has properties similar to the top layer and, during fouling, obscures the PSU echo.

This hypothesis was tested by mathematical modelling and repeated variation of the parameters. The final input parameters used for the flat cell configuration are given in Table 4.1.

The results of the modelling are presented in Figure 4.2. It shows the modelled echoes up to and including the polyester layer. It is a reasonable likeness of the echo records shown in Figure 4.1 and appears to confirm the above hypothesis. However, according to the nature of a hypothesis it is not proof but a good indication that layers can 'fuse' as far as their echoes are concerned, if the acoustic parameters are close enough. It would, in such a case, not be possible to calculate the thickness of a fouling layer directly from the ultrasonic record in the conventional way. Modelling would be a support in finding the correct approach. Mathematical modelling could therefore play an important role in the handling and understanding of ultrasonic test records. The detail applications of URM are presented in the following Chapters 7 and 8.

Table 4.1: Input parameters used for modelling PSU membrane fouled by paper mill effluent

Layers\Parameters	Velocity [m/s]	Thickness [m]	Density [g/cm^3]
Perspex	2762	0.00569	1.18
Water/feed	1483	0.002	1.0
Fouling	2300	0, 50, 100, 150 μm	1.05
PSU_1	2500	0.00001	1.13
PSU_2	2450	0.00015	1.1
Polyester	3100	0.00002	1.53
Metal backing	4590	0.003	3.2

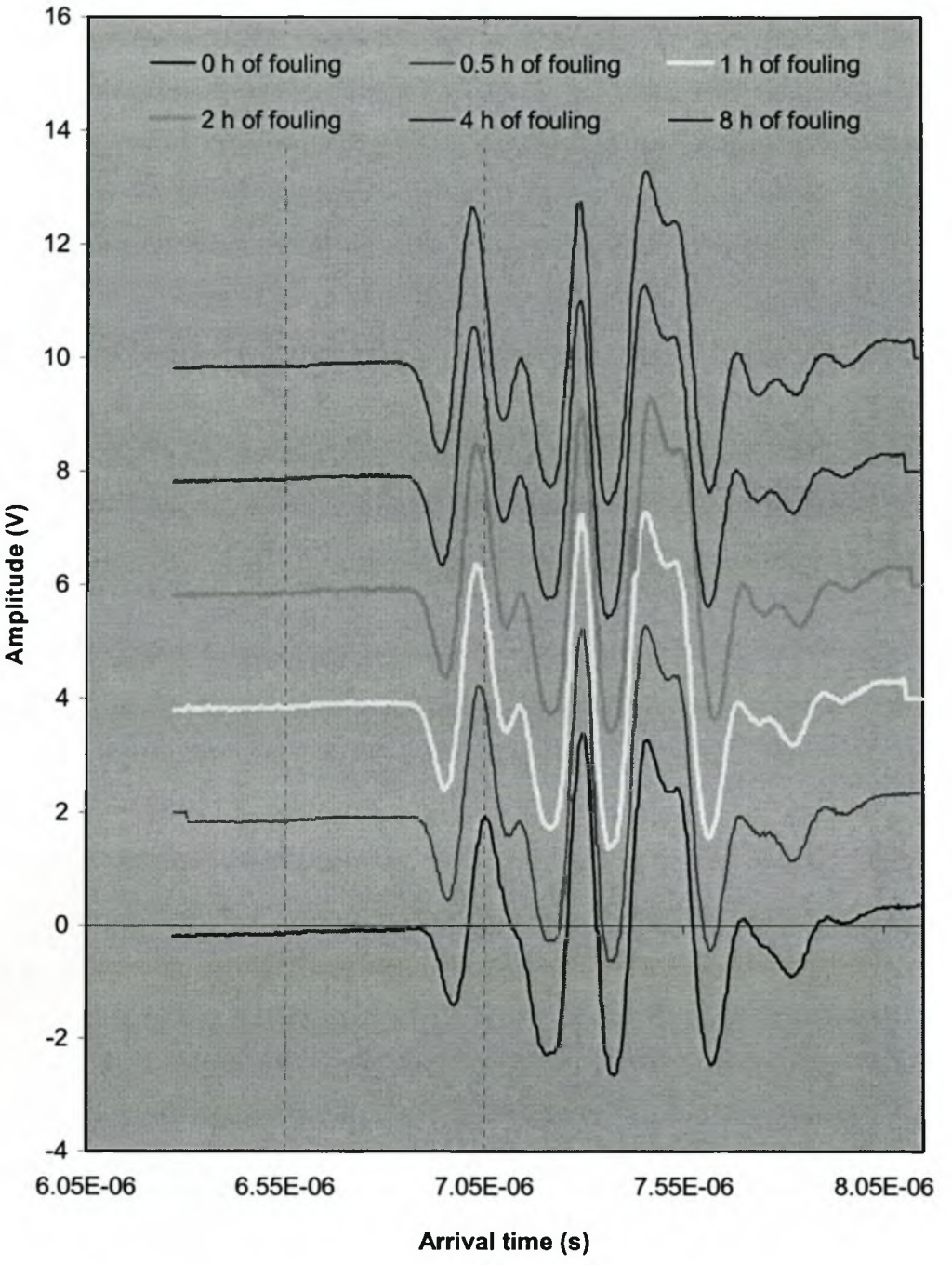

Figure 4-1: Ultrasonic reflectometry during filtration of paper mill effluent by PSU membranes.

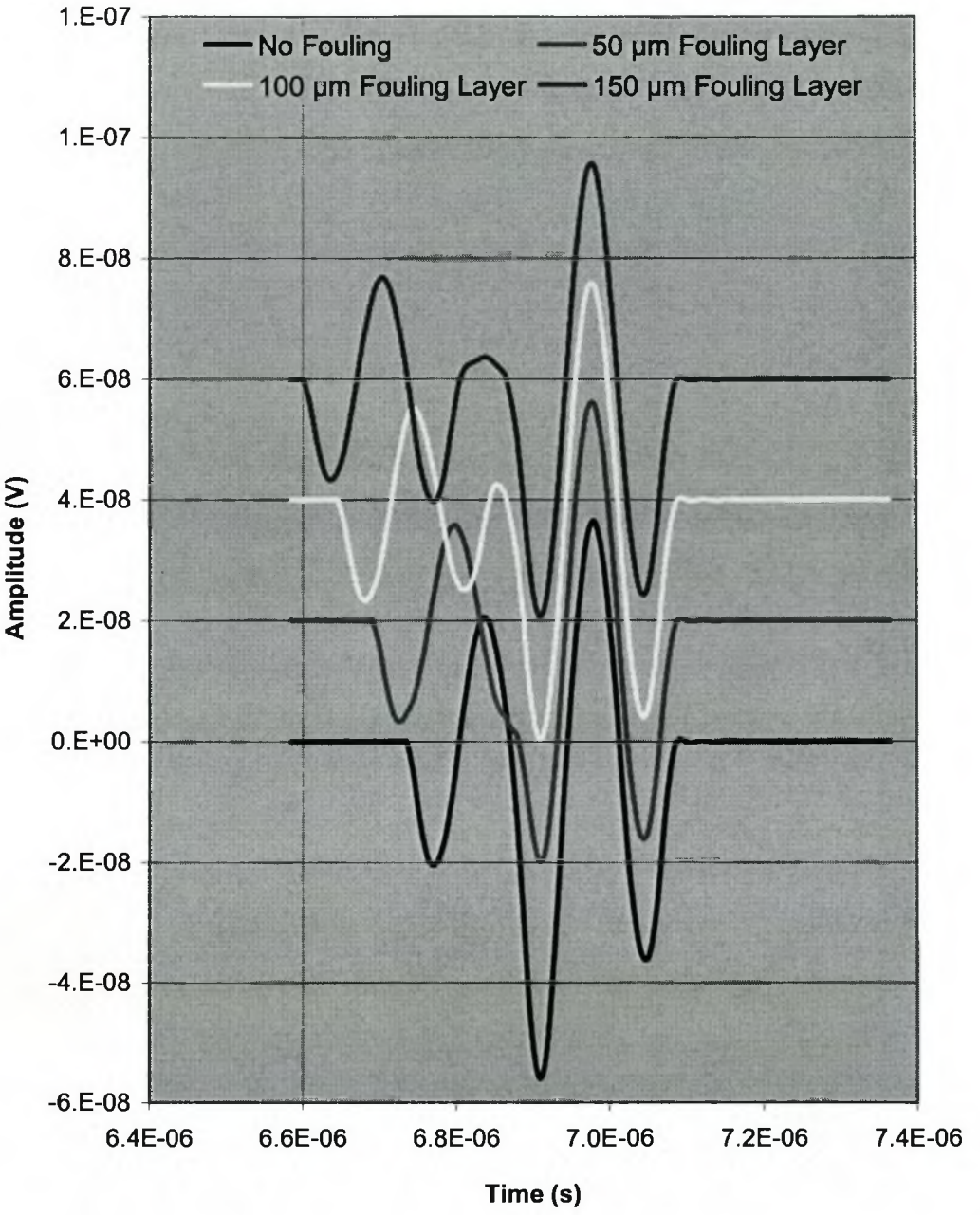

Figure 4.2: Modelling of fouling layers on PSU membranes.

CHAPTER 5

IN SITU MEASUREMENT OF PARTICLE DEPOSITION AND ITS REMOVAL IN MICROFILTRATION

5.1 SCOPE OF THIS CHAPTER

This chapter describes the use of the ultrasonic time-domain reflectometry (UTDR) technique for the non-invasive, *in situ* measurement of particle deposition and its removal during crossflow microfiltration with nylon membranes. The study was carried out with 0.5 g/l kaolin (average particle size 2 μm). Ultrasonic response signals were obtained upon particle deposition and subsequent cake layer formation on the membrane surface. A cake layer echo appeared in the time domain. The UTDR technique was also used to quantify the thickness of a fouling layer on the membrane surface. Moreover, UTDR was applied to monitor membrane cleaning and evaluate the effectiveness of different cleaning methods in MF. The UTDR results corroborated flux measurements and SEM analyses.

5.2 INTRODUCTION

It is generally recognized that one of the major problems associated with the more widespread use of microfiltration (MF) for separation is the significant flux decline during operation. This is because of particle deposition and the build-up of a filter cake on the surface of a MF membrane.

The development of a non-invasive visualization technique that is sensitive to changes in the condition of a membrane surface is of considerable interest. Direct analysis of the fouling deposits on membranes has been done using SEM, XRD and XRF [Butt et al. 1995; Dudley and Dorrton, 1996]. However, these invasive methods cannot be used to measure the fouling process in real time. The use and advantages of UTDR for the nondestructive analysis of a variety of materials has been previously described

[Lynnoworth, 1989; Kool et al. 1998; Peterson et al. 1998]. In particular, UTDR has been used to study membrane formation and compaction, and fouling [Mairal et al. 1999 and 2000; Koen, 2000]. To date, its use for studying membrane fouling has been restricted to RO membranes.

The present study describes the application of the non-destructive, *in situ*, UTDR technique to investigate particle deposition and its removal in a MF system. The further capabilities of the UTDR technique and its applicability in different types of membrane separation systems are evaluated. Ultrasonic response signals obtained provide quantitative information on the occurrence of kaolin fouling on MF membranes.

5.3 EXPERIMENTAL

5.3.1 MF SYSTEM AND ULTRASONIC SET-UP

Figure 5.1 is a schematic representation of MF separation system. The assembly consisted of a 10-litre feed tank for storage and supply of the fouling solution, a peristaltic pump (WATSON-MARLOW 313S, Watson-Marlow Limited, England) for pressurization of the feed solution, the rectangular test module (see Figures 3.3 and 3.4), a temperature control system for the feed tank, pressure gages, valves and a flow meter.

The ultrasonic measurement system consisted of a 10 MHz ultrasonic transducer (Panametrics V111-RB), a pulser-receiver (Panametrics 5058PR) and a digital oscilloscope (HP Model 54602B) (Figure 5.1). The oscilloscope connected to the pulsar-receiver captures and displays the data as amplitude changes on its front panel. Each set of ultrasonic data generated consisted of 500 data points. This data can be stored on a computer's hard drive. Commercially available salad oil was used to couple the transducer to the top plate surface.

Nylon MF membranes (disc Φ 290 mm) made by Pall Ltd., England, with a nominal pore size of 0.2 μm, were used in all of the fouling experiments. Kaolin was chosen as

a potential foulant because kaolin occurs frequently in the mining and paper industries, especially in the mining wastewater treatment in South Africa. Fouling experiments were carried out with 0.5 g/l kaolin (average particle size 2 μm).

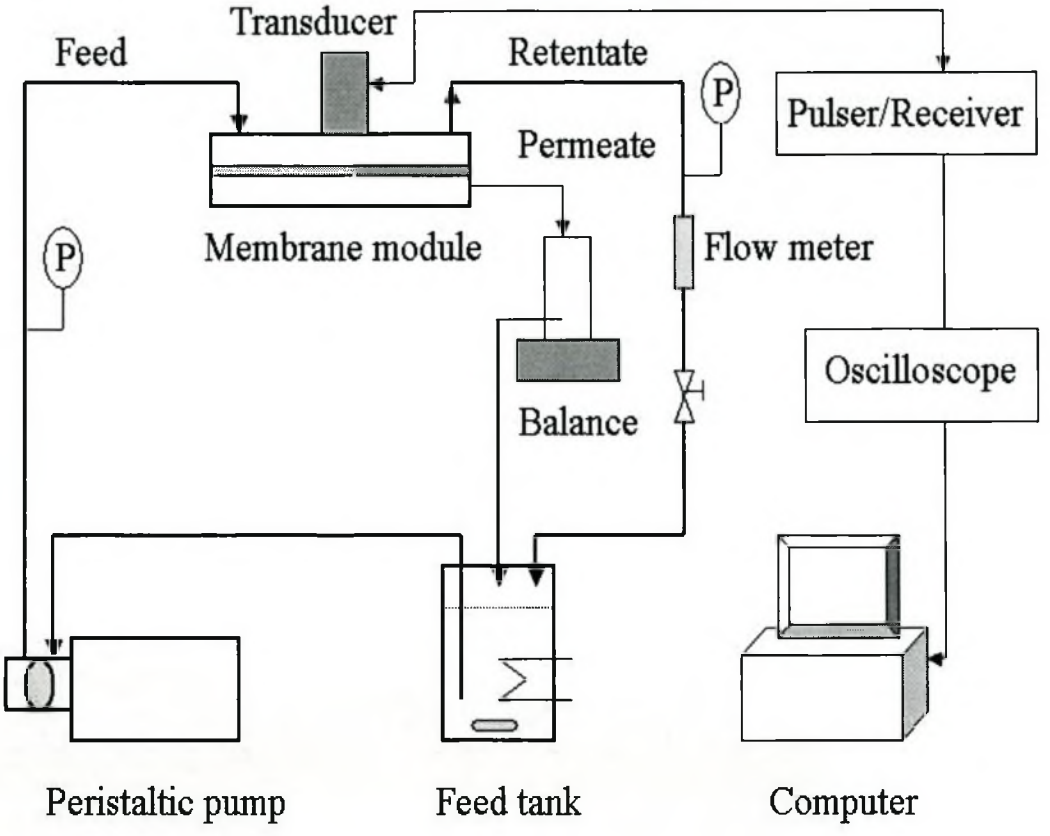

Figure 5.1: Schematic representation of MF separation system and ultrasonic measurement.

5.3.2 EXPERIMENTAL PROCEDURE AND FOULING

Each experiment commenced with pure water being circulated through the system at the desired flow rate and applied pressure for 1 h to compress the membrane and to build up a stable flow field. Once steady state was attained, the feed was switched to the kaolin solution to initiate the fouling phase. The fouling experiment was carried out at a flow rate of 6.97 ± 0.07 cm/s (*Re* = 253 ± 2.5), applied pressure 100 ± 5 kPa and temperature 24 ± 1°C. This phase was allowed to continue until the ultrasonic response and permeate flux had stabilized.

5.3.3 CLEANING EXPERIMENT

After the membranes were fouled with kaolin, they were cleaned by two methods, consecutively, namely: reverse flushing (at a flow rate of 50 cm/s) and ultrasonic cleaning, for cleaning times of 5 min each. The feed solution was changed from effluent to water under the same operating conditions as used in the fouling phase in order to compare the cleaning efficiencies of these three methods. The cross-flow filtration cell was immersed in a water bath at temperature 24 ± 1°C during ultrasonic cleaning. The cell was irradiated with a horn ultrasonic cleaner (Model W-375, Ultrasonics INC.) with a frequency of 20 kHz and a power of 375 W.

To investigate the cleaning efficiency of each cleaning method, the cleaned membrane was used to filter pure water under the same operating condition as used in the fouling phase. The UR measuring system captured the changes in ultrasonic signal responses after the different cleaning methods. These data can be stored on a computer's hard drive.

5.4 RESULTS AND DISCUSSION

5.4.1 ULTRASONIC REFLECTOMETRY IN A CELL

Before investigating fouling by UTDR, it is necessary to understand the basic principle of ultrasonic measurements and distinguish or recognize various response signals from ultrasonic records in the flat-sheet cell (refer to Figures 3.3 and 3.4). A representative waveform obtained during pure water operation with a clean nylon membrane is shown in Figure 5.2.

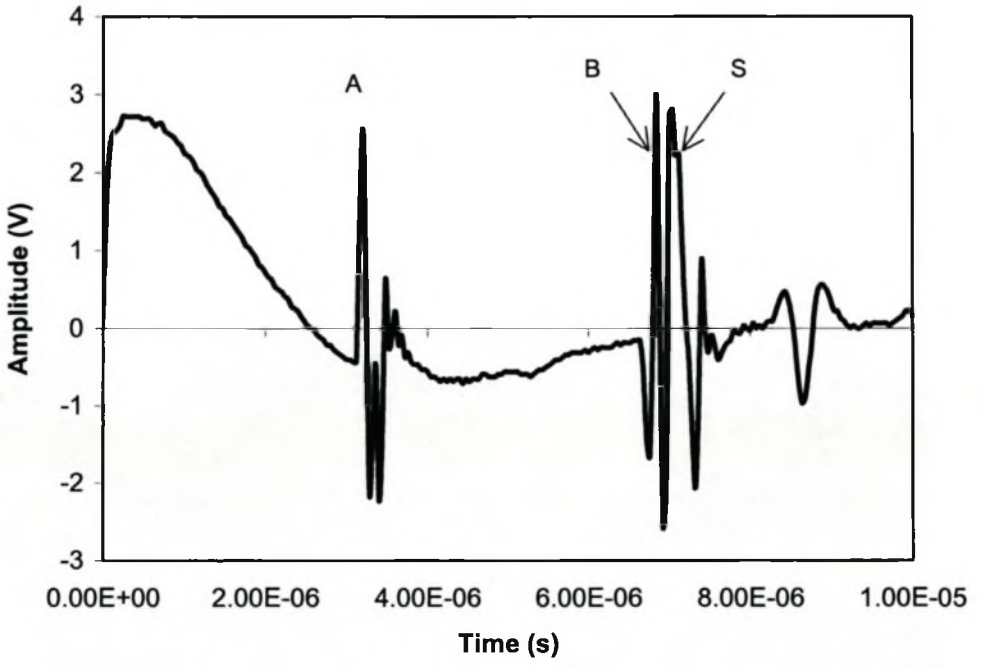

Figure 5.2: Ultrasonic spectrum inside the flat sheet cell during pure water filtration at operation pressure of 100 kPa.

Figure 5.2 plots the ultrasonic signal amplitude in volts (V) vs. the time in seconds (s). Each peak corresponds to a reflected acoustic wave from one of the multiple interfaces in the flat cell. Peaks A, B and S were generated from the following interfaces: perspex plate/feed (water), water/nylon membrane and membrane/porous metal support. Peak B is a single echo that exhibits the structure of the nylon membrane - a symmetric layer. The UTDR measurement was focused on the front of Peak B (as a observed peak), which indicates the membrane surface.

In order to prove the above observation, a mathematical model of the reflections inside the flat-sheet cell was designed and the results were compared to the actual cell and nylon membrane dimensions measured by vernier. Figure 5.3 is a cross-sectional view of the cell with the received reflections supposed from the various interfaces where

A : echo between top plate of the cell and water interface;

B : echo between water and nylon membrane interface;

S : echo between nylon membrane and porous metal support.

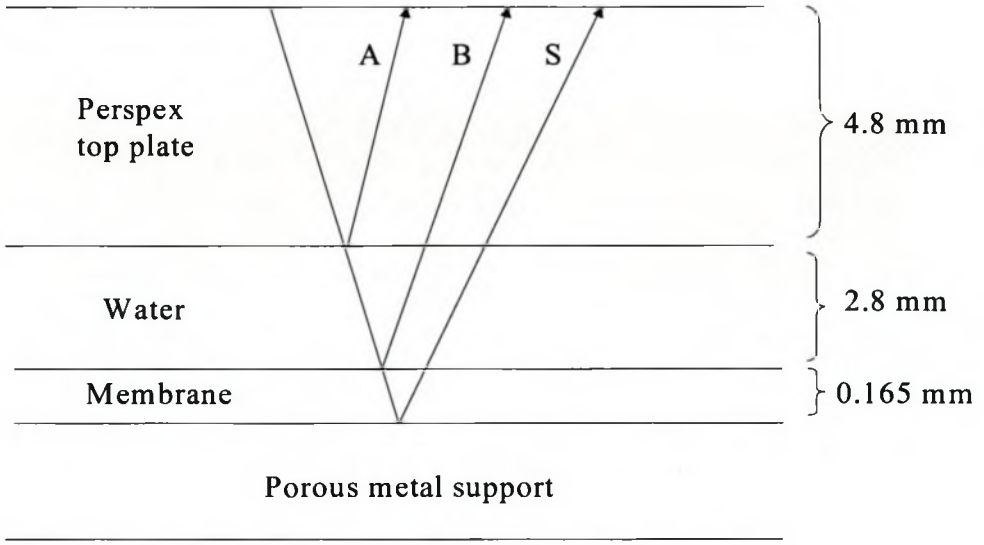

Figure 5.3: Mathematical model in a flat-sheet cell.

The arrival time of the response signals as measured by UTDR (Figure 5.2) was:

$t_A = 3.40\ \mu s$

$t_B = 6.84\ \mu s$

$t_S = 7.00\ \mu s$

If the speed of sound in Perspex, water and a nylon membrane is known, the thicknesses of them can be mathematically correlated, by using the received echo time and Equation 3.1 with

$V_{perspex} = 2730$ m/s;

$V_{water} = 1438$ m/s

$V_{polyimade\ (nylon)} = 2200$ m/s [Krautkrämer, 1969].

$$dS_{perspex} = 0.5 \times V_{perspex} \times t_A$$
$$= 0.5 \times 2730 \times 3.40$$
$$= 4.64 \times 10^{-3}\ m$$
$$= 4.64\ mm$$

$$dS_{water} = 0.5 \times V_{water} \times (t_B - t_A)$$
$$= 0.5 \times 1438 \times (6.84 - 3.40)$$
$$= 2.47 \times 10^{-3}\ m$$
$$= 2.47\ mm$$

$$dS_{nylon} = 0.5 \times V_{polyimade\ (nylon)} \times (t_S - t_B)$$
$$= 0.5 \times 2200 \times (7.00 - 6.84)$$
$$= 0.176 \times 10^{-3}\ m$$
$$= 0.176\ mm$$

The calculated thickness of the Perspex plate is 4.64 mm, which is very close to the measured value of 4.80 mm by vernier. The calculated value of the water (feed channel) thickness of 2.47 mm is smaller than the measured value of 2.8 mm because of the compaction of the rubber O-ring. The thickness of the nylon membrane was measured by vernier under dry conditions, hence the measured value of 0.165 mm is thinner than the calculated value of 0.176 mm (probably due to compaction). Overall, the model showed excellent correlation between the echoes received and the measured cell dimensions.

5.4.2 FOULING EXPERIMENT AND ULTRASONIC MEASUREMENT

As shown in Figure 5.4, the value of the permeate flux declines rapidly after commencement of fouling and then reaches a near steady-state flux. The rapid flux decline to 34.2% of its initial value after 60 min of operation implies that significant membrane fouling occurs.

The UTDR echo signals during the fouling experiments are shown in Figure 5.5. Generally, once foulants (particles) are deposited on the membrane surface, the acoustic impedance difference and the topographical characteristics at the feed solution/membrane interface will change, resulting in a change in the amplitude of the membrane echo, as shown after 5 min of fouling operation in Figure 5.5b. Further, if a cake layer builds up on the membrane surface, a new echo signal (Peak C) will be seen, as seen after 10 min of fouling operation in Figure 5.5c. An increase in the amplitude of Peak C and its movement in the time-domain can be observed at 0.5, 2 and 7 h of operation in Figure 5.5 d–f. Peaks B' and C were generated from the interfaces: the kaolin layer/ nylon membrane and the feed/kaolin layer (Figure 5.5).

Figure 5.4 also shows the amplitude of Peak C as a function of operation time during kaolin fouling. At the beginning of the fouling experiment an instantaneous and rapid increase in the amplitude is observed, followed by a more gradual increase after 1 h of operation. The instantaneous amplitude increase results primarily from particle deposition and the formation of a dense kaolin layer. The gradual amplitude increase is presumed to occur as result of the effective density of the fouling deposit, which does not change significantly once the fouling layer becomes reasonably dense and thick. Indeed, the flux decline corresponds to the changes in the amplitude of peak C.

The decline in the amplitude of peak B with operating time is related to the growth of the echo signal of the bottom of the kaolin layer. This has an effect on the reflection signal of the membrane as a result of the build up and consolidation of the fouling layer on the membrane surface.

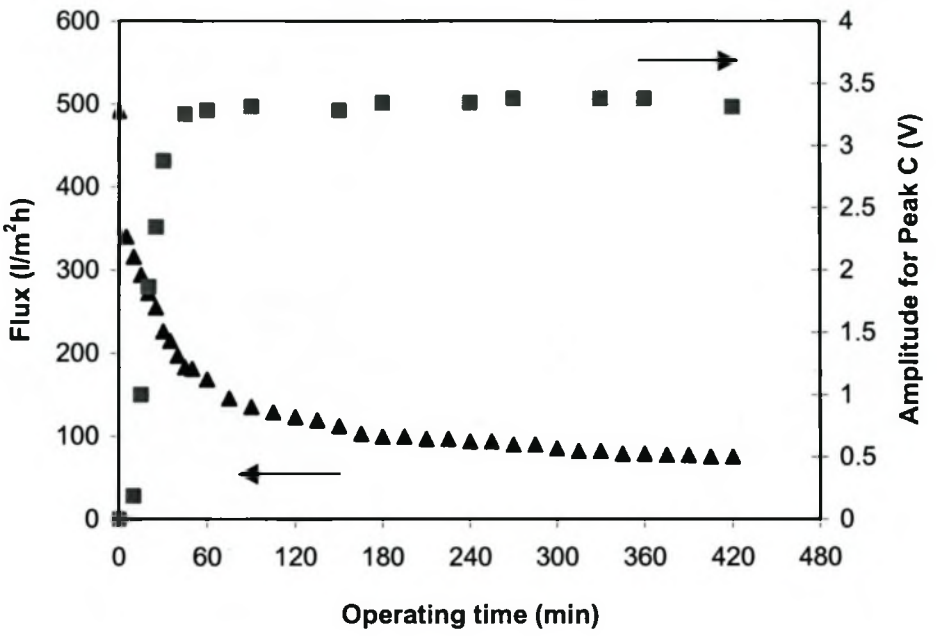

Figure 5.4: Effect of kaolin fouling on permeate flux decline and amplitude of Peak C (echo of fouling layer) with operating time, at pressure 100 kPa and flow rate 6.97 cm/s in MF.

Ultrasonic responses:

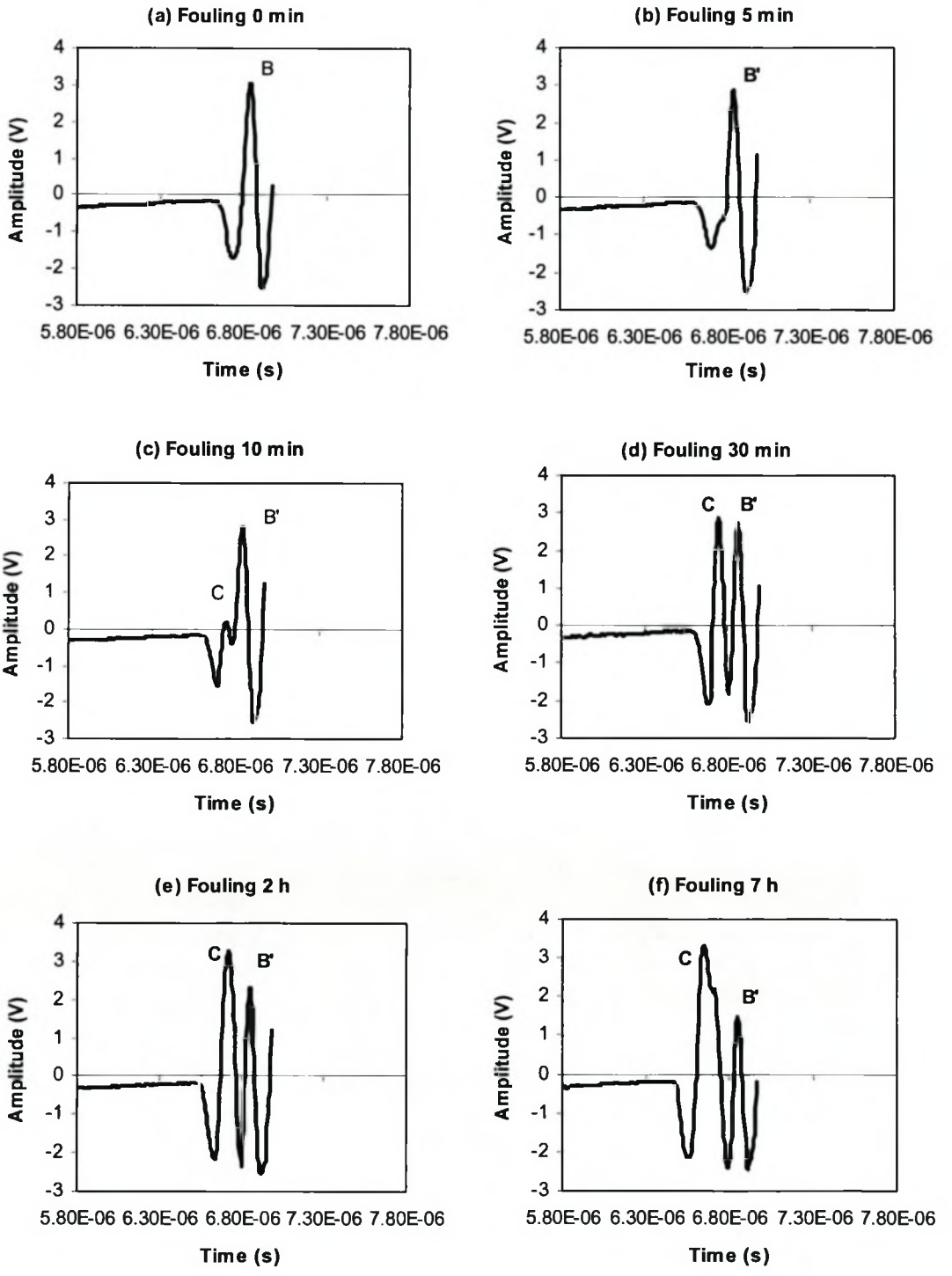

Figure 5.5: Ultrasonic response signals after (a) 0 min (start), (b) 5 min, (c) 10 min, (d) 30 min, (e) 2 h and (f) 7 h of operation in the fouling experiment carried out with kaolin (0.5 g/l) in MF.

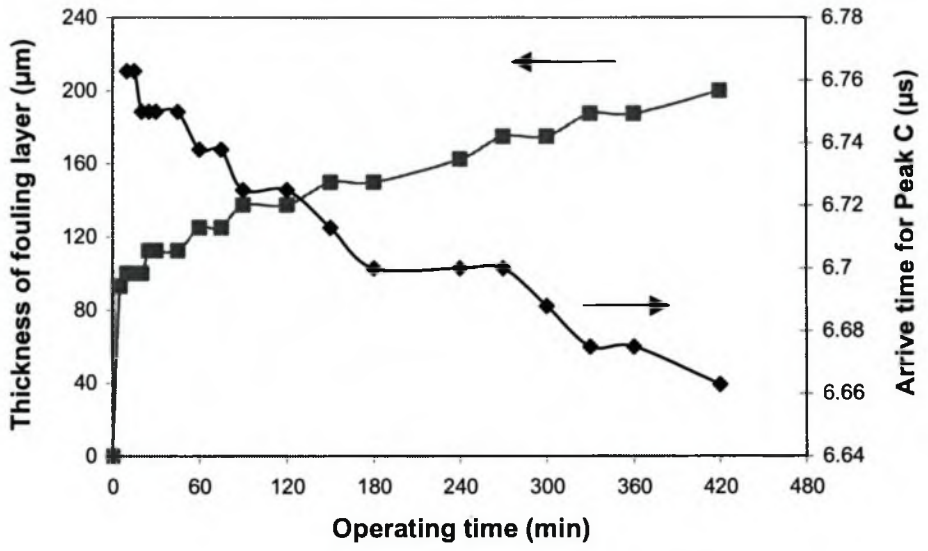

Figure 5.6: Plots the thickness of fouling layer and arrival time of peak C during kaolin fouling in MF.

Figure 5.6 plots the arrival time of peak C during the fouling process. According to the difference in arrival times, dt, between echoes B and C, the thickness of the kaolin layer on the membrane surface can be calculated from Equation 3.1 (V = 2000 m/s), as shown in Figure 5.6. Although there is an obvious change (with time) in the thickness of the kaolin layer, there is little change in flux. This implies that the pore size of the top kaolin layer is bigger than that of the bottom layer.

In order to study the correlation between the measurement of UTDR and membrane coverage by the fouling layer, membrane samples were taken for SEM analysis. Results are shown in Figure 5.7. Morphological characterization of the membrane surface after 5 min of fouling operation revealed particle deposits on the membrane surface (Figure 5.7a). Complete membrane coverage with aggregate kaolin particles and layers was observed after 30 min and 2 h of operating (Figure 7b and c). After 7 h of fouling operation, there was a dense kaolin layer covering on the membrane surface (Figure 5.7d).

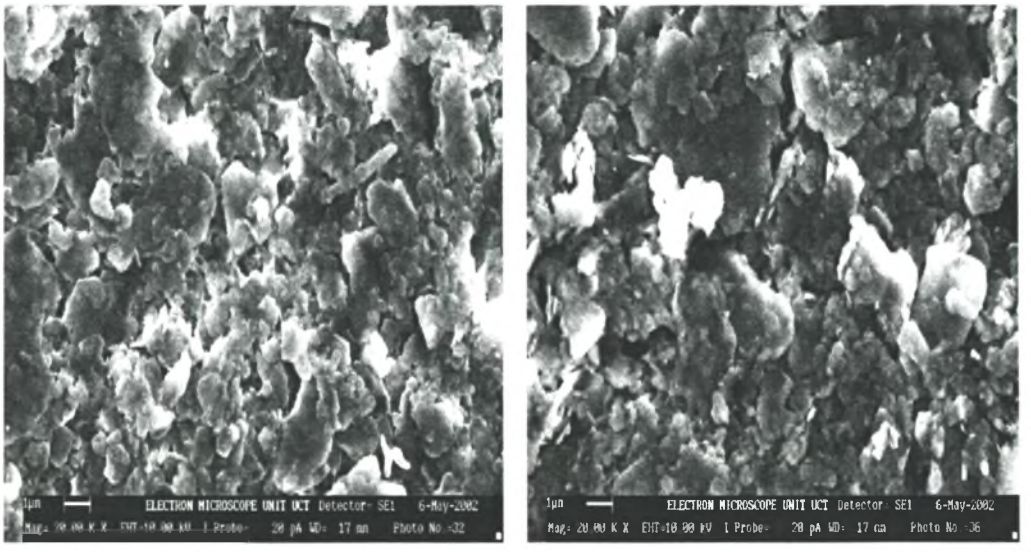

(a) (b)

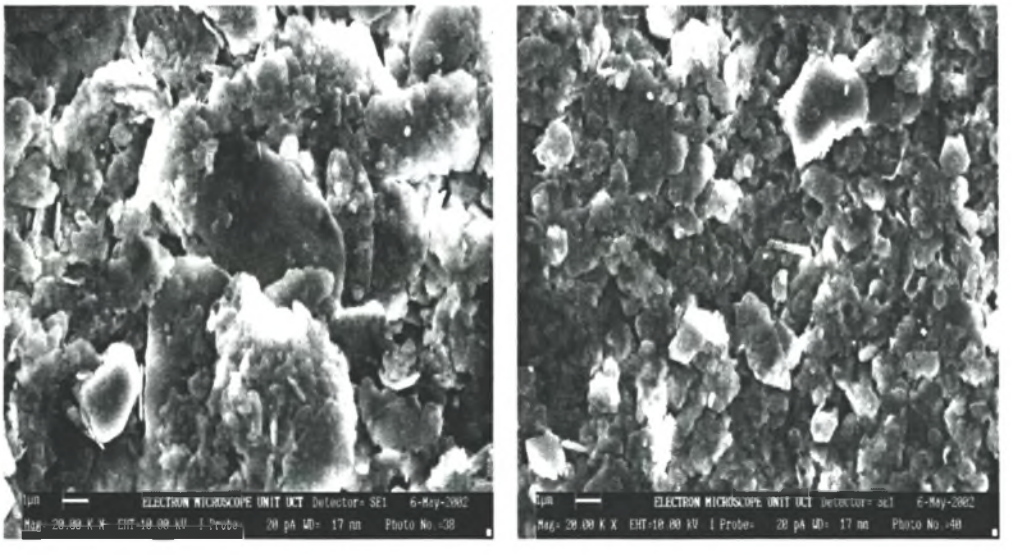

(c) (d)

Figure 5.7: Microscopic images of a fouled Nylon membrane after (a) 5 min, (b) 30 min, (c) 2 h and (d) 7 h of fouling operation in MF.

5.4.3 CLEANING EXPERIMENT

To investigate the possibility of using the UTDR technique for monitoring fouling removal in real time, cleaning experiments were carried out by reverse flushing and ultrasonic cleaning, consecutively. The results of the UTDR response signals and permeate fluxes after the cleaning processes are shown in Figures 5.8 and 5.9.

Reverse flushing can reduce the cake layer covering on the membrane surface and enhance the permeate flux, although not to the original value (Figure 5.8). The UTDR response signal in Figure 5.9a shows that a fouling layer still covered the membrane. The disappearance of peak C (fouling echo after ultrasonic irradiation) indicates that the fouled membrane was cleaned by ultrasonic irradiation, as shown in Figure 5.9b. The recovery of flux after ultrasonic cleaning confirms this observation (see Figure 5.8). The amplitude of peak B for ultrasonic cleaning (Figure 9b) is, however, only 84.2% of that of peak B for fouling start [Figure 5.5 (a)]. This suggests that there are still some particles that remain on the membrane surface after ultrasonic cleaning. The microscope image of the membrane surface cleaned by ultrasonic cleaning proves the above observation (Figure 5.10 b). These results therefore demonstrate that the UTDR technique can indeed monitor removal of the fouling layer and membrane cleaning.

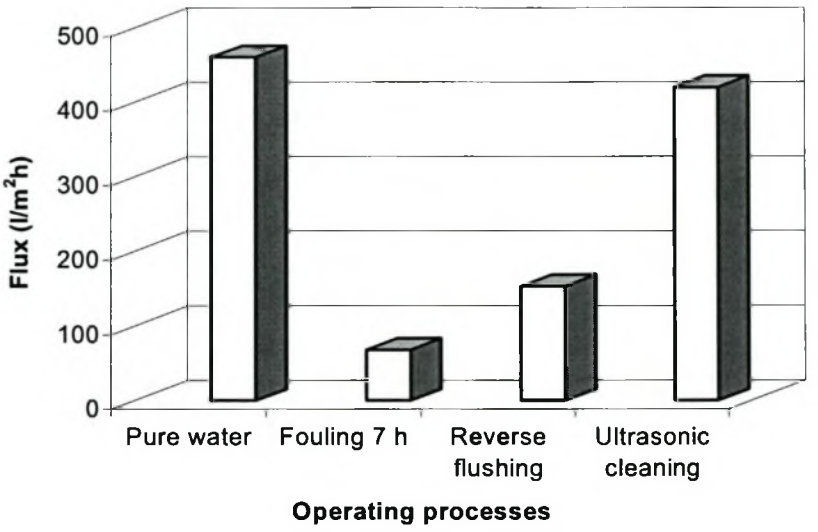

Figure 5.8: Change in flux during fouling and cleaning processes (at pressure 100 kPa and flow rate 6.07 cm/s).

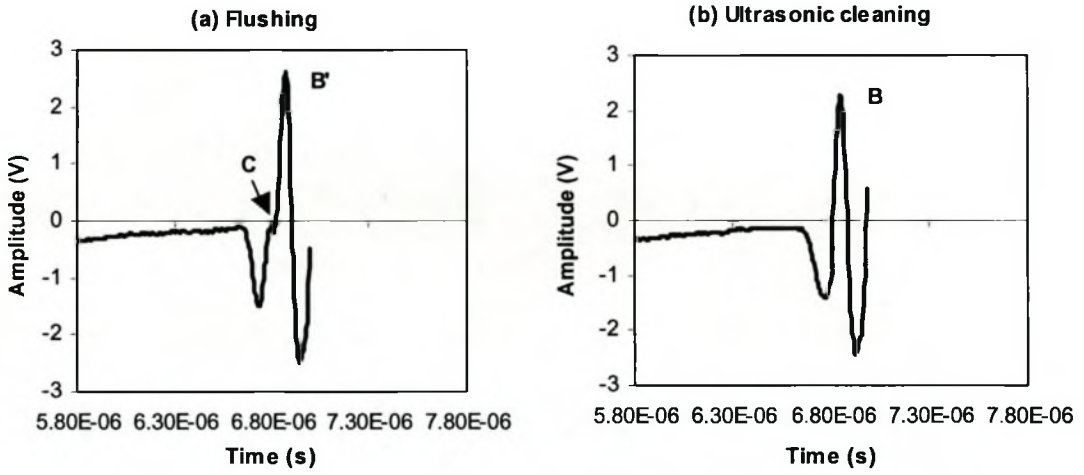

Figure 5.9: Ultrasonic echo signals in the cleaning processes: reverse flushing and ultrasonic cleaning.

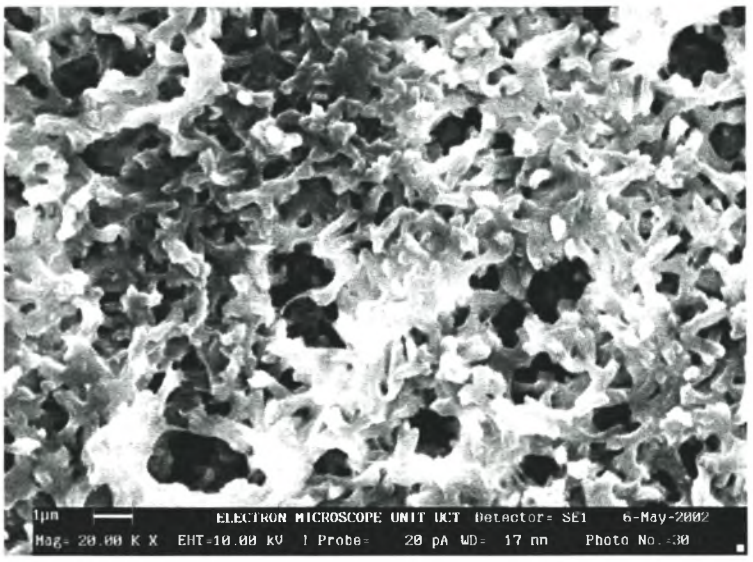

(a)

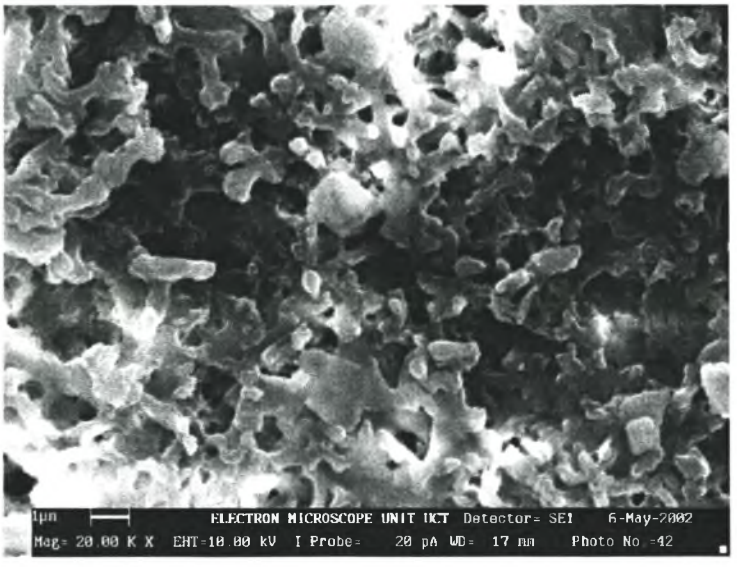

(b)

Figure 5.10: Microscope images: (a) a clean nylon membrane surface; (b) the membrane surface cleaned by ultrasonic cleaning.

5.5 SUMMARY

The mathematical model analysis revealed good correlation between the echoes received and the measured cell dimensions.

Both the UTDR signal amplitude and arrival time of a fouling peak as a function of operating time provide usefully quantitative information on the fouling processes. Results show that UTDR can monitor particle deposition, and the build up and consolidation of a fouling layer on a MF membrane surface in real time.

A dense cake layer formed in a short time, with a corresponding flux decline. Although there is an obvious change (with time) in the thickness of the kaolin layer after the formation of a dense layer, there is little change in flux. This implies that the pore size of the top kaolin layer is larger than that of the bottom layer.

UTDR can also be used to monitor membrane cleaning. Ultrasonic cleaning is an effective cleaning method. The UTDR results corroborate the flux measurements and SEM analyses

CHAPTER 6

ULTRASONIC CLEANING OF NYLON MICROFILTRATION MEMBRANES

6.1 SCOPE OF THIS CHAPTER

An ultrasonic technique was successfully applied to remove fouling and recover the permeate flux of flat-sheet MF membranes. Three kinds of cleaning methods were used to clean MF membranes: forward flushing, ultrasonic cleaning and ultrasound with forward flushing, and their cleaning efficiencies compared. It was found that ultrasound associated with forward flushing was a new effective method for the recovery of permeate flux. Scanning electron microscopy (SEM) analysis indicated that this method was able to remove fouling layers from a membrane surface and restore the original structure of the membrane surface. The operating conditions during cleaning were investigated. In general, a high forward-flushing velocity and low cleaning solution (water) temperature, under the same ultrasonic conditions, gave higher cleaning efficiency. Moreover, online ultrasound reduced membrane fouling and enhance permeate flux. The horn sonicator employed had a frequency of 20 kHz and a power of 375 w. Fouling and cleaning experiments were performed with nylon membranes with 0.2 μm average pore diameter. The membranes were fouled by Kraft paper mill effluent.

6.2 INTRODUCTION

Wastewater reclamation in the pulp and paper industry is important because of the large volume of water used in this field [Ahn et al. 1998]. It has gathered ever more attention as the regulations on the effluent become more stringent. Many technologies, including: adsorption, chemical oxidation, ion exchange, evaporation and membrane processes have been used to purify wastewater from the paper industry. Of these technologies, membrane processes can be tailored according to the required degree of purification [Nourtila-Jokinen and Nystrom, 1996]. One of the limiting aspects in

applying MF and UF for wastewater treatment is that of problems with membrane fouling and consequent flux reduction.

Membrane fouling is characterized by an "irreversible" decline in flux. Most of the literature that appeared over the past two decades focused on fouling rather than cleaning, even though what appears to be a fouling problem may really be a cleaning problem. Considerable progress has been made in understanding the interactions between the foulants, the membrane and the operating conditions [Potts et al, 1981; Fane and Fell, 1987; Robertson and Zydney, 1990; Belfort et al., 1994]. However, although many techniques have been developed to overcome fouling, membrane cleaning techniques need to be improved.

The typical methods of membrane cleaning that have been used in practice have been crossflushing (spiral-wound and tubular) and backwashing (hollow fibre) [Redkar and Davis, 1995; Parnham and Davis, 1996; Pontie et al. 1997; Cheryan, 1998; Kennedy et al. 1998]. Crossflushing and backwashing may be especially useful with colloidal suspensions and some tubular membranes. Further, chemicals such as detergents, acids or alkalis are often used to clean fouled membranes [Jaffar, 1994; Mukherjee, 1996]. However, the chemical methods used sometimes damage the membrane materials and causes secondary pollution. Electrical techniques have also been used to enhance permeate flux in membrane filtration [Lentdch et al. 1993; Muralidhara, 1994; Huotari et al. 1999; Tarleton and Wakeman, 1991 and 1992]. Charged particles will move away from the membrane surface, depending on the electric field strength applied, thus reducing the extent of concentration polarization and increasing flux. There is, however, the danger of electrolysis taking place at the electrodes and gas being generated. Change in the pH of the product stream will be proportional to the applied voltage. Corrosion of electrodes and high power costs have inhibited the commercial implementation of this technique [Cheryan, 1998].

Ultrasound has been widely used as a method for cleaning materials because of the cavitation phenomenon [Price, 1992]. Cavitation is defined as the formation, growth and collapse of bubbles, which are formed when a large negative pressure is applied to a liquid medium. When ultrasound is transmitted through a liquid medium, such as the feed solution, alternate compression and expansion cycles of the medium occur. The

compression cycle can cause micro bubbles to collapse, with a release of energy, which causes cleaning of the membrane surface. The collapse of the cavities has sufficient energy to overcome the interaction between the foulant and the membrane and remove the foulant from the membrane surface.

Many studies have been carried out to enhance the solvent permeate flux and clean the membrane using ultrasound treatment [Hruvey {1965; Lenart and Auslander, 1980; Kost and Langer, 1988; Li et al., 1995; Chai et al., 1999] (refer to section 2.3.5.4 and 2.3.4.5]. The above studies provided valuable information on flux enhancement by ultrasonic irradiation, but use of the ultrasonic method and its effectiveness is limited. Online ultrasonic irradiation has low efficiency and high cost. An ultrasonic bath is only useful in laboratory studies because there is a high waste of acoustic energy in the bath during the cleaning process that cannot be tolerated in industrial process.

In the present study, a horn ultrasonic cleaner was employed. Research was focused on the effect of ultrasound on the cleaning of fouled membranes and a comparison of results obtained from cleaning by forwardflushing, ultrasonic cleaning and ultrasound associated with forwardflushing. The operating conditions during cleaning and the effect of online ultrasound on the permeate flux was also investigated.

6.3 EXPERIMENTAL

6.3.1 MF AND ULTRASONIC CLEANING SYSTEMS

Nylon MF membranes (disc Φ 290 mm) made by Pall Ltd., England, with a nominal pore size of 0.2 μm, were used in all of the fouling experiments. The feed solution selected was the effluent from a wastewater treatment plant of the Mondi Kraft mill at Piet Retief, South Africa. This plant has looked for ways for further reduce membrane fouling. The effluent from the paper mill contains breakdown products of lignin and lignosulphonate. The wastewater treatment plant comprised the following processes: pretreatment, dissolved air flotation (DAF), MF and UF. Samples were taken from the DAF product. The characteristics of the effluent are summarized in Table 6.1.

Table 6.1: Characteristics of paper mill effluent[a]

ITEMS	VALUE	ITEMS	VALUE
pH	4.96	Conductivity, μS/cm	5550
Aluminum as Al, mg/l	16	Boron as B, mg/l	2
Calcium as Ca, mg/l	353	Iron as Fe, mg/l	3
Magnesium as Mg, mg/l	27	Sodium as Na, mg/l	908
Potassium as K, mg/l	30	Sulphur as S, mg/l	1075
Bicarbonate as HCO_3, mg/l	98	Nitrate as NO_3, mg/l	50
Chloride as Cl, mg/l	10	M-Alkalinity as $CaCO_3$, mg/l	27.2
Turbidity, NTU	64	Suspended solids (SS), mg/l	6636

[a]This data from Mondi Piet Retief, Mondi Ltd, South Africa.

The flat-sheet MF experimental set-up, shown in Figure 6.1, allows for the accurate control of inlet pressure, retentate flow rate and temperature. In each MF experiment, continuous stirring in the feed tank was provided. The permeate flux was measured by an electrical balance. During the experiments both the retentate and permeate were recycled to the feed tank after flux measurements. Figure 6.1 is also a schematic representation of the ultrasonic cleaning system used. A horn ultrasonic cleaner (Model W-375, Ultrasonics INC.), with a frequency of 20 kHz and a power density of 82.9 W/cm^2, was used in this study. The cross-flow filtration cell was immersed in a water bath during ultrasonic cleaning. The cell was irradiated with the sonicator.

The flat cell had the following specifics: the thickness of the top plate 20 mm, a recess with 90 × 35 ×14 mm on the top plate, and the height of feed channel 2.5-3 mm (See Figure 3.3). The horn transducer was fixed by a rack to clamp so as to maintain the same distance between transducer and cell in each experiment.

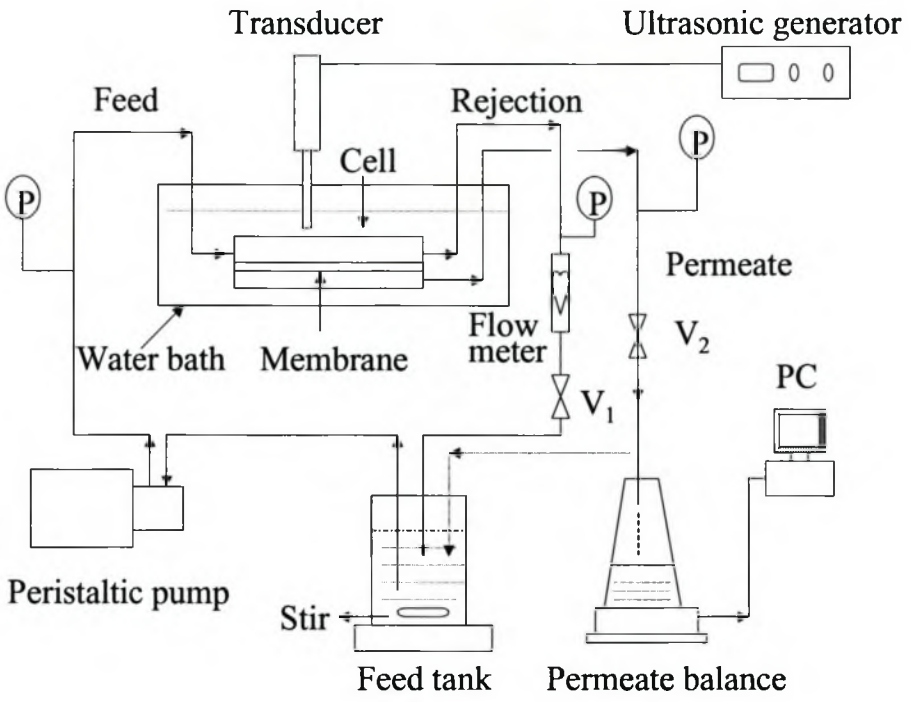

Figure 6.1: Experimental set-up for cross-flow MF and ultrasonic cleaning.

6.3.2 MF FOULING EXPERIMENTS

6.3.2.1 Fouling Experiments

Each experiment commenced with pure water being circulated through the system at a fixed flow rate and applied pressure for about half an hour to compress the membrane and to build up a stable flow field. The flux values for a new, clean membrane, referred to as J_w, were recorded after 30 min of pure water filtration. The pure water was then replaced by effluent. The flow rate of the feed and operating pressure were fixed at 0.125 m/s and 50 kPa, respectively, for the duration of the filtration experiments. The turbidity of the feed and permeate solutions were 64 and 1, respectively.

6.3.2.2 Online Ultrasound

The following experiment was conducted in order to investigate the effect of online ultrasound on the permeate flux during the fouling. The fouling experiment was carried out with a feed of paper mill effluent at 0.125 m/s axial velocity and 50 kPa, after an initial 30 min period of pure water filtration. The sonicator was turned on after fouling filtration for 90 min.

6.3.3 CLEANING EXPERIMENTS

After the membranes were fouled with paper mill effluent, the feed solution was changed from effluent to pure water. The fouled membranes were cleaned by three methods, namely: forward flushing, ultrasonic cleaning, and ultrasound associated with forward flushing. The duration was 10 min. Forward flushing was performed with valve V2 closed. Valve V1 was opened only after the transmembrane pressure differential over the membrane subsided and reached zero, under the pre-determined flushing velocity. Ultrasound associated with forward flushing was performed with intermittent flushing under a pre-determined flushing velocity during ultrasonic irradiation. To investigate the cleaning efficiency of each cleaning method, the cleaned membrane was used to filter pure water under the same operating condition as used during the fouling phase (section 6.3.2).

6.4 RESULTS AND DISCUSSION

6.4.1 EFFECT OF ONLINE ULTRASOUND ON THE FLUX DURING FOULING

Figure 6.2 shows the influence of online ultrasound on the permeate flux. A rapid decline in permeate flux is observed because of the presence and formation of a fouling layer on the nylon membrane surface. A final permeate flux value of 21.45 l/m^2h was reached after 90 min of fouling operation. The flux increased to 28.8 l/m^2h

when the sonicator was turned on for 5 min, then slightly decreased from 28.8 l/m^{2}h to 25.98 l/m^{2}h after ultrasonic irradiation for 30 min.

Figure 6.2 also shows the results of online ultrasonic cleaning for 20 min, after 90 min of fouling operation. Online ultrasonic irradiation can enhance the permeate flux from 21.45 to 29.4 l/m^{2}h. But the flux also slightly decreased from 29.4 l/m^{2}h to 23.04 l/m^{2}h after 30 min of fouling operation under ultrasonic irradiation.

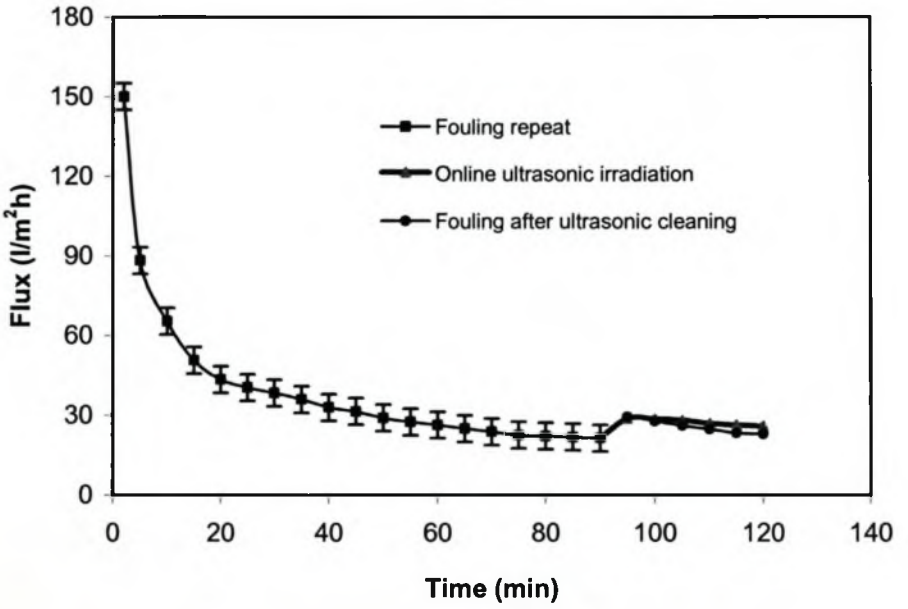

Figure 6.2: Permeate flux change with filtration time during paper effluent fouling experiment in the absence and presence of ultrasound (20 kHz), and fouling again after online ultrasonic cleaning for 20min, after fouling time of 90 min.

Further experiments were carried out with and without ultrasonic irradiation during the paper-mill effluent fouling experiment. Figure 6.3 shows the changes in the permeate flux with and without ultrasonic irradiation. Without ultrasonic irradiation, the flux value declined from an initial 172 l/m^{2}h to 66 l/m^{2}h and 40 l/m^{2}h at 10 and 30 min. On the other hand, when ultrasonic irradiation was used at the beginning of fouling, the flux decline was slower and the flux values obtained were 81 l/m^{2}h and 51

l/m^2h at 10 and 30 min. Results of this experiment suggest that ultrasonic irradiation can enhance the flux during MF. However, no flux difference was found between membrane treated with and without ultrasonic irradiation after 50 min of fouling operation. There may be two reasons why the flux enhancement cannot be obtained over long periods of online ultrasonic treatment. First, the sound energy will decrease because of the increase temperature of the transducer during operation. Second, the agitation due to the ultrasonic irradiation is likely to be complicated by the substantial increase in the number of cavitation nucleation sites generated on the new particle surface. When larger particles exist in the feed (average particle size: 0.947 μm in the paper mill effluent), ultrasound can lead to a reduced flux rate. Presumably the momentum needed to re-suspend these particles is more than that which can be supplied by the application of the ultrasound, and the motion that is imparted to the particles in the fouling layers cause them to 'jostle' and pack more densely [Tarleton and Wakeman, 1992].

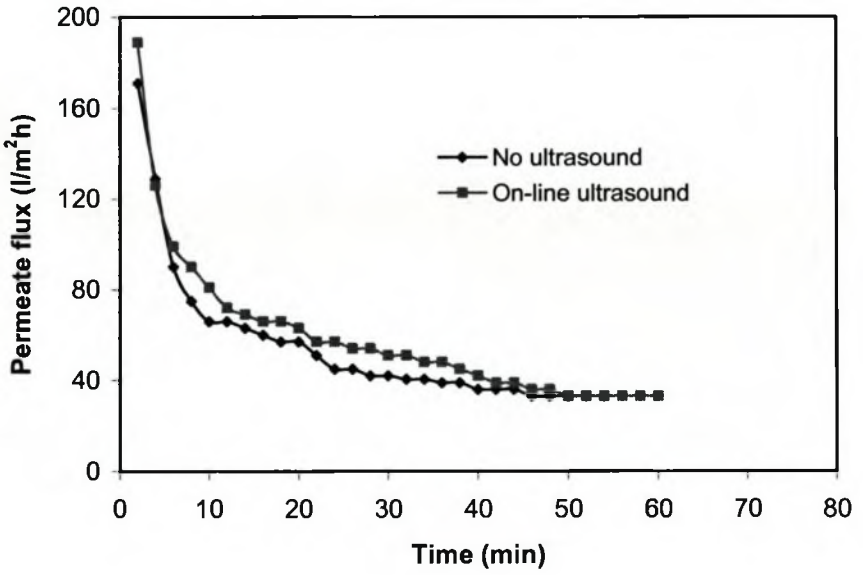

Figure 6.3: Changes in the permeate flux with and without ultrasonic irradiation during paper effluent fouling experiment at 50 kPa and 0.125 m/s.

6.4.2 RECOVERY OF FLUX BY DIFFERENT CLEANING METHODS

The effect of membrane cleaning was investigated by three different cleaning methods: forward-flushing, ultrasonic cleaning and ultrasound associated with forward-flushing. To compare the efficiencies of these methods, nylon membranes were fouled, under the same conditions, with effluent fouled by the DAF product from the paper industry, after pure water filtration. Each cleaning process was then applied, individually, for 10 min, after 80 min of fouling operation. These nylon membranes were used to filter pure water, under the same conditions and their permeate fluxes determined. A graphical representation of permeate flux versus time is shown in Figure 6.4.

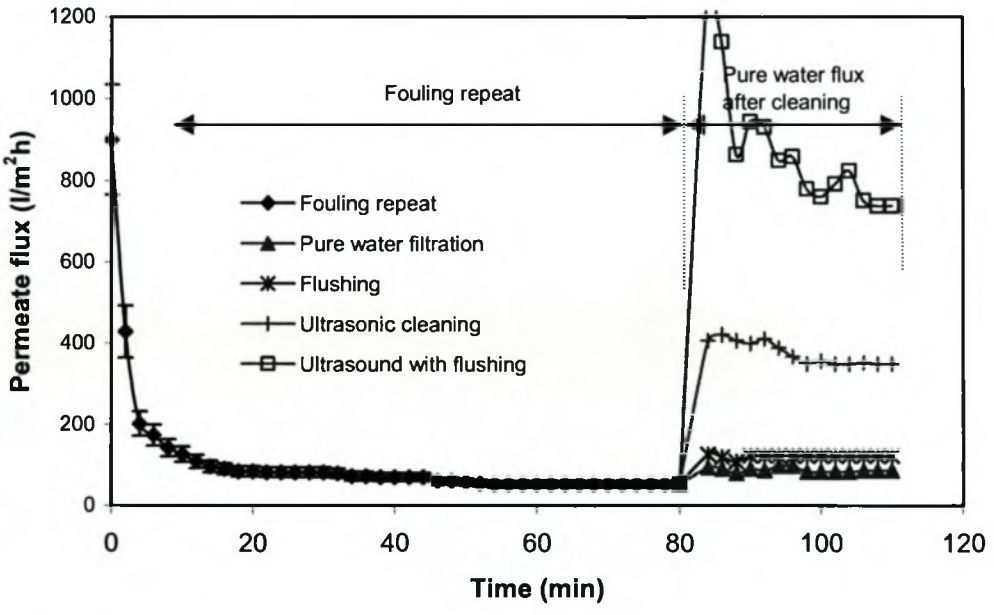

Figure 6.4: Effect of different cleaning methods on the water flux through a membrane after 80 min of fouling operation by paper-mill effluent: water filtering, forward-flushing, ultrasonic cleaning and ultrasound with forward-flushing.

At the beginning of fouling operation the permeate flux declined rapidly, followed by a more gradual decline after 20 min fouling (Figure 6.4). The permeate flux was 52.8 l/m^2h after an 80-min fouling period. When the feed was changed from the effluent to pure water, the permeate flux increased to 86.4 l/m^2h after 30 min of pure water filtration, because of a reduction in concentration polarization. Forward-flushing increased the water permeate flux from 86.4 l/m^2h to 122.4 l/m^2h after 110 min of operation. An increase in the water permeate flux was observed after ultrasound cleaning. It is suggested that ultrasonic irradiation can effectively clean membrane fouling in MF. The value of 350 l/m^2h at 30 min of pure water operation obtained after ultrasonic cleaning was however still lower than the original water flux of 900 l/m^2h. Hence, ultrasound associated with forwardflushing was applied in an effort to restore the permeate flux of the membrane. The water permeate flux of the membrane cleaned by ultrasound with forwardflushing was 738 l/m^2h at 30 min of pure water operation. In this case results showed that ultrasound associated with flushing was the most effective of the cleaning methods investigated.

In an effort to obtain a better understanding of the fouling and cleaning processes we calculated the various resistances of the membrane during the fouling and cleaning procedures. The permeate flux during MF is usually written in terms of transmembrane pressure difference (ΔP) and a total resistance, according to the resistance model [Jiraratannon and Chanachai, 1996; Mulder, 1991]:

$$J = \Delta P/(\mu R_t) \qquad (6.1)$$

where J = permeate flux of solution (m/s), ΔP = transmembrane pressure difference (kPa), R_t = total resistance (m^{-1}) and μ = viscosity of permeate solution (Pa.s). The viscosity of the paper effluent in the experiments was measured to be 1.02×10^{-3} Pas at 20 °C. In this study, the total resistance R_t is defined as

$$R_t = R_m + R_r + R_f \qquad (6.2)$$

where R_m, the resistance of new or clean membranes, can be calculated from Equation 6.1, written for pure water, i.e.

$$J_w = \Delta P/(\mu_w R_m) \quad (6.3)$$

where *Jw* is the pure-water permeate flux for a new membrane (m/s) (at 30 min of pure water operation in here); μ_w is the viscosity of pure water (Pas). R_r is a reversible resistance i.e. particle polarization, cake layer, R_f is a fouling resistance, an irreversibly adsorbed layer which cannot be removed by water cleaning. R_r is removed by cleaning the membrane with water at a low flow rate (<12.5 cm/s). The water flux measured after different cleaning methods is J'_w. Therefore,

$$R_m + R_f = \Delta P/(\mu_w J'_w) \quad (6.4)$$

Each resistance can be calculated using the experimental data and Equations 6.1 to 6.4.

Table 6.2: Various resistances *R* ($\times 10^{12}$ m^{-1}) and their percentages during fouling

Resistances	R ($\times 10^{12}$ m^{-1})	%
R_m	0.4	6
R_r	2.33	34.9
R_f	3.95	59.1
R_t	6.68	100

Note: R_m, the resistance of new or clean membranes; R_r, a reversible resistance; R_f, fouling resistance; R_t, total resistance.

Table 6.2 shows various resistances and their percentages during fouling. The membrane resistance was 6 % of the total resistance. Therefore, the main resistances of the fouled membrane were R_r and R_f. This is because concentration polarization and fouling layers appeared on the membrane surface during fouling. The reversible resistance, R_r, is 34.9% of the total resistance. It is known that changing operating conditions or using flow destabilization can reduce reversible resistance, enhance the mass transfer coefficient and increase permeate flux. Fouling resistance, R_f, is 59.1 %

of the total resistance. R_f was 1.7 R_r, meaning that fouling was the main cause of the decrease in permeates flux in MF.

To compare the effectiveness of these cleaning methods, the cleaning efficiency E_c was defined as follows:

$$E_c\,(\%) = (R_f - R_c) / R_f \times 100 \qquad (6.5)$$

where R_f and R_c represent the resistance (m^{-1}) of fouling layer and residual fouling layer, respectively. (This allows R_c to be zero for a perfect clean and gives E_c = 100%.) R_c was calculated from Equation 6.4. Table 6.3 shows R_c and E_c for each cleaning method. It is seen that flushing can decrease the fouling resistance by only 8.8%. It is suggested that paper effluent fouling is difficult to clean using only water cleaning or flushing. In this case, membrane fouling is caused by the adsorption of foulant both on and inside the membrane. This membrane fouling is irreversible and additional cleaning methods are needed.

Ultrasonic cleaning is an effective method to decrease membrane fouling in MF. It was determined that ultrasonic irradiation can reduce the fouling resistance by 84%. Under similar conditions, the cleaning efficiency of ultrasound associated with flushing was 97.8%. This suggests that both procedures are necessary to completely remove the foulant from a membrane. It is known that in many liquids high-energy ultrasound (a horn transducer with a frequency of 20 kHz and a power density of 82.9 W/cm^2 in this study) produces observable effects such as caviatation, the rapid movement of fluid caused by variations of sonic pressure, and micro-streaming [Wakeman and Tarleton, 1991].

Table 6.3: The resistance of the residual fouling layer R_c ($\times 10^{11}$ m^{-1}) and cleaning efficiency E_c (%) of different cleaning methods

Cleaning methods	R_c ($\times 10^{11}$ m^{-1})	E_c (%)
Flushing	36	8.8
Ultrasound	6.3	84
Ultrasonic flushing	0.88	97.8

6.4.3 SEM MICROSCOPY

To further investigate the effect of different cleaning methods on the fouling layer of a nylon membrane, Figure 6.5 shows SEM micrographs of new, fouled and cleaned MF membranes. The image of a new membrane surface (Figure 6.5a) shows the typical membrane surface structure, including the membrane pores. Figure 6.5b shows that after 80 min of operation, only some larger pores remained partially unblocked. Inductively coupled plasma analysis showed that the main chemical composition of the fouling layer is breakdown products of lignin or lignosulphonate [Domingo, 2001].

The surface of the fouled membrane appeared to have more pores after forward flushing (Figure 6.6 a). This result indicated that forward flushing could partly reduce fouling resistance. It was, however, difficult to remove all fouling matter by flushing alone. Ultrasonic irradiation can loosen, break and disperse the fouling layer because of ultrasonic cavitation and acoustic streaming (Figure 6.6 b). Hence, the permeate flux increased after ultrasonic cleaning although some fouling still remained on the membrane surface. The clear pore structure of the cleaned membrane (Figure 6.5) was seen again after ultrasound with forward flushing because this method can completely remove the fouling from the membrane surface.

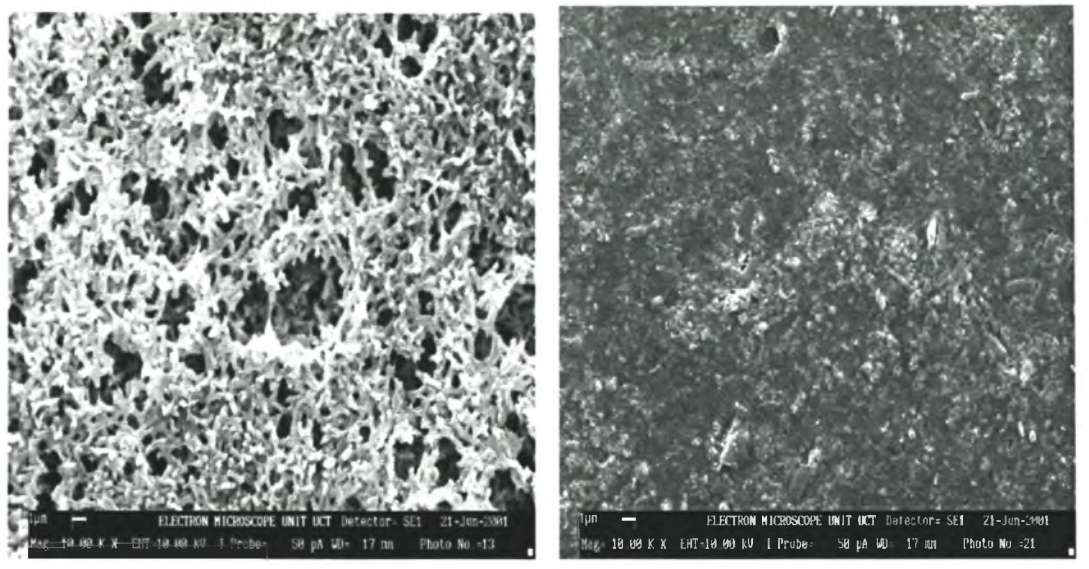

(a) (b)

Figure 6.5: SEM micrographs of nylon membranes: (a) new membrane; (b) fouled membrane, magnification 20,000×.

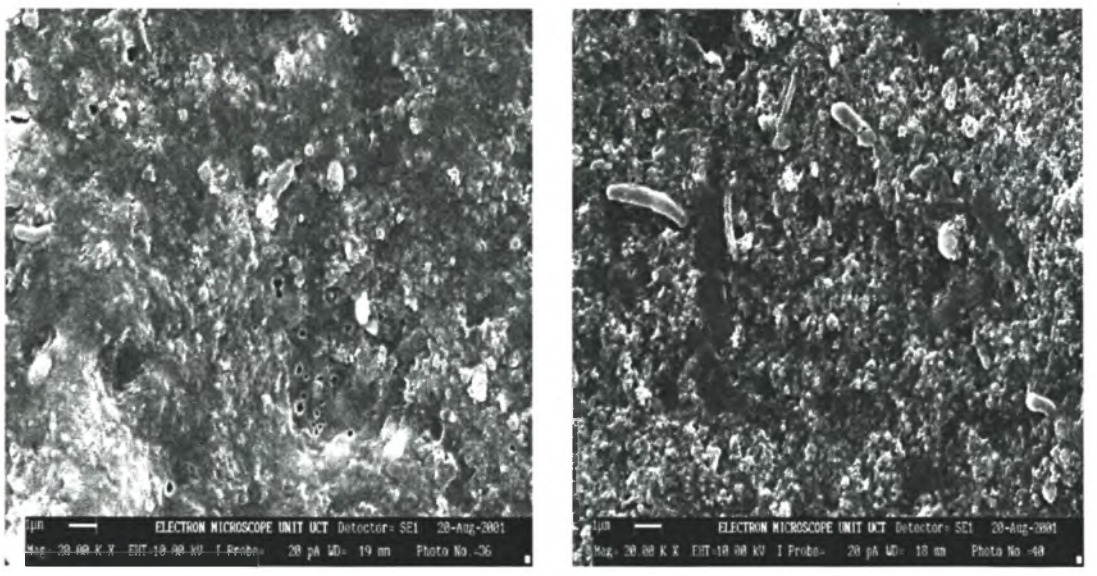

(a) (b)

Figure 6.6: SEM micrographs of nylon membranes cleaned by (a) forward flushing; (b) ultrasonic irradiation, magnification 20,000×.

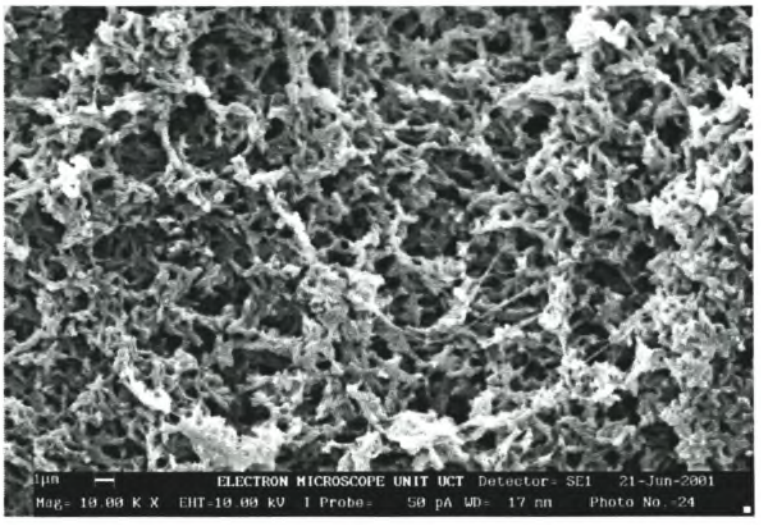

Figure 6.7: SEM micrographs of nylon membrane cleaned by ultrasonic forwardflushing, magnification 20,000×.

6.4.4 EFFECT OF DIFFERENT CROSSFLOW RATES DURING ULTRASONIC IRRADIATION

Fouling involves the accumulation and compaction of retained material at a membrane surface, while the solvent (water) passes through the pores. The deposited fouling layer is expected to become re-suspended and swept away by tangential- or cross-flow [Perusich and Alkire, 1991]. So, the different forward-flushing velocities resulted in different cleaning efficiencies.

The effect of different forwardflushing velocities with ultrasonic irradiation is shown in Figure 6.8. Forwardflushing slightly increased the water permeate flux (compared with water flow) even when the velocity was increased from 0.21 to 0.56 m/s. This indicated that a fouling layer accumulated and compacted on/within the membrane surface and that it was difficult to clean it and sweep it away by the forwardflushing method only. Figure 6.8 also shows that ultrasound with forwardflushing can apparently enhance water permeate flux, as the forwardflushing velocity increased

from 0.21 to 0.56 m/s under ultrasonic irradiation. This is because of the effectiveness of ultrasound and forwardflushing. The forwardflushing produces a high tangential or cross-flow rate on fouling layers as the forwardflushing velociy increases.

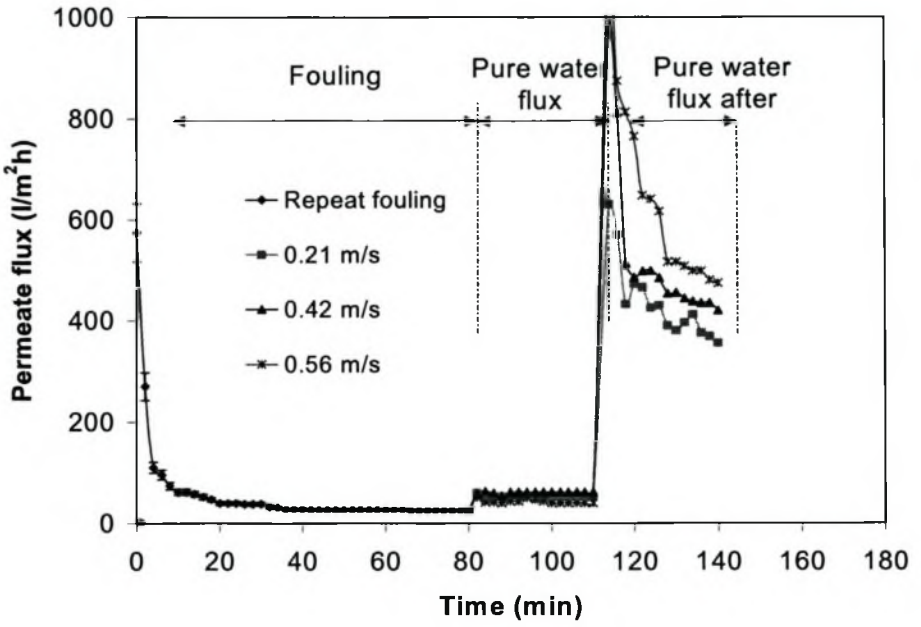

Figure 6.8: Effects of different forward flushing velocities on the recovery of permeate flux.

Note: The water filtration is used for cleaning and examining the recovery of permeate flux after an 80 min fouling period at the same pressure and flow rate as used in the fouling phase.

6.4.5 EFFECT OF DIFFERENT CLEANING TEMPERATURES ON FLUX

Since temperature influences the cleaning efficiency of ultrasound [Zhu and Liu, 2000], the cleaning performance of flushing under ultrasound was examined at different cleaning temperatures. Nylon membranes were again fouled for 80 min, then cleaned by ultrasound associated with forward flushing (velocity: 0.4 - 0.5 m/s) at temperatures of 23, 30 and 40°C, for 10 min. The pure water fluxes of the cleaned membranes were determined under the same operating conditions.

Figure 6.9 shows the changes in the permeate fluxes during fouling and after cleaning. It is seen that the water permeate flux of the nylon membrane decreases as the cleaning temperature increases from 23 to 40°C. Firstly, this is due to a change in the ultrasonic cavitation intensity as the temperature decreases [Zhu and Liu, 2000]. Ultrasonic cleaning of the MF membrane is mainly caused by ultrasonic cavitation and the acoustically excited bubble break-ups on the membrane surface. An increase in solution temperature gives rise to an increase in the vapor saturation pressure in the bubble so that the shock-wave intensity during the bubble break-up is reduced. In other words, the cavitation effectiveness decreases. Secondly, the fluid viscosity also changes with temperature and could have caused the change in ultrasonic effectiveness. An increase in the viscosity of a liquid will result in an increase in the threshold of cavitation [Mason, 1989]. There will probably be several different types of cavity in the liquid: (a) an empty cavity (true cavitation), (b) a vapour-filled cavity, (c) a gas-filled cavity, and (d) a combination of vapour and gas filled cavities. A lower temperature favours the formation of empty cavities.

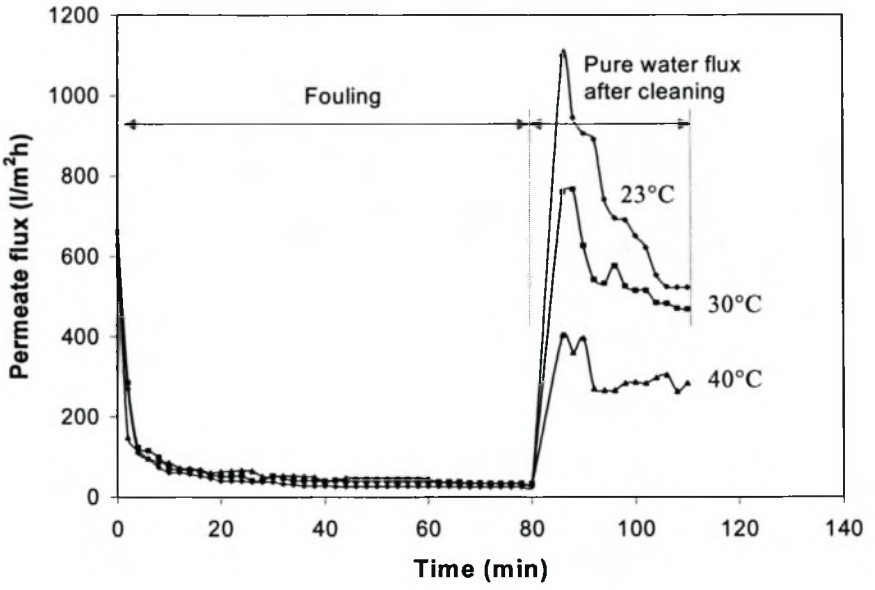

Figure 6.9: Effects of different temperatures under ultrasound on the recovery of permeate flux.

6.5 SUMMARY

This study described the effect of ultrasound on the cleaning of nylon MF membranes. Nylon membrane were fouled by pulp paper effluent and cleaned by the methods of forward flushing, ultrasonic cleaning and ultrasound associated with forward flushing. The cleaning efficiencies were determined by pure water flux comparisons.

Experimental results showed that ultrasound associated with flushing was the most effective of these cleaning methods. Cleaning by this method cleaned fouled membranes and restored the original membrane morphology. Resistance analysis indicated that the cleaning efficiencies of ultrasonic cleaning and ultrasound with forward flushing were 87% and 97.8%, respectively. It was also found that high forward flushing velocity combined with ultrasound was also beneficial for cleaning.

To be effective, the flushing velocity should be greater than the normal operating velocity. At different cleaning temperatures, under ultrasonic irradiation, the pure water flux increased as the cleaning temperature decreased from 40 to 23°C.

These findings indicate that placing an ultrasonic generator on an operating plant would be costly and inefficient, but removing modules and cleaning them individually in an ultrasonic bath would preclude purchasing new modules, as irreversible fouling can be removed to 97.8%.

CHAPTER 7

MEASUREMENT OF CAKE-LAYER DEPOSITION, GROWTH, COMPRESSIBILITY AND ITS REMOVAL IN MICROFILTRATION

7.1 SCOPE OF THIS CHAPTER

Further investigation of cake-layer deposition, growth and compressibility in MF by UTDR was required. The study was carried out with paper mill effluent from a wastewater treatment plant. Nylon membranes Nylon MF membranes with a nominal pore size of 0.2 μm, were used in all of the fouling experiments.

Ultrasonic response signals were recorded as particles deposited and a cake layer formed on a nylon membrane surface. The ultrasonic testing technique can measure the cake thickness as a function of time. Results also showed that the ultrasonic unit is a suitably programmed microprocessor, and can be used to compare reference and test waveforms. It produced a separated signal (from reference and test waveforms), indicating the state and progress of the cake layer on the membrane surface under operating conditions.

A predictive modelling program - ultrasonic reflection modelling (URM) was developed, to better understand the processes related to the deposition of cake layers on the membrane surface. The modelling program can predict the shape of the curve of the ultrasonic wave at the beginning of the signals, indicating the cake compressibility. In MF, the flux decline is related to not only the layer thickness but also the cake density (compressibility). The changes in the densities of cake layers as well as the thicknesses can be substantiated by the modelling. The predicted results were in good agreement with the actual measurements.

7.2 INTRODUCTION

Cross-flow microfiltration is an increasingly important technique for processing particulate suspensions in areas such as biotechnology, water and wastewater treatment, and food and mineral processing [Tanny et al., 1982; Treffry-Goatley et al., 1987; Ginn et al,. 1997; Cheryan, 1998]. It is generally recognized that one of the major problems associated with the more widespread use of microfiltration systems is the significant flux decline during operation. This is as a result of particle deposition and the build-up of a filter cake on the surface of a septum or a membrane.

A variety of theoretical models quantitatively describing the fouling phenomenon during microfiltration have been developed [Vyas et al. 2001]. These can be classified mainly into: (1) resistance models, including the standard blocking model [Hermia, 1982]; the cake filtration model [Persson and Nilsson, 1991]; blocking law [Persson and Nilsson, 1991] and the resistance in series model [Persson et al, 1993]; (2) particle back-transport models, including Brownian diffusion [Green and Belfort, 1980]; shear-induced diffusion [Zydney and Colton, 1986] and inertial lift [Altena and Belfort, 1984]; (3) flowing cake and surface transport models [Vyas et al. 2001].

The compressible cake filtration model describing the filtration behaviour of particulate suspensions is applicable to cross-flow microfiltration [Shirato et al. 1969, Tiller, 1975; Murase et al. 1995; Tiller and Kwon, 1998; Tiller and Li, 2001]. From practical experience, it is acknowledged that flow through compressible cakes composed of deformable particles results in a highly non-uniform structure, with a tight skin layer of very low porosity next to the supporting medium. This skin layer often has adverse effects, such that, increasing the filter pressure has little effect on the flow rate or average porosity. This usually results in an erroneous prediction of the filtration rate if a rigid particle cake is assumed when using the conventional cake filtration theory. Therefore, various theoretical models to describe concentration polarization and to predict the filtration rate during crossflow filtration are based upon the assumption of the incompressibility of the fouling layer and the rigidity of suspensions [Altena and Belfort, 1981; Zydney and Colton, 1986; Davis and Leighton,

1987; Romero and Davis, 1990; Blake et al. 1992]. Although these models are able to quantitatively predict the steady-state flux for some types of particles, they provide no detailed information about how the skin layer is formed on the filter septum/membrane because of the unavailability of a suitable non-destructive measurement technique to measure fouling build-up in real-time.

Most crossflow microfiltration studies have typically been limited to measurements of filtrate flux alone because cake thickness information was not available. Over the last ten years, numerous methods have been used to study cake deposition and characterization so as to infer the possible mechanisms. The numerous experimental methods used to measure cake layer thickness can be classified into two broad categories: destructive [AI-Malack and Anderson, 1996; Schmidt and Löffeler, 1990; Vyas et al. 2000] and non-destructive measuring methods [Tiller et al. 1995; Wakeman, 1994; McDonogh et al. 1995; Li and Fane, 1998; Mores and Davis, 2001]. Destructive measuring methods include bake weighting [AI-Malack and Anderson, 1996], freeze slicing [Schmidt and Loffeler, 1990] and reconstruction of the cake layer [Vyas et al. 2000]. Although these destructive measuring methods can measure cake thickness and porosity, they provide little information regarding the actual and dynamic build-up of the cake on the membrane surface.

Methods used to try to non-destructively measure or monitor cake thickness as a function of time have included nuclear magnetic resonance spectroscopy (NMR) [Wandelt et al.1992; La Heij et al. 1996], CATSCAN [Tiller et al. 1995], optical laser beam [Altmann and Ripperger, 1997], optical methods [Hamachi and Mietton-Peuchot, 1999; Tung et al. 2001; Mores and Davis, 2001; Lu et al. 2002; McDonogh et al. 1995], photography [Mackley and Sherman, 1992; Wakeman, 1994; Li et al. 1998], X-ray [Bierck et al. 1988; Bierck and Dick] ultrasonic imaging and reflectometry [Hutchins and Mair, 1989; Haerle and Haber, 1993].

The present study aims to contribute to a further understanding of the ultrasonic response signals including differential signals obtained and the deposition, growth and compressibility of a cake layer on the membrane surface. A predictive modelling program - ultrasonic reflection modelling (URM) was developed, to better understand the processes related to the deposition of cake layers.

7.3 EXPERIMENTAL

7.3.1 MF SYSTEM AND ULTRASONIC MEASUREMENT

In this study investigations were carried out into a MF separation system that is the same as that in Section 5.3.1 (Figure 5.1). The ultrasonic measurement system, flat-sheet module and nylon MF membrane used are also the same as those in Section 5.3.1. The feed was taken from the wastewater treatment plant of Mondi Kraft Mills, Mondi Ltd, South Africa. The characteristics of the effluent are summarized in Table 6.1

7.3.2 EXPERIMENTAL PROCEDURE AND FOULING

The MF experimental set-up (Figure 5.1) allows for the accurate control of inlet pressure, retentate flow rate and temperature. Each experiment commenced with pure water being circulated through the system at the desired flow rate and applied pressure, for 2 h, to compress the membrane and to build up a stable flow field. Once steady state was attained, the feed was switched to the effluent solution to initiate the fouling phase in which fouling occurred. This phase was allowed to continue until the ultrasonic response and permeate flux had stabilized. The fouling experiment was carried out at flow rates of 1.83 ± 0.02 cm/s (Re = 65 ± 0.7) and 6.97 ± 0.07 cm/s (Re = 253 ± 2.5), applied pressure 150 ± 5 kPa and temperature 24 ± 1°C. All runs were made in the laminar flow regime with Re < 400. The total operating time for the fouling experiments was about 7-18 h, depending upon the specific axial velocity employed.

7.3.3 CLEANING EXPERIMENT

To investigate the suitability of the UTDR technique for fouling removal strategies, the following fouling and cleaning experiments were carried out. A new fouling experiment was carried out with paper mill effluent at a flow rate of 4.2 ± 0.05 cm/s (Re=150 ± 1.5), applied pressure 100 ± 5 kPa and temperature 24 ± 1°C. The total

operating time for the fouling experiments was 16 h. After the membranes were fouled with paper effluent they were cleaned by three methods, in turn, namely: forward flushing, ultrasonic cleaning and ultrasound together with forward flushing for cleaning times of 20 min each. The feed solution was changed from effluent to pure water filtration at the same operating conditions as used in the fouling phase in order to compare the cleaning efficiencies of these three methods.

In Figure 6.1, forward flushing was performed with valve V1 opened and V2 closed. The cross-flow filtration cell was immersed in a water bath at temperature 24 ± 1°C during ultrasonic cleaning. The cell was irradiated with a horn ultrasonic cleaner (Medal W-375, Ultrasonics INC.) with a frequency of 20 kHz and a power of 375 w. Ultrasound associated with forward flushing was performed with intermittent forward flushing with a flow rate (40-50 cm/s) during ultrasonic irradiation. To investigate the cleaning efficiency of each cleaning method, the cleaned membrane was used to filter pure water under the same operating condition as used in the fouling phase. The UR measuring system captures the changes in ultrasonic signal responses after different cleaning methods. These data can be stored on a computer's hard drive.

7.4 RESULTS

7.4.1 CROSSFLOW MF AND ULTRASONIC MEASUREMENTS

The pure water filtration was carried to investigate the resolution capabilities of the UR technique and obtain pure water flux of the membrane and reference waveform inside the cell during the steady state. Figure 7.1 plots the ultrasonic signal amplitude in volts (V) vs. the arrival time in seconds (s) inside the cell. Each peak corresponds to a reflected acoustic wave from one of the multiple interfaces in the flat cell. Note: Peak A is a reverse signal because the sound wave travels from high impedance Perspex ($W_{perspex}$ = 2.4 kg/m^{2}s) to low impedance water (W_{water} = 1.0 kg/m^{2}s). The UR measurement was focused on at the front of Peak B, which indicates the membrane surface.

Changes in flux with operation time at velocities of 1.83 and 6.97cm/s are summarized in Figure 7.2.

The UTDR echo signals during the fouling experiments at 1.83 cm/s are shown in Figures 7.3 and 7.4. Peaks B, B' and C were generated from the interfaces: water/nylon membrane, cake layer/nylon membrane and feed/cake layer. Morphological characterisation of the fouled membrane is shown in Figure 7.5.

Results of the UTDR responses during the fouling experiments at 6.97 cm/s are shown in Figures 7.6 - 7.8. A new echo (Peak C) appeared after 5 h of fouling operation at 6.97 cm/s (see Figure 7.7a). As fouling layer growth progressed, an increase in echo amplitude was observed in Figures 7.7 and 7.8. SEM analysis showed complete membrane coverage with the cake layer in Figure 7.9. The cross-section showed the dry fouling layer and membrane thicknesses to be 40 μm and 90 μm (Figure 7.9d).

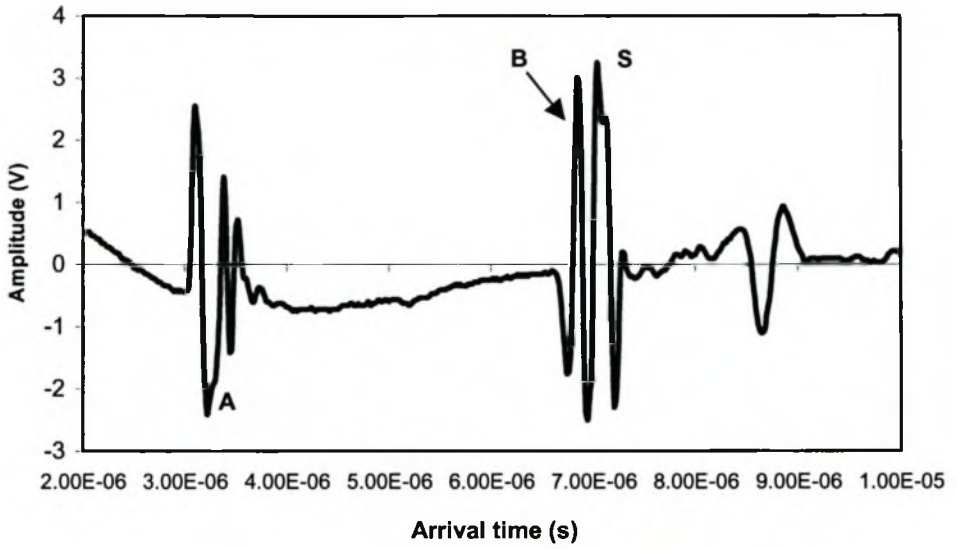

Figure 7.1: Ultrasonic spectrum inside the flat sheet cell during pure water filtration at operating pressure of 150 kPa.

Note: Peaks A, B and S were generated from the following interfaces: perspex plate/feed (water), water/nylon membrane and membrane/porous metal support.

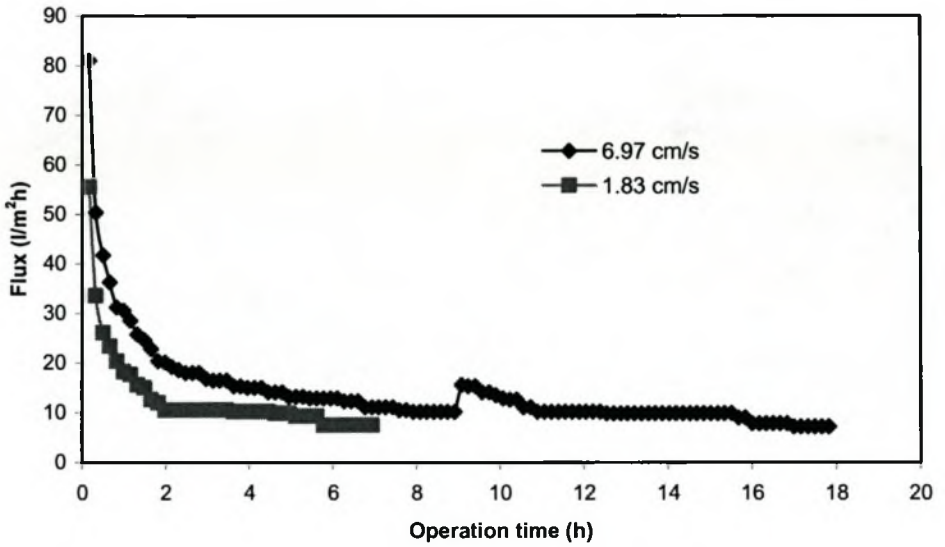

Figure 7.2: Flux decline with time in the paper mill effluent fouling experiment at flow rates of 1.83 and 6.97cm/s (stop & restart of the fouling operation at 9 h).

Ultrasonic responses:

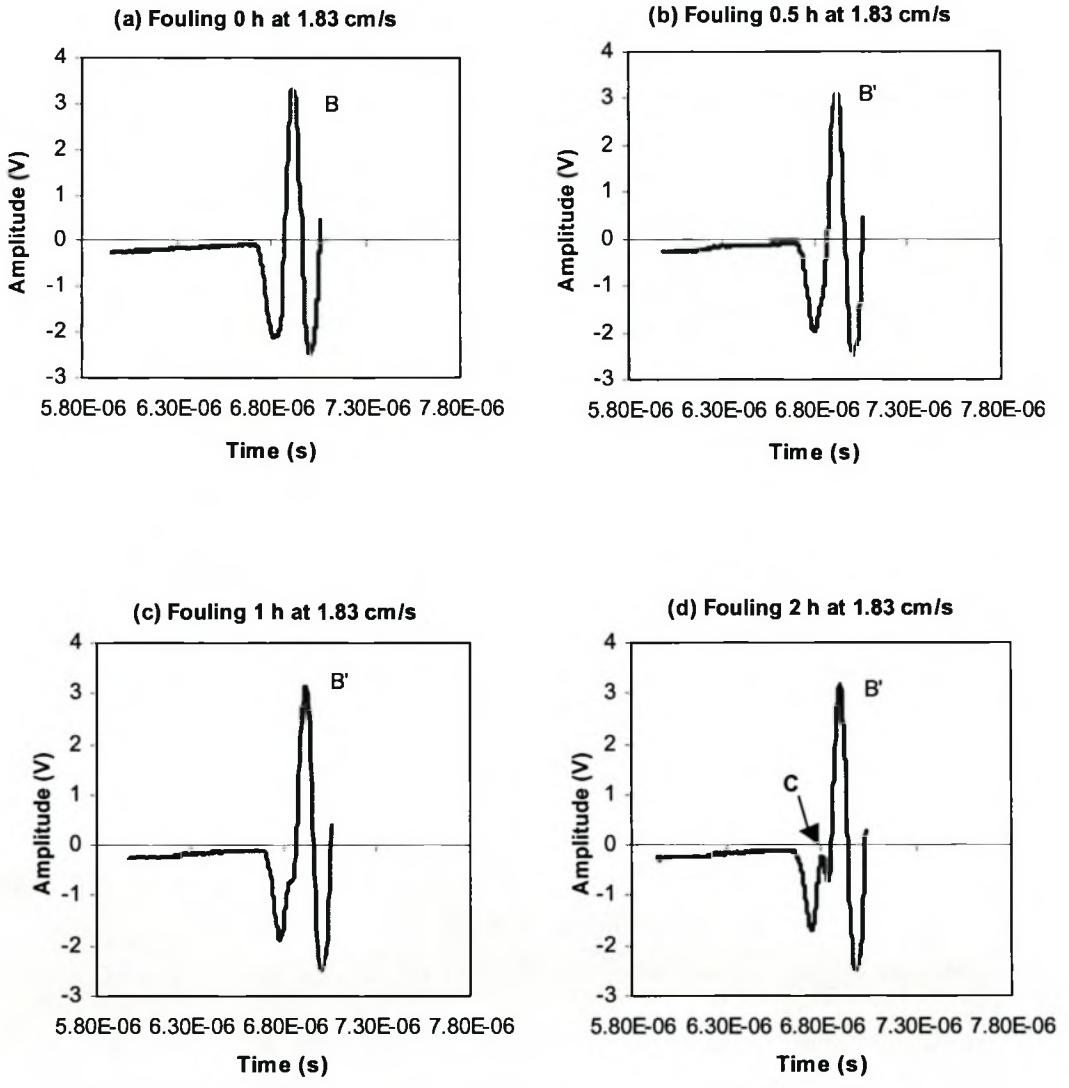

Figure 7.3: Ultrasonic responses (a) at 0 h (start), (b) after 0.5 h, (c) 1 h and (d) 2 h of operation in the fouling experiment carried out with paper mill effluent at a flow rate of 1.83 cm/s.

Note: Peaks B, B' and C were generated from the interfaces: water/nylon membrane, cake layer/nylon membrane and feed/cake layer.

Ultrasonic responses

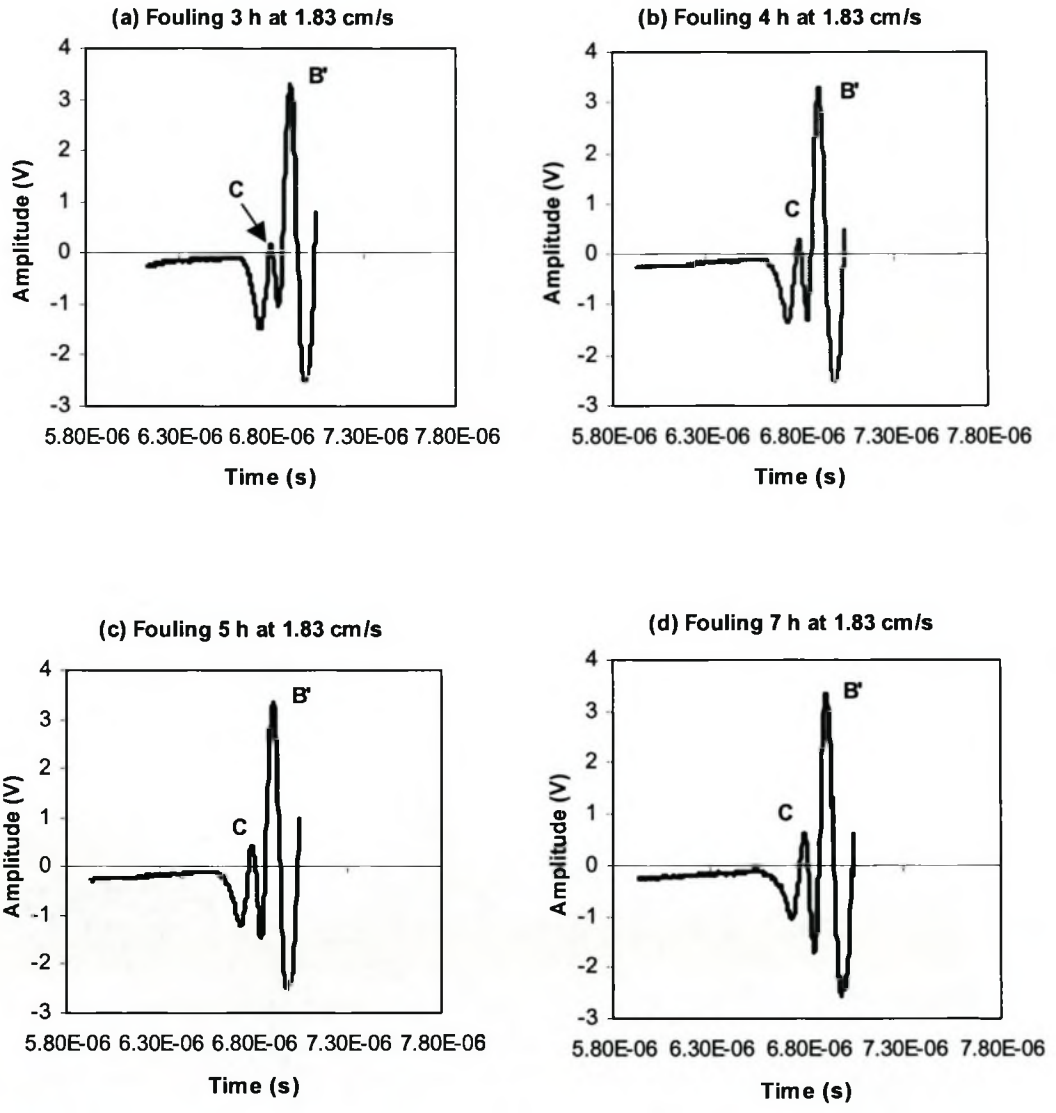

Figure 7.4: Ultrasonic responses after (a) 5 h and (b) 7 h of operation in the fouling experiment carried out with paper mill effluent at a flow rate of 1.83 cm/s.

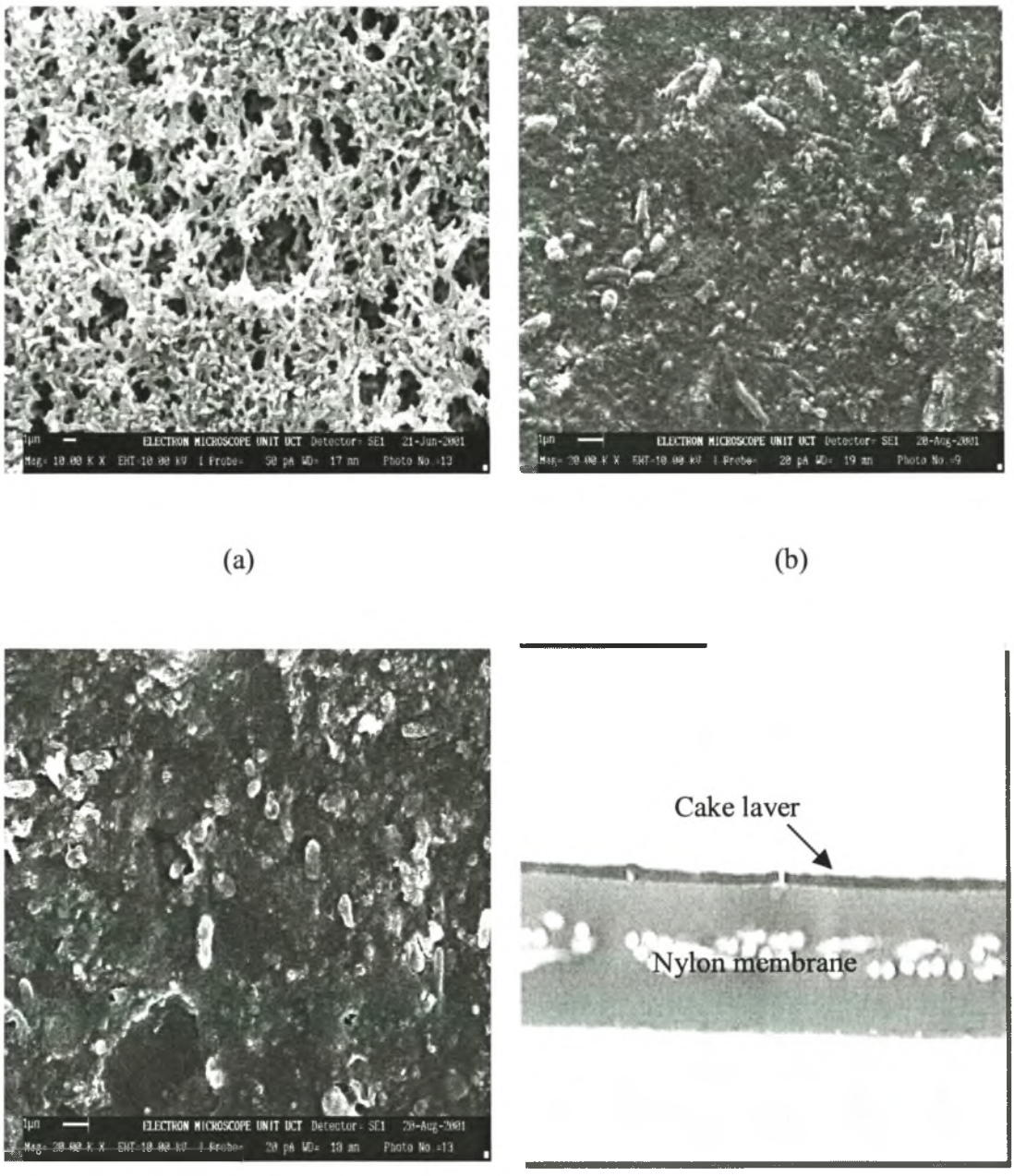

(a) (b)

(c) (d)

Figure 7.5: SEM micrographs of the nylon membrane surfaces: (a) clean nylon membrane; fouled membranes after (b) 2 h and (c) 7 h of fouling operation; (d) optical micrograph: cross-section of nylon membrane fouled by paper mill effluent (1.83 cm/s, 150 kPa), magnification 100 ×.

Ultrasonic responses

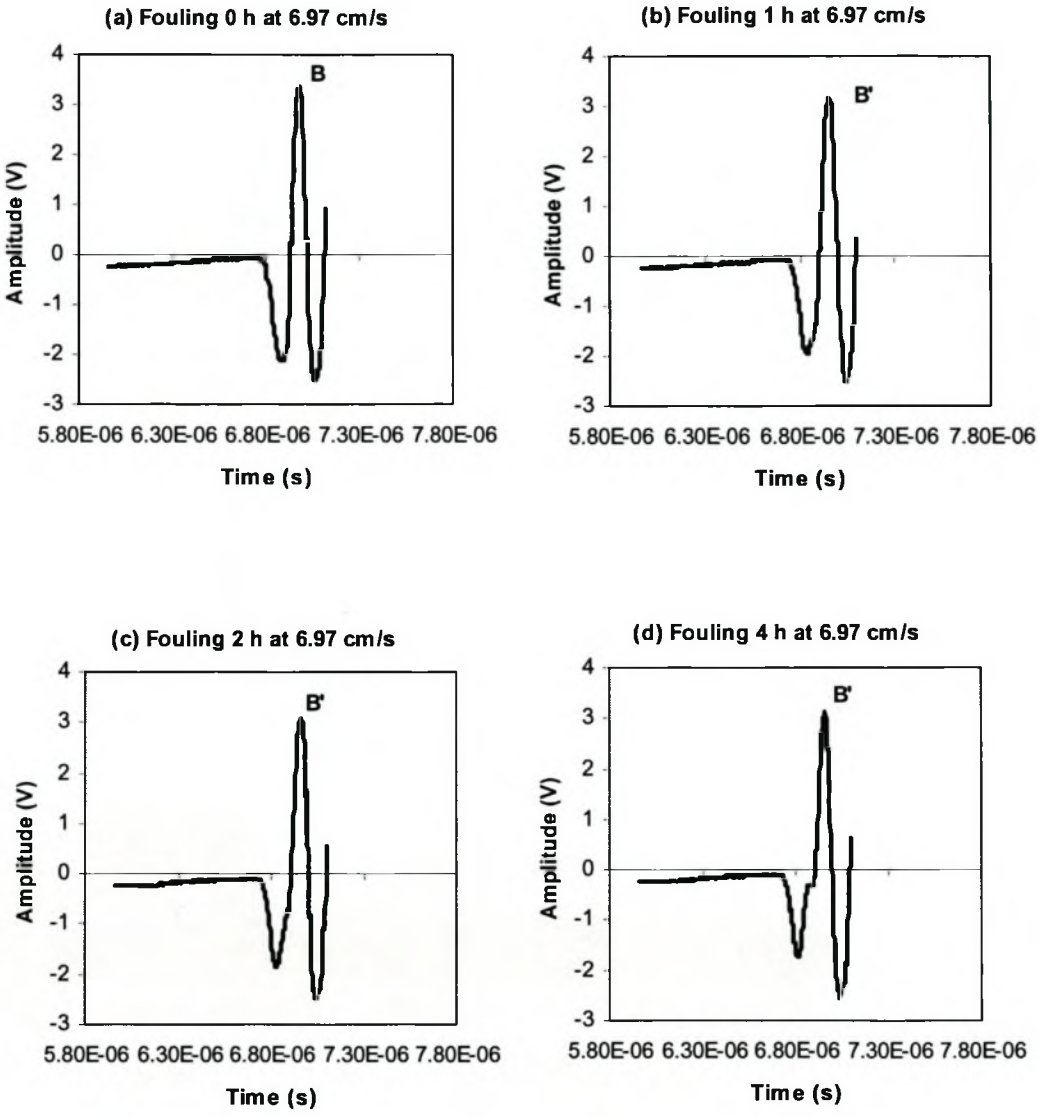

Figure 7.6: Ultrasonic responses at (a) 0 h, after (b) 1 h, (c) 2 h and (d) 4 h of operation in the fouling experiment carried out with paper mill effluent at a flow rate of 6.97 cm/s.

Note: Peaks B and B' were generated from the interfaces: feed (water)/nylon membrane, fouling/nylon membrane.

Ultrasonic responses

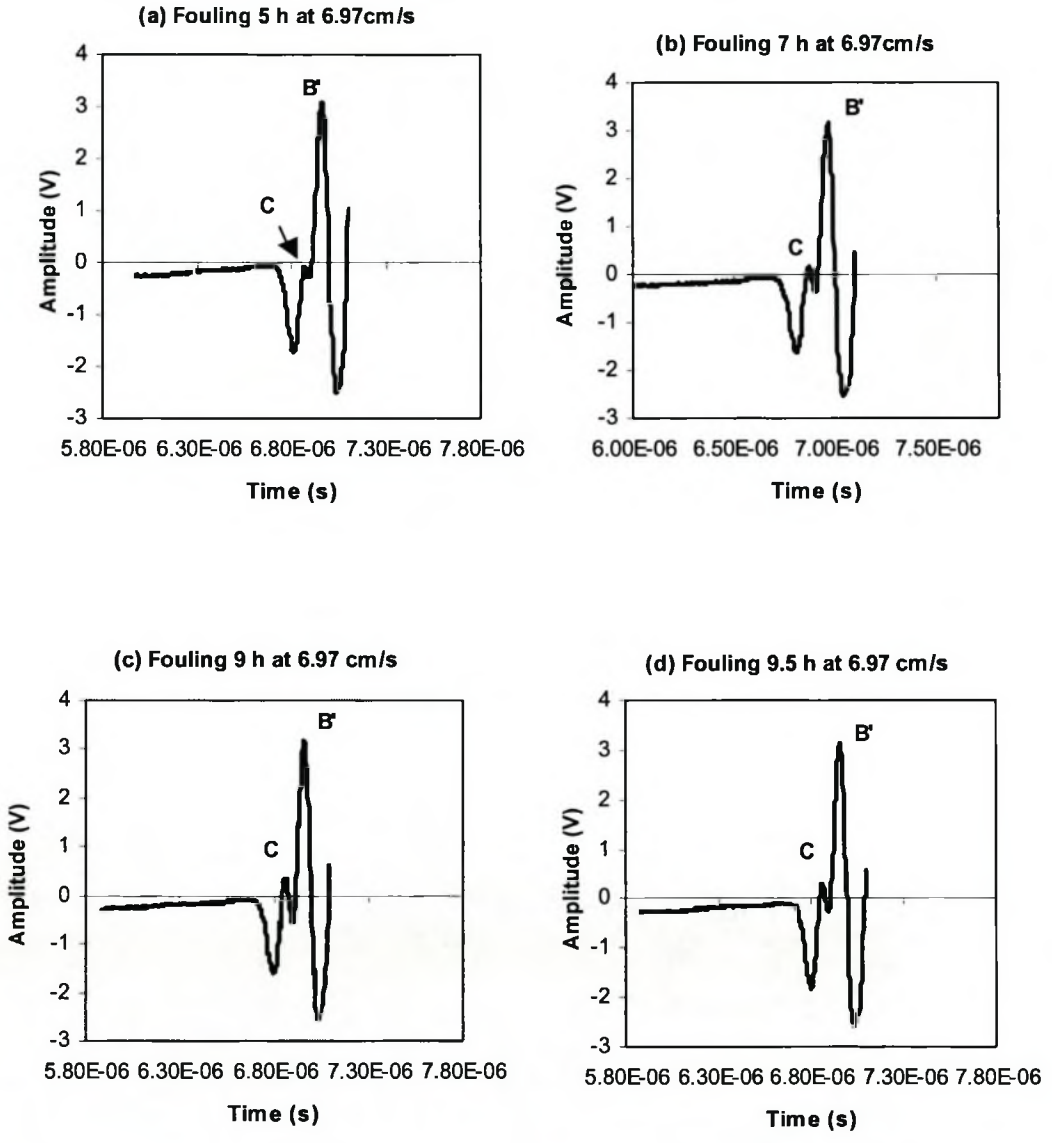

Figure 7.7: Ultrasonic responses after (a) 5 h, (b) 7 h, (c) 9 h and (d) 9.5 h of operation in the fouling experiment carried out with paper mill effluent at a flow rate of 6.97 cm/s.

Note: Peaks B, B' and C were generated from the interfaces: water/nylon membrane, cake layer/nylon membrane and feed/cake layer.

Ultrasonic responses

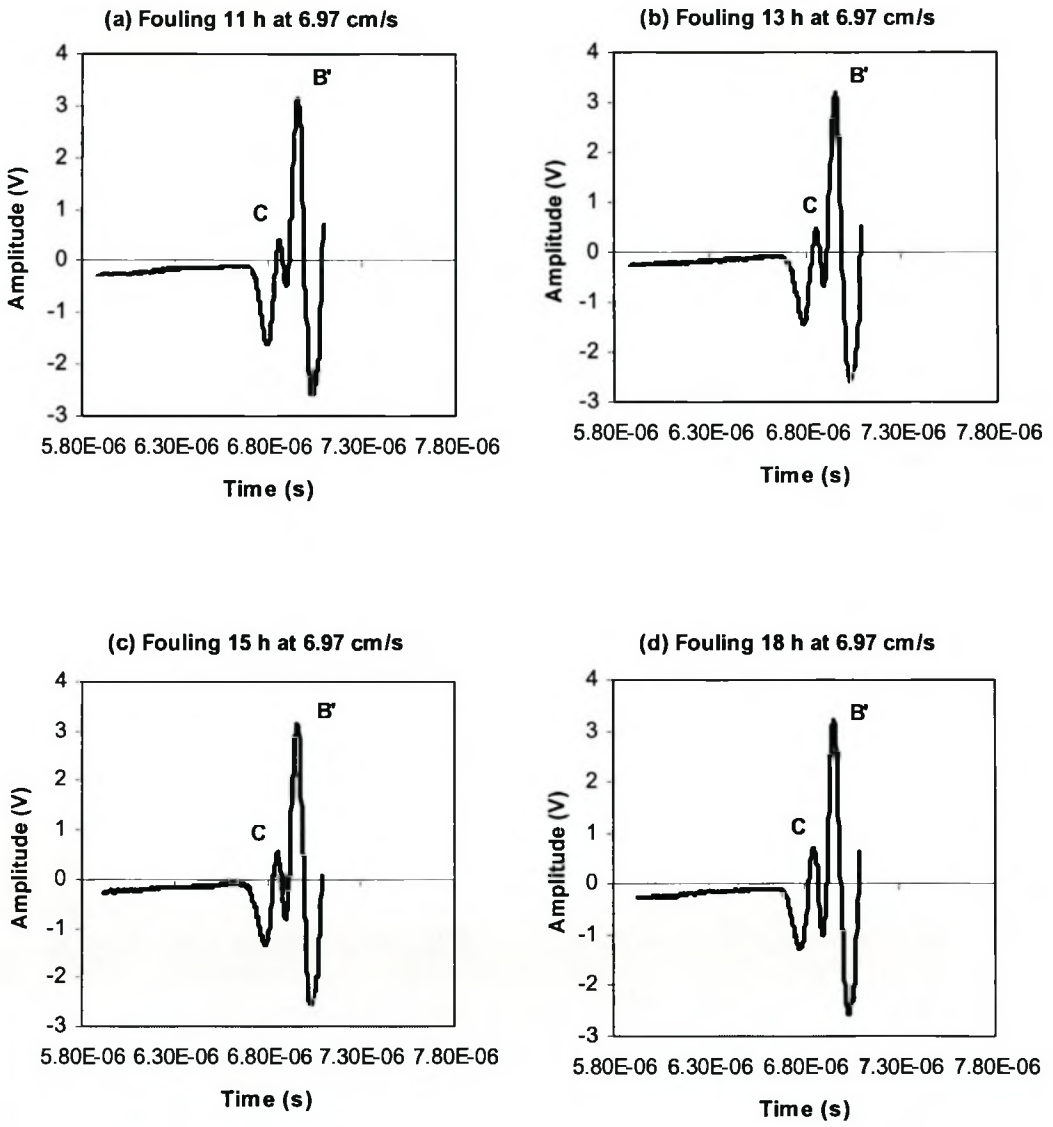

Figure 7.8: Ultrasonic responses after (a) 11 h, (b) 13 h, (c) 15 h and (d) 18 h of operation in the fouling experiment carried out with paper mill effluent at a flow rate of 6.97 cm/s.

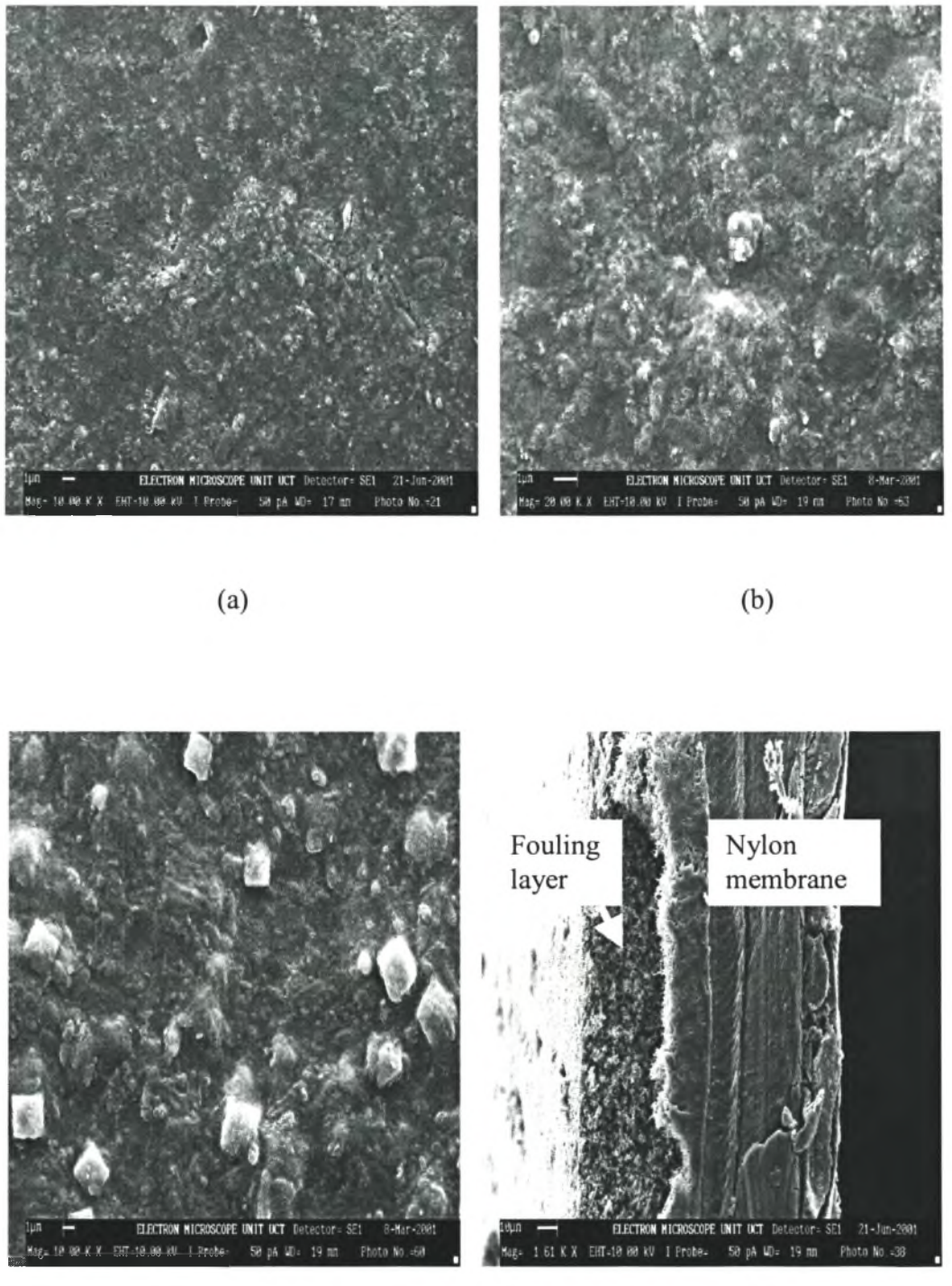

Figure 7.9: Representative SEM micrographs of the membrane surface after (a) 2 h, (b) 4 h, (c) 18 h of fouling operation (6.97 cm/s, 150 kPa) and (d) cross-sectional view of the fouled membrane after 4 h, with paper mill effluent.

7.4.2 DIFFERENTIAL SIGNALS

Further studies were carried out to investigate the build-up of a cake layer and its physical state on a membrane surface so as to interpret the results observed in the above experiments. This study showed that the UTDR technique provides a means of producing a differential signal (an echo signal of a fouling layer) by comparing the difference between reference and test waveforms, according to the principle of waveform fold. A clean membrane waveform obtained upon pure-water filtration or at fouling start (0 h) is used as a reference waveform for later use during fouling and cleaning process. A fouled membrane waveform obtained during the fouling processes can be used as a test waveform. Hence, a differential signal equals the difference between test waveform and reference waveform. The differential signal represents an echo signal of a cake layer on a membrane surface. This technique is used in order to observe minor differences in a shape, far below the resolution limit that the wavelength imposes [Cilliers, 2002].

Results of differential signals during the fouling experiments carried out with the paper mill effluent at flow rates of 1.83 and 6.97 cm/s are shown in Figures 7.10 – 7.14. Note: Peak B is an echo of a clean nylon membrane (white line); Peak C' is an echo of a cake layer on the membrane surface. The growth and movement of Peak C' can be seen in Figures 7.10 – 7.14.

Changes in time- and amplitude-domain of Peak C with operation time during fouling are summarized in Figure 7.15. According to the difference in arrival times, dT, between echoes B and C', the thickness of the cake layer on the membrane surface can be calculated from Equation 3.1, as shown in Figure 7.16. The calculation is based on the parameter: v = 1500 m/s in the cake layer. Quantitative information about the cake layer during fouling processes was obtained, for instance cake layer thickness down to 15 μm, i.e. better than theoretical resolution measured. In fact there is not a lower limit.

Differential signals:

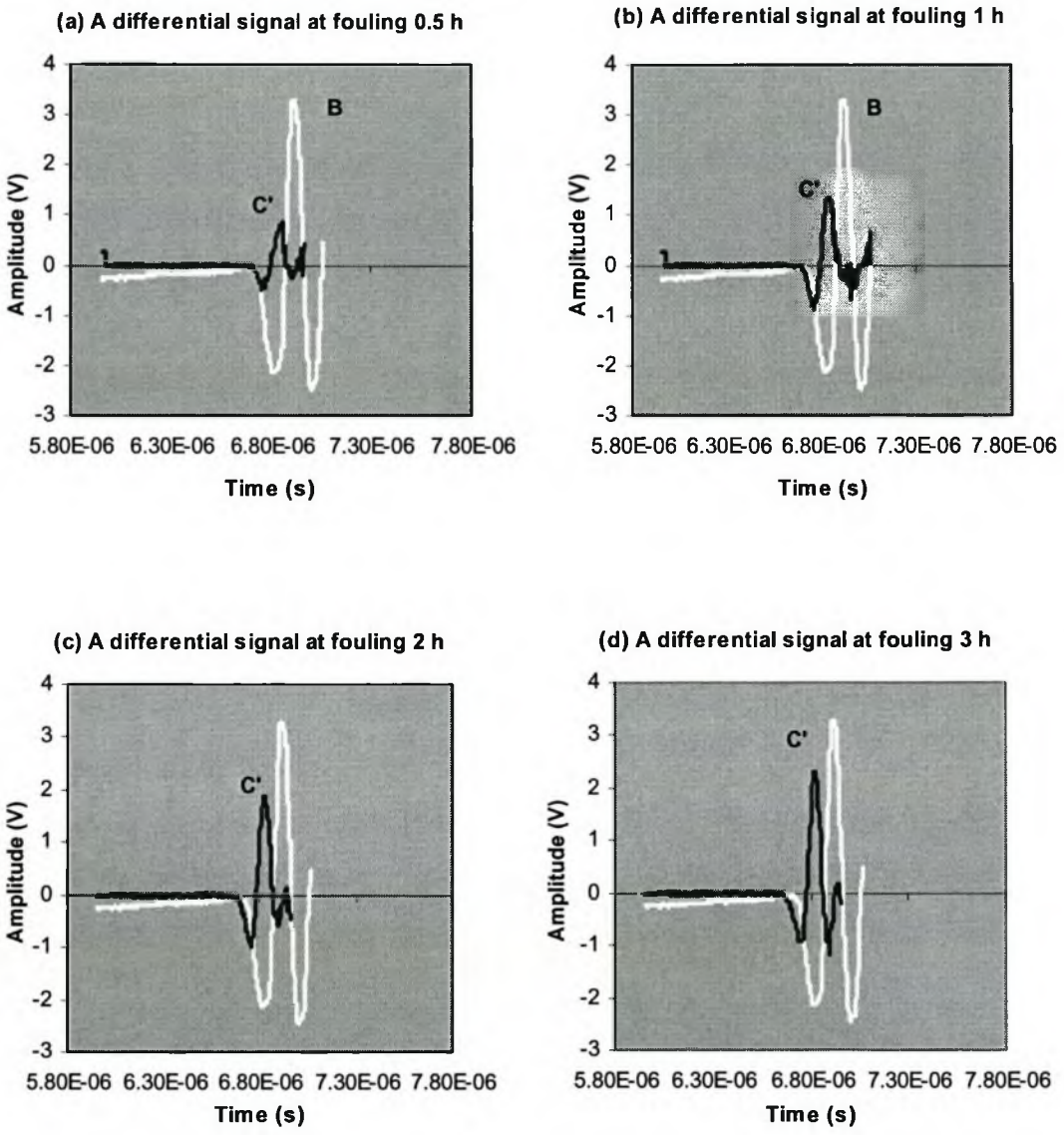

Figure 7.10: Differential signals after (a) 0.5 h, (b) 1 h, (c) 2 h and (d) 3 h of operation in the fouling experiment carried out with paper mill effluent at a flow rate of 1.83 cm/s.

Note: Peak B – echo of clean Nylon membrane (white line), Peak C' - echo of a cake layer.

Differential signals:

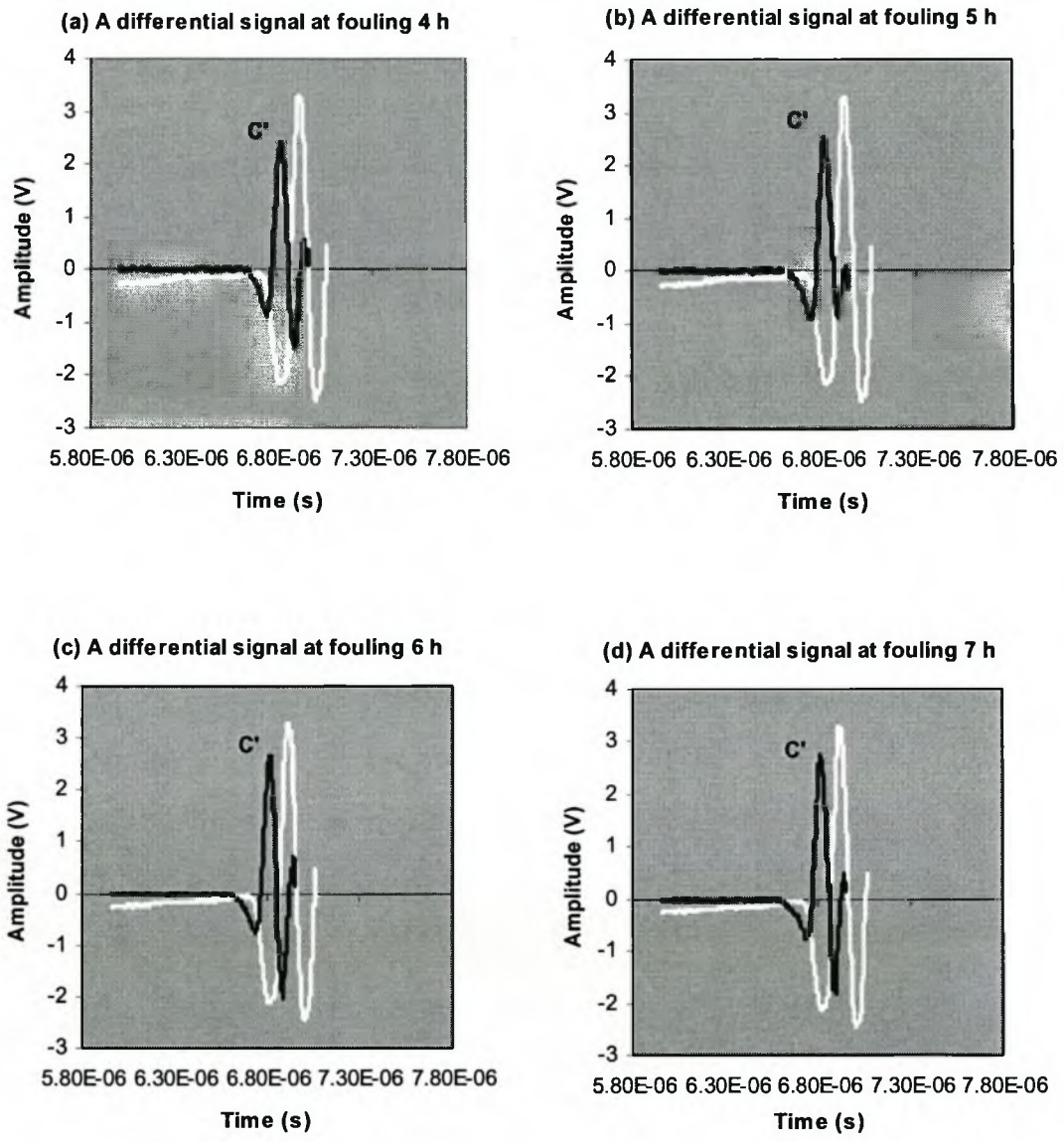

Figure 7.11: Differential signals after (a) 4 h, (b) 5 h, (c) 6 h and (d) 7 h of operation in the fouling experiment carried out with paper mill effluent at a flow rate of 1.83 cm/s.

Note: Peak B – echo of clean Nylon membrane (white line), Peak C' - echo of a cake layer.

Differential signals:

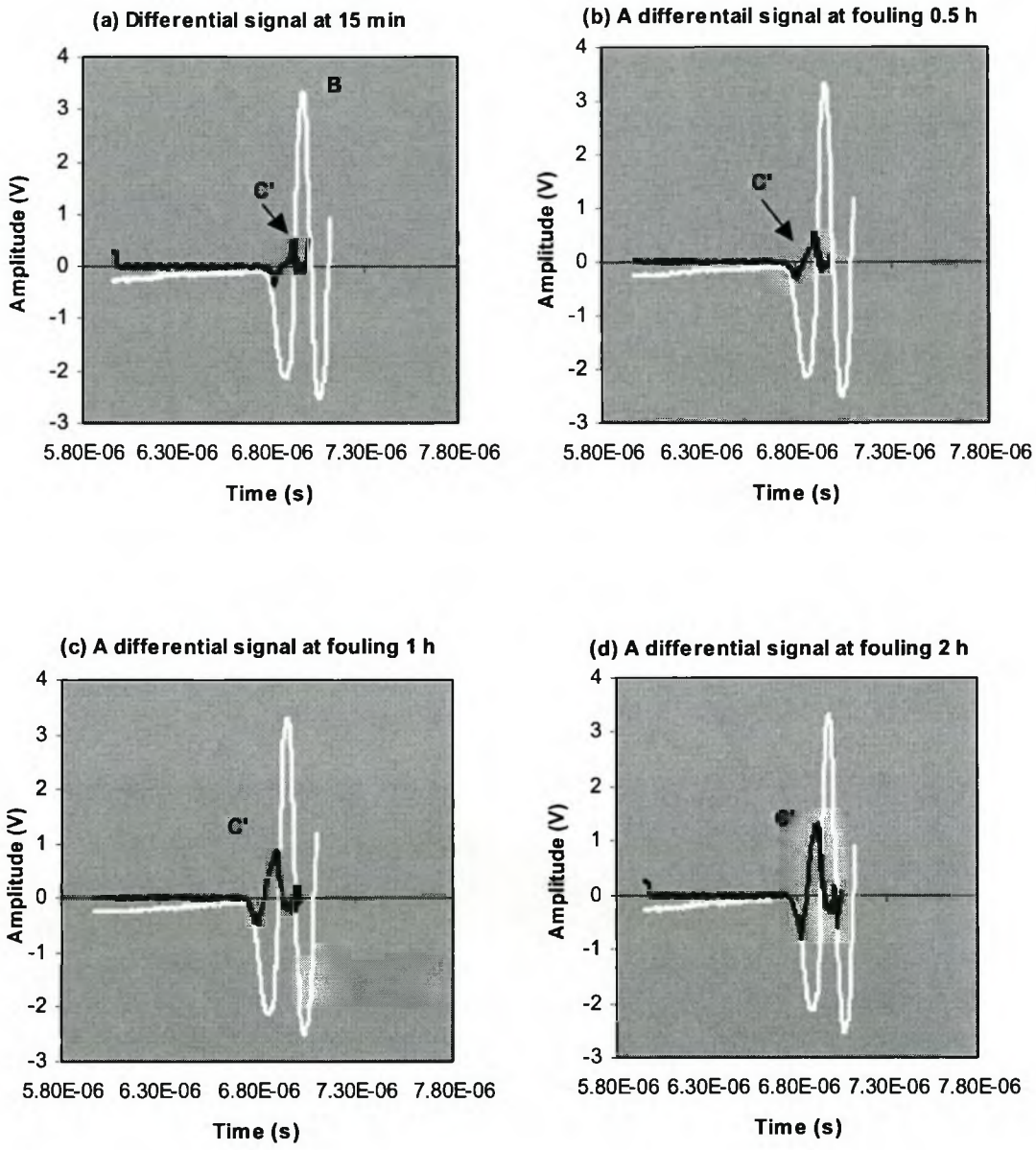

Figure 7.12: Differential signals after (a) 15 min, (b) 0.5 h, (c) 1 h and (d) 2 h of operation in the fouling experiment carried out with paper mill effluent at a flow rate of 6.97 cm/s.

Differential signals:

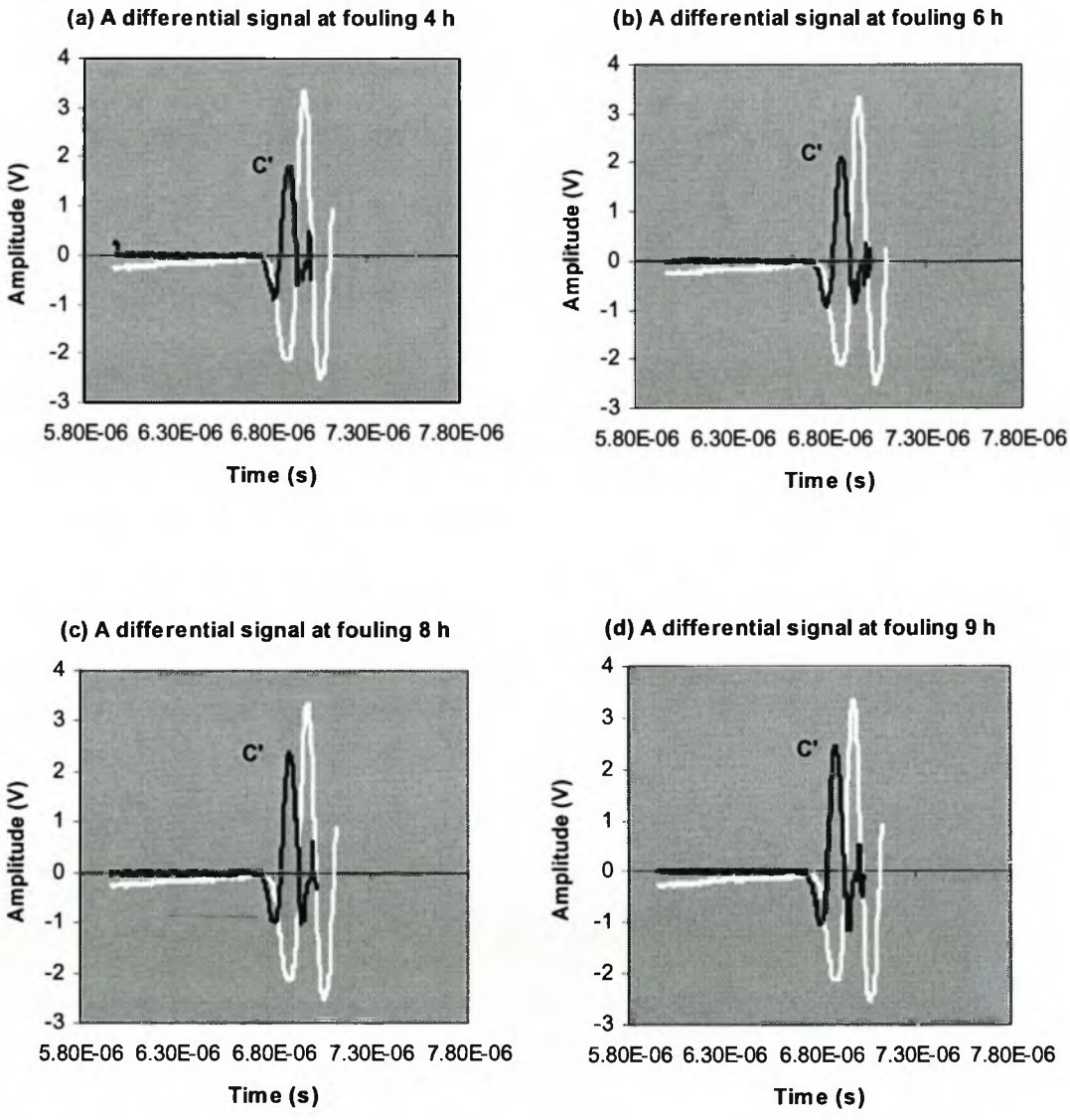

Figure 7.13: Differential signals after (a) 4 h, (b) 6 h, (c) 8 h and (d) 9 h of operation in the fouling experiment carried out with paper mill effluent at a flow rate of 6.97 cm/s.

Differential signals:

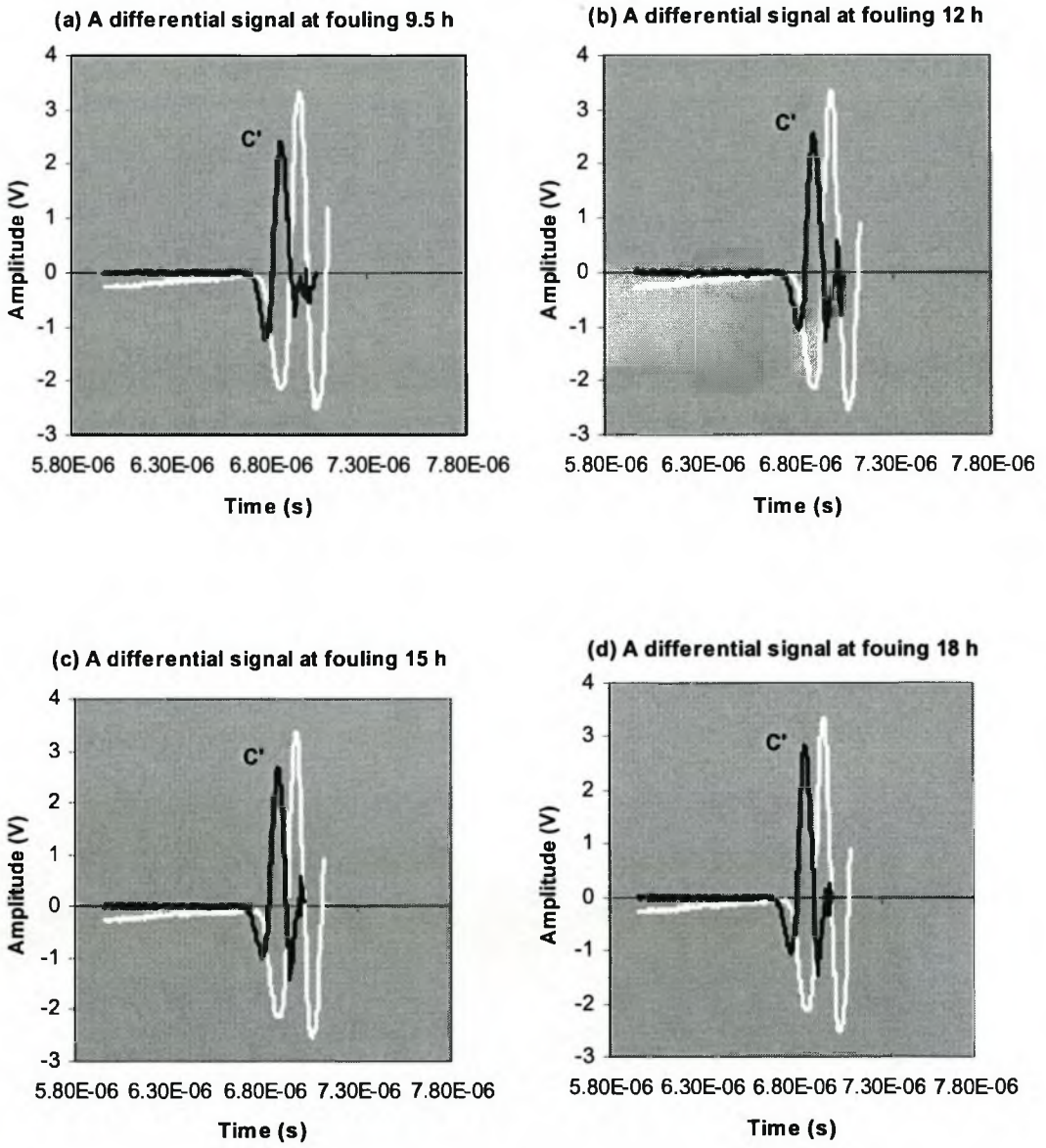

Figure 7.14: Differential signals after (a) 9.5 h, (b) 12 h, (c) 15 h and (d) 18 h of operation in the fouling experiment carried out with paper mill effluent at a flow rate of 6.97 cm/s.

Note: Stop and restart at fouling 9 h of operation.

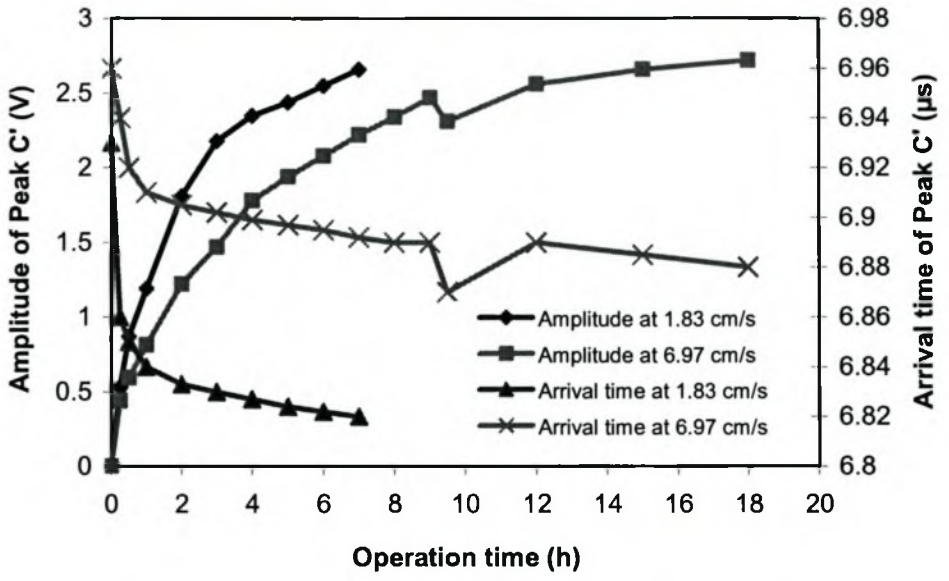

Figure 7.15: Amplitude and arrival time of differential signal (Peak C') versus operation time during the fouling experiments with paper mill effluent at flow rates of 1.83 and 6.97 cm/s (stop and restart of the fouling operation at 9 h).

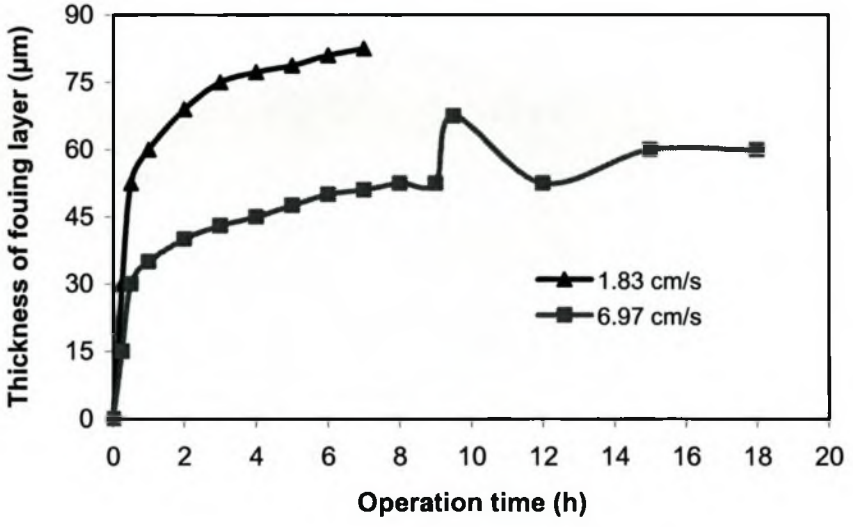

Figure 7.16: Thickness of fouling layer vs. operation time at flow rates of 1.83 and 6.97 cm/s (Stop and restart of the fouling operation at 9 h).

7.4.3 CLEANING EXPERIMENTS AND ULTRASONIC MEASUREMENTS

As mentioned earlier (section 7.3.3), to investigate the suitability of the UR technique for fouling removal strategies, a new fouling experiment was carried out with paper mill effluent at a flow rate of 4.2 cm/s and applied pressure 100 kPa. Results of ultrasonic reflections in the fouling experiment are shown Figure 7.17. SEM analysis of the fouled membrane is shown in Figure 7.18.

Figure 7.19 shows the results of ultrasonic response signals during the cleaning experiments. Results of differential signals during the cleaning processes are shown in Figures 7.20 and 7.21. Figure 7.22 displays changes in the amplitude of differential signal - Peak C' during cleaning. Pure water flux recovery of the cleaned membrane obtained by different cleaning methods is shown in Figure 7.23.

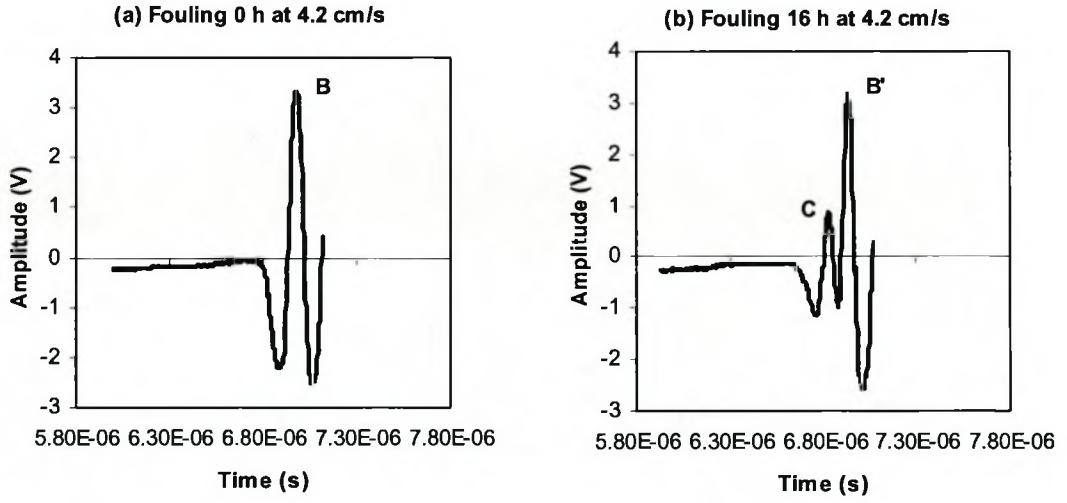

Figure 7.17: Ultrasonic responses (a) at the start, (b) after 16 h of operation in the fouling experiment carried out with paper mill effluent at a flow rate of 4.2 cm/s and applied pressure 100 kPa.

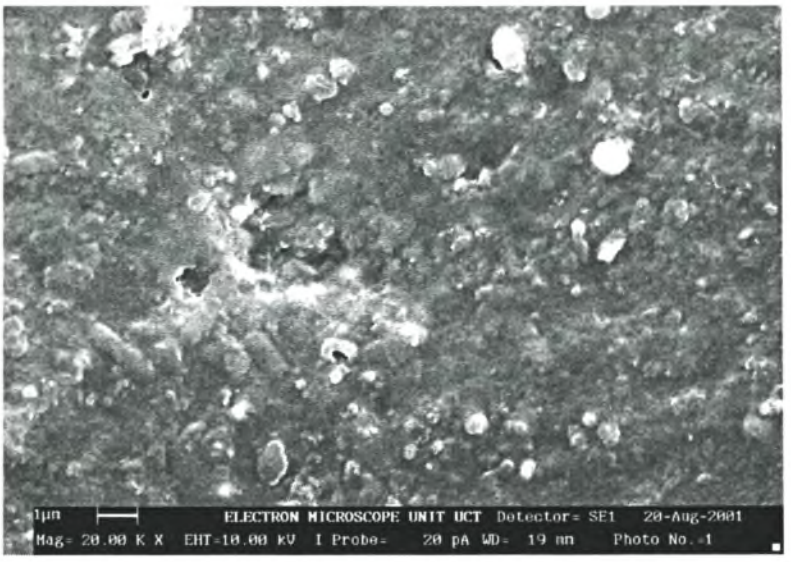

(a)

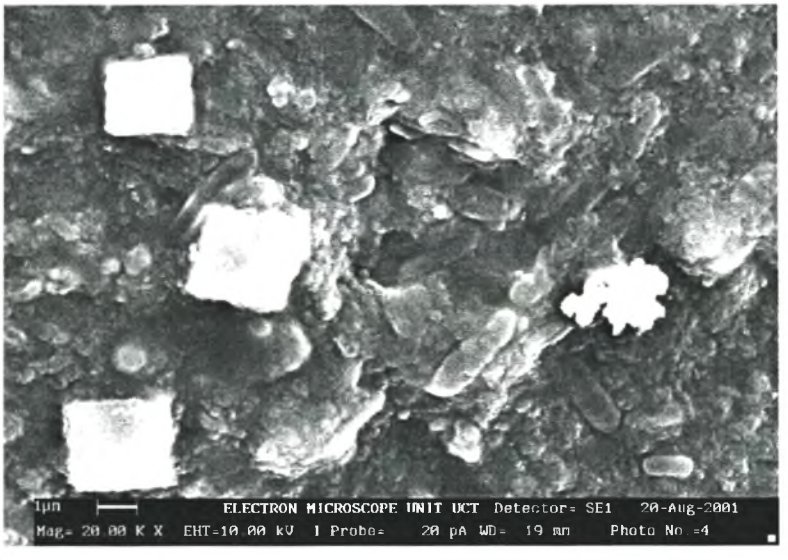

(b)

Figure 7.18: Microscope images of the Nylon membrane surface during paper mill effluent fouling experiments: after (a) 4 h and (b) 16 h of operation (4.2 cm/s and 100 kPa).

Ultrasonic responses

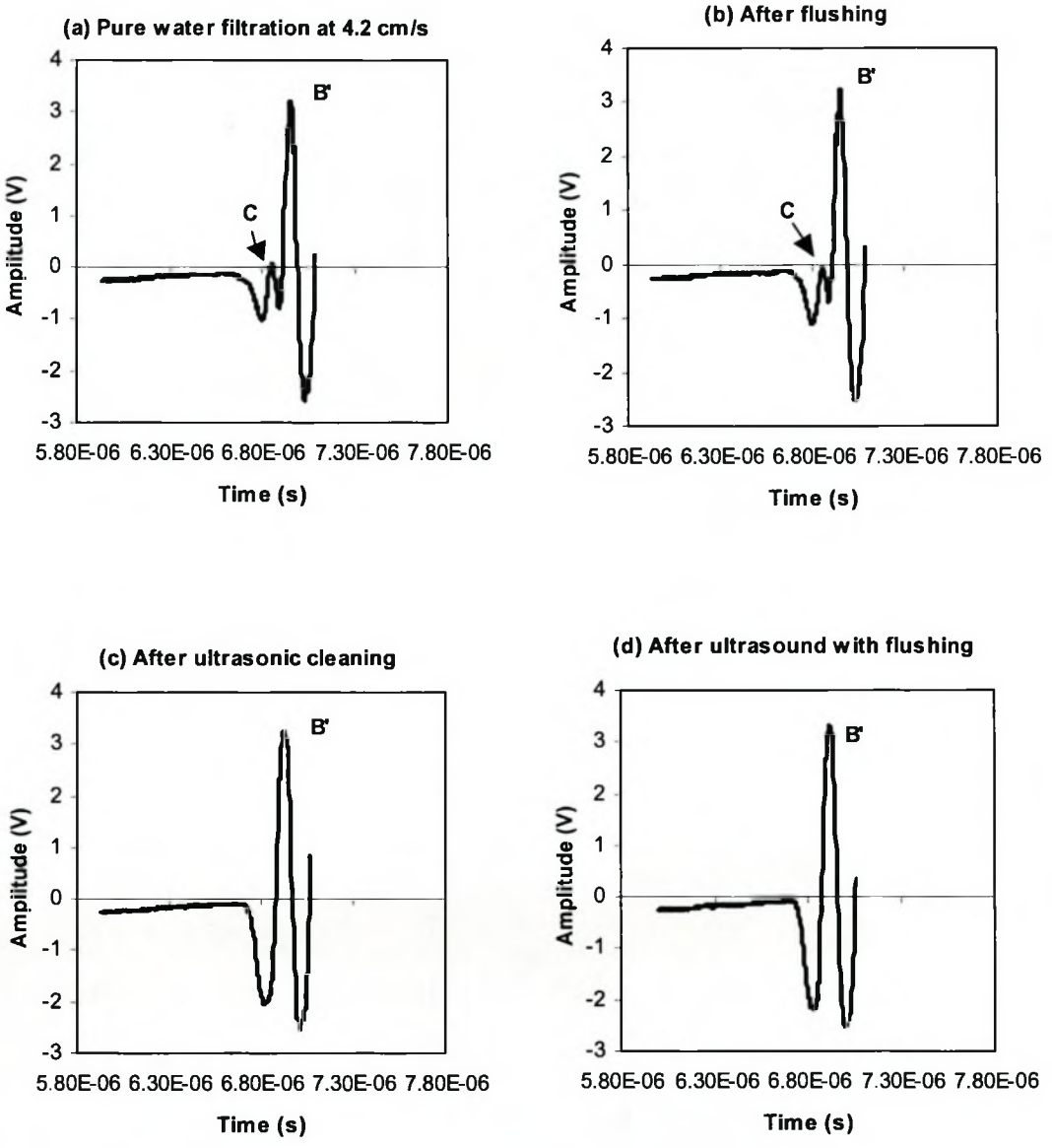

Figure 7.19: Ultrasonic responses during the cleaning experiments: (a) pure water filtration After 16 h of fouling operation, (b) flushing, (c) ultrasonic cleaning and (d) ultrasound associated with flushing.

Note: Peaks B, B' and C were generated from the interfaces: water/nylon membrane, cake layer/nylon membrane and feed/cake layer.

Differential signals

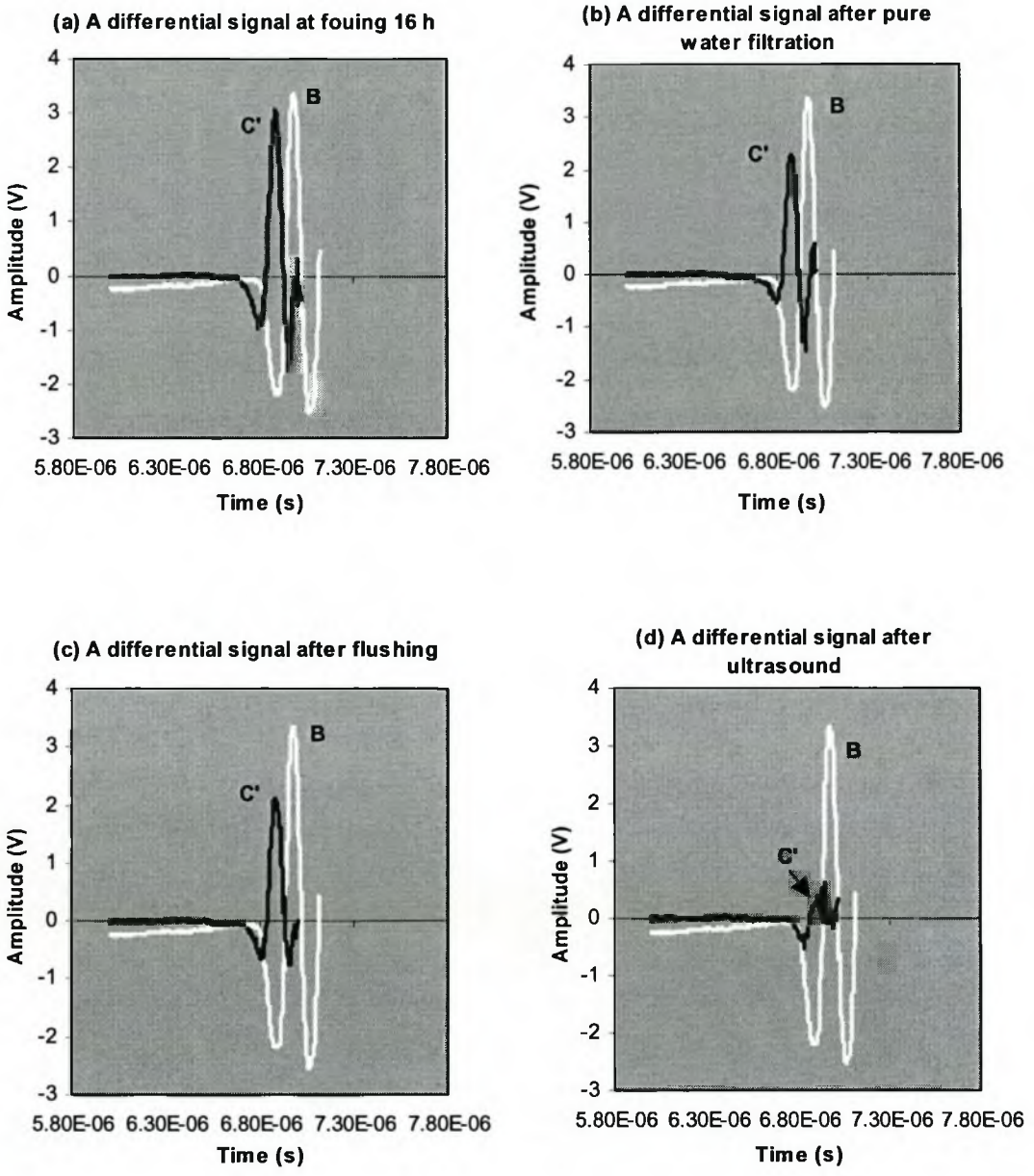

Figure 7.20: Differential signals after (a) 16 h of fouling operation, (b) pure water filtration after fouling, (c) flushing and (d) ultrasonic cleaning.

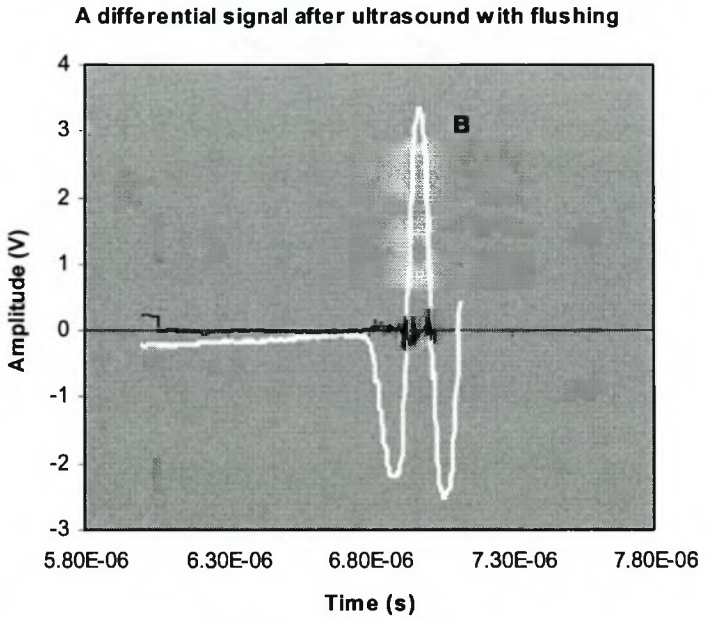

Figure 7.21: Differential signals after ultrasound with flushing.

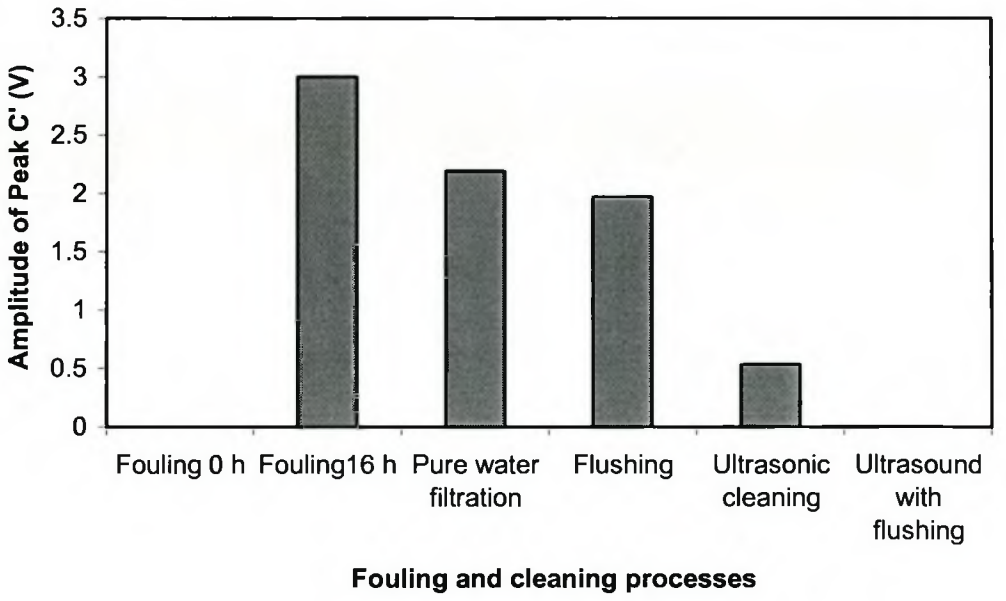

Figure 7.22: Changes in the amplitude of differential signal - Peak C' during cleaning.

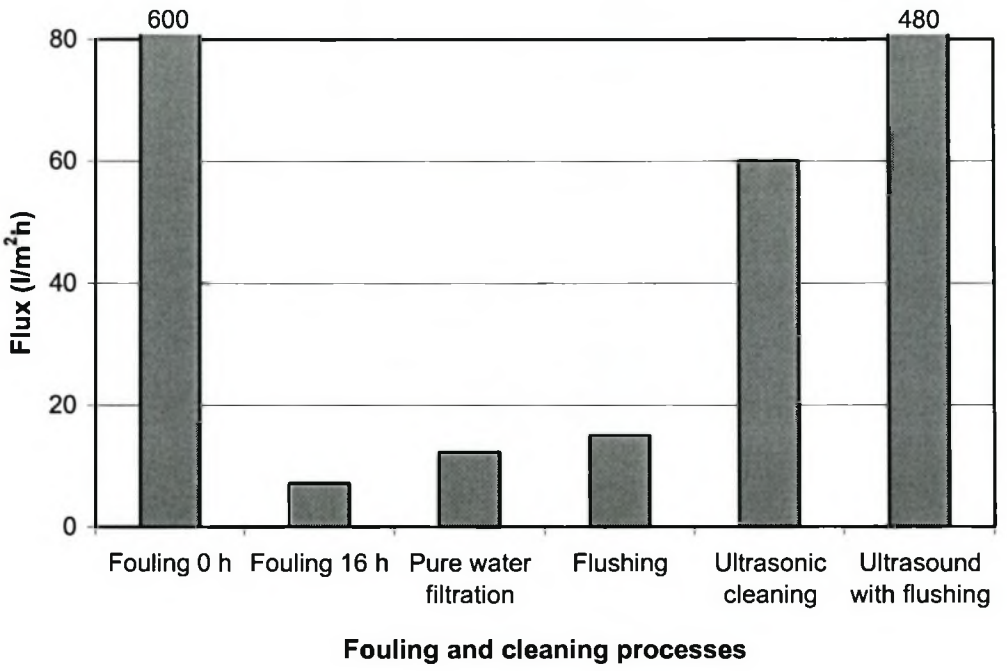

Figure 7.23: Changes in flux during fouling and cleaning processes.

7.5 INTERPRETATION OF RESULTS

7.5.1 FOULING AND ULTRASONIC MEASUREMENT

As shown in Figure 7.2, at the beginning of the fouling experiment an instantaneous and rapid decline in the flux was observed, followed by a more gradual decline after 2 h of operation. The instantaneous flux-decline results primarily from particle deposition and the formation of a cake layer on the membrane surface, whereas the gradual decline is presumed to occur as a result of the slow growth of the cake layer and consolidation the cake layer. Figure 7.2 also shows that the decrease in flux was faster at the flow rate of 1.83 cm/s than at 6.97 cm/s. It may be that high shear rates generated at the membrane surface tend to shear off deposited material and thus reduce the hydraulic resistance of the cake layer. Both fluxes had similar values. This suggests that the high flow rate does not mitigate the fouling.

Consistent with above observation, the corresponding ultrasonic measurements exhibit relatively rapid changes in ultrasonic response signals. The peak B represents the clean nylon membrane echo in Figure 7.3a. Generally, once foulants are deposited on the membrane surface, the acoustic impedance difference and the topographical characteristics at the feed solution/membrane interface will change, resulting in a change from echo B to echo B', as shown in Figure 7.3b and c, after 0.5 and 1 h of fouling operation at 1.83 cm/s. The formation of a very thin cake layer (compared with the nylon membrane layer) on the membrane surface generated an echo signal of the cake layer, which combined with the echo signal of the clean nylon membrane layer to form a new waveform B' (although the echo signal of the cake layer could not be seen at this moment). Inductively coupled plasma analysis showed that the main chemical composition of the fouling layer is breakdown products of lignin or lignosulphonate [Domingo, 2001].

Further, if the cake layer is thick enough as the cake layer grows, the echo signal (Peak C) of the cake layer will be seen (Figure 7.3d). If still more particles or fouling covers the membrane surface, a denser fouling layer is formed and a greater acoustic impedance change between the bulk solution and the membrane is expected. This

would be detected as a sharper reflection. Thus, an echo signal (Peak C) with greater amplitude is observed at 3 – 7 h of fouling operation in Figure 7.4. This is because of the gradual increase in the density and thickness of the cake layer (the amplitude of the reflected wave related to material density, see Equations 2.13 and 2.26). However, it is also important to note that the initial slope of the echo signal changed significantly during the experiment, from a steep slope (Figure 7.3a or b) to a shallow slope (Figure 7. 4b - d). This implies that the lower layers resemble bound aggregates and the upper layers have a more loosely flocculated structure. This observation will be discussed on the basis of URM (section 7.6).

In order to study the correlation between the measurement of UTDR and membrane coverage by the fouling layer, membrane samples were taken for SEM analysis. Results are shown in Figure 7.5a -d. The SEM micrograph of a clean membrane with a clear pore structure is shown in Figure 7.5a. Morphological characterization of the fouled membrane surface after 2 h of fouling operation revealed complete membrane coverage with the cake layer (Figure 7.5b). There are more and bigger particles on the membrane surface after 7 h than 2 h of fouling operation (Figure 7.5c). A cross-sectional view of a fouled membrane displayed a cake layer covering on the membrane surface. This suggests that morphological observations of the fouling layer corroborate the ultrasonic signal response of the fouling layer.

Similar results of ultrasonic responses in the fouling experiment at the 6.97 cm/s flow rate can be seen in Figures 7.6 – 7.8. Peak B (Figure 7.6a) was changed into Peak B' when fouling initiated on the membrane surface (Figure 7.3b – c). By comparison with results recorded at a flow rate of 1.83 cm/s (Figure 7.3), it was found that the fouling echo Peak C at 6.97 cm/s appeared later that that at 1.83 cm/s. A new echo (Peak C) appeared at the front of the membrane echo Peak B' after 5 h of fouling operation at 6.97 cm/s (Figure 7.7a). The growth of Peak C can be seen in Figure 7.7 as fouling proceeded. A sharp reflection Peak C (cake layer echo) emerged after 13 – 18 h of fouling operation at 6.97 cm/s in Figure 7.8. However, a large Peak C arose only after 3 h of operation at 1.83 cm/s. The fouling echo appeared and grew quickly at a low flow rate because of the low shear rate. This indicates that the UTDR technique is able to detect the fouling rates under different operation conditions.

Morphological characterization of the membrane surface after 2, 4 and 18 h of fouling operation revealed complete membrane coverage with the fouling layer (Figure 7.9). There were more and bigger particles on the membrane surface after 18 h of fouling operation. A SEM cross-sectional view of the fouled membrane revealed that the thickness of the fouling layer was about 40 μm after 4 h of fouling (Figure 7.9d).

7.5.2 DIFFERENTIAL SIGNAL ANALYSIS

In the case of a very thin fouling layer, it is difficult to calculate the thickness of the fouling layer directly from the ultrasonic record in the conventional way. Differential signal analysis (the difference between test waveform and reference waveform) would be a correct approach to track the real echo of a cake layer. It is shown in Figures 7.10 and 7.11 that a differential signal (Peak C') appeared within 0.5 h of fouling operation at 1.83 cm/s, and grew over the period 1, 2, 3, 4, 5 and 6 h as fouling proceeded. A sharp signal emerged after 7 h of fouling due to a denser cake layer on the membrane surface (Figure 7.11d). Time-domain movement was also observed and obtained by the ultrasonic digital device as a result of an increase in the thickness of the fouling layer.

Differential signals obtained in the fouling experiment by paper mill effluent at a flow rate of 6.97 cm/s are shown in Figures 7.12 – 7. 14. Results also reveal the echo of cake layer appeared in a very short time measurement, namely, 15 min after start of fouling (Figure 7.12a). The growth of Peak C' was observed as the fouling proceeded. It is as a result of the build up of cake layer. A sharp Peak C' also emerged after 18 h of fouling operation at 6.97 cm/s (Figure 7.14), although the Peak C' arose slower at 6.97 cm/s than at 1.83 cm/s.

Changes in amplitude and arrival time of the differential signals (Peak C) with operating time during crossflow filtration are summarized in Figure 7.15. These indicated that the amplitude of the differential signals increased as fouling proceeded. The cake build-up and growth results from increases in the acoustic impedance of the cake layer ($W = V\rho$), meaning that the density of the cake covering on the membrane surface increased due to particle deposition and compressibility as fouling proceeded.

In the early stages of crossflow filtration, the filtration flux dominates the fluid mechanism and particles are advected directly onto the membrane and cake layer. So a rapid increase in amplitude of differential signal (the density of the cake layer) was observed in the early stages. In the later stages, the gradual amplitude increase is presumed to occur as result of the effective density of the cake deposit, which does not change significantly once the cake layer becomes reasonably dense and thick. At this stage, the crossflow velocity dominated the fluid mechanics. The particles are highly selective as to where they finally reside and packing efficiency will be increased [Mackley et al. 1992]. Indeed, the flux decline corresponds to the changes in amplitude of the differential signal (Peak C).

Another basic quantity measured in non-destructive ultrasonic testing is the time of flight, or the amount of time taken for the sound to travel through the sample. Figure 7.15 illustrates changes in the amplitude and arrival time of the differential signal (Peak C) with operation time in the paper mill effluent experiments. The arrival time of Peak C declines with time as a result of an increase in the thickness of the fouling layer. Figure 7.16 illustrates an increase in the thickness of the fouling layer with time.

The thickness of the cake layer increased rapidly at the beginning of fouling because of particle deposition and cake layer formation, followed by a slow increase because of gradual growth and compressibility of the cake layer (Figure 7.16). Although the thickness (82.5 μm) of the fouling layer obtained after 7 h of operation at crossflow 1.83 cm/s is thinner than the thickness (60 μm) obtained after 18 h of operation at 6.97 cm/s, the flux of 7.5 l/m^2h obtained after 7 h of operation at 1.83 cm/s is higher than the flux of 7.2 l/m^2h obtained after 18 h of operation at 6.97 cm/s. The amplitudes of differential signals are 2.66 and 2.72 V, after 7 h of operation at 1.83 cm/s and 18 h of operation at 6.97 cm/s, respectively. This indicates that the 60-μm cake layer (obtained after 18 h of operation at 6.97 cm/s) is denser than the 82.5-μm cake layer (obtained after 7 h of operation at 1.83 cm/s). The compressibility of cake layer contributes the flux decline.

Something particularly interesting is seen to occur at 9 h of operation at 6.97 cm/s, in Figure. 7.15. At this point the amplitudes show a decrease for a period longer than 30

min, followed by an increase. These changes in amplitude coincided with a stop and restart of the fouling operation (at 9 h). Interrupting the fouling experiment resulted in flow destabilization and relaxation of the fouling layer. An increase in the thickness of the fouling layer from 52.5 to 67.5 μm and a decrease in amplitude of the cake layer from 2.47 to 2.31 V (density reduction) are seen in Figures 7.15 and 7.16.

Changes in flow- and shear-rates upon re-commencement of the fouling experiment resulted in a decrease in the fouling layer thickness or partial dissolution of the fouling layer and. These factors resulted in a rapid increase in the ultrasonic amplitude as the fouling layer conformation on membrane surface was altered. Indeed, the flux increase observed (Figure 7.2) corresponded to the substantial amplitude change. The results obtained from this study suggest that the combination of flux determination and UTDR measurements can provide a much clearer view of the fouling behavior than the flux measurement alone.

An important distinction should be noted between the flux-decline behavior and the ultrasonic response in Figure 7.2. While there is no change in the flux-decline curve after operating for 11h at 6.97 cm/s, there are significant differences in the ultrasonic measurements logged. This may indicate that the UTDR technique is more sensitive to fouling layer growth than the flux-decline behavior is towards transport resistance.

7.5.3 CLEANING EXPERIMENT

Results of the fouling experiment (4.2 cm/s and 100 kPa) show the appearance of a cake layer echo and coverage of the cake layer on the membrane surface in Figures 7.17 and 7.18, indicating that membrane fouling occurs. When the feed was changed from the effluent to pure water, flux increased from 7.2 to 12.3 l/m^2h and amplitude of Peak C' decreased from 3 to 2.19 V (Figures 7.20, 7.22 and 7.23). It is because of a reduction in concentration polarization.

Ultrasonic responses and differential signals revealed a change in the fouling echo after flushing (Figures 7.19 and 7.20). The amplitude of peak C', the fouling echo, decreased from 2.19 to 1.97 V after flushing because fouling was reduced (Figure 7.20). Indeed, forward flushing slightly increased the water permeate flux from 12.3 to 15 l/m^2h (Figure 7.23). This suggests that forward flushing can reduce the reversible fouling cake layer by reversing the pressure differential across the membrane. The deposited cake layer on the membrane is expected to become re-suspended and swept away by tangential- or cross-flow [Redkar and Davis, 1995]. Therefore, the UR technique is able to explore the presence and the removal of the cake layer in real-time. In addition, it was found that the paper effluent fouling on the nylon membrane is difficult to clean using only flushing (see SEM image in Figure 6.6a). Additional cleaning methods are required.

Figures 7.22 and 7.23 show that the pure water flux increased from 15 to 60 l/m^2h and the amplitude of differential signal - Peak C' decreased from 1.97 to 0.53 V after ultrasonic cleaning. This suggested that ultrasonic treatment could effectively disperse the fouling layer on the membrane because of the cavitation phenomenon and acoustic steaming [Zhu and Liu, 2000]. Collapse of the cavities has sufficient energy to remove the foulants from the membrane. The disappearance of Peak C in Figure 7.19 indicated the fouling layer was removed. However, the amplitude of Peak C' is 0.53 V, signifying that there is still some fouling on the membrane. Hence, ultrasound associated with flushing was applied in an effort to remove the membrane fouling.

Results in Figure 7.23 also show that the pure water flux enhanced from 60 to 480 l/m^2h, after ultrasound associated with flushing, although it is still lower than the original pure water flux of 600 l/m^2h. The disappearance of Peak C' (Figure 7.21) after ultrasound with flushing indicated that the fouling on the membrane was removed. This is because ultrasonic cavitation results in hydraulic pressure impulses on the deposited fouling layer by impinging actions, similar to the water-hammer effect [Perusich and Alkire, 1991]. Acoustic streaming jets give rise to an enhanced convection and mixing, in terms of a series of micro-vortices, near the membrane surface. The crossflushing produces a high tangential or cross-flow rate (40-50 cm/s) on fouling layers. Thus, ultrasound associated with flushing was the most effective of the cleaning methods used; this method cleaned the fouled membranes (refer a SEM image of cleaned membrane in Figure 6.7). These results demonstrate that the UTDR technique can monitor removal of the fouling layer and membrane cleaning. It is suitable to study the effectiveness of various cleaning techniques.

7.6 APPLICATION OF MODELING TO UNDERSTANDING CAKE-LAYER DEPOSITION AND GROWTH

In order to aid in the interpretation of the results and to gain an understanding of the formation of fouling, a series of mathematical models based on the physical parameters of the above actual experiments were conducted. A full wave recording (near $1\frac{1}{2}$ sine signals) was produced in the mathematical modelling. The physical parameters used for modelling were closely related to actual parameters, although some assumptions had to be made. In particular, no or little information was available on the acoustic velocities of membrane materials. Some published information on the properties of polymers had to be adopted and adjusted in order to produce echo patterns similar to the measured ones. For example, the sound (longitudinal) velocity of nylon 6-6 is 2620 m/s [Lawrence, 1962]. However, no information be focused on the sound velocity of a porous nylon membrane. We adjusted the sound velocity of a porous nylon membrane to 2200 m/s according to our results obtained from Section 7.4. We also adjusted the sound velocity of PSU membrane with dense layer PSU_1, porous layer PSU_2 and polyester support, and the velocity and density of the cake layer (in paper mill effluent experiments) as shown in Table 4.1.

Nylon membrane was modelled on the basis of an actual membrane. Figure 7.24 shows the modelling echo response for a nylon membrane, in response to its reflecting properties and position in the cell based on internal velocities, thicknesses and densities. A signal frequency of 10 MHz was used in the actual experiments. In order to produce a smooth signal curve, points were calculated at intervals of 3×10^{-9} s.

A further model was based on the assumption that a cake layer consisting of lignin and lignosulphonate (ρ = 1.05 g/cm^3), with a thickness of 20 μm, had been deposited on the membrane. Results of modeling are presented in Figure 7.25. A response very similar to the signal obtained during actual measurements (Figure 7.10a) was obtained. A small echo peak formed in front of the membrane peak. The arrival time for the fouling peak is 6.92 μs (Figure 7.25). A further increase in the thickness of the

fouling layer to 40 μm led to a small movement ahead in the time domain (the arrival time for the fouling peak: 6.89 μs in Figure 7.26). However, maintaining the density and increasing the thickness of the layer to 80 μm resulted in a further movement ahead in the time domain (the arrival time for the fouling peak: 6.84 μs in Figure 7.27), without significantly changing the shape and peak height of the 'fouling peak'.

In Figures 7.3 and 7.4 the initial slope of the echo signal, recorded at a flow rate of 1.83 cm/s, became shallower with increasing thickness of the fouling layer. However, in the fouling experiment in which the flow rate was 6.97 cm/s, no obvious changes in the slope of the echo were observed with increasing thickness of the fouling cake (Figures 7.6 –7.8). This indicates that the cake layer obtained in paper mill effluent experiments is composed of compressible materials. The cake layer obtained at 6.97 cm/s is more compressible than that obtained at 1.83 cm/s. This is because a high shear force under a high flow rate (6.97 cm/s) affected to the cake layer. A similar phenomenon was observed in experiments where dispersed clay (kaolin) was used as fouling agent (Figure 5.5). The kaolin used was the moderately compressible material [Tiller and Kwon, 1998].

If, in the case of the Kraft fluid (paper mill effluent), the initial fouling layer has a high density, the ultrasonic response signal will be as shown in Figure 7.3b-c. Decreasing density (in the upper layers) in the subsequent fouling deposit would, however, produce a different response, resulting in a shallow slope of the echo signal in Figures 7.4. Such a case was modelled and, in the following model, the density of a 30 μm - fouling layer was increased from 1.005 to 1.4 g/cm^3. An increase in peak height of the fouling echo was obtained as the density of the fouling layer increased (Figure 7.28). A concomitant change of the initial slope with changing density is apparent, supporting the earlier interpretation that foulants such as Kraft fluids produce a non-uniform fouling layer of decreasing density towards its top. This also suggests that changes in the densities of the fouling layer can be predicted by the shape of the curves. In addition, maintaining the thickness and increasing the density of the fouling layer to 1.4 g/cm^3 resulted in a further increase in peak height and a slight change in slope at the beginning of the signal, without changing the position of the fouling echo.

In order to understand the process of the cake formation and the character of the cake layer, results of differential signals (from 0.5 to 7 h) during the fouling operation at 1.83 cm/s are summarized in Figure 7.29. Firstly, the movement of the differential signals in the time-domain were observed (Figure 7.29) as the fouling time increased from 0.5 hours to 7 h as a result of an increase in the thickness of the cake layer (as shown in Figure 7.15). Secondly, it is seen that the amplitude of the differential signal increases with operating time due to the compressibility of cakes or an increase in the density of the cake layer. Thirdly, the initial slope of the differential signal became shallower with an increase in the thickness of the cake layer or operating time. It implies that the cake layer covering on the membrane surface is a non-uniform layer. Its density decreases from the lower layers to the upper layers. However, results of differential signals during the fouling operation at 6.97 cm/s show in Figure 7.30 that a uniform cake layer was obtained under a high shear force. It implies that the operation at a high flow rate could not reduce fouling. These results indicate that growth of the cake layer in thickness and density results in an increase in the deposit resistance.

For a given thickness of deposit, the resistance grows with pressure, and this growth becomes all the more significant with increasing thickness of a cake layer. At the same time, stress applied to the cake decreases porosity and increases resistance to flow. The observed increase in deposit resistance is mainly due to the compressibility [Tiller and Kwon, 1998; Tiller and Li, 2001].

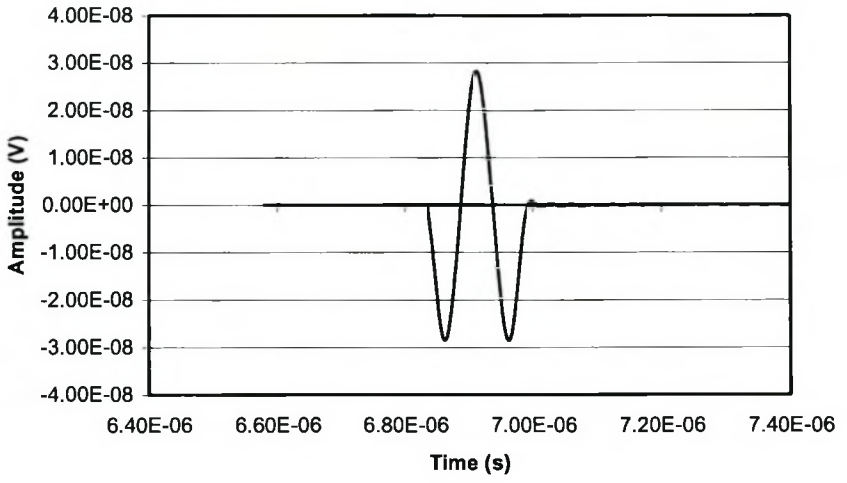

Figure 7.24: Mathematical model of the arrival times and echo for a clean nylon membrane (using a 10 MHz signal input).

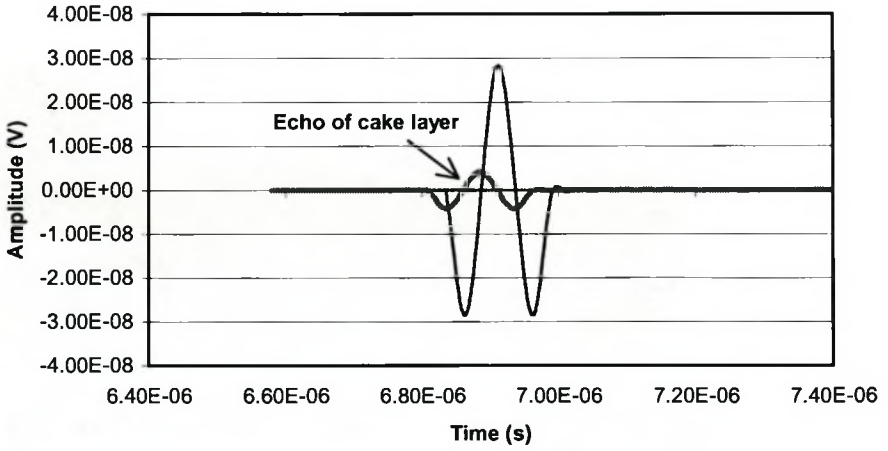

Figure 7.25: Model of a 20 μm thick cake layer (ρ = 1.05 g/cm^3) on a nylon membrane.

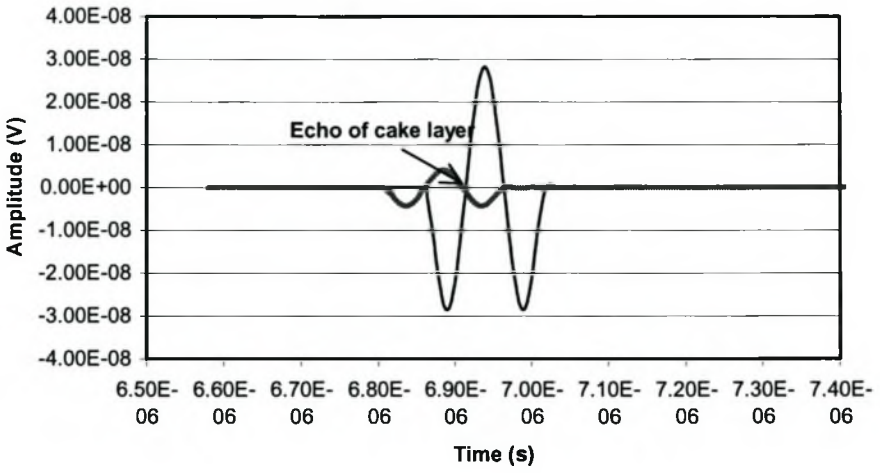

Figure 7.26: Model of a 40 μm thick cake layer (ρ = 1.05 g/cm^3) on a nylon membrane.

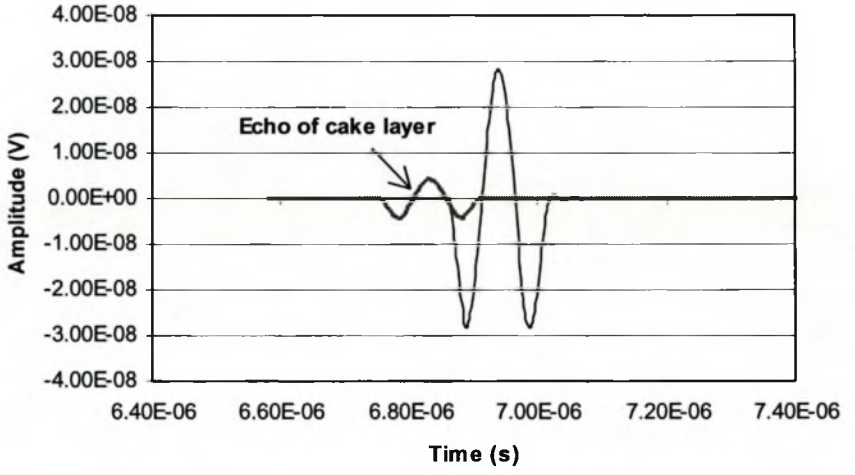

Figure 7.27: Model of an 80 μm thick cake layer (ρ = 1.05 g/cm^3) on a nylon membrane.

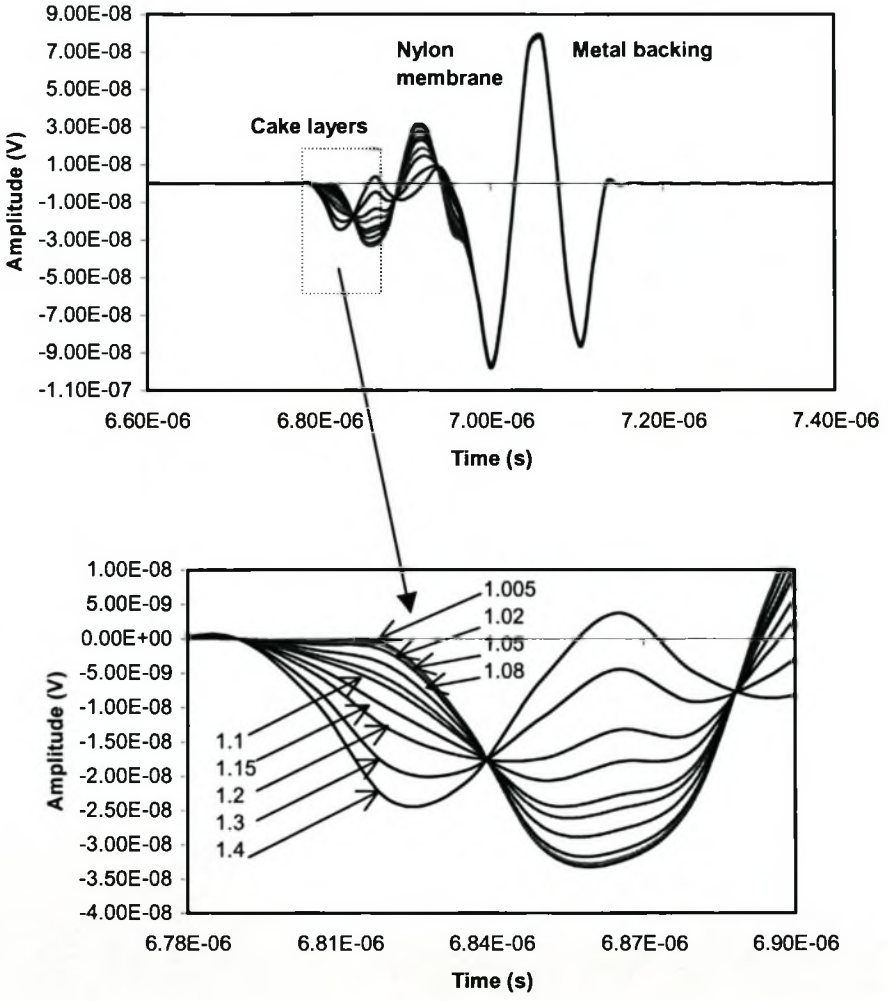

Figure 7.28: Mathematical model of density increases in a cake layer (ρ = 1.005 - 1.4 g/cm^3).

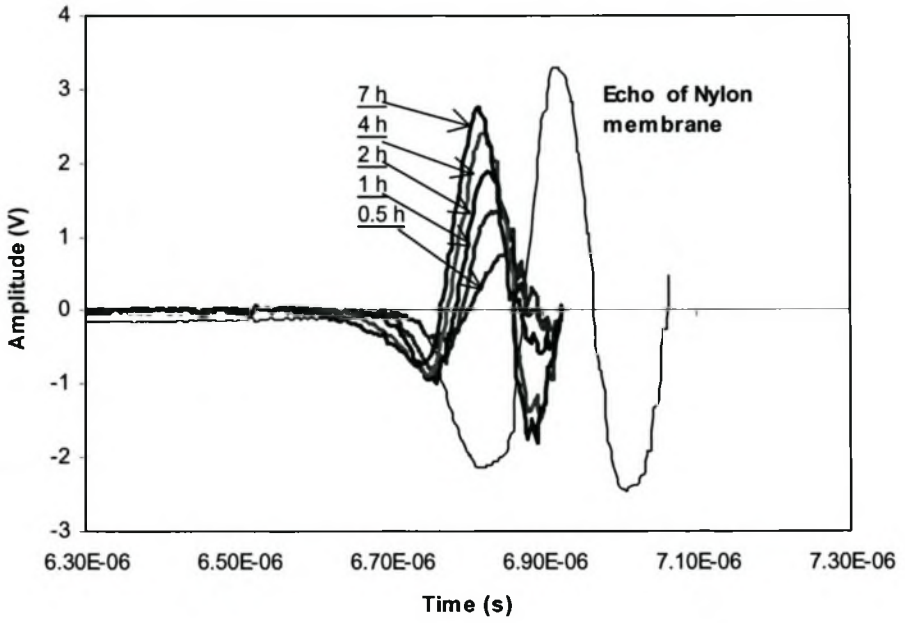

Figure 7.29: Actual ultrasonic response signal of a clean nylon membrane and differential signals after 0.5 - 7 h of operation in a fouling experiment (150 kPa, 1.83 cm/s) carried out with paper mill effluent.

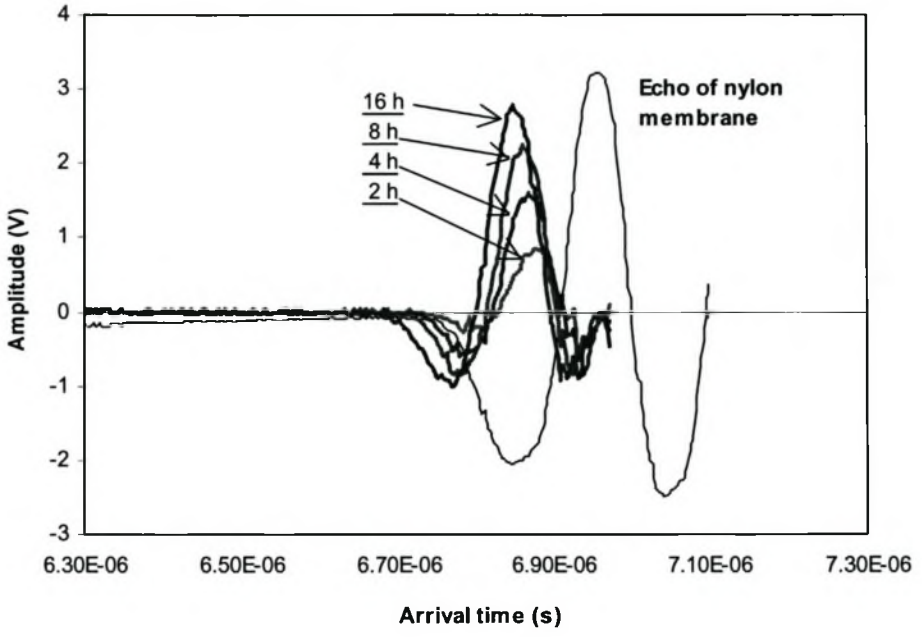

Figure 7.30: Actual ultrasonic response signal of a clean nylon membrane and differential signals after 0.5 - 18 h of operation in a fouling experiment (150 kPa, 6.97 cm/s) carried out with paper mill effluent.

7.7 SUMMARY

In crossflow microfiltration, cake formation, growth and compressibility were observed by an ultrasonic testing method. Results show that the ultrasonic testing technique can monitor the particle deposition, and the formation and growth of a cake layer on the membrane surface. The ultrasonic technique can measure the rate of cake layer formation at different flow rates.

The UTDR technique is also capable of detecting subtle changes such as stop and restart operation. In cleaning experiments, results show that a cake-layer echo decreased after flushing and disappeared after ultrasonic irradiation. UTDR results consolidate the results obtained in Chapter 5, namely that ultrasound associated with flushing is the most effective cleaning method for membranes fouled with paper mill effluent. The fact that the UTDR technique monitors changes on the membrane surface makes it very suitable to study membrane cleaning and determine effectiveness of various cleaning techniques.

Results further show that the differential signal of a fouling layer echo was obtained, indicating the state and progress of a cake layer on the membrane surface in actual operations. Both amplitude and arrival time of differential signals as a function of operation time provide useful quantitative information in the fouling processes. The UTDR technique can overcome the conventional way to quantify the thickness of a very thin cake layer on a membrane surface, using a differential signal. UTDR results corroborated the flux measurements and SEM analyses.

A predictive modelling program - ultrasonic reflection modelling (URM) was developed to better understand the processes related to the deposition of cake layers on membrane surfaces. Changes in the densities of the cake layer as well as the thickness can be substantiated by the mathematical modelling. In microfiltration the deposit resistance is not only related to the layer thickness but also the cake density (compressibility). The cake layer covering on the membrane surface is a non-uniform layer in the fouling experiment at a flow rate of 1.83 cm/s, and a uniform layer in at

6.97 cm/s. UTDR proves that raising flow rate in the actual operation could not reduce fouling. The predictive results are in good agreement with the actual measurements.

In sum, the echo signal of the cake layer can indicate the density state and progress of the cake layer on the membrane surface in real time and provide an early warning to adjust system-operating parameters, often faster then observable flux reduction.

CHAPTER 8

DIRECT MONITORING OF MEMBRANE FOULING AND CLEANING DURING ULTRAFILTRATION

8.1 SCOPE OF THIS CHAPTER

UTDR has been used as a non-destructive, real-time, *in situ* measuring technique for the non-invasive study of fouling and cleaning during UF with polysulfone (PSU) membranes. Paper-mill effluent from a wastewater treatment plant was used as feed solution. Firstly, the structure and compaction of an asymmetric PSU membrane and its compaction were detected by UTDR. The experimental results showed a good correspondence between the UTDR signal response and the development of the fouling layer on the membrane surface. Secondly, the UTDR technique was successfully used to monitor membrane cleaning and evaluate the cleaning effectiveness of various cleaning methods in UF. Moreover, a differential signal obtained indicated the state and progress of the fouling layer on a membrane surface. Such a signal gives warning of advanced fouling during realistic operation. Results showed the nature and thickness of the fouling layer as a function of operating time. Ultrasonic reflection modeling (URM) was applied to model the density and thickness of a fouling layer on a membrane surface so as to predict the fouling behaviour. Overall, UTDR is a most useful technique for the non-destructive investigation of fouling and cleaning in membrane applications.

8.2 INTRODUCTION

UF has become an increasingly important separation process. It is used for product recovery and pollution control in industrial effluents, oil emulsions, wastewater, ultra-pure water, biological macromolecules, colloidal paint suspensions and medical therapeutics [Lonsdale, 1982; Jönsson and Trägärdh, 1990; Cheryan, 1998]. The main problem related to UF however is the flux decrease caused by concentration polarization and fouling.

An *in-situ* visualization technique can not only characterize and distinguish between the various phenomena causing the flux decline, but also aid in elucidating the exact mechanism and nature of the fouling layer growth. The development and utilization of a suitable non-invasive technique for on-line monitoring of fouling in industrial and laboratory applications would also enable the effectiveness of fouling remediation and cleaning strategies to be quantified.

In Chapters 5 and 7 we described the use of an ultrasonic reflectometry technique for the *in-situ*, non-invasive observation of fouling deposition and growth on MF membranes. The present study aims to further understand the UTDR technique for the real-time, non-invasive investigation of organic fouling deposition and removal during UF, so as to further evaluate the capabilities of the UTDR technique and its applicability in different membrane separation systems. The multi-layer structure and compactness of an asymmetric PSU membrane was detected by UTDR. The different signals obtained and ultrasonic reflection modeling provided correct approaches to gain an understanding of the processes of ultrasonic testing related to fouling deposition.

8.3 EXPERIMENTAL

8.3.1 UF SYSTEM AND ULTRASONIC MEASUREMENT

The effluent from a wastewater treatment plant of Mondi Kraft Mills, Mondi Ltd, South Africa, was used as the feed solution. The wastewater treatment plant comprised the following processes: pretreatment, dissolved air flotation (DAF), MF and UF. Samples were taken from the MF product. The characteristics of the effluent are summarized in Table 8.1.

Flat-sheet polysulfone (PSU) membranes with a molecular weight cut-off (MWCO) of about 35 kD were prepared and used in all the fouling experiments. In order to monitor and determine the onset and advancement of fouling on a membrane surface, a flatbed filter cell was designed and used (Figure 3.3). A PSU membrane was placed between two Perspex plates.

Investigations were carried out with the UF separation system described in Section 5.3.1 (Figure 5.1). The ultrasonic measurement system used was the same as the one described in Section 5.3.1

Table 8.1: Characteristics of paper mill effluent from MF products[a]

ITEM	VALUE	ITEM	VALUE
pH	5.33	Sulphate, SO_4, mg/l	1232
Conductivity, μS/cm	315	Fluoride, F, mg/l	0.2
Suspended solids (SS), mg/l	720	Silica as Si, mg/l	5.8
Total Dissolved Solids, mg/l	4545	Chloride, Cl, mg/l	103
Chemical Oxygen Demand, mg/l	4090	Soap, oil & grease, mg/l	2.8
Biochemical Oxygen Demand, mg/l	900	Potassium, K, mg/l	24
Aluminum as Al, mg/l	12.6	Iron as Fe, mg/l	3
Calcium, Ca, mg/l	122	Sodium, Na, mg/l	1270
Total Iron, Fe, mg/l	3.3	Magnesium, Mg, mg/l	16.2
Total Dissolved Iron, mg/l	3.3	Potassium as K, mg/l	30

[a]The data from Mondi Piet Retief, Mondi Ltd, South Africa.

8.3.2 EXPERIMENTAL PROCEDURE AND FOULING EXPERIMENTS

In each UF experiment, continuous stirring in the feed tank was provided. Each experiment commenced with pure water being circulated through the system at the desired flow rate and applied pressure, for 0.5 h, to compress the membrane and to build up a stable flow field. Once steady state was attained, the feed was switched to the effluent solution to initiate the fouling phase in which concentration polarization and fouling occurred. This was allowed to continue until the ultrasonic response and permeate flux had stabilized.

Both cross-flow and dead-end filtrations were investigated. The fouling experiment was carried out at flow rates of 0 and 12.5 ± 0.12 cm/s (*Re* = 454 ± 4.5), applied pressure 175 ± 5 kPa and temperature 20 ± 1°C. The total operating time for the fouling experiments was 8.5 h.

8.3.3 UF CLEANING EXPERIMENT

Further fouling experiments were carried out at flow rates of 2.1 ± 0.02 cm/s (*Re*=532 ± 5.3), applied pressure 185 ± 5 kPa and temperature 20 ± 1°C. The total operating time for the fouling experiments was 20 h. Before commencing with the cleaning experiments, the feed solution was changed from effluent to pure water at 185 kPa and an axial velocity of 2.1 cm/s, in order to obtain pure water flux (PWF) of a fouled membrane. The fouled membrane was cleaned with pure water by three methods, in turn, namely: forward flushing, ultrasonic cleaning and ultrasound together with forward flushing, for cleaning times of 20 min each. The cross-flow filtration cell was immersed in a water bath during ultrasonic cleaning. The cell was irradiated with a horn ultrasonic cleaner (Medal W-375, Ultrasonics INC.) with a frequency of 20 kHz and a power of 375 w.

Ultrasound associated with forward flushing was performed with intermittent forward flushing at a flow rate of 40-50 cm/s during ultrasonic irradiation. To investigate the cleaning efficiency of each cleaning method, the cleaned membrane was used to filter pure water under the same operating condition as used in the fouling phase. The UTDR measuring system captured the changes in ultrasonic signal responses after the different cleaning methods. These data can be stored on a computer's hard drive.

8.4 RESULTS

8.4.1 ULTRASONIC REFLECTIONS AND HYDROSTATIC PRESSURE EXPERIMENT

Ultrasonic reflections in a flat cell are shown in Figure 8.1. The representative waveform plots the ultrasonic signal amplitude in volts (V) versus the arrival time in second (s). Each peak corresponds to a reflected acoustic wave from one of the multiple interfaces in the flat cell. Peaks A, B, C and D are generated from the following interfaces: Perspex plate/feed (water), water/PSU layer, PSU layer/polyester backing layer and polyester backing layer/metallic porous support.

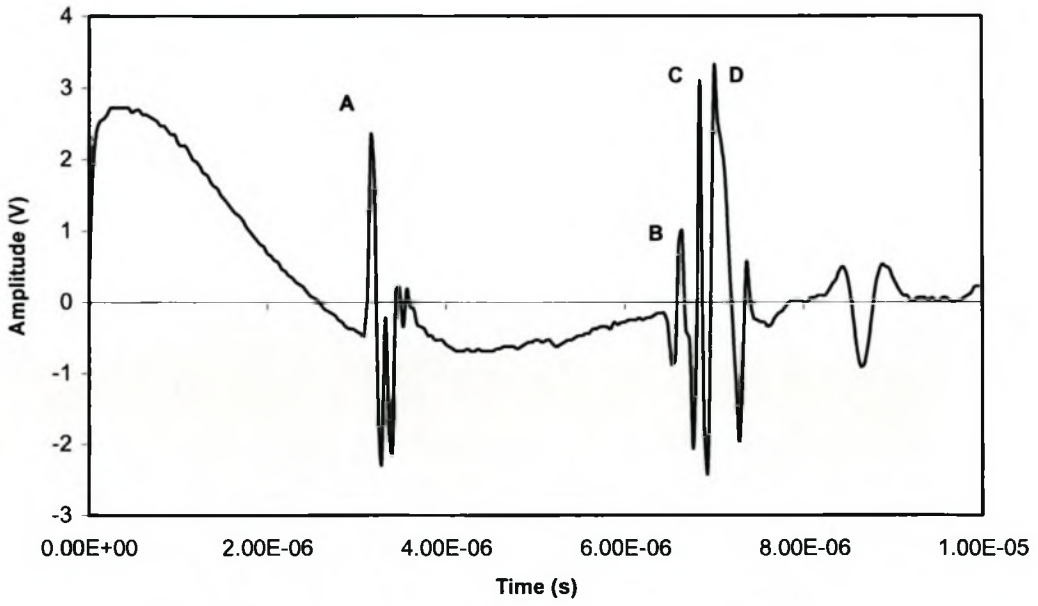

Figure 8.1: Ultrasonic reflections in a flat cell.

Note: Peaks A, B, C and D are generated from the following interfaces: Perspex plate/water, water/PSU layer, PSU layer/polyester backing, polyester backing/ porous metal support.

A hydrostatic pressure experiment with pure water was first carried out to investigate the resolution capabilities of the UTDR technique. Figure 8.2 shows ultrasonic response signals of a clean PSU membrane at hydrostatic pressures of 0 and 160 kPa during the hydrostatic pressure experiment.

Figure 8.3 shows the changes in the arrival time and shift distance of peak B (as a reference/observed signal) with hydrostatic pressure. The hydrostatic pressures ranged from 0 to 220 kPa.

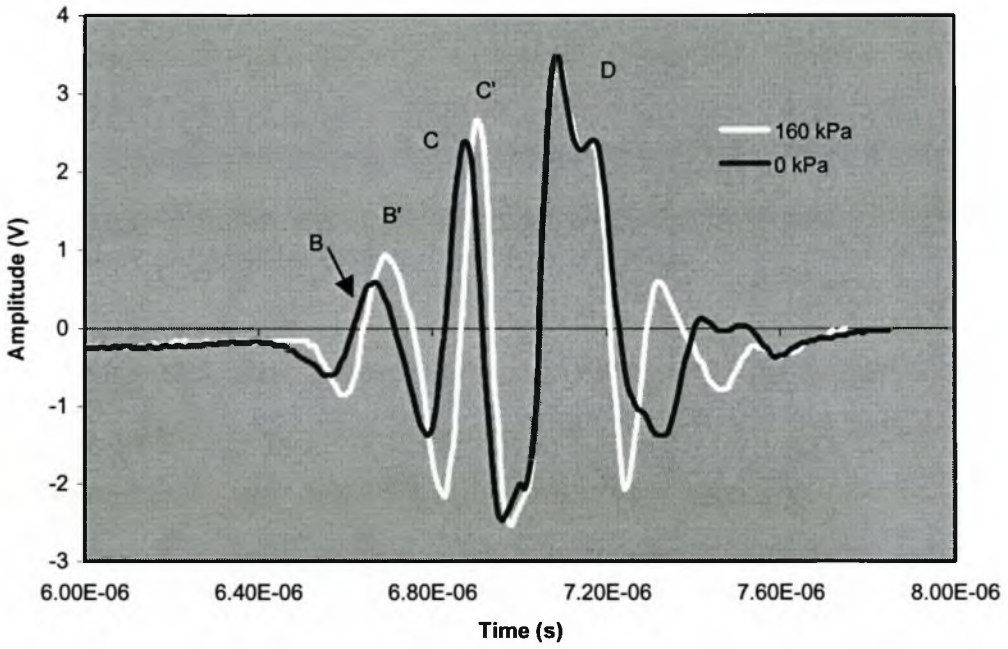

Figure 8.2: Ultrasonic response signals of a composite PSU membrane at hydrostatic pressures of 0 and 160 kPa during a hydrostatic pressure experiment with pure-water.

Note: the changes in slope and amplitude of peak B' while show density changes with hydrostatic pressure.

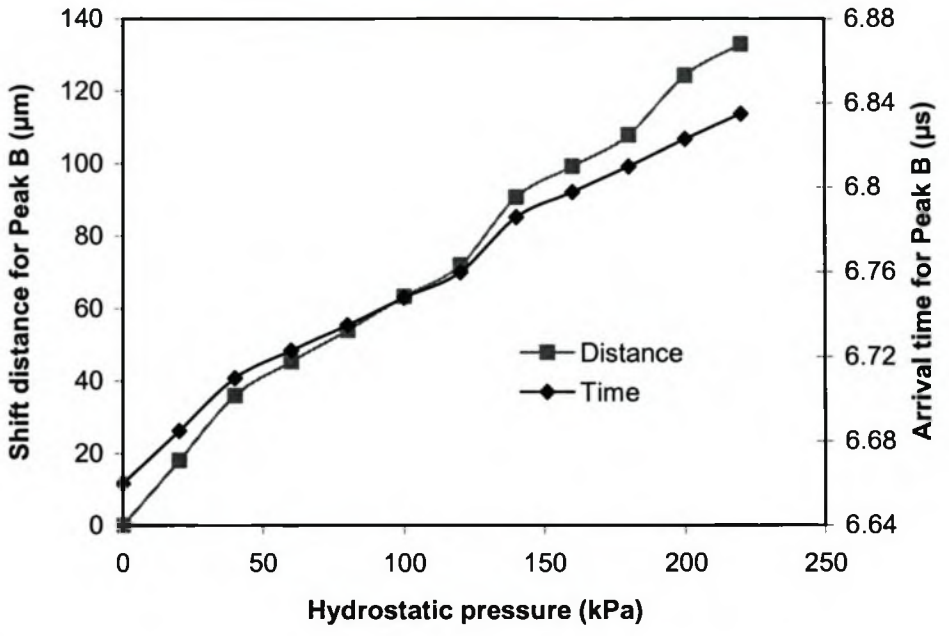

Figure 8.3: Time delay and shift distance of Peak B versus hydrostatic pressure.

8.4.2 FOULING EXPERIMENT AND UTDR MEASUREMENT

Figure 8.4 shows changes in the permeate flux with operating time during the fouling experiments carried out with paper mill effluent in dead-end and crossflow (12.5 cm/s) filtration.

Results of ultrasonic response signals during dead-end fouling experiments are shown in Figures 8.5 and 8.6. Figure 8.7 shows a scanning electronic microscope (SEM) cross-sectional view of a clean PSU membrane and an optical microscope cross-sectional view of a PSU membrane fouled by paper mill effluent during dead-end filtration.

Further experiments were carried out with paper mill effluent at a crossflow rate 12.5 cm/s and pressure 175 kPa. Results of ultrasonic response signals during crossflow fouling experiments are shown in Figures 8.8 and 8.9.

Figure 8.10 shows the microscopic images of PSU membranes fouled by paper mill effluent after 8 h of fouling operation at (a) dead-end and (b) 12.5 cm/s crossflow rate.

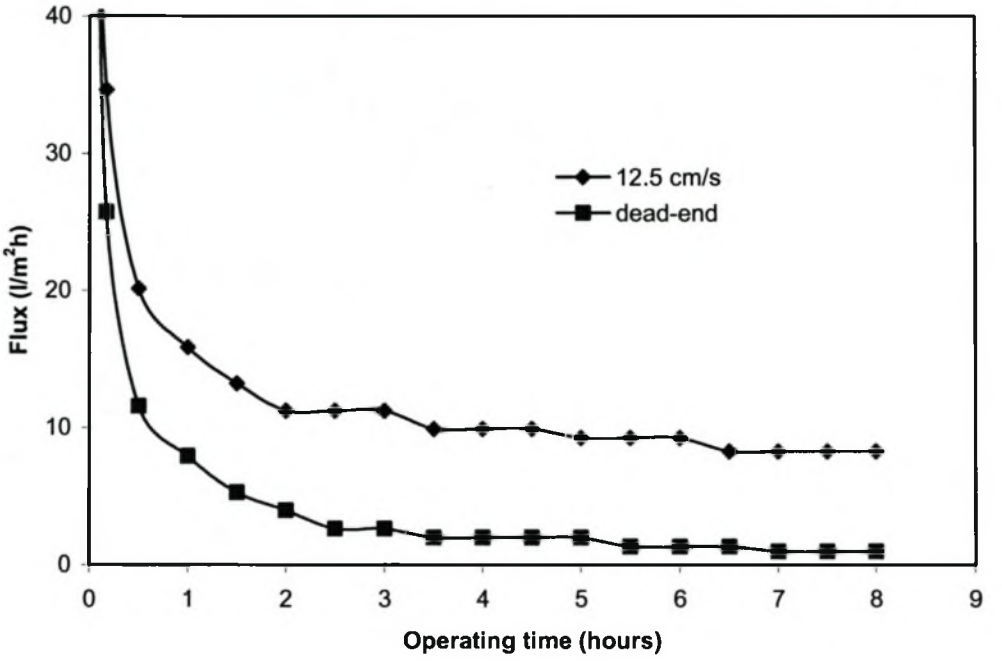

Figure 8.4: Permeate-flux vs. operation time in the fouling experiment carried out with paper mill effluent at flow rates: dead-end and 12.5 cm/s, and pressure 175 kPa.

Ultrasonic responses at dead-end:

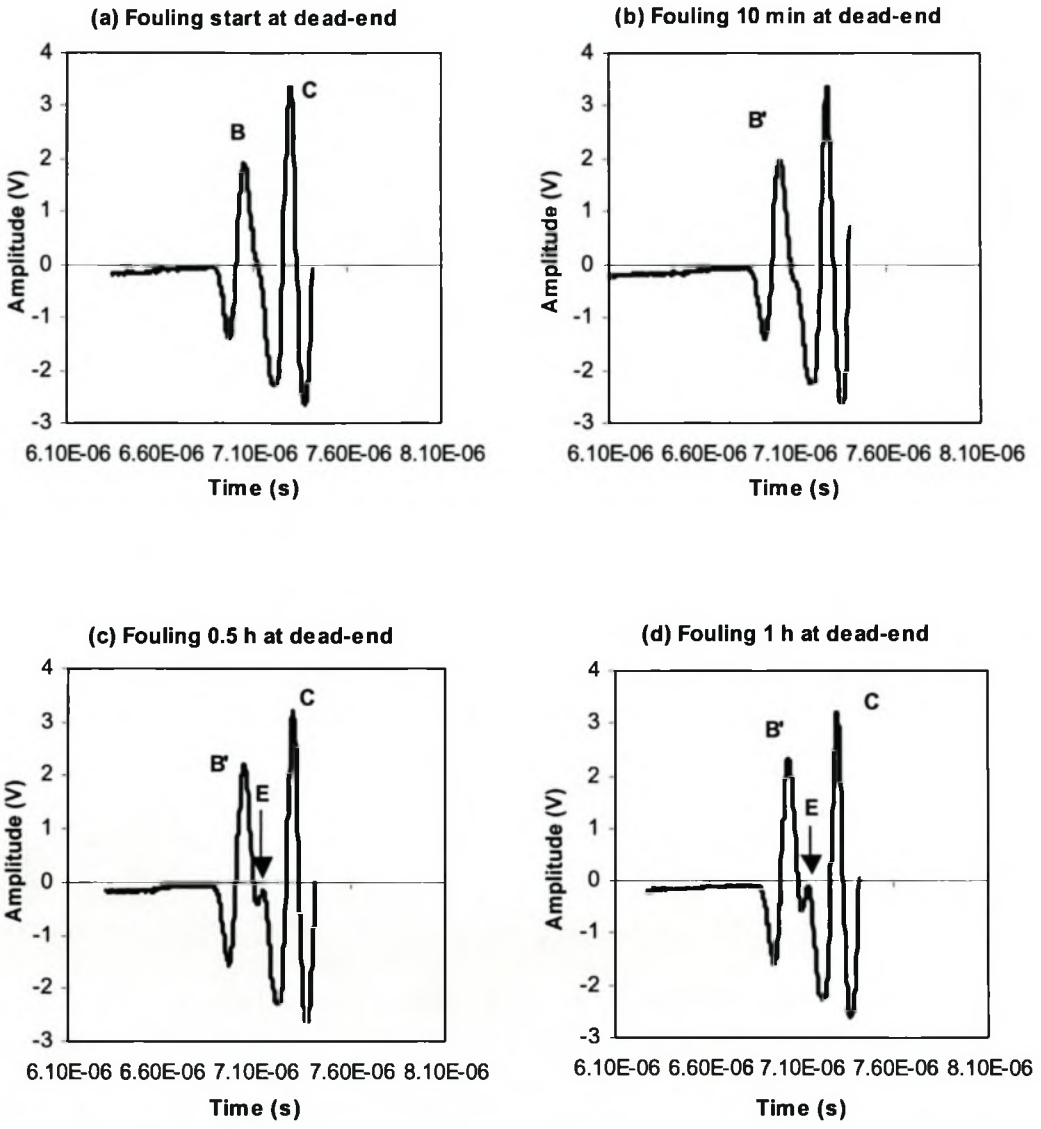

Figure 8.5: Ultrasonic signal responses after 0 (start), 10 min, 0.5 and 1 h of operation in the fouling experiment (175 kPa, dead-end) carried out with paper mill effluent.

Note: The reflection signals B, B', C and E are generated from the interfaces: water/PSU_1 layer, feed/fouling layer (combined PSU_1), PSU_2 layer/polyester backing, PSU_1 layer/ PSU_2 layer.

Ultrasonic responses at dead-end:

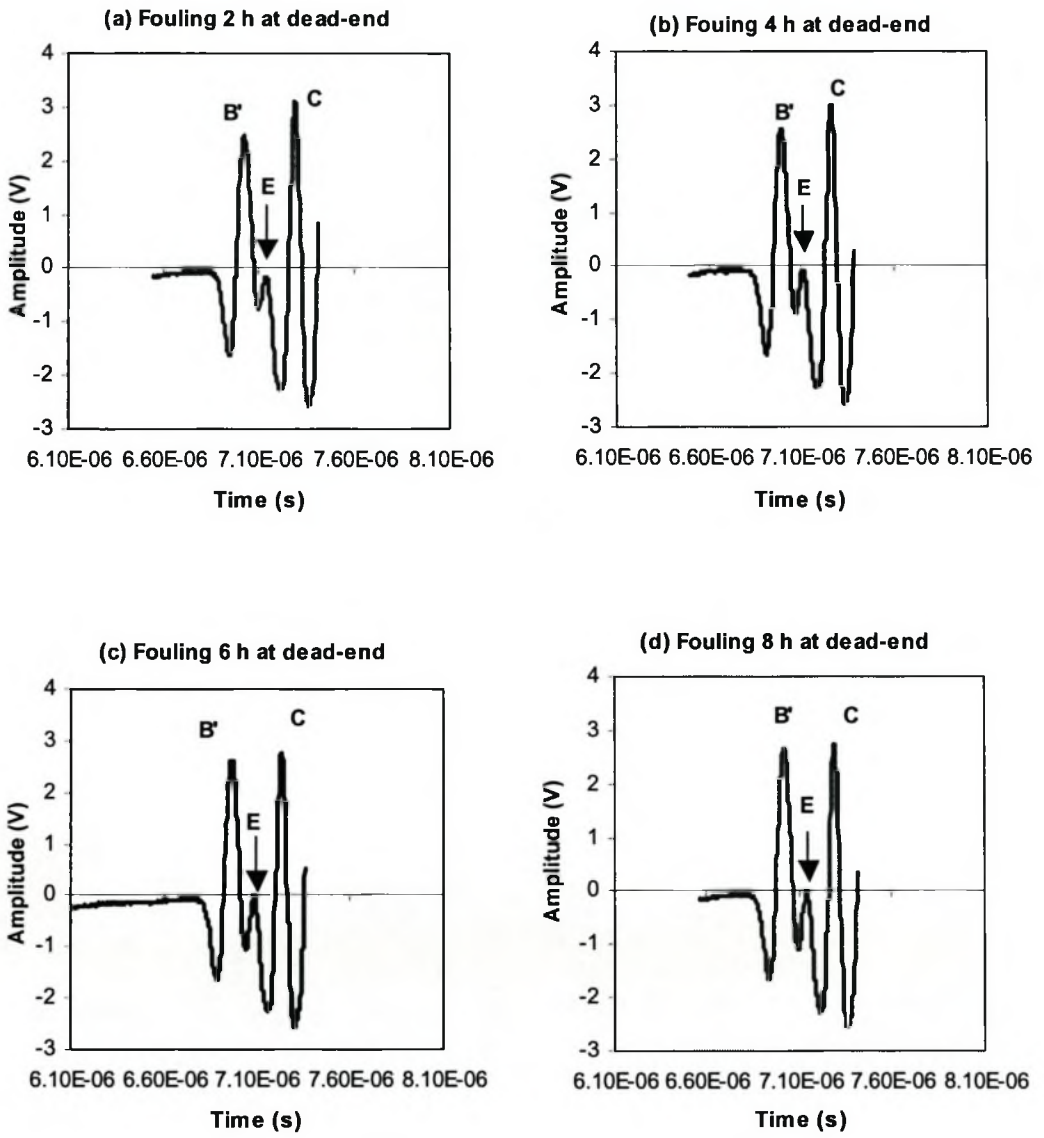

Figure 8.6: Ultrasonic signal responses after 2, 4, 6 and 8 h of operation in the fouling experiment (175 kPa, dead-end) carried out with paper mill effluent.

Microscopic images:

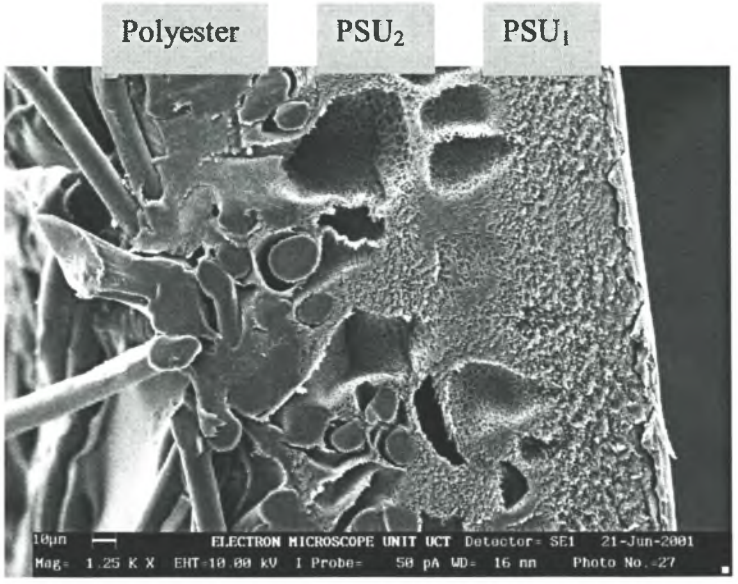

(a)

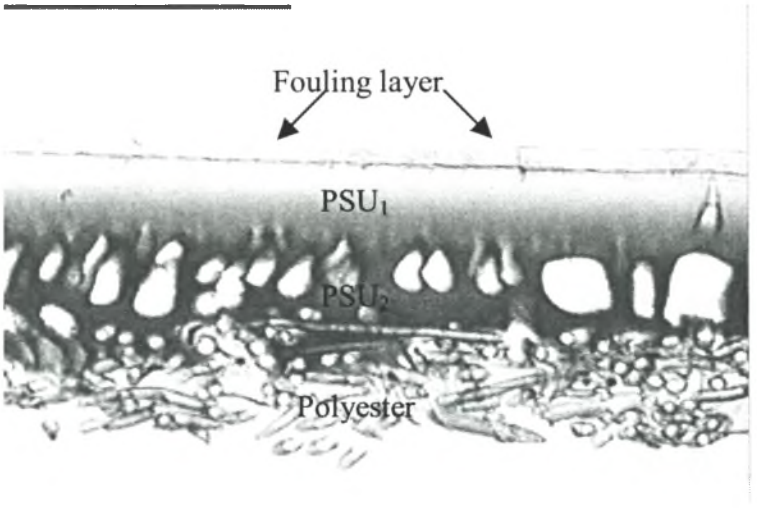

(b)

Figure 8.7: (a) SEM micrograph: cross-sectional view of a clean PSU membrane, magnification 1250×; (b) micrograph of cross-sectional view of PSU membrane fouled by paper effluent, magnification 250 ×. PSU_1 – a dense PSU layer, PSU_2 – a porous PSU layer, polyester – a non-woven polyester backing.

Ultrasonic responses at crossflow:

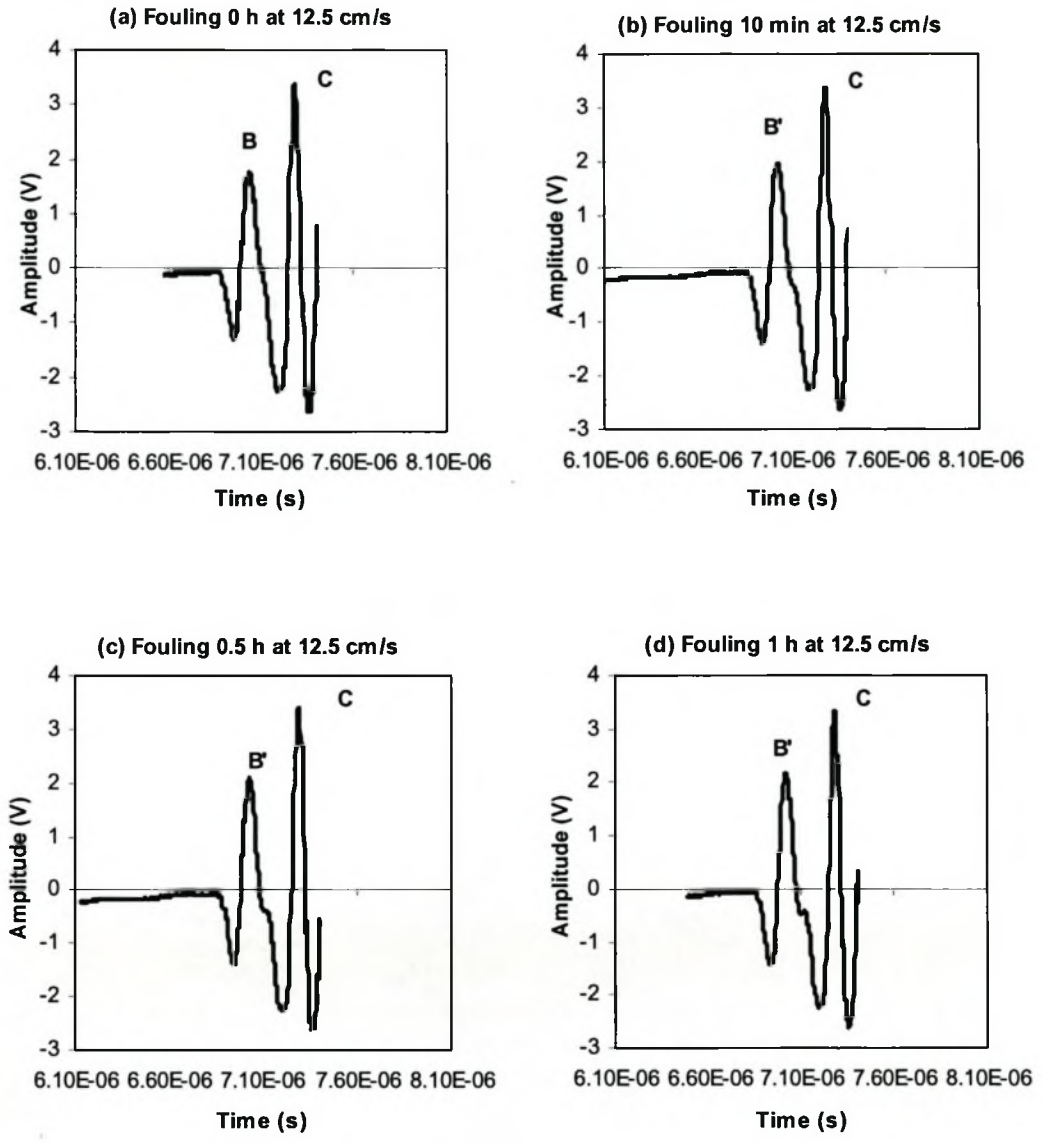

Figure 8.8: Ultrasonic signal responses after 0 (start), 10 min, 0.5 and 1 h of operation in the fouling experiment (175 kPa, 12.5 cm/s) carried out with paper mill effluent.

Ultrasonic responses at crossflow:

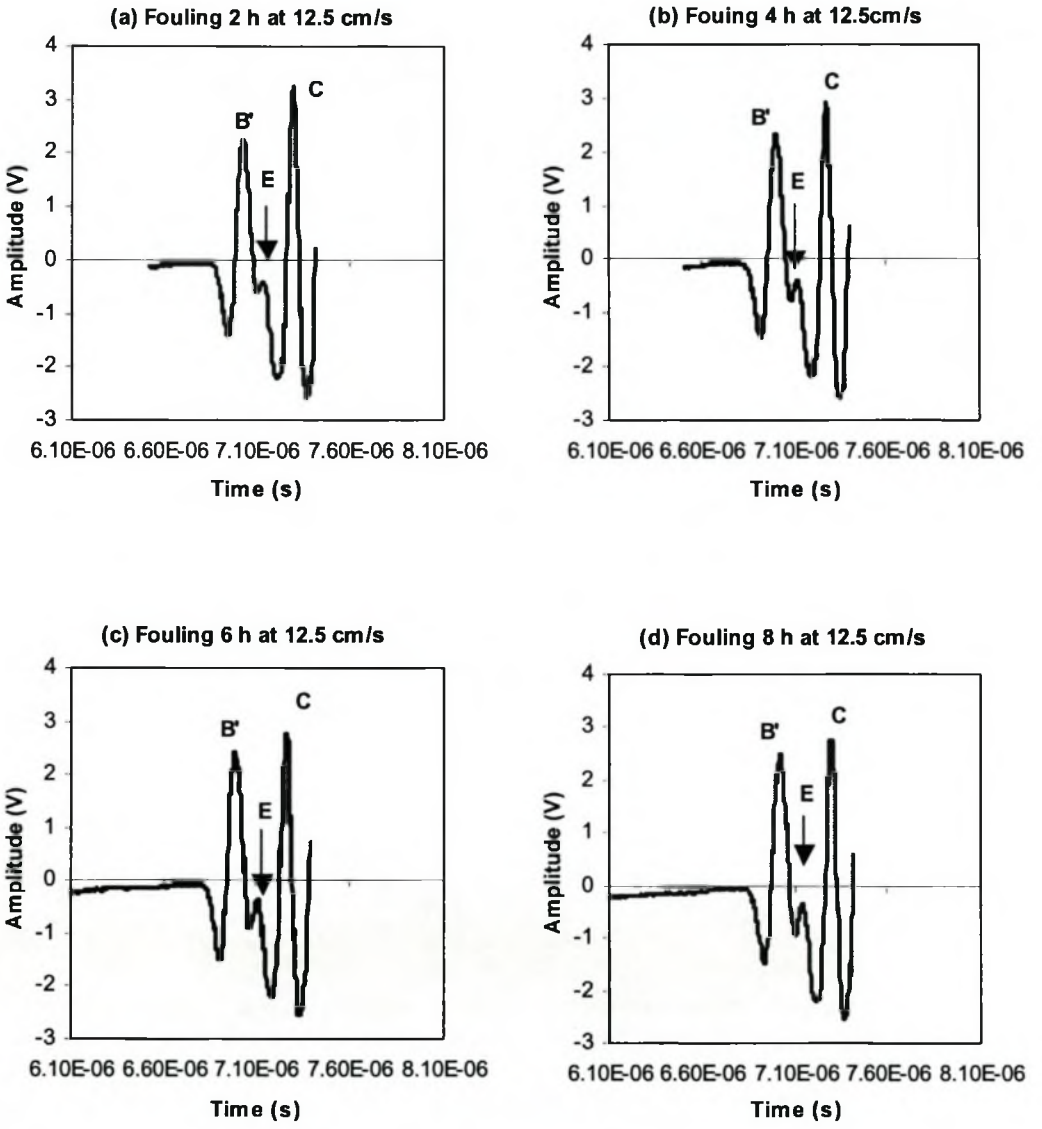

Figure 8.9: Ultrasonic signal responses after 2, 4, 6 and 8 h of operation in the fouling experiment (175 kPa, 12.5 cm/s) carried out with paper mill effluent.

Note: The reflection signals B, B', C and E are generated from the interfaces: water/PSU_1 layer, feed/fouling layer (combined PSU_1), PSU_2 layer/polyester backing, PSU_1 layer/ PSU_2 layer.

Microscopic images:

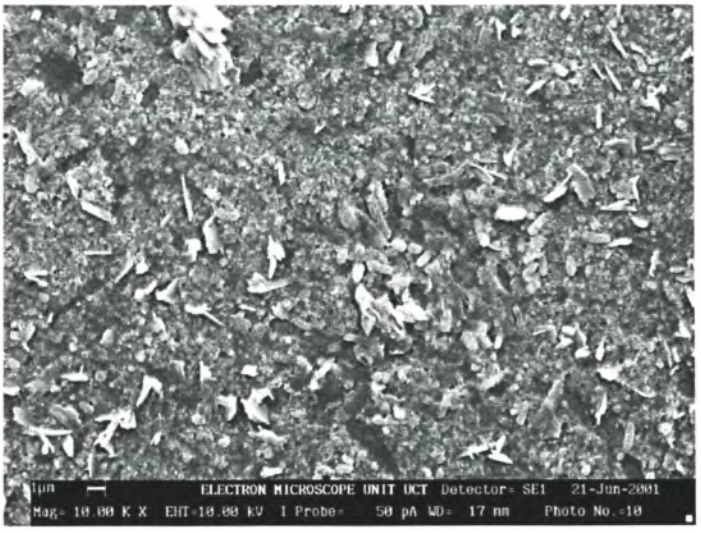

(a)

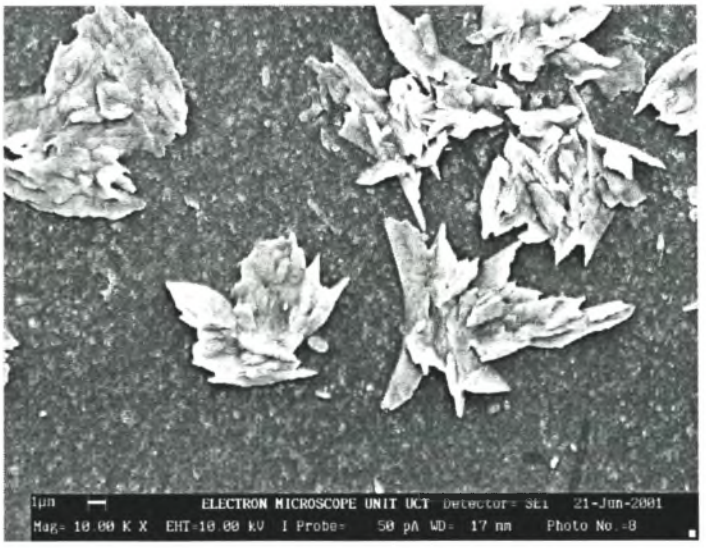

(b)

Figure 8.10: Microscopic images of PSU membranes fouled by paper mill effluent after 8 h of fouling operation at flow rates (a) dead-end and (b) 12.5 cm/s; magnification: 10,000 ×.

8.4.3 DATA ANALYSIS – DIFFERENTIAL SIGNALS

Further studies were carried out to investigate build-up of a fouling layer and its physical state on a membrane surface so as to interpret the results observed in the above experiments. It was found from this study that the UTDR technique provides a means of producing a differential signal (an echo signal of a fouling layer) by comparing a reference waveform and a test waveform according to wave superimposition principles [Bland, 1988]. A clean membrane waveform obtained upon pure-water filtration or at fouling start is used as a reference waveform for later use during fouling (or cleaning) processes. A fouled membrane waveform obtained during fouling process can be used as a test waveform.

Results of differential signals during dead-end and crossflow (12.5 cm/s) experiments are shown in Figures 8.11 and 8.12.

Changes in amplitude of the differential signals during dead-end and crossflow (12.5 cm/s) filtration are shown in Figure 8.13.

Figure 8.14 illustrates the thickness of the fouling layer as a function of operation time during fouling experiments with paper mill effluent at flow rates of dead-end and 12.5 cm/s.

Differential signals at dead-end:

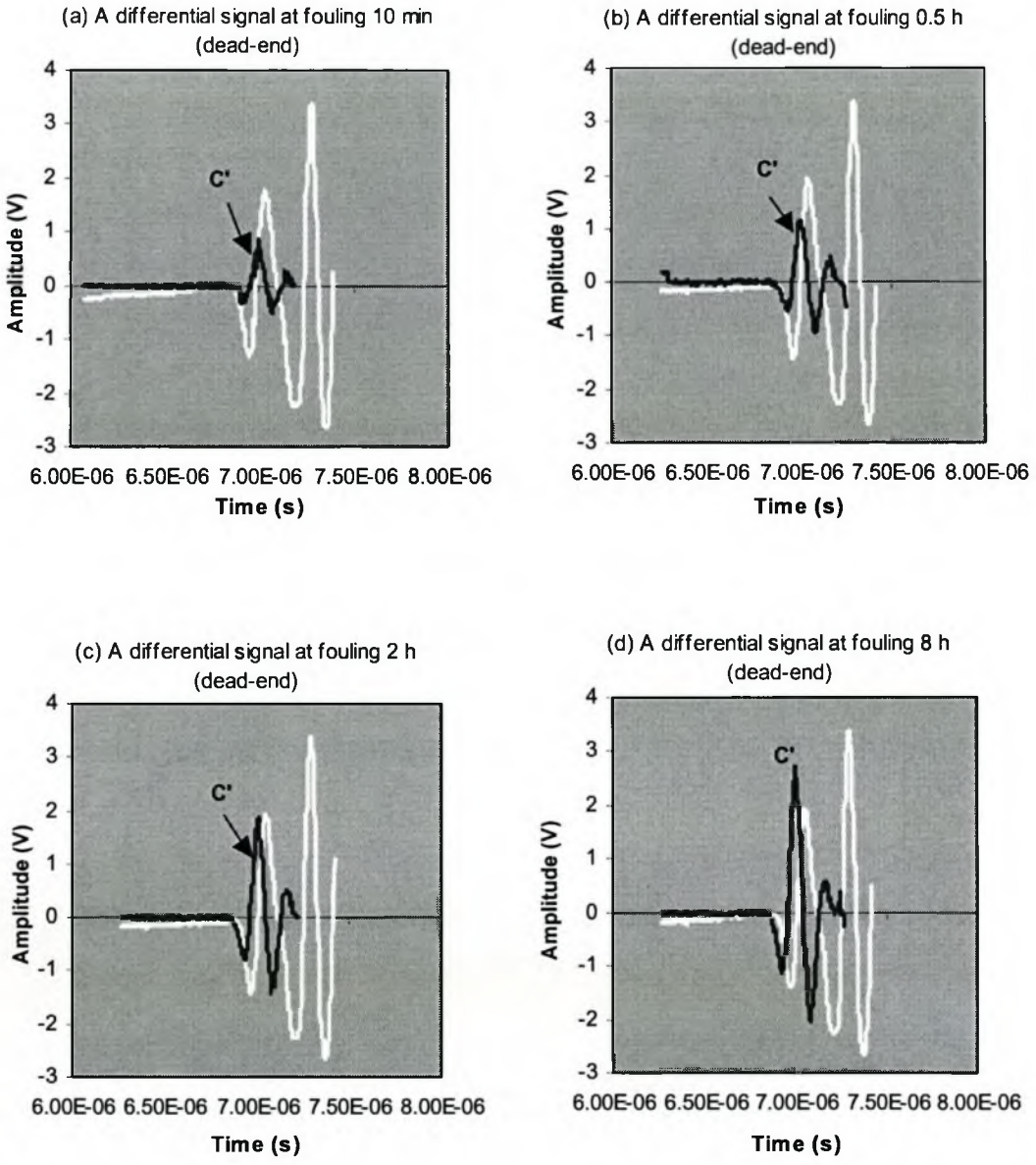

Figure 8.11: Differential signals (Peak C') after 10 min, 0.5, 2 and 8 h of operation in the fouling experiment carried out with paper mill effluent at pressure 175 kPa and dead-end filtration.

Note: the white line represents ultrasonic signal responses of a clean PSU membrane.

Differential signals at crossflow:

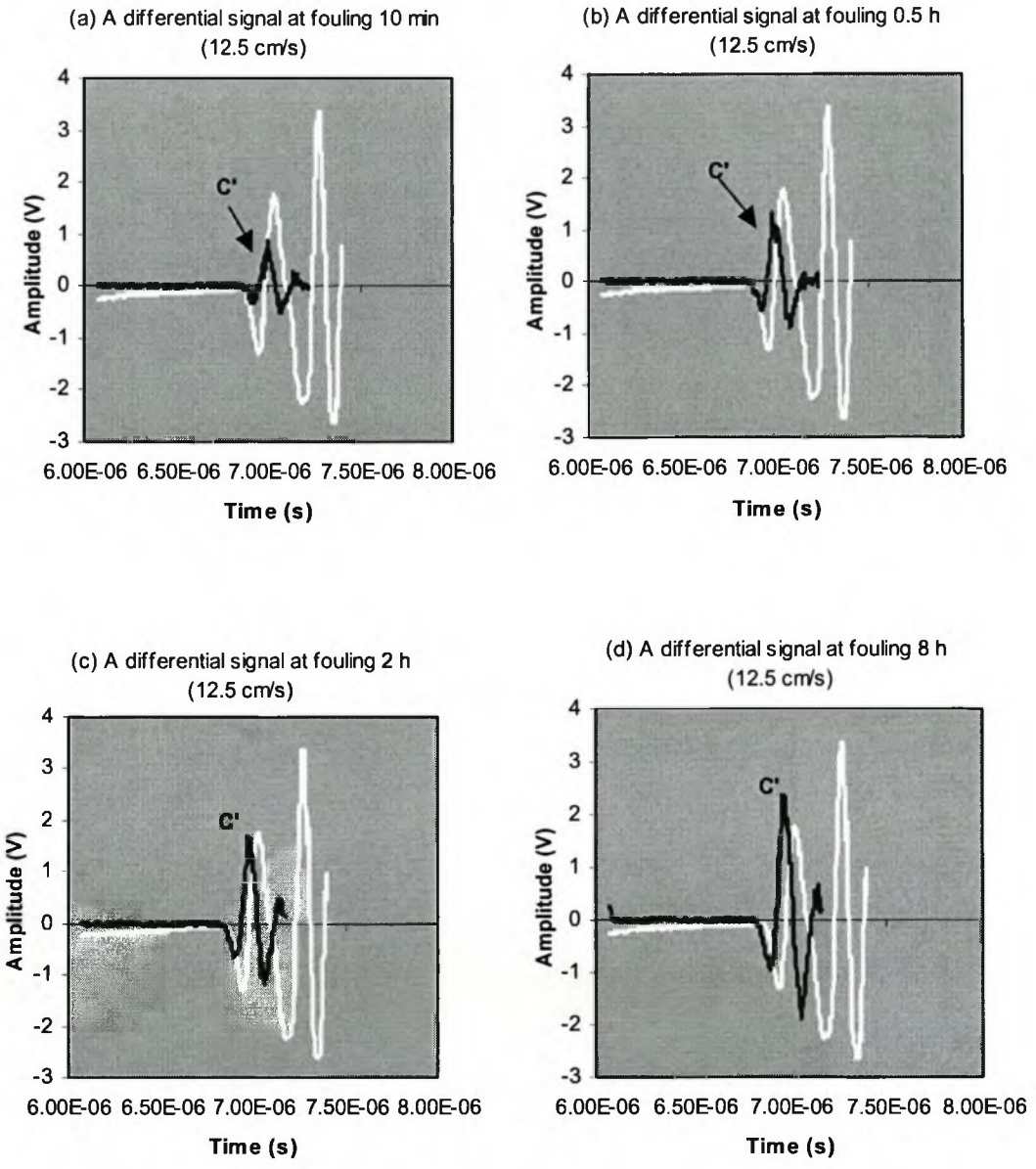

Figure 8.12: Differential signals (Peak C') after 10 min, 0.5, 2 and 8 hours of operation in the fouling experiment carried out with paper mill effluent at pressure 175 kPa and crossflow rate 12.5 cm/s.

Note: The white line represents ultrasonic signal responses of a clean PSU membrane.

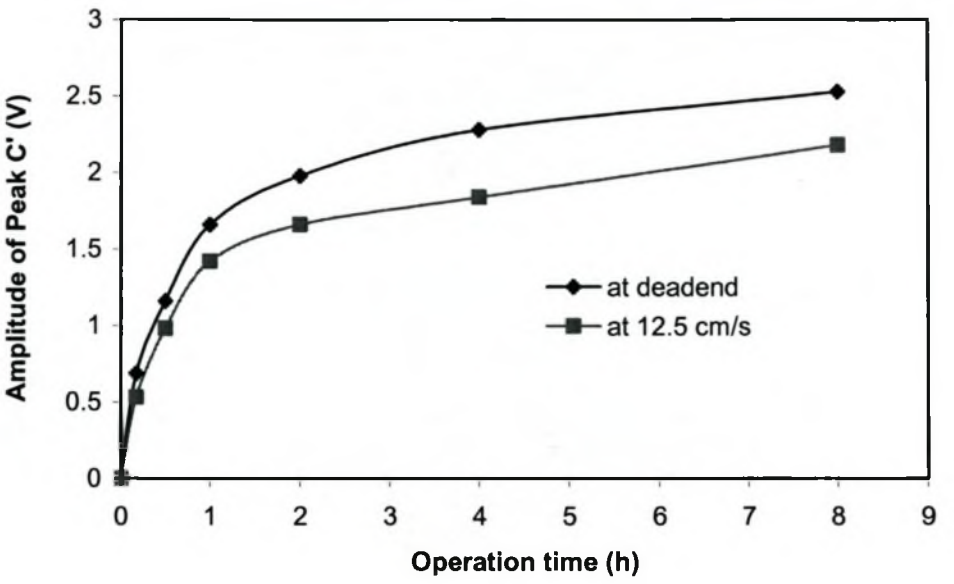

Figure 8.13: Amplitude of differential signal (Peak C') versus operation time during fouling experiments carried out with paper effluent at flow rates of dead-end and 12.5 cm/s.

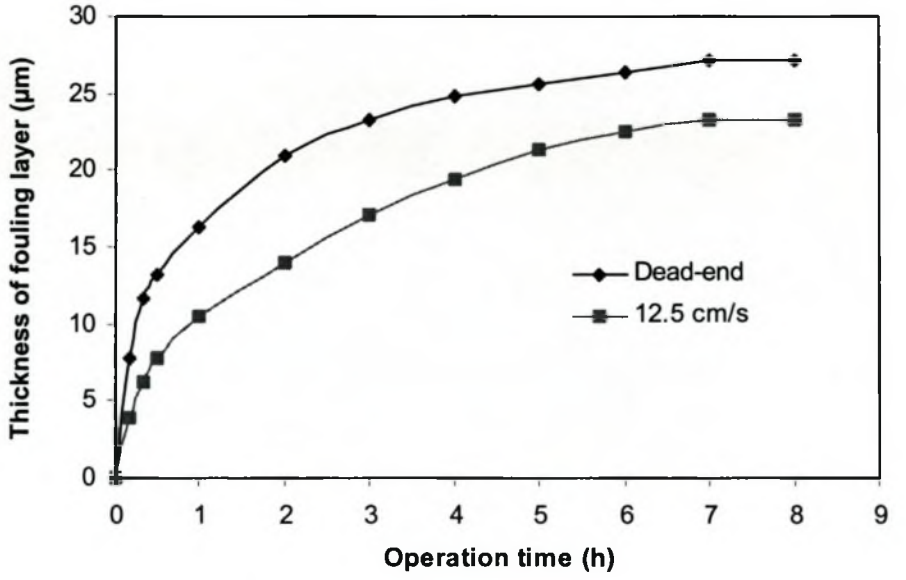

Figure 8.14: The thickness of fouling layer as a function of operation time during fouling experiments at flow rates of dead-end and 12.5 cm/s.

8.4.4 CLEANING EXPERIMENT AND UTDR MEASUREMENT

To investigate the suitability of the UTDR technique for fouling removal strategies, the following fouling and cleaning experiments were carried out. A further fouling experiment was carried out with paper mill effluent at a flow rate of 2.1 cm/s and applied pressure 185 kPa. The total operating time for the fouling experiments was 20 h. Results of ultrasonic reflections in the fouling experiment are shown Figure 8.15. Figure 8.16 displays SEM analysis of clean and fouled membranes.

Figure 8.17 shows the results of ultrasonic response signals during the cleaning experiments. Pure water flux recovery of the cleaned membrane obtained by different cleaning methods is illustrated in Figure 8.18. SEM micrographs of the cleaned samples were also recorded (Figures 8.19 and 8.20). Results of differential signals recorded during cleaning processes are shown in Figure 8.21.

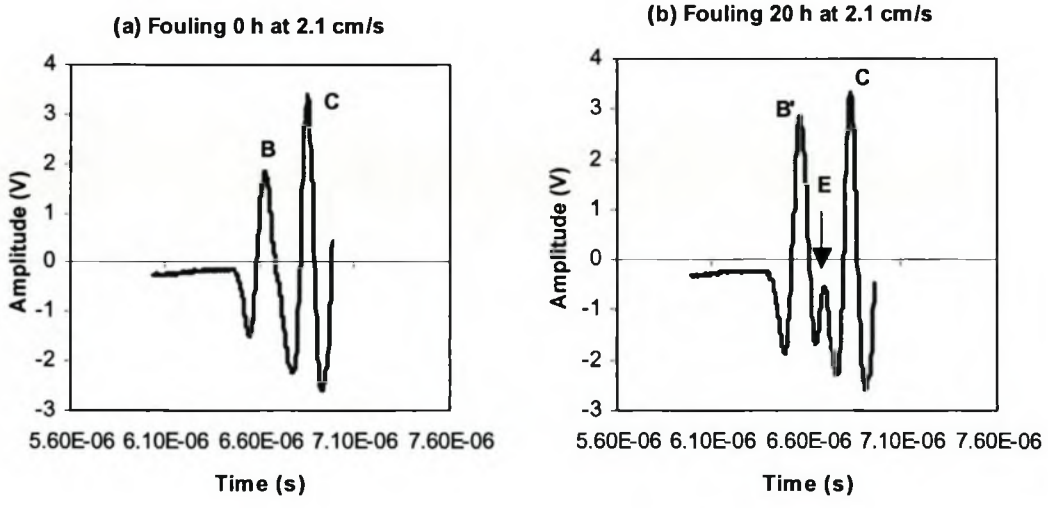

Figure 8.15: Ultrasonic signal responses after 0 (start) and 20 h of operation in the fouling experiment carried out with paper mill effluent at pressure 185 kPa and flow rate 2.1 cm/s.

Microscopic images:

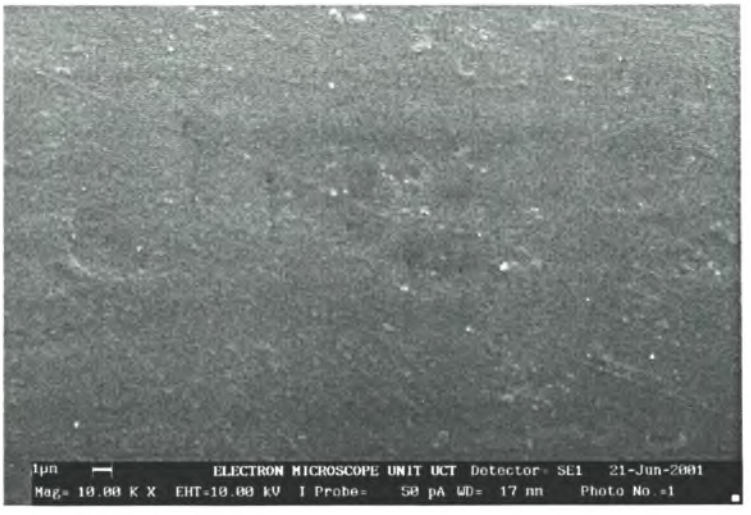

(a)

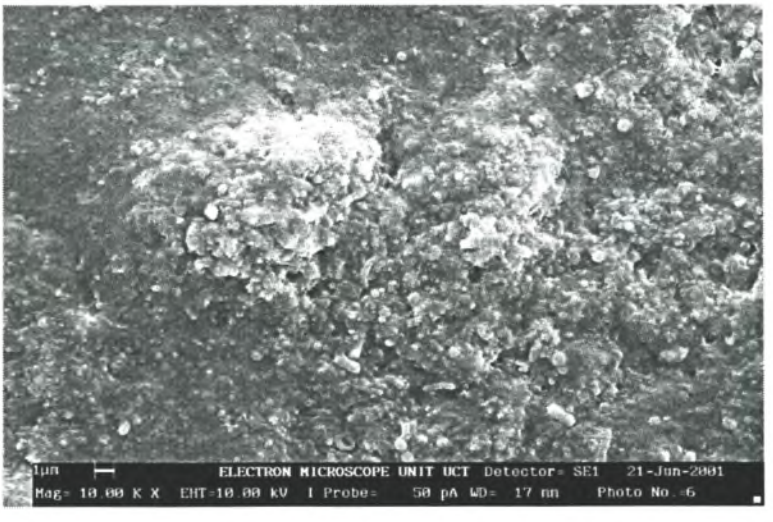

(b)

Figure 8.16: Microscopic images of (a) a clean PSU membrane and (b) a PSU membrane fouled by paper mill effluent after 20 h of operation, magnification: 20,000×.

Ultrasonic responses:

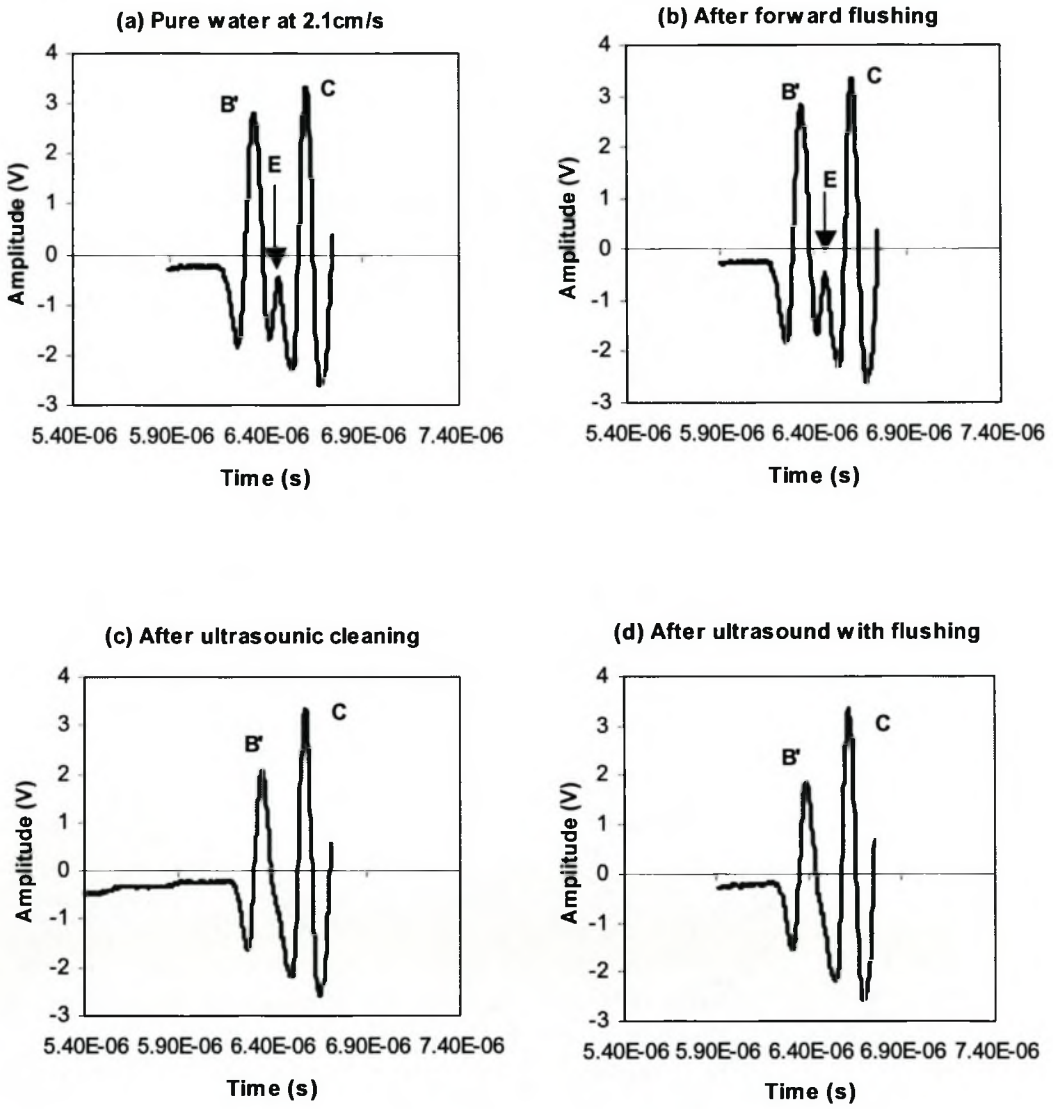

Figure 8.17: Ultrasonic signal responses during pure water experiments after different cleaning methods: forward flushing, ultrasonic irradiation and ultrasound with forward flushing.

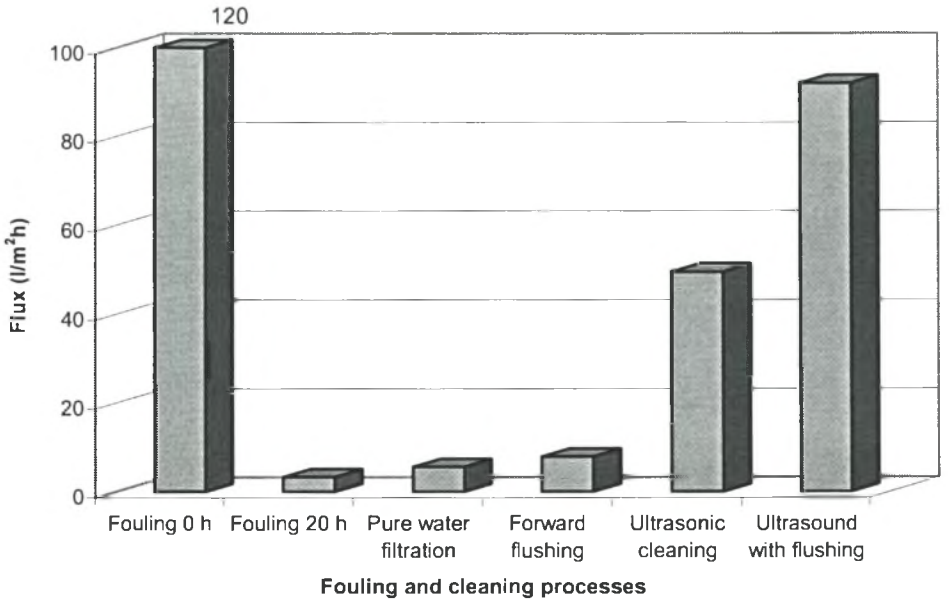

Figure 8.18: Changes of permeate flux during fouling and cleaning processes (at 2.1 cm/s and 185 kPa): fouling 20 h; pure water filtration; forward flushing; ultrasonic cleaning and ultrasound associated with flushing.

Figure 8.19: Microscopic image of the cleaned PSU membrane surface by forward flushing, magnification: 20,000×.

Microscopic images:

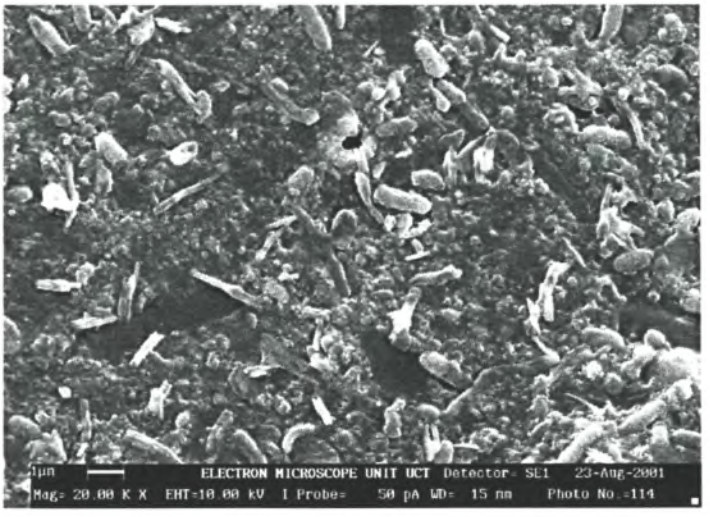

(a)

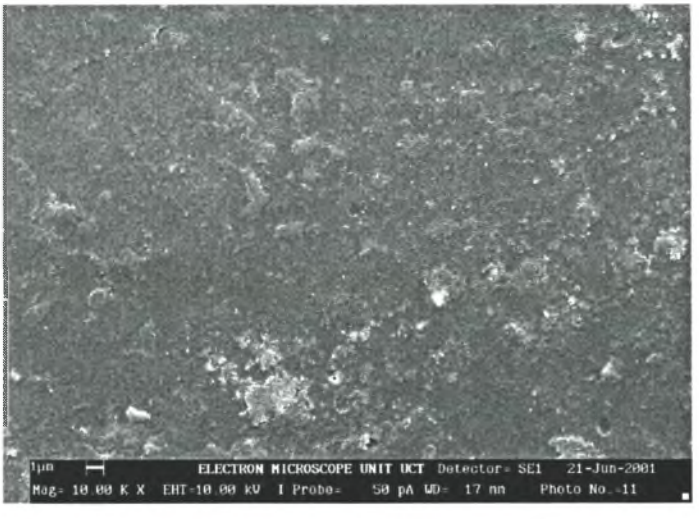

(b)

Figure 8.20: Microscopic images of the cleaned PSU membrane surface: after cleaning by (a) ultrasonic cleaning; (b) ultrasound with forward flushing; magnification: 20,000×.

Differential signals:

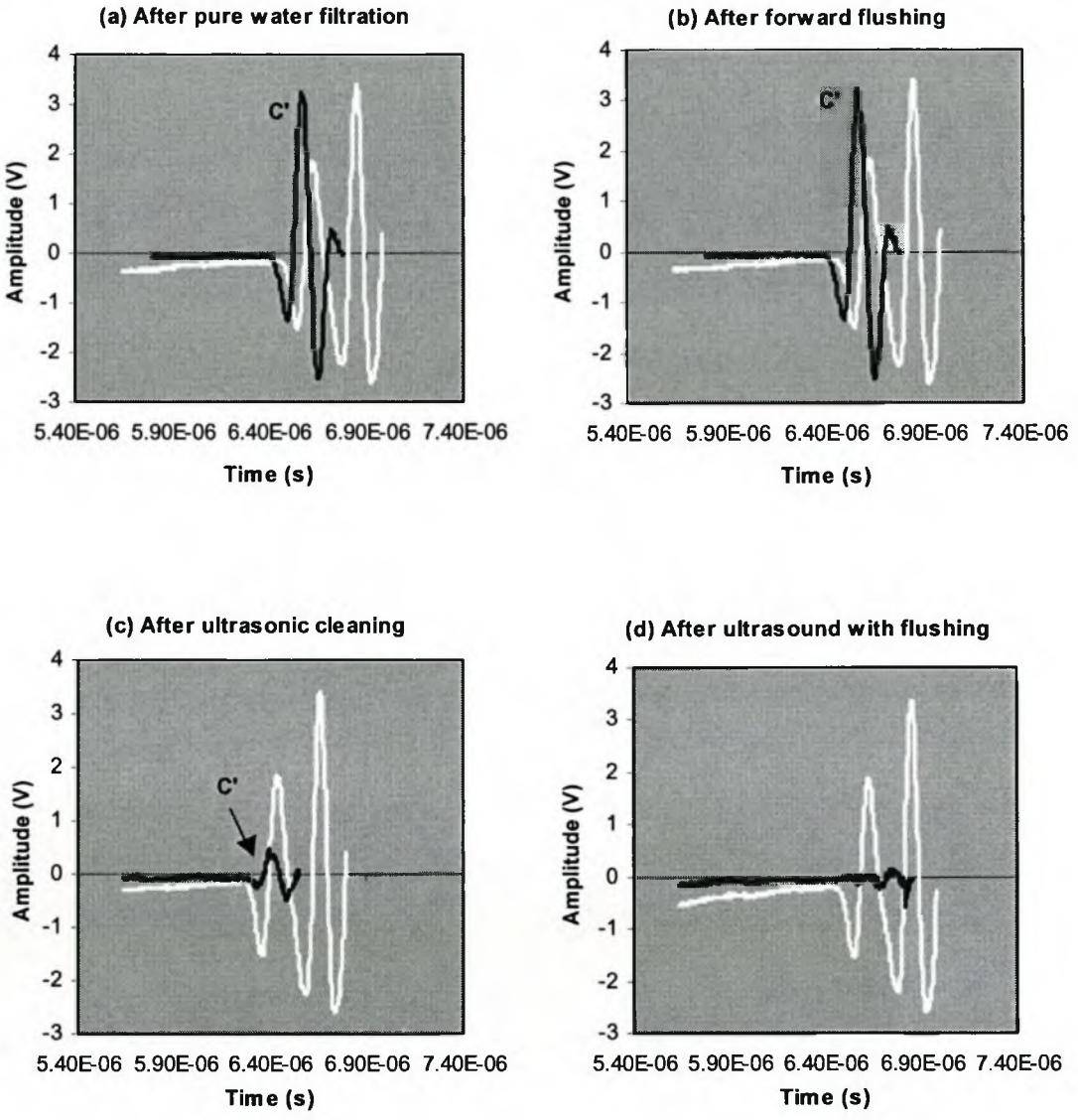

Figure 8.21: Differential signals after (a) pure water filtration after 20 h of fouling operation; cleaning by (b) forward flushing; (c) ultrasonic cleaning; (d) ultrasound with flushing.

Note: The white line represents ultrasonic signal responses of a clean PSU membrane.

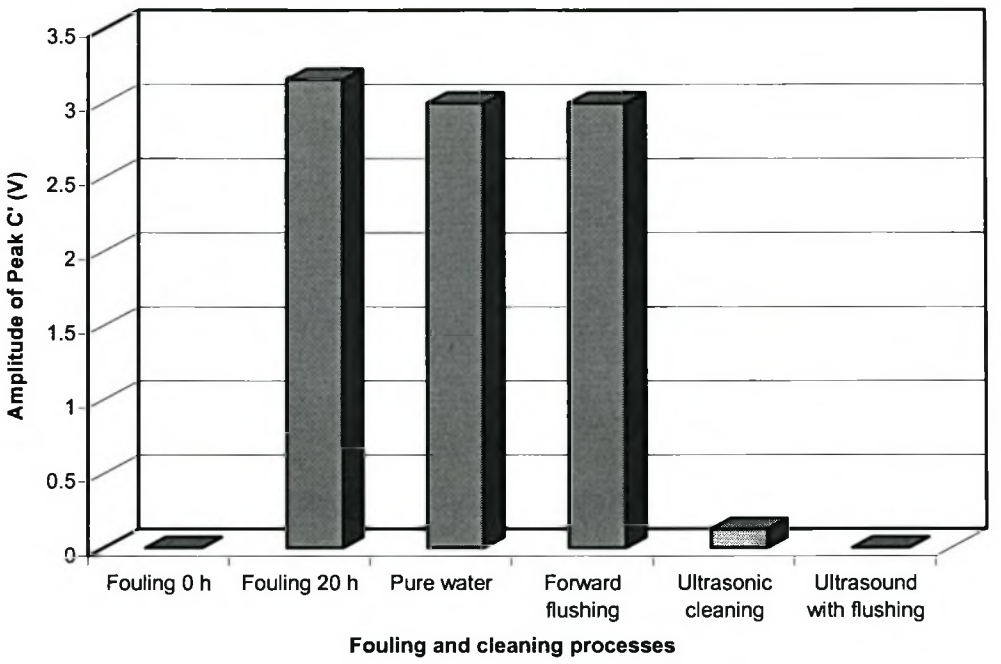

Figure 8.22: Differential signals during fouling and cleaning processes.

8.5 INTERPRETATION OF RESULTS

8.5.1 HYDROSTATIC PRESSURE EXPERIMENT

The ultrasonic response signals revealed a PSU composite membrane that is composed of a PSU layer and a polyester backing layer. The UTDR measurement was focused on Peak B, which indicates the membrane surface (Figure 8.1).

The membrane echo signals B and C shifted to signals B' and C' when the hydrostatic pressure increased from 0 to 160 kPa (Figure 8.2). Figure 8.2 also shows that reflection signals B' and C' are sharper at a hydrostatic pressure of 160 kPa than at 0 kPa. This suggests that the PSU membrane is compacting, causing changes in acoustic impedance under a higher hydrostatic pressure, and becomes denser.

As the hydrostatic pressure increased, the membrane moved farther from the transducer. A near linear relationship exists between the hydrostatic pressure and the arrival time of the reflected signal from membrane signal B (Figure 8.3). The shift distance of Peak B with the hydrostatic pressure can be calculated by Equation 3.1 (the sound velocity in pure water is 1438 m/s) as shown in Figure 8.3. This corresponds to a change in spacing between the top plate and the membrane. The shift distance from Peak B to Peak B' is 133 μm as the hydrostatic pressure increased from 0 to 220 kPa. The distance also includes the shift because of the membrane compaction. As shown in Figure 8.3, the difference in the arrival times between Peaks B and C is 0.22 μs and the difference in the arrival times between Peaks B' and C' is 0.2 μs. The thickness of PSU membrane decreases by 24 μm with an increase in pressure from 0 to 160 kPa (the average sound velocity in a PSU membrane: 2400 m/s). Results of the hydrostatic pressure experiments proved the membrane compaction.

8.5.2 FOULING EXPERIMENT AND UTDR MEASUREMENT

As shown in Figure 8.4, the value of the flux declined rapidly at the beginning and then reached a near steady-state flux after 2 h of operation. Further, the decline in the permeate flux was faster at dead-end filtration (0 cm/s) than crossflow (12.5cm/s). It implies that significant membrane fouling occurred.

Consistent with the above observation, the corresponding ultrasonic signal responses exhibited rapid changes in amplitude as fouling proceeded (Figure 8.5). Peak B (Figure 8.5a) represents the PSU layer(s). Peak B has a shoulder, showing that the PSU membrane has two layers, a thin and dense layer (PSU_1) and a porous layer (PSU_2, small shoulder, later a peak). In general, once fouling is initiated on the membrane surface, the acoustic impedance difference at the feed solution/membrane interface will change, resulting in a change in the amplitude of echo B. As shown in Figure 8.5c, an increase in the amplitude from Peak B (1.687 V) to B' (2.06 V) can be seen after 0.5 hours of fouling, as a result of the deposition and growth of a fouling layer on the membrane surface. The ultrasonic response of the fouling layer combined with that of PSU_1 formed Peak B'. The difference in arrival times, dT, between Peaks B and B' is 20 ns, due to an increase in the thickness of the fouling layer. Simultaneously a 'new' peak E appeared. It was generated from the interface between PSU_1 and PSU_2. It is because the PSU membrane has two layers: PSU_1 and PSU_2. PSU_1 is so thin compared to PSU_2 that the two traces appear merged (following from waves superimposition principles) before fouling has taken place. After fouling, the fouling layer with PSU_1 becomes thick enough, relative to the PSU_2 layer, to form a distinct echo. The ultrasonic response models related to fouling deposition processes are illustrated in Figure 8.23.

As the chemical composition of the fouling layer is mainly lignin or lignosulphonate [Domingo, 2001], both of which have densities similar to the PSU_1 layer, the fouling layer and PSU_1 give a single peak in the UTDR. Hence the reflected signals B, B', C and E were generated from the interfaces: water/PSU_1, feed solution/fouling layer (combined PSU_1), PSU_2 layer/polyester backing and PSU_1/PSU_2. SEM and optical microscope cross-sectional views of a PSU membrane revealed a composite PSU

membrane structure - a denser skin layer PSU_1, a porous layer PSU_2 and a non-woven polyester backing as shown in Figure 8.7. These observed results are consistent with real-time ultrasonic measurements.

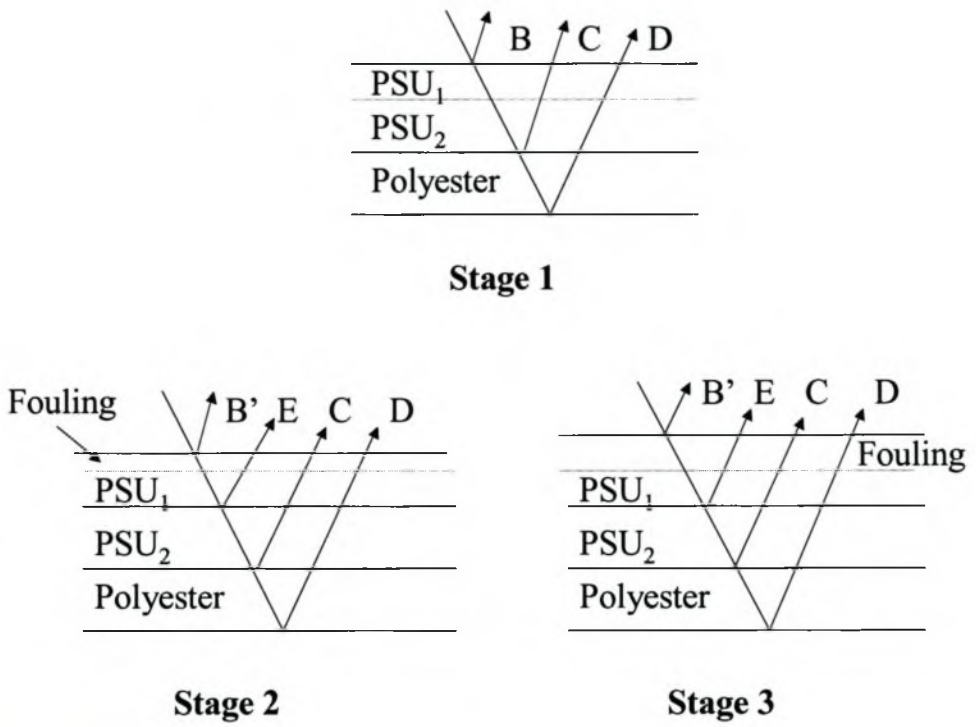

Figure 8.23: Ultrasonic reflection models in the fouling processes. Stage 1: a clean two-layer PS membrane with polyester backing; Stage 2: deposition of a fouling layer on the membrane surface; Stage 3: growth of a fouling layer.

As fouling layer growth progressed, more fouling covers the membrane surface, a denser fouling layer is formed and a greater acoustic impedance change between the bulk solution and the membrane is expected. This will be detected as a sharper reflection. Thus, an echo with greater amplitude was observed at 1, 2, 4, 6 and 8 h of fouling operation in Figure 8.5 and 8.6. The time-domain movement (ahead) of the fouling echo signal (B') was observed as a result of an increase in the fouling layer thickness. The arrival time of peak B was 7.07 μs. After 8 h of fouling operation, the amplitude and arrival time of Peak B' were 2.468 V and 7.028 μs, respectively.

Similar results of ultrasonic responses can be observed in Figures 8.8 and 8.9 as further experiments were carried out with paper mill effluent at a crossflow rate 12.5 cm/s and pressure 175 kPa. It was found that the amplitude of peak B' at crossflow 12.5 cm/s increased at a slower rate than that at dead-end. An apparent peak E at 12.5 cm/s appeared after 2 h of operation (Figure 8.9a). However, after 0.5 h of operation Peak E was already present in dead-end (Figure 8.5c). The fouling layer on the membrane surface appeared and grew fast at lower axial velocity because of the lower shear rates. This indicates that the ultrasonic testing technique is able to distinguish between the growth rates of a fouling layer on a membrane surface in dead-end and crossflow operations.

In order to study membrane coverage, the fouled membranes were taken for SEM analysis to confirm the ultrasonic measurement and membrane coverage in Figure 8.10. The micrographs of the membrane surface after 8 h of fouling operation under dead-end and crossflow (12.5 cm/s) revealed complete membrane coverage with a fouling layer. Figure 8.10a shows that mixed (fine and large) particles were left on the membrane surface because of dead-end operation. This suggests that the sharper echo peak was reflected from the fouled membrane surface with a denser fouling layer (Figure 8.6d). Fine particles were removed and big particles were retained on the membrane surface at crossflow (12.5 cm/s) with higher shear rates. The big particles resulted in the formation of a loose fouling layer with a weak reflection compared with dead-end. A rough/sparse fouling layer surface covering on the membrane surface resulted in some sound distribution (Figure 8.9d). Hence, reflection signals during crossflow operation are weaker than that during dead-end operation. It is concluded that the in situ ultrasonic measurements corroborated the flux decline and morphological observations of membrane coverage.

8.5.3 DIFFERENTAIL SIGNALS

It is shown in Figure 8.11 that a differential signal was observed within a short time, namely 10 min of fouling operation, and grew at 0.5, 2 and 8 h as fouling proceeded. The size of the presupposes pores that even shorter time measurements should be possible. A sharper differential signal emerged due to a denser fouling layer on the membrane surface after 8 h of fouling operation at dead-end. Time-domain movement from Peaks B to B' can be also observed as a result of an increase in the thickness of fouling layer. Figure 8.12 shows similar results achieved at 10 min, 0.5, 2 and 8 h of fouling operation during crossflow filtration.

Changes in amplitude of the differential signals during dead-end and crossflow (12.5 cm/s) filtrations are shown in Figure 8.13. These indicated that the amplitude of the differential signals increased as fouling proceeded. Furthermore, the increase in the ultrasonic amplitude became slower as the axial velocities increased. This suggests that the rate of fouling was lower at a higher axial velocity.

Another basic quantity measured in non-destructive ultrasonic testing is the time of flight or the amount of time required for the sound to travel through the sample. That is to say that the ultrasonic technique can quantify the thickness of a fouling layer (on a membrane surface) by comparing ultrasonic response signals. The thickness of a fouling layer on a membrane surface can be calculated by Equation 3.1 (the sound velocity in the fouling layer is 1550 m/s). The thickness of the fouling layer increased rapidly at the beginning of fouling because of concentration polarization and fouling layer formation, followed by a slow increase due to gradual growth of the fouling layer (Figure 8.14). Moreover, an increase in the thickness of the fouling layer grew faster during dead-end filtration than during crossflow (12.5 cm/s). The thickness of the fouling layer after 8 h of fouling operation was 27.1 μm at dead-end filtration, and 23.2 μm at crossflow (12.5 cm/s), respectively.

8.5.4 CLEANING EXPERIMENT

Results of a further fouling experiment showed an increase in amplitude-domain and movement in time-domain from Peaks B to B' after 20 h of fouling operation in Figure 8.15. Peak E also appeared after 20 h of fouling operation. It indicated that a dense fouling layer was formed on the membrane surface. SEM analysis of the fouled membrane (Figure 8.16) corroborated this observation.

An increase in permeate flux and a decrease in the amplitude of the ultrasonic response signal of the fouling layer, in comparison with the 20 h fouling echo signal, were observed (Figures 8.18 and 8.22) because of changing the bulk solution from effluent to pure water. The change in the bulk solution from effluent to pure water resulted in the reduction of concentration polarization on the membrane surface. This again suggests that the UTDR technique is able to detect subtle changes on the membrane surface.

Flushing slightly increased the pure water flux (Figure 8.18) and decreased the amplitude of the ultrasonic response signal of the fouling layer (Figures 8.21b and 8.22). This again suggests that forward flushing can reduce the rate of membrane fouling. The deposited fouling layer on the membrane surface is expected to become re-suspended and swept away by tangential- or cross-flow [Redkar and Davis, 1995]. The peak of the fouling echo signal decreased because the density of fouling layer was reduced after forward flushing. Therefore, the UTDR technique is able to explore the presence and the removal of the fouling layer in real-time.

In addition, it was found that the paper effluent fouling on the PSU membrane is difficult to clean using only forward flushing. SEM analysis revealed that there is still a dense fouling layer on the membrane surface after forward flushing, although many pores produced by forward flushing appeared on the fouling layer (Figure 8.19). Hence, membrane fouling is caused by the adsorption of foulants both on and inside the membrane. Additional cleaning methods are needed.

Figure 8.18 shows that the pure water flux increased from 7.92 l/m^{2}h after forward flushing to 49.5 l/m^{2}h after ultrasonic cleaning. The disappearance of the echo signal E showed that the fouling layer was destroyed by ultrasonic irradiation (Figure 8.17c). There is a significant decrease in ultrasonic amplitude of the differential signal, from 3.0 volts after forward flushing to 0.125 volts after ultrasonic irradiation (Figures 8.22c and 8.23). This suggests that ultrasonic treatment can effectively break the fouling layer on the membrane. However, Figure 8.21c shows that the amplitude after ultrasonic cleaning is 0.125 volts, signifying that there is still some fouling on the membrane as shown in Figure 8.21a. Furthermore, the permeate flux of 49.5 l/m^{2}h obtained after ultrasonic cleaning is still lower than the original pure water flux of 190 l/m^{2}h.

After ultrasound associated with flushing, the pure water flux was 92 l/m^{2}h (Figure 8.18). Although it is still lower that the original water flux of 120 l/m^{2}h, the ultrasonic signal response shows that the differential signal disappeared after ultrasound with forward flushing (Figure 8.21). Hence, the fouled membrane was cleaned by ultrasound associated with flushing. Morphological analysis of the cleaned membrane showed that there is almost no fouling layer on the membrane surface (Figure 8.20b). This is because forward flushing produces a high tangential or cross-flow rate (40-50 cm/s) on fouling layers. These results demonstrate that the UTDR technique can monitor the removal of the fouling layer and membrane cleaning. It is suitable to study the effectiveness of various cleaning techniques.

8.6 APPLICATION OF MODELING

The PSU composite membrane was modeled on the basis of an actual membrane. Figure 8.24 shows the modelled individual and combined response signals of a clean two-layer PSU membrane with polyester backing. The modeling for an asymmetric PSU membrane in response to its reflecting properties was based on internal velocities, thicknesses and densities of multi-layers made of the PSU. A signal frequency of 10 MHz was used in the actual experiments. In order to produce a smooth signal curve, points were calculated at intervals of 3×10^{-9} s. Results of this mathematical modeling display a composite PSU membrane, which is composed of two layers (PSU_1 and PSU_2) and polyester backing.

The next model was based on the assumption that a fouling layer consisting of lignin and lignosulphonate ($\rho = 1.05$ g/cm^3), with a thickness of 20 μm, had been deposited on the membrane. The results of modeling a 20-μm fouling layer on a PSU membrane are presented in Figure 8.25. A response very similar to the signal obtained during actual measurements of fouling deposition carried out with paper mill effluent in Figures 8.11b or 8.12b was obtained. A small echo peak formed in front of the membrane peak. Further, maintaining the density and increasing the thickness of the layer to 80 μm resulted in a movement ahead in the time domain (Figure 8.26), without any significant change in the shape and peak height of the "fouling peak".

In the following model the density of a 50 μm fouling layer was increased from 1.03–1.4 g/cm^3. An increase in peak height of the fouling echo was obtained as the density of the fouling layer increased (Figure 8.27). In addition, maintaining the thickness and increasing the density of the fouling layer to 1.4 g/cm^3 resulted in a further increase in peak height and a slight change in slope at the beginning of the signal, without changing the position of the fouling echo. The differential signals obtained in Figures 8.28 and 8.29 corroborate the modeling results. Results of the UTDR indicate that growth of a fouling layer in thickness and density results in flux decline.

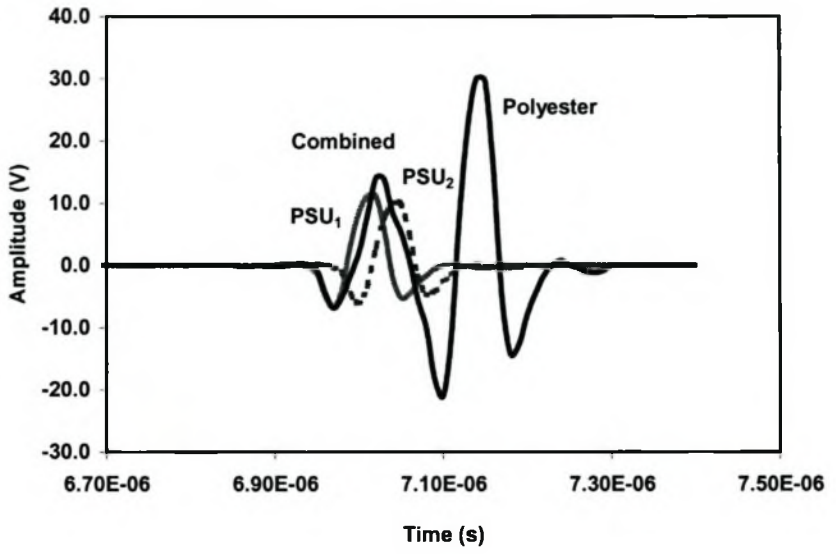

Figure 8.24: Modeling individual and combined response signals of a clean two-layer PSU membrane with a polyester backing.

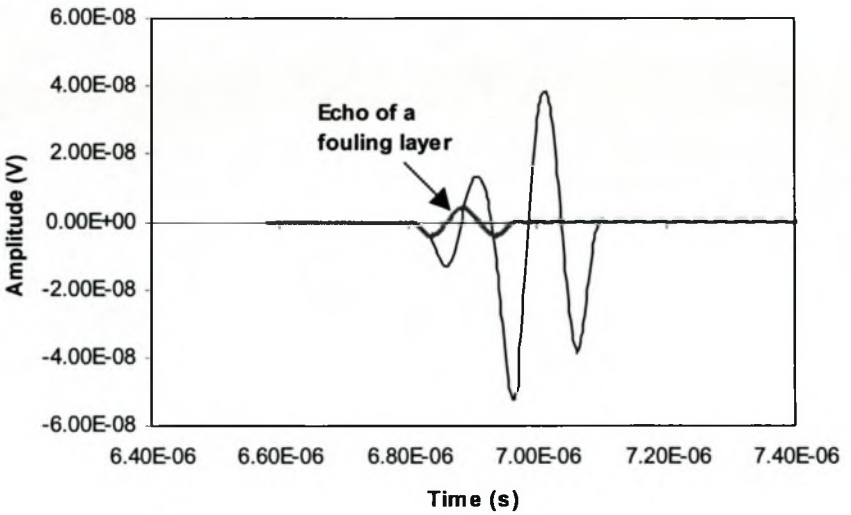

Figure 8.25: Model of a 20 μm thick fouling layer (ρ = 1.05 g/cm^3) on a PSU membrane.

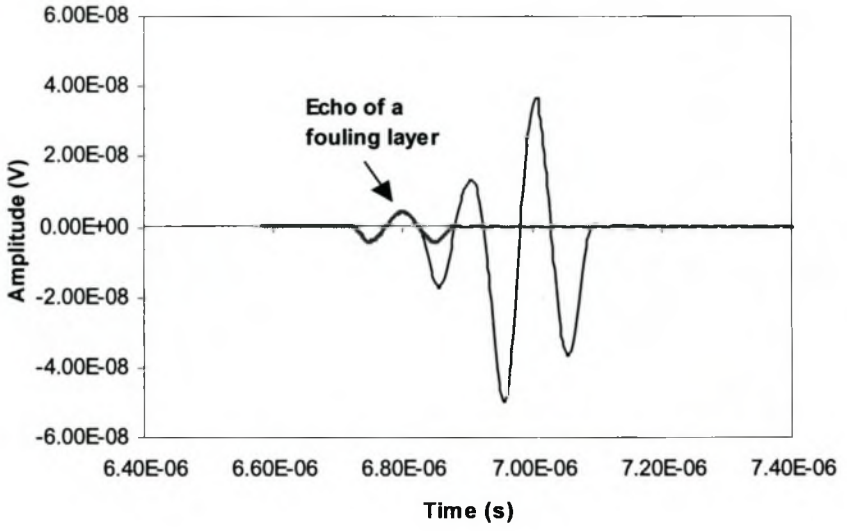

Figure 8.26: Model of an 80 μm thick fouling layer (ρ = 1.05 g/cm^3) on a PSU membrane.

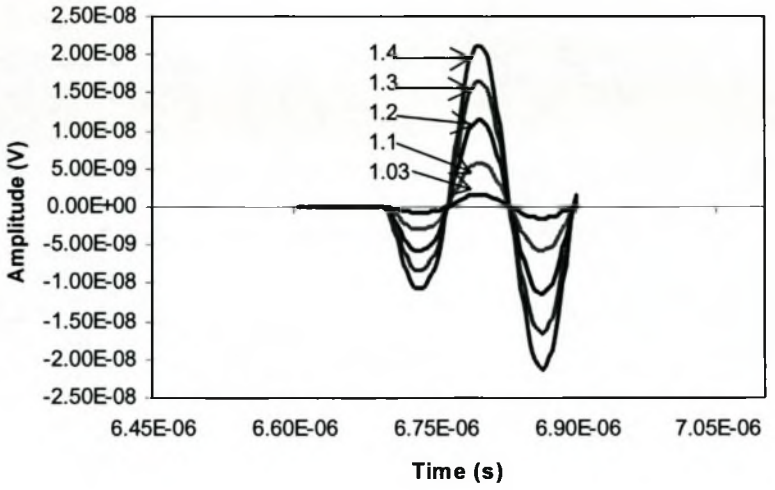

Figure 8.27: Mathematical model of density increases from1.03 to1.4 g/cm^3 in a 50 μm fouling layer.

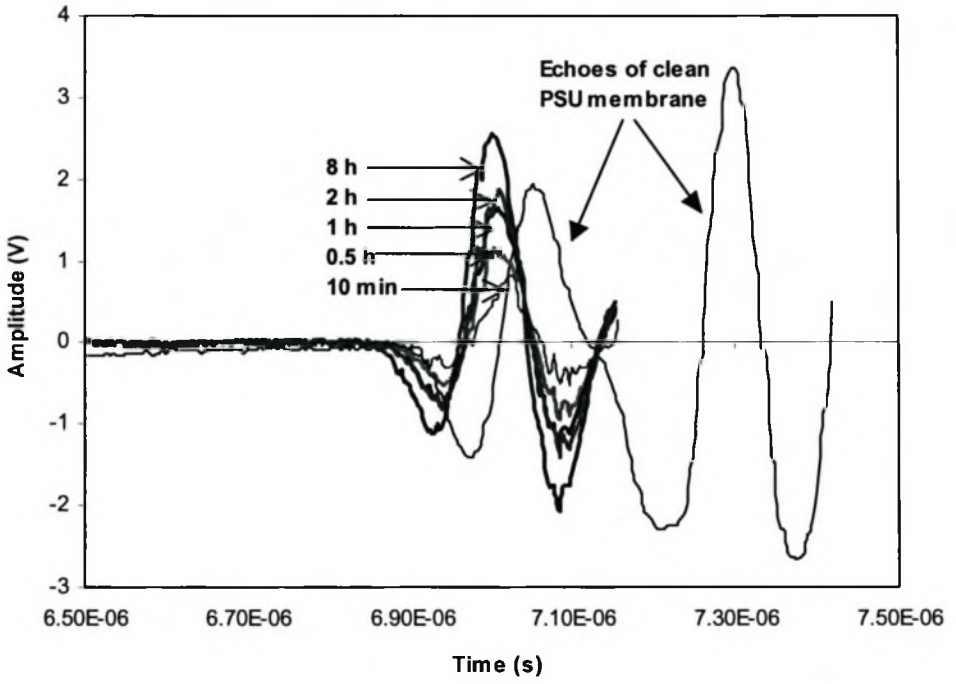

Figure 8.28: Actual ultrasonic response signal of a clean PSU membrane and differential signals after 10 min - 8 h of operation in the fouling experiment carried out with paper mill effluent at applied pressure 175 kPa and dead-end.

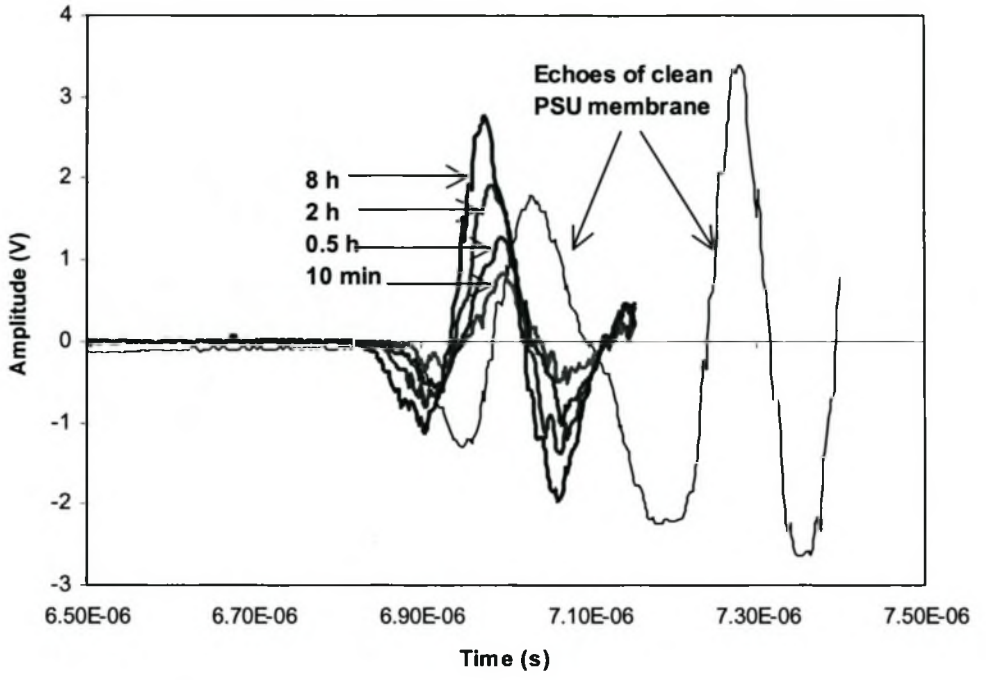

Figure 8.29: Actual ultrasonic response signal of a clean PSU membrane and differential signals after 10 min - 8 h of operation in the fouling experiment carried out with paper mill effluent at applied pressure 175 kPa and a flow rate of 12.5 cm/s.

8.7 SUMMARY

This chapter describes the UTDR technique as a non-destructive method by which to monitor and measure organic fouling and cleaning in real time in UF. An asymmetric, composite PSU membrane and its compaction can be detected by UTDR. Results show a good correspondence between the UTDR signal response and the development of the fouling layer on the membrane surface. The ultrasonic technique can measure the rate of fouling layer formation at the different operating conditions: dead-end and crossflow filtrations.

The most important finding is the differential signal obtained. Both amplitude and arrival time of differential signals as a function of operation time provide useful quantitative information such as the thickness of a fouling layer and its density changes in the fouling processes.

The UTDR technique can effectively not only detect deposition and growth of a fouling-layer on a membrane in real-time, but also monitor the progress of membrane cleaning and evaluate the cleaning effectiveness of various cleaning methods. The UTDR results corroborated traditional flux measurements and analysis of the membrane surface by microscopy.

Ultrasonic reflection modeling (URM) was applied to model the density and thickness of a fouling layer on a membrane surface so as to predict the fouling behaviour. The growth of a fouling layer in thickness and density results in flux decline. The modeling results are consistent with the actual observations. All indicate that the URM program is a useful tool with which to gain an understanding of the processes of ultrasonic testing related to fouling deposition and density changes of the cake layer.

CHAPTER 9

MEASUREMENT OF PROTEIN FOULING IN TUBULAR ULTRAFILTRATION

9.1 SCOPE OF THIS CHAPTER

Membrane filtration is an attractive process for the concentration and separation of bioproductions. Protein fouling is however a phenomenon, affecting filtration operation and membrane performance. One of the greatest challenges is the development of non-invasive methods that allow for early, *in-situ* protein fouling detection, especially in tubular membrane modules.

A new non-invasive ultrasonic technique has been applied to the *in-situ* monitoring of protein fouling in UF. A focal transducer with a frequency of 7.5 MHz was designed and employed in this study. A tubular UF module was used to investigate the capabilities of the ultrasonic technique and its applicability for different configuration modules. The tubular membrane was a polyethersulphone (PESU) UF membrane with MWCO 40 kDa. The feed used was 0.08 and 3 g/l Bovine serum albumin (BSA) solution. The experiments were conducted at a flow rate of 0.04 cm/s and applied pressure 150 kPa.

The ultrasonic technique can distinguish and recognize various response signals from ultrasonic measurements in a tubular cell. Protein fouling was successfully detected in tubular UF by the ultrasonic technique. The degree of the observed signal amplitude change correlated well with BSA fouling behaviour, such as adsorption, deposition and gelation on the membrane. The ultrasonic technique can provide an approach to understanding the nature and severity of protein fouling related to flux decline. Flux will decline due to the adsorption, concentration polarization and then as retentate concentration increases. Moreover, the ultrasonic technique is capable of detecting membrane cleaning. Flux measurements and UV analysis corroborate the ultrasonic

testing. Ultrasonic frequency spectra obtained may be useful as an additional tool for fouling detection.

9.2 INTRODUCTION

Ultrafiltration has been generally recognized as one of the most effective methods for the concentration and separation of bioproducts, and widely applied in the pharmaceutical and food industry [Cheryan, 1998]. The most serious operation restraint is, however, the flux decline. Such flux decline is mainly ascribed to concentration polarization [Kimura and Sourirajan, 1967], adsorption and deposition of small particles and proteins or other macromolecules [Robertson and Zydney, 1990; Opong and Zydney, 1991], pore constriction and/or pore blockage [Ititani et al. 1992; Tracey and Davis, 1994], the build-up of a filter cake of macromolecular solutes on the top surface of the membrane [Iritani et al., 2002] or a combination of these factors.

Understanding protein fouling behavior would greatly assist in developing strategies that may prevent this phenomenon from occurring, or minimizing its impact. Although a significant amount of research has been conducted to better understand the dynamics of UF, the real mechanism of separation remains incompletely understood. This is because there was no method that allows for *in-situ*, real time detection of protein fouling in membrane processes, and practical counter measures are only initiated when significant flux decline has occurred. Detecting the earliest stages of protein fouling formation is critical to the efficient and cost-effective management of membrane separations, and real-time protein fouling monitoring could be used to initiate appropriate counter measures against the maturation of protein fouling and help avoid the detrimental effects associated with their irreversible attachments.

This chapter focuses on development of a new ultrasonic technique to detect in situ protein fouling and cleaning in UF, and further investigate the capabilities of the ultrasonic technique and its applicability for different membrane module configurations. A focal transducer with a frequency of 7.5 MHz was used. Ultrasonic frequency spectra and differential signal were applied to describe the sensitivity of ultrasonic testing.

9.3 ULTRASONIC FREQUENCY SPECTRA

Ultrasonic resonance spectroscopy or ultrasonic absorption/attenuation spectroscopy is a well-known physical method of analysis having a variety of applications [Ford, 1970; Bhatia, 1985; Migliori et al. 1993 and 1996; Darling et al. 1997]. Ultrasonic frequency spectra are defined as the distribution of the frequency components of ultrasonic signals used in the non-destructive testing of materials [Lavrentyev and Rokhlin, 2001]. They are obtained by using the well-known Fast Fourier Transform procedure (FFT) and applied to ultrasonic measurements.

Ultrasonic testing uses short pulses of vibration energy, which have characteristics similar to white light. According to Fourier's theorem such short pulses can be regarded as arrays of various radiation frequencies and can be called frequency spectra. Figure 9.1 shows a typical signal waveform and frequency spectrum for a focal transducer used, having a central frequency of 7.5 MHz.

A spectrum analysis of these short pulses, carried out after they have passed through and interfered with materials to be tested, can be expected to yield information related to the physical properties of the material. Ultrasonic sound waves represent elastic waves. An ultrasonic frequency spectrum thus contains information on the elastic behaviour and properties of the material. Changes in density, as one example, should be contained as elastic information in such a spectrum [Lavrentyev and Rokhlin, 2001].

Most metals show low attenuation or absorption of ultrasonic waves, whereas many polymers and organic materials exhibit strong absorption [Ford, 1970]. At this stage in time little information is available on the interpretation of ultrasonic spectra and the causes for absorption/dissonance in certain materials. In here, ultrasonic frequency spectra are firstly used to further study the processes of fouling deposition related to ultrasonic responses in membrane separations.

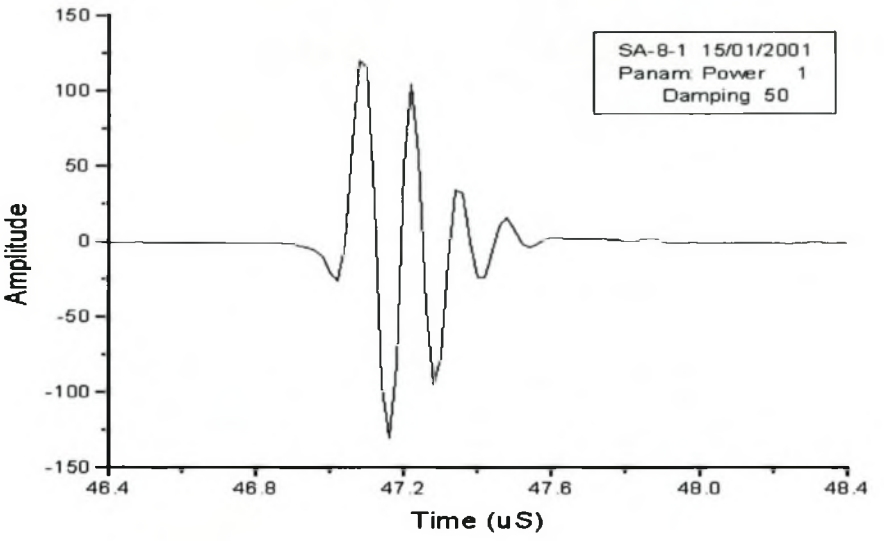

(a)

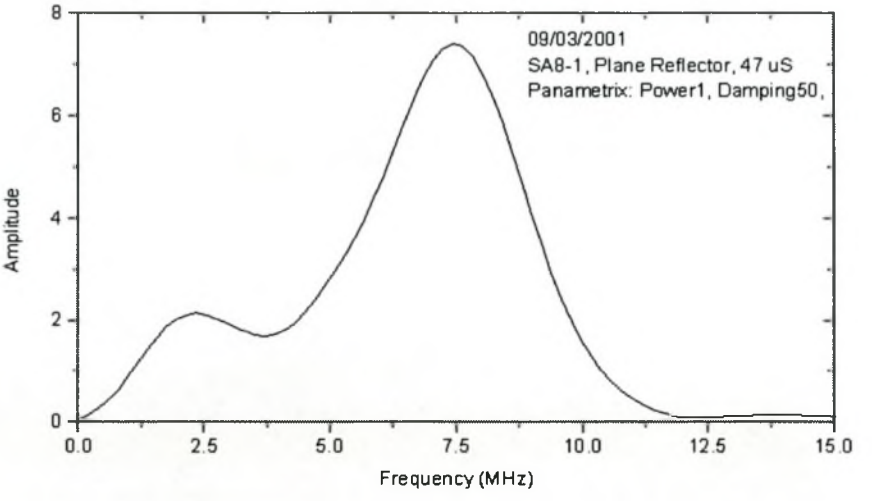

(b)

Figure 9.1: Typical signal waveform in (a) time domain and (b) frequency domain for a focused transducer with a frequency of 7.5 MHz used.

9.4 EXPERIMENTAL

9.4.1 MATERIAL AND APPARATUS

Bovine serum albumin (BSA) (Franction V, Boehringer Mannheim Gmbh, Germany) with molecular weight of 67 kDa was used in this study. Powdered BSA was dissolved in distilled water. Feed concentrations of BSA solution investigated were 0.08 g/l (pH = 6.9) and 3 g/l (pH = 6.2). The BSA concentration was measured with a UV spectrophotometer (Model Lambda 20 UV/VIS, PerkinElmer Ltd.) at 280 nm.

The tubular membrane was a polyethersulphone (PESU) UF membrane (Weir-Envig Ltd. South Africa) with a molecular weight cut-off (MWCO) of 40 kDa. The dimensions of the membrane were Φ 14 × 21 mm. A tubular test cell was designed as shown in Figure 3.5 and used in this study.

The ultrasonic measurement system consisted of a 7.5 MHz focal ultrasonic transducer; a pulser-receiver (Panametrics 5058PR) and a digital oscilloscope (HP Model 54602B) with sweep speeds 2 μs/div and 1mv/div sensitivity. The focal transducer emitting signals to and receiving them from the various layers within the tubular cell was externally mounted, in contact with the tubular test cell. The couplant used to couple the transducer was salad oil.

9.4.2 EXPERIMENTAL PROCEDURE AND FOULING EXPERIMENT

Figure 9.2 is a schematic representation of a UF experimental system and an ultrasonic measurement system. The UF system allows for the accurate control of inlet pressure, retentate flow rate and temperature.

In each UF experiment, continuous stirring in the feed tank was provided. Each experiment commenced with pure water being circulated through the system at the desired flow rate and applied pressure, for 2 h, to compress the membrane and to build up a stable flow field. Ultrasonic spectra inside the tubular test cell and echoes of a

tubular membrane during the pure water phase were obtained. Once steady state was attained, the feed was switched to the BSA solution to initiate the fouling phase. This phase was allowed to continue until the ultrasonic response and permeate flux had stabilized.

The fouling experiment was carried out at flow rate 0.04 cm/s and applied pressure 150 ± 5 kPa and temperature 26 ± 1°C. The total operating time for the fouling experiments was 4 h.

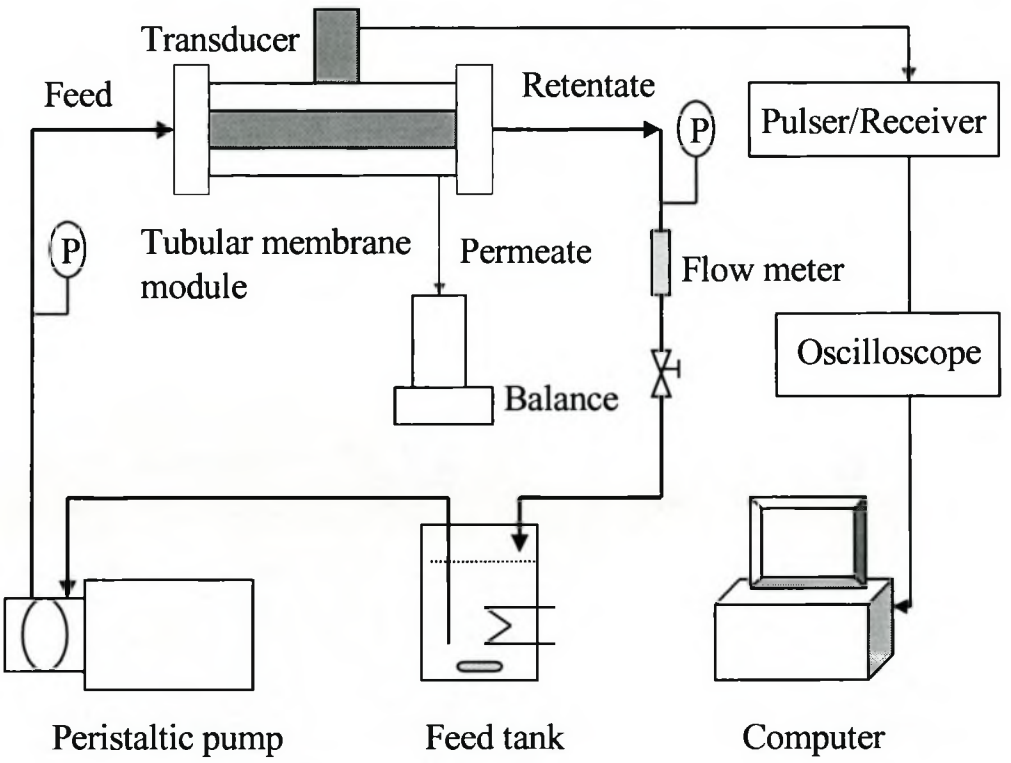

Figure 9.2: Schematic representation of the tubular UF separation system and the ultrasonic measurement system.

9.5 RESULTS AND DISCUSSION

9.5.1 ULTRASONIC SPECTROMETRY IN A TUBULAR CELL

The pure water filtration was carried to investigate the resolution capabilities of the UTDR technique and distinguish or recognize various response signals from ultrasonic records in the tubular cell

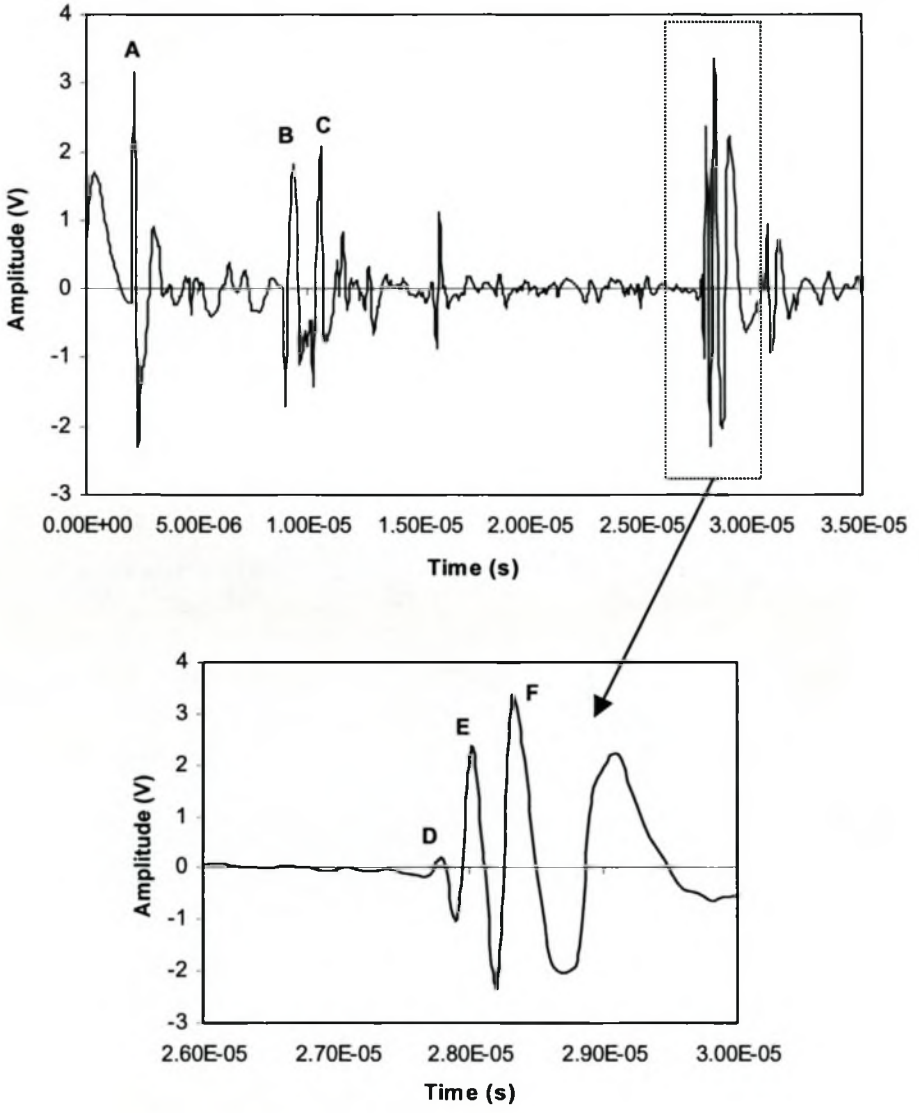

Figure 9.3: Ultrasonic spectrum inside tubular UF cell.

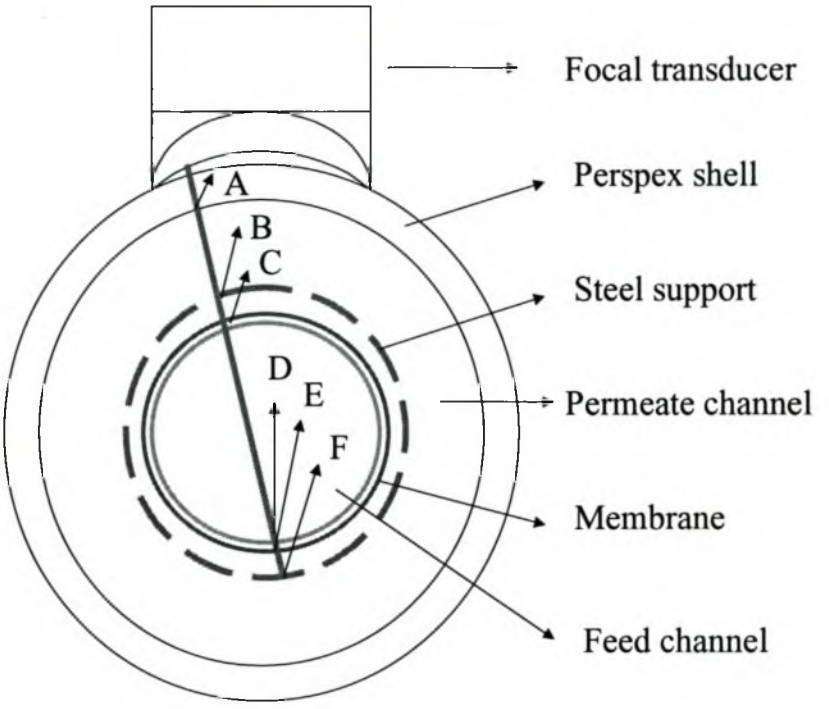

Figure 9.4: Cross-sectional view of tubular UF cell and ultrasonic reflections for set-up in Figure 9.3.

Figure 9.3 plots the ultrasonic signal amplitude in volts (V) vs. the time in seconds (s) inside the tubular cell. Each peak corresponds to a reflected acoustic wave from one of the multiple interfaces inside the tubular cell. Peaks A, B, C, D, E and F were generated from the following interfaces: Perspex shell/water, water/steel support, PESU membrane/water, water/PESU membrane, PESU membrane/polyester backing, polyester backing/steel support. The ultrasonic responses show the structure of the tubular cell as shown in Figure 9.4.

The ultrasonic response signals revealed a PESU membrane that is composed of a PESU layer and a polyester backing. The UTDR measurement was focused on the front of Peak D, which indicates the membrane surface. The pure water flux and echoes of the clean PESU membrane as reference waveform were also obtained during the pure water phase.

9.5.2 BSA FOULING EXPERIMENT AND ULTRASONIC MEASUREMENT

Figure 9.5 shows the variation of the permeate flux with operation time during the fouling experiments carried out with 0.08 and 3 g/l BSA. Flux first decreased rapidly to 26.2 % and 35. 4 % of the pure water flux in 10 min of fouling operation with 0.08 and 3 g/l BSA, followed by a gradual decline. The BSA rejection was > 99.5 % and 92.4 % in the fouling experiments with 0.08 and 3 g/l BSA (Table 9.1). The instantaneous flux-decline results primarily from the adsorption and concentration polarization of BSA on the PESU membrane [Aimar et al., 1986; Mulder, 1991]. The flux gradually declined due to the formation of gel layer and then as retentate concentration increases (such as 0.08 to 0.22 g/l after 4 h of fouling operation with 0.08 g/l BSA solution in Table 9.1). This is because the diffusivity of the BSA macromolecules is rather low and the retention is normally very high. This implies that the solute concentration at the membrane surface attains a very high value, the gel concentration may be reached for a number of macromolecular solutes [Mulder, 1991].

The corresponding ultrasonic responses at 0 and 4 h of fouling operation carried out with 0.08 and 3 g/l BSA are shown in Figures. 9.6 and 9.7. Peaks D and E combined together represent the clean PESU membrane. Once BSA foulants are initiated on the membrane surface, the acoustic impedance difference and the topographical characteristics at the feed solution/membrane interface will change, resulting in a change in the amplitude of echo D. The echo of BSA gel layer combined Peak D to form a new echo D'. Figure 9.8 shows changes in amplitude of Peak D' and time domain movement of Peaks D' with operation time. An amplitude decline of the observed Peak D' and an increase in the arrival time difference between Peaks D' and E with operation time were observed by UTDR. This is relative to the deposition and formation of a gel layer [Noble and Stern, 1995]. However, the gel layer is so thin that two successive echoes cannot be separated. Further observation is limited by the interference of ultrasonic signals reflected from the BSA thin layer and membrane.

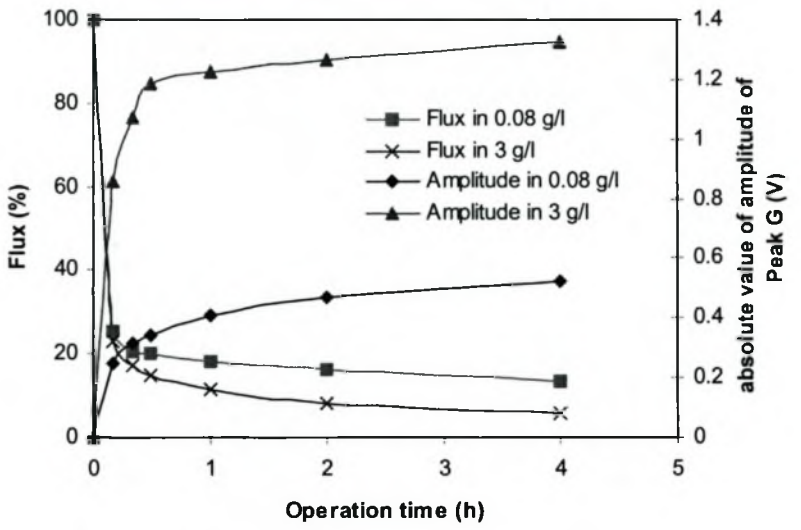

Figure 9.5: Permeate flux and amplitude of differential signal (Peak G) as a function of operation time during the fouling experiments carried out with BSA 0.08 and 3 g/l.

Table 9.1: BSA concentration in retentate and rejection during fouling experiments carried out with 0.08 and 3 g/l BSA

Operation time (h)	0.08 g/l BSA solution		3 g/l BSA solution	
	BSA concentration in retentate (g/l)	BSA rejection (%)	BSA concentration in retentate (g/l)	BSA rejection (%)
0	0.08		3.00	
0.25	0.09	99.70	4.00	
0.50	0.12	99.70	4.80	
1			5.20	92.50
2.50	0.14	99.50		
4			7.20	92.70
5	0.22	99.50		

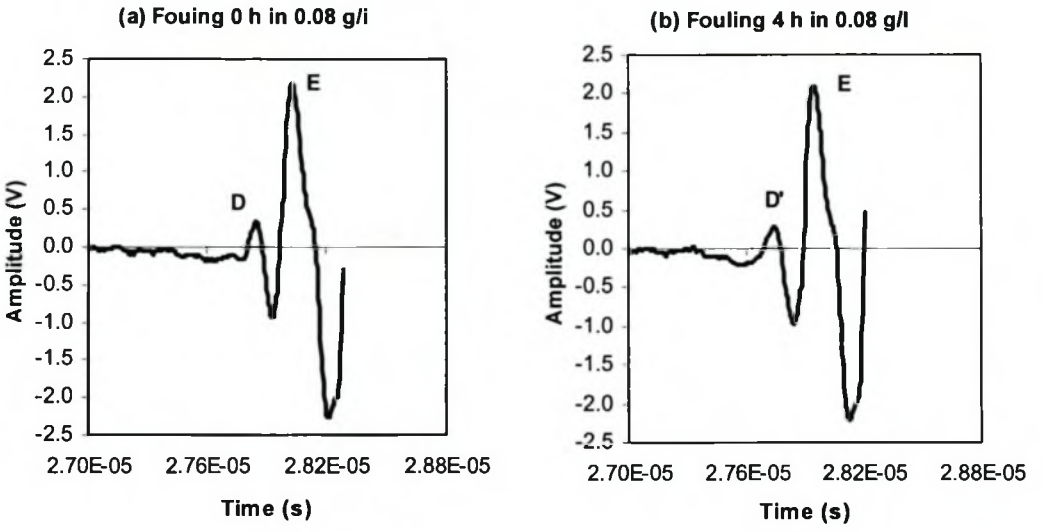

Figure 9.6: Ultrasonic signal responses after 0 (start) and 4 h of operation in the fouling experiment carried out with 0.08 g/l BSA at flow rate 0.04 cm/s and applied pressure 150 kPa.

Note: Peaks D, D' and E are generated from the following interfaces: water/PESU layer, BSA solution/BSA gel layer combined PESU layer, PESU layer/polyester backing.

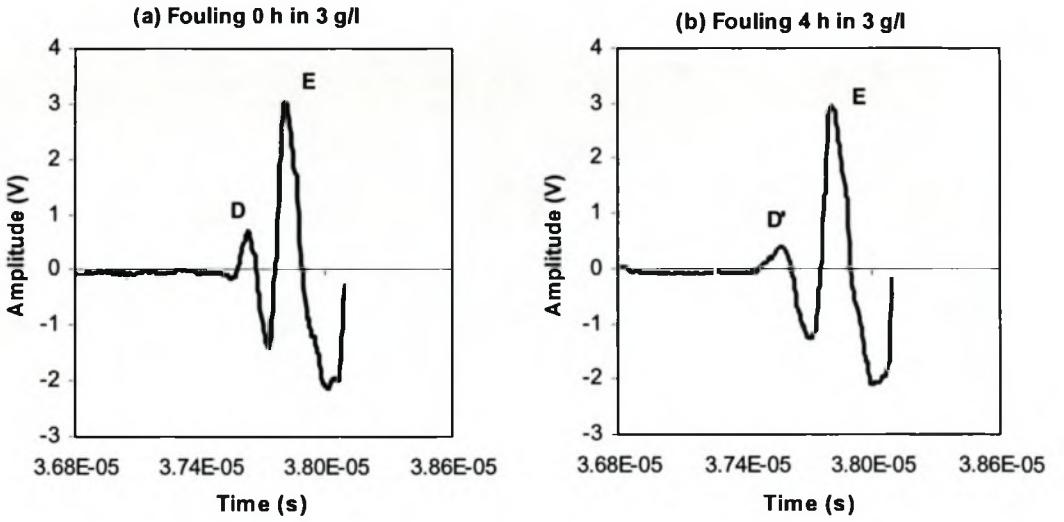

Figure 9.7: Ultrasonic signal responses after 0 (start) and 4 h of operation in the fouling experiment carried out with 3 g/l BSA at flow rate 0.04 cm/s and applied pressure 150 kPa.

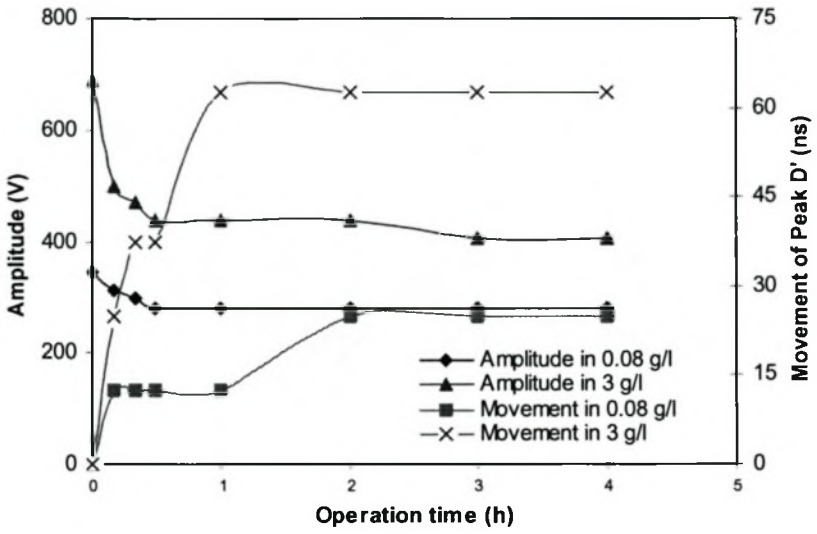

Figure 9.8: Changes in amplitude and time domain movement of Peaks D' with operation time in the fouling experiments with 0.08 and 3 g/l BSA.

9.5.3 DIFFERENTIAL SIGNALS

Results of differential signals during BSA fouling experiments are shown in Figures 9.9 and 9.10. Figure 9.5 also plots the amplitude of the differential signal (fouling echo G) as a function of operation time during BSA fouling experiments.

It is shown in Figure 9.9 that a clear differential signal had appeared within a short time, as was measured at 10 min of fouling operation, due to the adsorption of BSA on the PESU membrane. The BSA adsorbed quite strongly in or on the membrane surface resulting in an 65 % flux decline, even at a low BSA solution concentration (0.08 g/l). The growth of differential signals also can be seen at 0.5, 2 and 4 h as fouling proceeded (Figures 9.5 and 9.9). Note: the differential signals are reverse signals. It might indicate the impedance of the BSA gel layer is lower that that of water. A differential signal with 0.524 V emerged after 4 h of fouling operation with 0.08 g/l BSA. Figure 9.10 shows similar results achieved at 10 min, 0.5 h, 2 h and 4 h of fouling operation with 3 g/l BSA. But the increase in the ultrasonic amplitude became faster as the 3 g/l BSA concentration in feed is higher than 0.08 g/l. (Figures 9.5 and 9.10). An increase from 3 to 7.2 g/l in retentate concentration can be seen as fouling proceeded (Table 9.1). The high BSA concentration might results in a low rejection (92.7 %). A sharp differential signal with 1.327 V appeared after 4 h of fouling operation with 3 g/l BSA. This is because aggregation and deposition of BSA formed a dense gel layer as a second barrier on the membrane surface. Further flux decline results from the formation of a dense gel layer on the membrane surface.

According to a resistance model [Mulder, 1991], the gel layer resistance can be calculated by Equations 6.1, 6.3 and 9.1.

$$R_t = R_g + R_m \qquad (9.1)$$

where R_g = gel resistance including reversible or irreversible resistance.

As shown in Figure 9.11, a linear relationship between absolute value of amplitude of differential signals and fouling resistance exists in the fouling experiment with 0.08 g/l BSA. It suggests that fouling resistance increase with operation time results from

the protein adsorption, aggregation and gelation. The ultrasonic technique is capable of detecting and quantifying theses changes on the membrane surface.

The thickness (dS) of the BSA gel layer was calculated by Equation 3.1 As shown in Figure 9.12 (assume a sound velocity of 1480 m/s in BSA gel), the thickness of the gel layer was 3.7 and 5.18 μm after 10 min of fouling operation with 0.08 and 3 g/l. The thickness increased very slow, even kept unchanged as fouling proceeded. However the very thin layer with high gel concentration results in the continuous flux decline.

Differential signals:

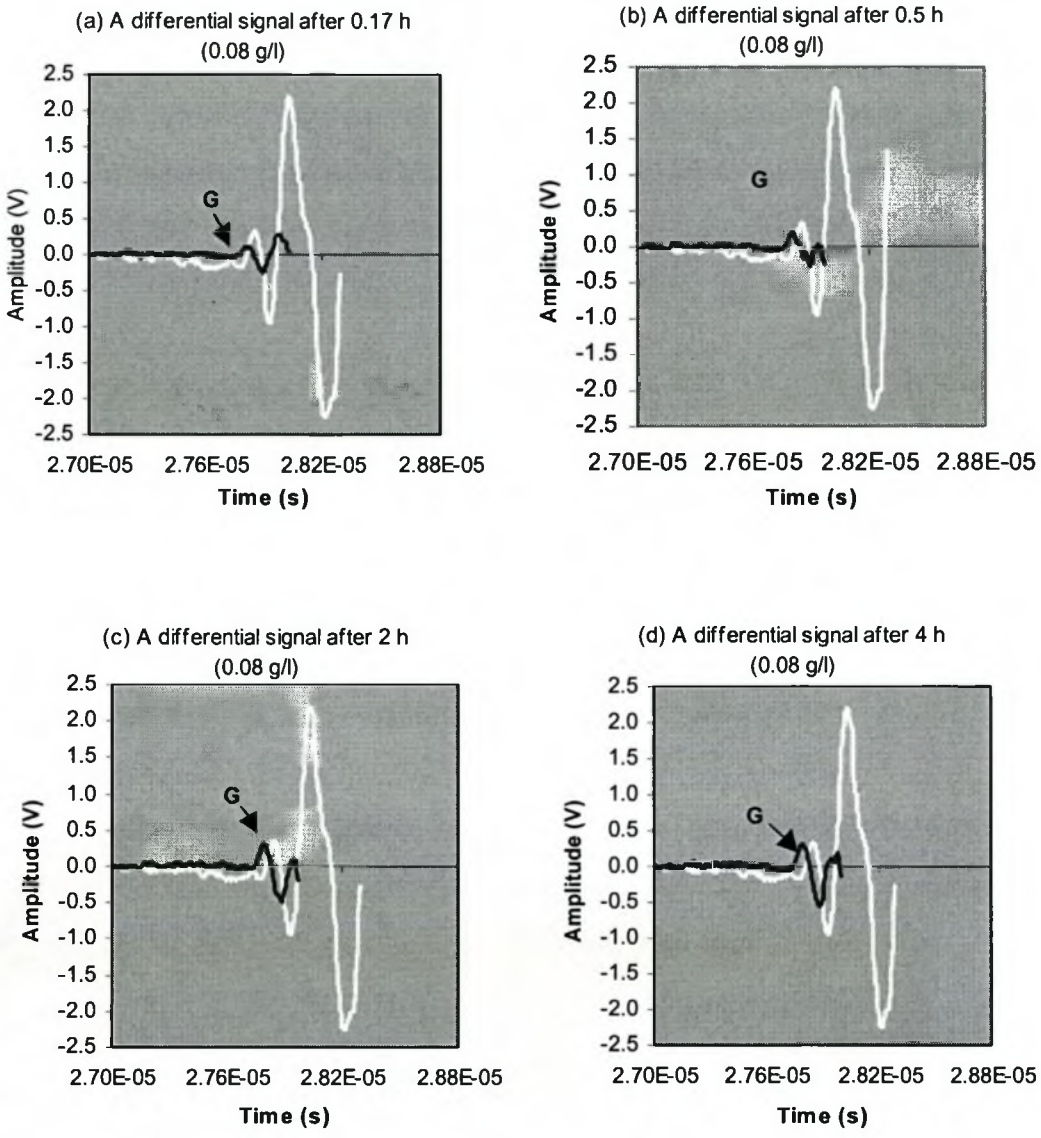

Figure 9.9: Differential signals (Peak G') after 10 min, 1 h, 2 h and 4 h of operation in the fouling experiment carried out with 0.08 g/l BSA.

Note: the white line represents ultrasonic signal responses of a clean tubular PESU membrane.

Differential signals:

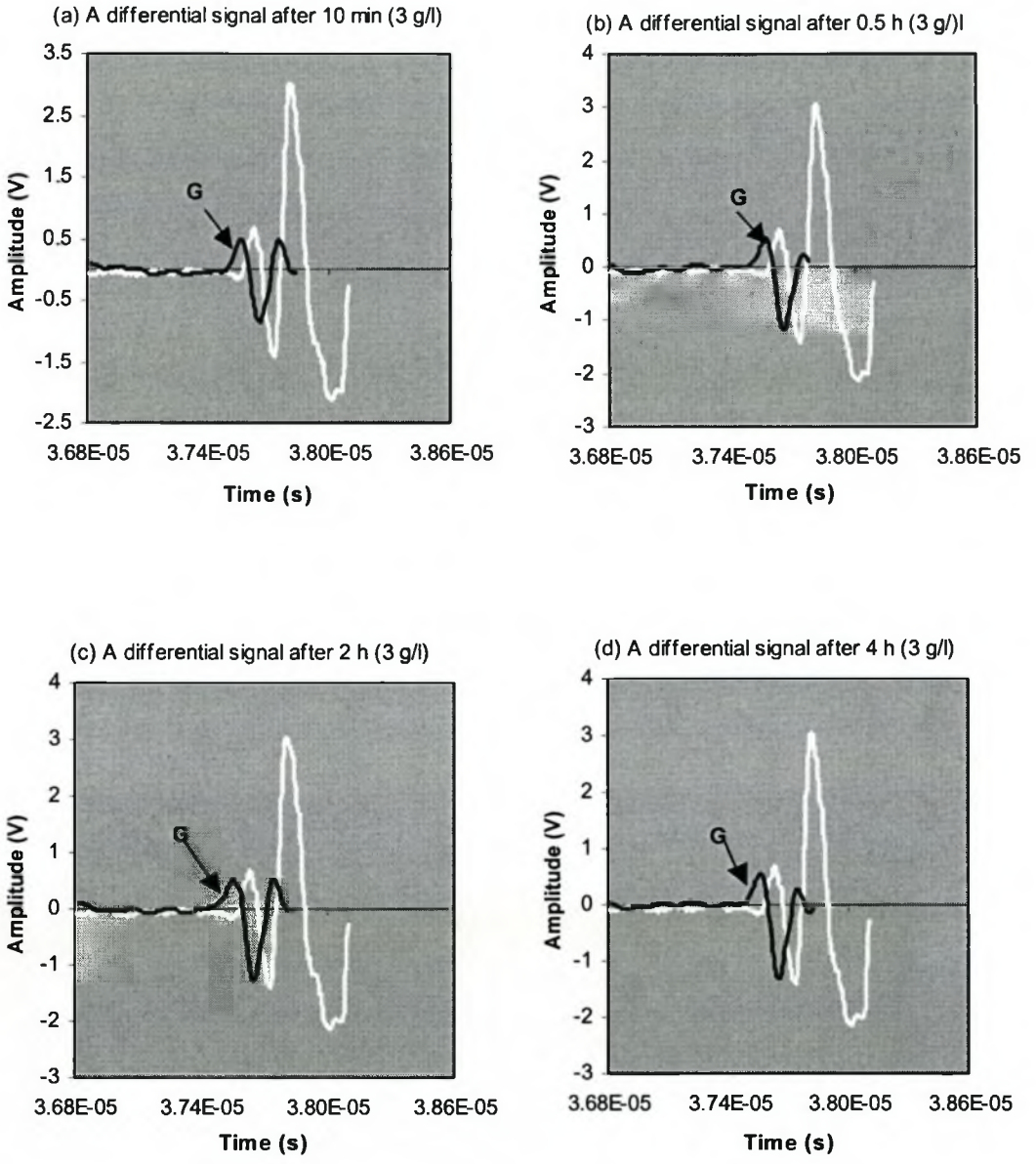

Figure 9.10: Differential signals (Peak G') after 10 min, 1 h, 2 h and 4 h of operation in the fouling experiment carried out with 3 g/l BSA.

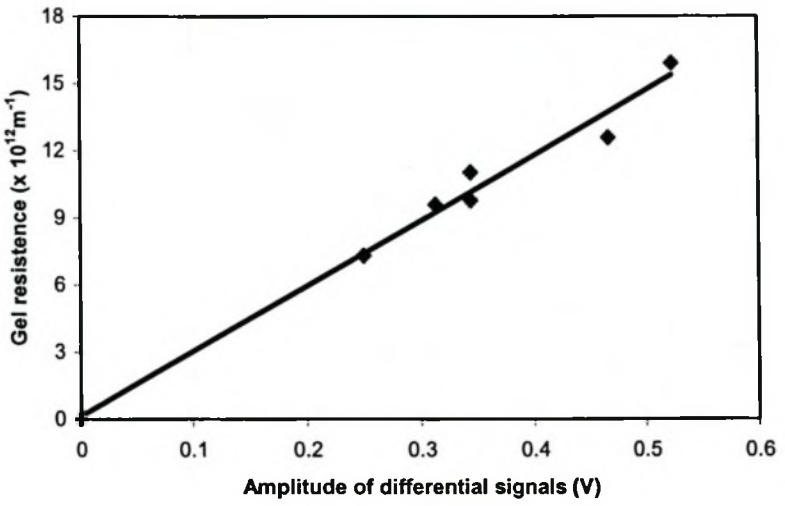

Figure 9.11: Relationship with the absolute value of amplitude of Peak G and gel resistance in the fouling experiments carried out with 0.08 g/l BSA.

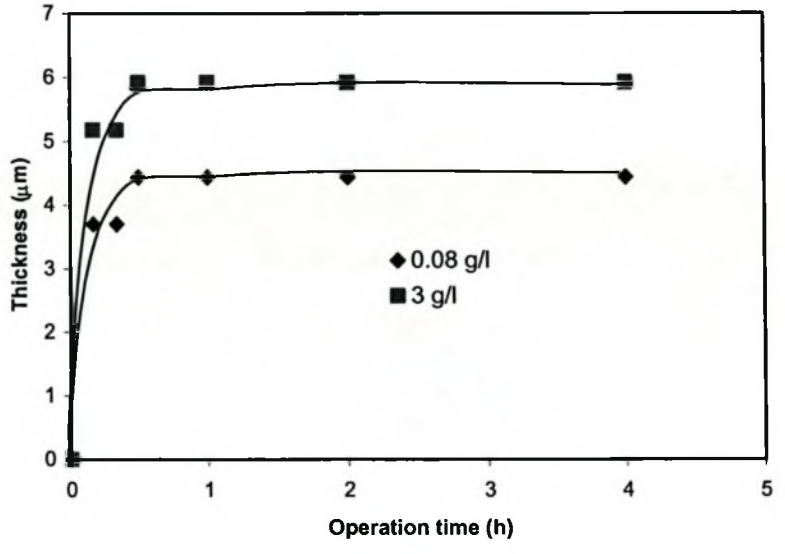

Figure 9.12: Thickness of BSA gel layer as a function of operation time in the BSA fouling experiments with 0.08 and 3 g/l BSA.

9.5.4 CLEANING EXPERIMENTS AND ULTRASONIC TESTING

Before commencing with the cleaning experiments, the feed solution was changed from 3 g/l BSA solution to pure water at 150 kPa and an axial velocity of 0.04 cm/s, in order to obtain pure water flux of a fouled membrane. The fouled membrane was cleaned with 0.1 g/l enzyme solution for 30 min. Pure water flux recovery of the cleaned membrane is shown in Figure 9.13. Figure 9.14 shows the results of ultrasonic differential signals during the cleaning experiments.

An increase in flux from 5.68 to 20.36 % and a decrease in absolute value of the amplitude of differential signal from 1.32 to 0.08 V were observed (Figures 9.13 and 14a) after pure water filtration because of changing the bulk solution from BSA to pure water. The change in bulk solution from BSA to pure water resulted in the reduction of concentration polarization on. Figure 9.13 shows that pure water flux increased from 20.36 to 68.38 % after by enzyme cleaning. The disappearance of the differential signal G showed the gel layer was taken away by enzyme cleaning (Figure 9.14b). However, the recovery flux by enzyme cleaning is still lower than the original flux. It might be because protein pore plug or protein-membrane interactions results from the irreversible fouling on or in the membrane [Robertson and Zydney, 1990; Huisman et al., 2000].

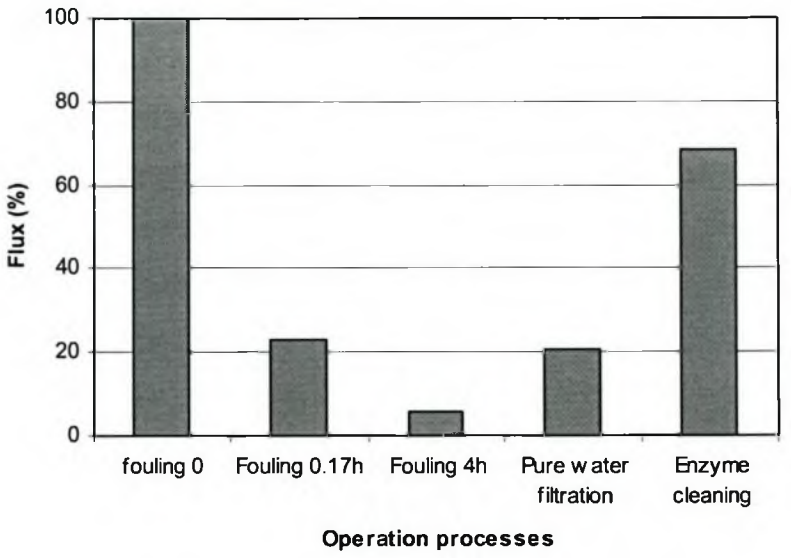

Figure 9.13: Changes in flux with operation processes during the fouling experiment with 3 g/l BSA.

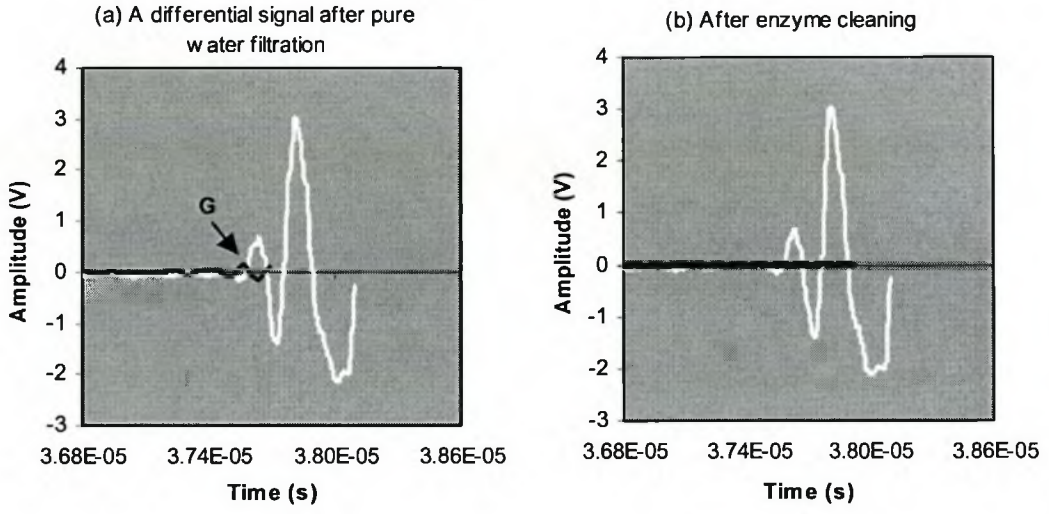

Figure 9.14: Differential signals after pure water filtration and enzyme cleaning in the fouling experiment with 3 g/l BSA.

9.5.5 ULTRASONIC FREQUENCY SPECTRUM

Figure 9.15 shows ultrasonic frequency spectra obtained from ultrasonic measurements by Fast Fourier Transform (FFT) during fouling (carried out by 0.08 g/l BSA). Each frequency spectrum contains a frequency band from 0 to 11 MHz. As indicated on Figure 9.15, the frequency spectra show obvious changes in ultrasonic resonance in the 9 MHz range. There is increasing resonance (increasing negative peaks) with fouling operation with 0.08 g/l BSA. Figure 9.16 shows the appearance and growth of differential signals of ultrasonic resonance minima with BSA fouling time. The broad resonance minima correspond to the properties of the fouling layer such as density and thickness etc. because the foulants were imbedded in or deposited on the membrane surface to form a smooth surface, which caused a stronger resonance with the membrane than membrane self [Migliori et al., 1993, Pierce, 1996]. Further attempts will be made to interpret the results in terms of physical behavior, i.e. elastic properties of the membranes and foulants involved and reported in a later paper. Much basic research still has to be performed to be able to correlate resonance bands to physical and/or chemical parameters.

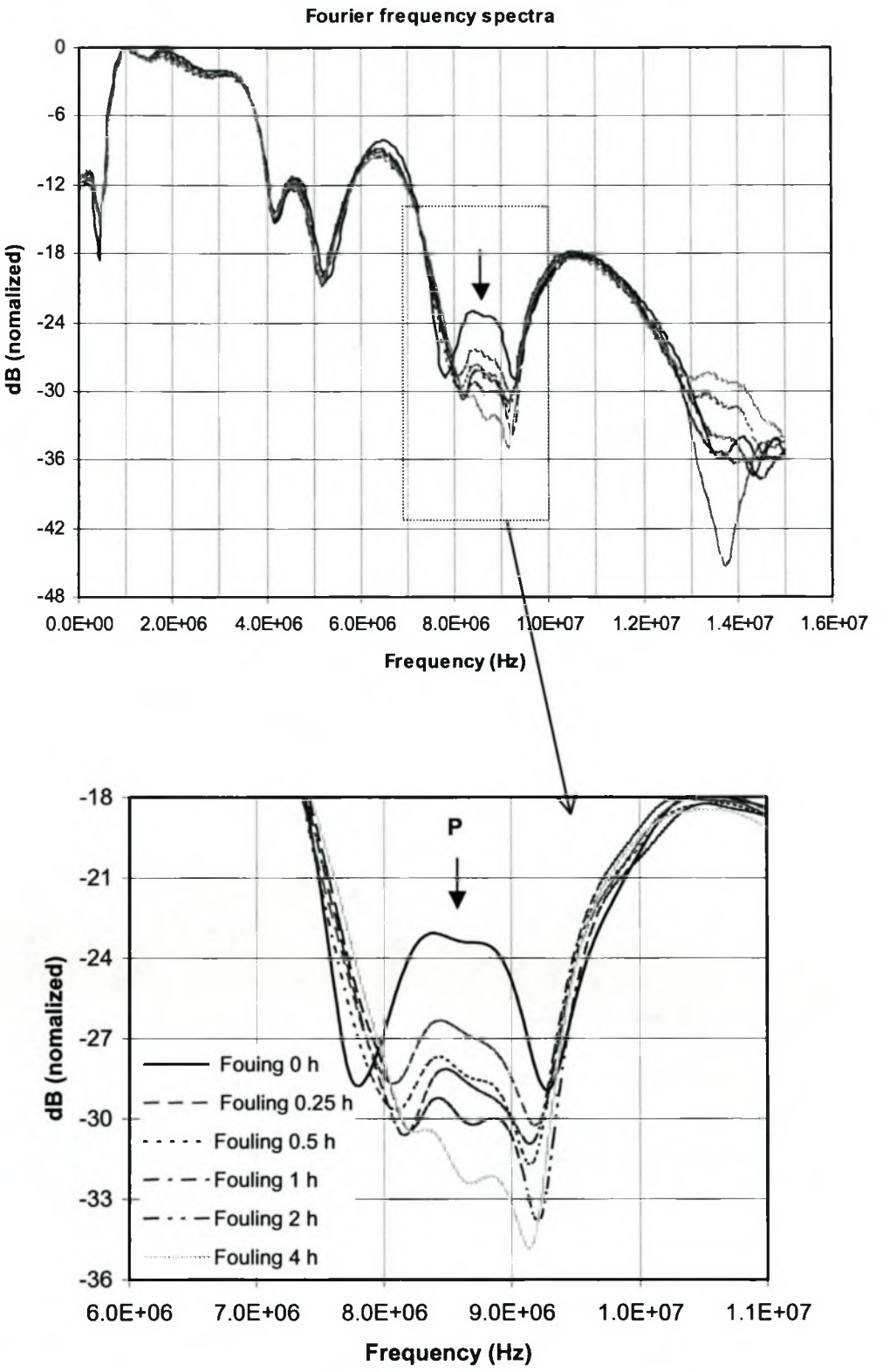

Figure 9.15: Ultrasonic frequency spectra from 0 to 4 h of fouling operation carried out with 0.08 g/l BSA in tubular UF.

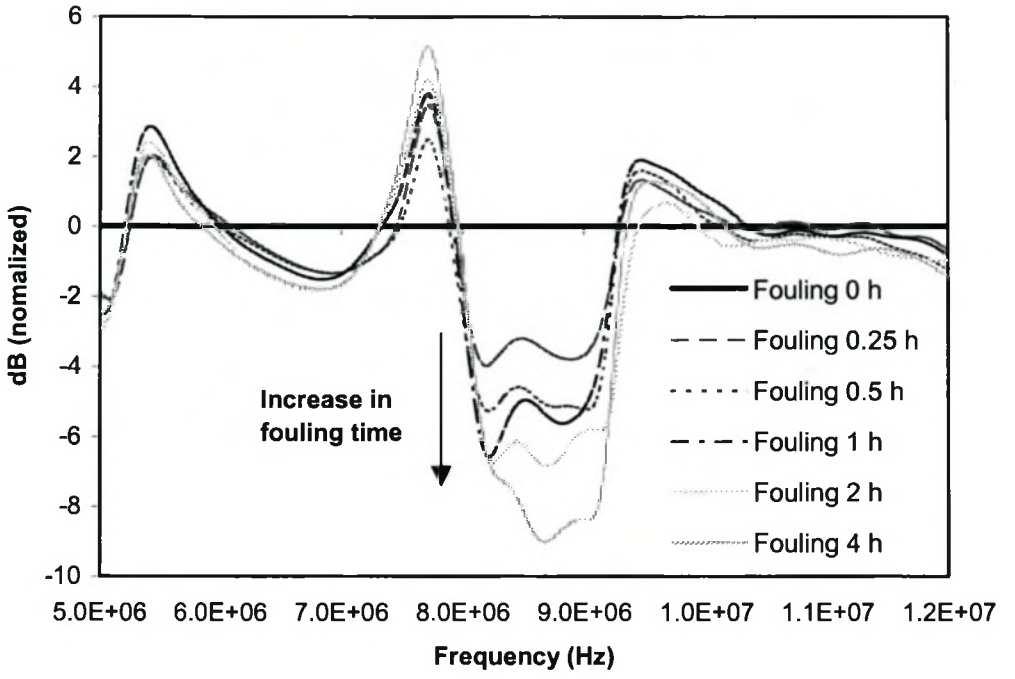

Figure 9.16: Differential signals of ultrasonic amplitude (dB) with operation time during the fouling experiment with 0.08 g/l BSA in tubular UF.

9.6 SUMMARY

This chapter has demonstrated the use of a new ultrasonic technique to monitor, *in-situ*, protein fouling in tubular UF membranes. Results show that the ultrasonic technique can distinguish and recognize various response signals from ultrasonic measurements in a tubular cell.

Protein fouling was successfully detected in tubular UF by the ultrasonic technique. Changes in the amplitude of the differential signals obtained provide useful quantitative information about adsorption, deposition and gelation of BSA on the membrane. A linear relationship between absolute value of amplitude of differential signals and fouling resistance exists in the fouling experiment with 0.08 g/l BSA. The ultrasonic technique can provide an approach to understand protein fouling behavior related to membrane flux decline. Flux will decline due to the adsorption, concentration polarization and then as retentate concentration increases.

The ultrasonic technique is capable of detecting membrane cleaning. Flux measurements and UV analysis corroborate the ultrasonic testing. Furthermore ultrasonic frequency spectra were developed and may be useful as an additional tool for detection of fouling.

CHAPTER 10

CONCLUSIONS

This study has resulted in the development of ultrasonic time-domain and amplitude-domain reflectometry as a real-time visualization technique for fouling monitoring in various pressure-driven membrane separations. The major conclusions of this study can be summarized as follows:

1. Ultrasonic response signals were obtained for kaolin particle deposition and subsequent cake layer formation on a nylon membrane surface. A cake layer echo appeared, increased in the amplitude domain and moved in the time domain as fouling proceeded in MF.

2. An ultrasonic cleaning technique was successfully applied to cleaning membrane fouling in MF. The horn sonicator employed had a frequency of 20 kHz and a power of 375 w. Results showed that ultrasound associated with forward flushing was a new effective method for cleaning fouled MF membranes. SEM analysis indicated that ultrasound with flushing was able to remove fouling layers from a membrane surface and restore the original structure of the membrane surface. Resistance analysis indicated that the cleaning efficiencies of ultrasound with forward flushing was 97.8%. It was also found that high forward flushing velocity combined with ultrasound was also beneficial for cleaning. In general, a high forward-flushing velocity and low cleaning solution (water) temperature, under the same ultrasonic conditions, gave higher cleaning efficiency. Moreover, online ultrasound reduced membrane fouling and enhanced permeate flux, but only moderately.

3. In MF, cake formation, growth and compressibility were observed by an ultrasonic testing method. UTDR can measure the rate of cake layer formation at different flow rates. UTDR is also capable of detecting subtle changes such as the stop and restart operation.

4. UTDR was successfully used for monitoring membrane cleaning and evaluating the cleaning effectiveness of various cleaning methods, namely: forward flushing, ultrasonic cleaning and ultrasound with flushing. Results showed that a cake-layer echo decreased after flushing and disappeared after ultrasonic irradiation in MF. UTDR results showed that ultrasound associated with flushing was the most effective cleaning method for cleaning membranes fouled by paper mill effluent.

5. In UF an asymmetric PSU membrane and its compaction could be detected by UTDR. Results showed a good correspondence between the UTDR signal response and the development of the fouling layer on the membrane surface in UF.

6. Fouling occurrence on a membrane leads to flux decline. The dynamic processes of deposition and growth of a fouling layer was confirmed by *in-situ* ultrasonic response signals. The sensitivity of ultrasonic responses revealed the coverage of a membrane surface with a fouling layer. UTDR results corroborated the flux measurements and SEM analyses.

7. The ultrasonic unit is a suitably programmed microprocessor, and can be used to compare reference and test signals to produce a differential signal (a fouling layer echo). A differential signal indicated the state and progress of a fouling layer on a membrane surface during actual operations. Both amplitude and arrival time of differential signals as a function of operation time provide useful quantitative information, i.e. changes in thickness and density of a fouling layer on the fouling processes. The resolution exceeds the theoretical limit by a considerable margin when using the differential signals.

8. A predictive modelling program - ultrasonic reflection modelling (URM) was developed to understand the processes of ultrasonic testing related to the deposition of fouling layers on membrane surfaces. Changes in the densities of the cake layer as well as the thickness could be substantiated by the mathematical modelling. Deposit resistance is not only related to the layer thickness but also the cake density (compressibility). The predicted results of

fouling layer deposition were in good agreement with the actual measurements obtained in MF and UF.

9. UTDR is very useful to investigate fouling mechanisms. An increase in flux could be seen when fouling operation was stopped and restarted. This is because interrupting the fouling experiment resulted in flow destabilization and relaxation of the fouling layer. UTDR showed an increase in the thickness of the fouling layer and a decrease in the density of the cake layer. Further, although the thickness (82.5 μm) of the fouling layer obtained after 7 h of operation at crossflow 1.83 cm/s was thicker than the thickness (60 μm) obtained after 18 h of operation at 6.97 cm/s in MF, the flux of 7.5 l/m^2h obtained after 7 h of operation at 1.83 cm/s was higher than the flux of 7.2 l/m^2h obtained after 18 h of operation at 6.97 cm/s. UTDR showed that the 60-μm cake layer (obtained after 18 h of operation at 6.97 cm/s) was denser than the 82.5-μm cake layer (obtained after 7 h of operation at 1.83 cm/s). The compressibility of the cake layer contributed to the flux decline. UTDR proved that increasing the flow rate during actual operation could not reduce fouling in MF carried out with paper mill effluent because a denser cake layer formed on the membrane surface at a high flow rate than it did at a low flow rate.

10. UTDR could also distinguish and recognize various response signals from ultrasonic measurements in a tubular cell. Protein fouling was successfully detected by UTDR in a tubular PESU UF membrane. Changes in the amplitude and time domain of the observed signals provided useful quantitative information about adsorption, deposition and gelation of BSA on the membrane. The thickness of the BSA gel layer was obtained. UTDR can provide an approach to understand protein fouling behavior related to flux decline. Ultrasonic frequency spectra could be useful as an additional tool for fouling detection

RECOMMENDATIONS FOR FUTURE RESEARCH

The present research has clearly shown that UTDR can be used successfully to monitor membrane fouling in MF and UF with different membranes, foulants and configuration modules. Further work is needed in the following areas:

1. Develop UTDR to measure fouling in capillary UF membrane module and submerged module.

2. Further advance UTDR to study and understand biofouling in biorectors and membrane separations.

3. Further develop ultrasonic frequency spectra, to be used as an additional tool for fouling detection.

4. Develop a more sensitive analysis of ultrasonic data to isolate fouling effects from all other reflections.

5. Advance UTDR to detect membrane formation and evaluate efficiencies of modification and pretreatment.

6. Apply the UTDR technique to commercial separation plants at a low-to-moderate cost and aim for even further improvements in fouling monitoring.

REFERENCES

Abdel-Jawad, M.; Ebrahim, S.; Al-Atram, F.; Al-Shammar, S. Pretreatment of the municipal wastewater feed for reverse osmosis plants, Desalination 109 (1997) 211-223.

Ahn, K.H.; Cha, H.Y.; Yeom, I.T. and Song, K.G. Application of nanofiltration for recycling of paper regeneration wastewater and characterization of filtration resistance, Desalination 119 (1998) 169-176.

Aimar, P.; Baklouti, S. and Sanchez, V. Membrane-solution interactions: influence on pure solvent transfer during ultrafiltration, J. Membr. Sci. 29 (1986) 207-224.

Alig, I. and Tadjbakhsch, S. Film formation and crystallization kinetics of polychloroprene studies by an ultrasonic shear wave reflection method, J. Polym. Sci B, 36 (1998) 1730-1740.

Alig, I.; S. Tadjbakhsch and Zosel, A. Comparison of ultrasonic shear wave and dynamic-mechanical measurements in acrylic-type copolymers, J. Polym. Sci. B 36 (1998) 1703-1711.

AI-Malack, M.H.; Anderson, G.K. Formation of dynamic membranes with crossflow microfiltration, J. Membr. Sci. 112 (1996) 287-296.

Altena, F.W. and Belfort, G., Lateral migration of spherical particles in porous flow channels: application to membrane filtration, Chem. Eng. Sci. 39 (3) (1984) 343355.

Altmann, J.; Ripperger, R. Particle deposition and layer formation at the crossflow microfiltration, J. Membr. Sci. 124 (1997) 119-128.

Amjad, Z. Applications of antiscalants to control calcium sulfate scaling in reverse osmosis systems, Desalination 54 (1985) 263-276.

Anderson, J. E., Heyde, M. E. and Plummer, H. K. Irreversible fouling caused by plasticization of asymmetric reverse osmosis membranes, Desalination 37 (1981) 307-311.

Applegate, L. E. and. Sackinger, C.T. Avoiding iron fouling in reverse osmosis desalination plants, Desalination 61 (1987) 39-48.

Bacchin, P.; Aimar P. and Sanchez, V. Model for colloid fouling of membrane, AIChE J, 41 (1995) 368-376.

Baker, J.S.; Judd, S.J. and Parson, S.A. Antiscale magnetic pretreatment of reverse osmosis feed water, Desalination 110 (1997) 151-165.

Band, M.; Gutman, M.; Faerman, V.; Korngold, E.; Kost, J.; Plath, P.J.; Gantar, V. Influence of specially modulated ultrasound on the water desalination process with ion-exchange hollow fibres, Desalination 109 (1997) 303-313.

Belfort G. and Marx, B. Artificial particulate of hyper filtration membranes – analysis and protection from fouling, Desalination 28 (1979) 13-30.

Belfort, G. and Altena, R.W. Toward in inductive understanding of membrane fouling, Desalination 47 (1983) 105-127.

Belfort, G. Fluid mechanics in membrane filtration: recent development, J Membr. Sci. 40 (1989) 123-147.

Belfort, G.; Davis R.H. and Zydney, A.L. The behavior of suspensions and macromolecular solutions in crossflow microfiltration, J Membr. Sci. 96 (1994) 1-58.

Bellhouse, B.J. Membrane Filter, International Patent Application WO 94/21362, 1994.

Bhatia, A.B. Ultrasonic absorption: an introduction to the theory of sound absorption and dispersion in gases, liquids and solids, Dover Publications, Inc., New York, 1985.

Bhattacharjee, S. and Bhattacharya, P.K. Flux decline behaviour with low molecular weight solutes during ultrafiltration in an unstirred batch cell, J. Membr. Sci. 72 (1992) 149-161.

Bierck, B. R. and Dick, R.I. In-situ examination of effects of pressure differential on compressible cake filtration, Water Sci. and Technol., 22 (12) (1990) 125-133.

Bierck, B.R.; Wells S.A. and Dick, R.I. Compressible cake filtation: monitoring cake formation and shrinkage using synchrotron X-rays, J Water Pollution Control 60 (5) (1988) 645-653.

Birks, Albert S.; Green, Robert E.; McIntire, P. 1. Ultrasonic testing in Non-destructive testing handbook (2nd ed.; v. 7), the American Society for Non-destructive testing, 1991.

Blake, N.J.; Cumming, I.W. and Streat, M. Prediction of steady state crossflow filtration using a force balance model, J. Membr. Sci. 68 (1992) 205-215.

Bland, D.K. Wave theory and application, Clarendon, Oxford, 1988.

Blokhra, R.L., and Joshi, J. Industrial Journal of Chemistry 33A (1994) 758-759.

Bond, L.J.; Greenberg, A.R.; Mairal, A.P.; Loest, G.; Brewster, J.H.; Krantz, W.B. in: Thompson, D.O.; Chimenti, D.E. (Eds.), Review of progress in quantitative non-destructive evaluation, vol. 14, Plenum Press, New York, 1995, pp. 1167-1173.

Bond, L.J.; Chai, G.Y.; Greenberg, A.R. and Krantz, W.B. Method and apparatus for determining the state of fouling/cleaning of membrane modules, US Patent No. 6161435, 2000.

Borden, J.; Gilron J. and Hasson, D. Analysis of RO flux decline due to membrane surface blockage, Desalination 66 (1987) 257-269.

Bowen, W.R.; Kingdon R.S. and Sabuni, H.A.M. Electrically enhanced separation processes: the basis of *in situ* intermittent electrolytic membrane cleaning (IIEMC) and *in situ* electrolytic membrane restoration (IEMR), J. Membr. Sci. 40 (1989) 219-229.

Brinkert, L.; Abidine, N. and Aptel, P. On the relation between compaction and mechanical properties for ultrafiltration hollow fibers, J. Membr. Sci. 77 (1993) 123-131.

Brunelle, M.T. Colloid fouling of reverse osmosis membranes, Desalination 32 (1980) 127-135.

Buckley, C. A.; Flemmer, R. L. C. and Groves, G. R. Fouling studies and mathematical modelling of ultrafiltration of textile desizing effluents, Desalination 47 (1983) 171-179.

Burch, G. Practical experiments with circulating sponge balls on UF membranes with paper mill effluent, 4th WISA-MTD Symposium-Membranes: Science & Engineering, Stellenbosch, South Africa, 26-27 March 2001.

Butt, F. H.; Rahman, F. and Baduruthamal U. Characterization of foulants by autopsy of RO desalination membranes, Desalination 114 (1997) 51-64.

Butt, F.H., F. Rahman and U. Baduruthamal, Identification of scale deposit through membrane autopsy, Desalination 101 (1995) 219-230.

Carter, J.W. and G. Hoyland, Fifth Inernat. Symp Fresh Water from Sea 4 (1976) 21.

Chai, X.; Kobayashi, T. and Fujii, N. Ultrasound-associated cleaning of polymeric membranes for water treatment, Separation and Purification Technology 15 (1999) 139-146.

Chai, X.; Kobayashi, T. and Fujii, Nobuyuki Fujii, N. Ultrasound-associated cleaning of polymeric membranes for water treatment, Separation and Purification Technology 15 (1999) 139-146.

Chakravorty, B. and Layson, A. Ideal feed pretreatment for reverse osmosis by continuous microfiltration, Desalination 110 (1997) 143-149.

Cheryan, M., Ultrafiltration and microfiltration handbook, Technomic Publishing Company, Inc., Lancaster, 1998.

Chung, K. Y.; Edelstein, W. A. and Belfort G. Dean vortices with wall flux in a curved channel membrane system; 6. Two dimensional magnetic resonance imaging of the velocity field in a curved impermeable slit, J. Membr. Sci. 81 (1993) 151-162.

Cilliers, P.J. Private communications with Professor P.J. Cilliers, Dept. of Electrical and Electronic Engineering, University of Pretoria, Pretoria 0002, South Africa, 2002.

Cooray, G., Mineral Water Development, Stellenbosch, South Africa, 7600, 1998.

Czekaj, P.; Mores, W.; Davis, R.H. Guell, C. Infrasonic pulsing for foulant removal in crossflow microfiltration, J. Membr. Sci. 180 (2000) 157-169.

Darling, T.W.; Migliori, M.; Strouse, G.; Swanson, B.; Johnson, S.; Hundley, M.F. and Thompson, J.D. Resonant ultrasound spectroscopy and comparative studies of a 1-D linear chain (MX) material, Synthetic metals 86 (1997) 2153-2154.

Davis K. and Leighton, D. Shear-induced transport of a particle layer along a porous wall, Chem. Eng. Sci. 42 (1987) 275- 281.

Davis, R.H. in Membranes Handbook, W.S.W. Ho and K.K. Sirkar (eds.), Chapman and Hall, New York, 1992.

Dejmek, P. PhD thesis, Lund Institute of Technology, Sweden, 1975.

Denisov, G. A. Theory of concentration polarization in cross-flow ultrafiltration: gel-layer model and osmotic-pressure model, J. Membr. Sci. 91 (1994) 173-187.

Diaz, M.A.; Mansfield, R.K.; Bhattacharyya, D. and Jay, M. Scintillation proximity assay for measuring benzene absorption in a polyethylene membrane, J. Membr. Sci. 69 (1992) 179-183.

Domingo, G. S. Cleaning and pre-treatment techniques for UF membranes fouled by pulp and paper effluent, M.Sc. thesis, University of Stellenbosch, South Africa, 2001.

Dresch, M.; Daufin G. and Chaufer, B. Integrated membrane regeneration process for dairy cleaning-in-place, Separation and Purification Technology 22-23 (2001) 181-191.

Du Pont de Nemours, E.I. & Co., Permasep Technical Bulletin, Wilmington, 1977.

Dudley, L.Y. and E.G. Darton, Membrane autopsy – a case study, Desalination 105 (1996) 135-141.

Dudley, L.Y.; Darton, E.G. Pretreatment procedures to control biogrowth and scale formation in membrane systems, Desalination 110 (1997) 11-20.

Ebrahim, S. Cleaning and regeneration of membranes in desalination and wastewater applications: State-of-the-art, Desalination 96 (1994) 225-238.

Ensminger, D. Ultrasonics, Marcel Dekker, New York, 1988.

Ethier C. R. and Lin, D.C. Refractometric measurement of polarized layer structure: studies of hyaluronic acid ultrafiltration, J. Membr. Sci. 68 (1992) 249-261.

Eykamp, W. Microfiltration and ultrafiltration, in Noble, R.D., and Stern, S.A., (eds), Membrane Separation Technology Principles and Applications, Elservier, Amsterdam, 1995, p1.

Fane, A.G. and Fell, C.J.D. A view of fouling and fouling control in ultrafiltration, Desalination 62 (1987) 117-136.

Fane, A.G. Ultrafiltration: factors influencing flux and rejection, In: Filtration and Separation (Edited by R.J. Wakeman), Vol. 4, Elsevier, Amsterdam, 1986, p.101.

Fárkorá, J., The pressure drop in membrane module with spaces, J. Membr. Sci., 64 (1991) 103-111.

Ford, R.D. Introduction to Acoustics, Elsevier, Armsterdam, 1970.

Fountoukidis, E., Marouls Z.B. and Marinos-Kouris, D. Modeling of calcium sulphate fouling of reverse osmosis membranes, Desalination 72 (1989) 294-318.

France, A.B.; Cabell, S.G., US patent no. 438,579, 1890.

Frederick, J.R. Ultrasonic Engineering, John Wiley and Sons, New York, 1965.

Gésan, G., Daufln, G., Merin, U., Labbé, J. -P. and Quémerais, A. Fouling during constant flux crossflow microfiltration of pretreated whey. Influence of transmembrane pressure gradient, J. Membr. Sci. 80 (1993) 131-145.

Gilron, J. and Hasson, D. Calcium sulphate fouling of reverse osmosis membranes: flux decline mechanism, Chem. Eng. Sci. 42 (1987) 2351-2360.

Ginn, M.; Cobb, G.L.; Broxton L.E. and McNeely, K.R. Method of filtering for mineral slurries, Minerals Engineering 10 (1997) 654.

Glater, J.; York J. L. and Campbell, K. S. Scale formation and prevention (Chapter 10), In: Spiegler K S and Laird, A D K (eds) Principles of Desalination Part B, Academic Press, New York, 1980, pp. 627-678.

Gravas, N. and Martin, B.W. Instability of viscous axial flow in annuli having inner cylinder, J. Fluid Mech. 86 (1978) 385-396.

Green, G. and Belfort, G. Fouling of ultrafiltration membranes: lateral migration and the particle trajectory model, Desalination 35 (1980) 129-147.

Grodzinsky, S. and Weiss, A. Separation and Purification Methods 14 (1985) 1-40.

Gupta, B.B.; Blanpain, P. and Jaffrin, M.Y. Permeate flux enhancement by pressure and flow pulsations in microfiltration with mineral membranes, J. Membr. Sci. 70 (1992) 257-266.

Gupta, B.B.; Zaboubi, B. and Jaffrin, M.Y. Scaling up pulsatile filtration flow methods to a pilot apparatus equipped with mineral membranes, J. Membr. Sci. 80 (1993) 13-20.

Gurvich, I.I., Seismic prospecting (Scismicheskoya razvedka), Gostoptekhizdat, Moscow, 1960.

Haerle, A.G. and Haber, R.A. Real-time monitoring of cake thickness during slip casting, J Mater. Sci. 28 (1993) 5679-5683.

Hallbauer-Zadorozhnaya, V. Y. Private communication, Polymer Science, Department of Chemistry, University of Stellenbosch, South Africa, 2001.

Hamachi, M.; Mietton-Peuchot, M. Experimental investigations of cake characteristics in crossflow microfiltration, Chem. Eng. Sci. 54 (1999) 4023-4030.

Harding, K., Brikdle, D. A. and Thorne, F. Chemical descaling of acid-dosed desalination plants, Desalination 27 (1978) 273-282.

Harvey, R. Cavitational reverse osmotic separation of water from saline solutions, US Patent No. 3,206,397, 1965.

Hendricks, T. J. and Williams, F. A. Diffusion-layer structure in reverse osmosis channel flow, Desalination 9 (1971) 155-180.

Hermia, J. Constant pressure blocking filtration laws - application to power-law non-Newtonian fluids, Instit. Chem. Eng. 60 (1982) 183-187.

Herrero, C.; Prádanos, P.; Calvo, J.I.; Tejerina, F. and Hernández, F. Flux decline in protein microfiltration: influence of operative parameters, J Colloid Interf. Sci. 187 (1997) 344-351.

Hildebrandt, J.R. and Saxton, J.B. The use of Taylor vortices in protein processing to enhance membrane filtration performance, in Dean, R.C., Neren (Eds.), Bioprocess Engineering Colloquium, ASME, New York, 1987.

Hodgson, P. H.; Pillay, V.L. and Fane, A.G. Visual study of crossflow microfiltration with inorganic membranes: resistance of biomass and particulate cake, Proceedings of the Sixth World Filtration Congress, Nagoya, 1993, pp. 607-610.

Holdich, R.G. and Zhang, G.M. Crossflow microfiltration in corporation rotational fluid flow, Trans IchemE 70 (1992) 527-536 Part A.

Howell, J.A., V. Sanchez and Field, R. W. Membranes in bioprocessing: theory and applications, Blackie Academic & Professional (published), Glasgow, 1993.

Huisman, I.H.; Prádanos, P.; Hernández, A. The effect of protein-protein and protein-membrabe interactions on the membrane fouling in ultrafiltration, J Membr. Sci. 179 (2000) 79-90.

Hung, C-C. and Tien, C. Effect of particle deposition on the reduction of water flux in reverse osmosis, Desalination 18 (1976) 173-187.

Huotari, H. M., G. Tragardh and I.H. Huisman. Crossflow membrane filtration enhanced by an external DC electric field: a review, Chem. Eng. Research and Design 77(1999) 461-468.

Hutchins, D.A. and Mair, H.D. Ultrasonic monitoring of slip-cast ceramics, J. Mater. Sci. Lett. 8 (1989) 1185-1187.

Iritani, E., Hattori, K., Murase, T., Analysis of dead-end ultrafiltration based on ultracentrifugation method, J. Membr. Sci. 81 (1993) 1-13.

Iritani, E.; Mukai Y. and Hagihara, E. Measurements and evaluation of concentration distributions in filter cake formed in dead-end ultrafiltration of protein solutions, Chem. Eng. Sci. 57 (2002) 53 – 62.

Jaffar, A.E. The application of a novel chemical treatment program to mitigate scaling and fouling in reverse osmosis units, Desalination 96 (1994) 71-79.

Jiraratannon, R. and Chanachai, A. A study of fouling in the ultrafiltration of passion fruit juice, J Membr. Sci. 111 (1996) 39-48.

Johnson, A.R. Experimental investigation of polarization effects in reverse osmosis, AIChE J 20 (1974) 966-974.

Jönsson, A.S. and Trägårdh, G. Fundamental principles of ultrafiltration, Chem. Eng. and Processing 27 (1990) 67-81.

Jönsson, A.S. and Trägårdh, G. Ultrafiltration applications, Desalination 77 (1990) 135-179.

Jönsson, G. and Boesen, C.E. in: Synthetic Membrane Processes, G. Belfort, ed., Academic Press, Orlando, 1984, pp. 101-130.

Jonsson, G., Boundary layer phenomena during ultrafiltration of dextran and whey protein solutions, Desalination 51 (1984) 61-77.

Karode, S.K. and Kumar, A. Flow visualization through spacer filled channels by computational fluid dynamics I. Pressure dropand shear rate calculations for flat sheet geometry, J. Membr. Sci. 193 (2001) 69-84.

Kennedy, M.; Kim, S.M.; Muteryo, I.; Broens, L. and Schippers, J. Intermittent crossflushing of hollow fiber ultrafiltration system, Desalination 118 (1998) 175-188.

Khulbe, K.C., Matsuura, T.; Singh, S.; Lamarche, G. and Noh, S.H. Study on fouling of ultrafiltration membrane by electron spin resonance, J. Membr. Sci. 167 (2000) 263-273.

Kim, K.J., Chen, V. and Fane A.G. Ultrafiltration of Colloidal Silver Particles: Flux, Rejection, and Fouling, J. Colloid and Interf. Sci. 155 (1993) 347-359.

Kimura, S. and Nakao, S-I. Fouling of cellulose acetate tubular reverse osmosis modules treating the industial water in Tokyo, 17 (1975) 267-275.

Kimura, S. and Sourirajan, S. Analysis of data in reverse osmosis with porous cellulose acetate membranes used, AIChE J. 13 (1967) 497-503.

Kobayashi, T., Chai, X. and Fujii, N. Ultrasound enhanced cross-flow membrane filtration, Separation and Purification Technology 17 (1999) 31-40.

Koen, L.J. Ultrasonic time-domain reflectometry as a real-time non-destructive visualization technique of concentration polarization and fouling on reverse osmosis membranes, M.Eng. thesis, University of Stellenbosch, South Africa, 2000.

Kools, W.F.C.; Konagurthu, S.; Greenberg, A.R.; Bond, L.J. and Krantz, W.B.; Van den Boomgaard, T. and Strathmann, H. Use of ultrasonic time-domain reflectometry for real-time measurement of thickness changes during evaporative casting of polymer films, J. Appl. Polymer Sci. 69 (1998) 2013-2019.

Kost, J. and Langer, R. Ultrasound enhancement of membrane permeability, US Patent No. 4,7802,212, 1988.

Krautkrämer, J. and Krautkrämer H. Ultrasonic testing of materials. Springer-Verlag, Berlin/Heidelberg, 1969.

Kronenberg, K.J. Magnetic water treatment de-mystified, http:/www.gcea.com/treatment, 1998.

La Heij, E. J.; Kerkhof-Kopinga, P.J.A.M. and Pel, L. Determining porosity profiles during filtration and expression of sewage sludge by NMR imaging, AIChE J. 42 (4) (1996) 953-959.

Laborie, S.; Cabassud, C.; Durand-Bourlier, L. and Laine, J.M. Flux enhancement by a continuous tangential gas flow in ultrafilltration hollow fibres for drinking water production: effects of slug flow on cake structure, Filtration & Separation, Oct. 1997, p886-891.

Lahoussine-Turcaud, V.; Wiesner, M.R. and Bottero, J.Y. Fouling in tangential-flow ultrafiltration: The effect of colloid size and coagulation pretreatment, J. Membr. Sci. 52 (1990) 173-190.

Lavrentyev, A.I. and Rokhlin, S.I. An ultrasonic method for determination of elastic moduli, density, attenuation and thickness of a polymer coating on a stiff plate, Ultrasonics 39 (2001) 211-221.

Leger, J. P. and Hawker, L.C. The composition and structure of reverse osmosis foulant deposits formed from Rand Water Roard water: A preliminary investigation, Desalination 61 (1987) 137-158.

Lenart, I. and Auslander, D. The effect of ultrasound on diffusion through membranes, 9 (1980) 216-218.

Lentdch, S.; Aimar P. and Orozco. J.L. Enhanced separation of albumin-poly(ethylene glycol) by a combination of ultrafiltration and electrophoresis, J Membr. Sci. 80 (1993) 221-232.

Li, H.; Fane, A.G.; Coster, H.G.L. and Vigneswaran, S. Direct observation of particle deposition on the membrane surface during crossflow microfiltration, J. Membr. Sci. 149 (1998) 83-97.

Li, H.; Ohdaria E. and Ide, M. Effect of ultrasonic irradiation on permeability of dialysis membrane, Jpn. J. Appl. Phys. 35 (5B) (1995) 3225.

Lin, I.J. and Nadiv, S. Magnetic Separation News 2(1988) 81.

Lipp, P.; Görge, B. and Gimbel, R. A comparative study of fouling-index and fouling-potential of waters to be treated by reverse osmosis, Desalination 79 (1990) 203-216.

Loeb, S. and Sourirajan, S. Adv. Chem. Ser, 38 (1962) 117.

Logan, D.P., and Kimura, S. Control of gypsum scale on reverse osmosis membranes, Desalination, 54 (1985) 321-331.

Lonsdale, H.K. The growth of membrane technology, J Membr. Sci. 10 (1982) 81-181.

Lonsdale, H.K. in: Desalination by Reverse Osmosis, Merten, U. (ed), MIT press, Cambridge, 1966, pp. 93-160.

Lu, W.M.; Tung, K.L.; Pan, C.S. and Hwang, K.J. Crossflow microfiltration of mono-dispersed deformable particle suspension, J. Membr. Sci. 198 (2002) 225-243.

Lynnworth, L.C. Ultrasonic measurement for process control theory, techniques, applications, Academic Press, San Diego, 1989.

Maartens, A.; Swart, P. and Jacobs, E.P. Feed water pretreatment: methods to reduce membrane fouling by natural organic matter, J Membr. Sci. 163 (1999) 51-62.

Maartens, A.; Swart, P. and Jacobs, E.P. Humic membrane foulants in natural brown water: characterization, Humic membrane foulants in natural brown water: characterization and removal, Desalination 115 (1998) 215-227.

Maartens, A.; Swart, P. and Jacobs, E.P. An enzymatic approach to the cleaning of ultrafiltration membranes fouled in abattoir effluent, J. Membr. Sci. 119 (1996) 9-16.

Mackley, M.R. and Sherman, N.E. Cross-flow cake filtration mechanisms and kinetics, Chem. Eng. Sci. 47 (1992) 3067-3084.

Mahlab, D.; Yosef, N.B. and Belfort, G. Concentration polarization profile for dissolved species in unstirred batch hyperfiltration (reverse osmosis) – II transient case, Desalination 24 (1978) 297-303.

Mairal, A.P.; Greenberg, A.R.; Krantz, W. B. and. Bond, L.J. Real-time measurement of inorganic fouling of RO desalination membranes using ultrasonic time-domain reflectometry, J. Membr. Sci. 159 (1999) 185-196.

Mairal, A.P.; Greenberg, A.R. and Krantz, W.B. Investigation of membrane fouling and cleaning using ultrasonic time-domain reflectometry, Desalination 130 (2000) 45-60.

Marshall, A.D.; Munro P.A. and Trägårdh, G. The effect of protein fouling in microfiltration and ultrafiltration on permeate flux, protein retentate and selectivity: a literature review, Desalination 91 (1993) 65-108.

Mashiko, Y., Kurokawa, Y. and Saito, S. Initial flux decline of the cellulose acetate butylate membranes with time under RO performance, Desalination 48 (1983) 147-160.

Mason, T.J and Lorimer, J. P. Sonochemistry: theory, applications and uses of ultrasound in chemistry, Ellis Horwood, Chichester, 1989, pp. 29.

Mason, T.J. and Lorimer, J. P. Sonochemistry: theory, applications and uses of ultrasound in Chemistry, Ellos Horwood Ltd, Chichester, 1988, pp. 1-17.

Masselin, S.; Chasseray, X.; Durand-Bourlier, L.; Lainé, J.M.; Syzaret, P.Y. and Lemordant, D. Effect of sonication on polymeric membranes, J. Membr. Sci. 181 (2001) 213-220.

Matthiasson E. and Sivik, B. Concentration polarization and fouling, Desalination 35 (1980) 59-103.

McDonogh, R.M.; Bauser, H.; Stroh, H. and Chmiel, H. Concentration polarization and adsorption effects in crossflow ultrafiltration of proteins, Desalination 79 (1990) 217-231.

McDonogh, R.M.; Bauser, H.; Stroh, H. and Grauschoph, U. Experimental in situ measurement of concentration polarization during ultra- and micro-filtration of bovine serum albumin and dextran blue solutions, J. Membr. Sci. 104 (1995) 51-63.

Michaels, A.S. New separation technique for the CPI, Chem. Eng. Prog. 64 (12) (1968) 31-43.

Migliori, A.; Sarrao, J.L.; Visscher, W.M.; Bell, T.M.; Kei, M.; Fisk, Z. and Leisure, R.G. Resonant ultrasound spectroscopic techniques for measurement of the elastic moduli of solids, Physica B 183 (1993) 1-24.

Migliori, A. and Darling, T.W. Resonant ultrasound spectroscopy for materials studies and non-destructive testing, Ultrasonics 34 (1996) 473-476.

Milisic, V., and Bersillon, J.L. Anti-fouling techniques in crossflow microfiltration, Filtration Separation 23 (1986) 347-356.

Millward, H. R.; Bellhouse, B. J.; Sobey, I. J and Lewis, R. W. H. Enhancement of plasma filtration using the concept of the vortex wave, J. Membr. Sci. 100 (1995) 121-129.

Min, K. and Lueptow, R.M. Hydrodynamic stability of viscous flow between rotating porous cylinders with radial flow, Phys. Fluids 6 (1) (1994) 144-152.

Mores, W.D. and Davis, R.H. Direct visual observation of yeast deposition and removal during microfiltation, J. Membr. Sci. 189 (2001) 217-230.

Mukherjee, D.; Kulkarni A. and Gill, W.N. Chemical treatment for improved performance of reverse osmosis membranes, Desalination 104 (1996) 239-249.

Mulder, M. Basic principles of membrane technology, Kluwer Academic Pubulishers, The Netherlands, 1991.

Muralidhara, H.S. Enhance separations with electricity, Chemtech. May (1994) 36-41.

Murase, T.; Ohn, T. and Kimata, L. Filtrate flux in crossfiow niicrofiltration of dilute suspension forming a highly compressible fouling cake-layer, J. Membr. Sci. 108 (1995) 121-128.

Nabe, A., Staude E. and Belfort, G. Surface modification of polysulfone ultrafiltration membranes and fouling by BSA solutions, J. Membr. Sci. 133 (1997) 57-72.

Nilsson, J.L. Protein fouling of ultrafiltration membranes: causes and consequences, J Membr. Sci. 52 (1990) 121-142.

Noble, R.D. and Stern, S.A. Membrane separations: technology principles and applications, Elsevier Science B.V., Amsterdam, 1995.

Nourtila-Jokinen, J. and Nystrom, M. Comparison of membrane separation processes in the international purification of paper mill water, J Membr. Sci. 119 (1996) 99-115.

Offringa, G. Membranes: the current technology for the future, Water Institute of Southern Africa (WISA) 2002, Durban, South Africa, 19-23 May, 2002.

Opong, W.S. and Zydney, A.L. Hydraulic permeability of protein layers deposited during ultrafiltrtion, J Colloid and Interf. Sci. 142 (1991) 41-60.

Oppenheim, S.F.; Buettner, G.R.; Dordick, J.S. and Rodgers, V.G.J. Applying electron paramagnetic resonance spectroscopy to the study of fouling in protein ultrafiltration, J. Membr. Sci. 96 (1994) 289-297.

PANAMETRICS, INC., Technical notes, 2000.

Parnham, C.S. and Davis, R.H. Protein recovery from bacterial cell debris using crossflow microfiltration with backpulsing, J Membr. Sci. 118 (1996) 259-268.

Parthun M.G.; Johari, G.P. Dynamics of a molecule's growth: ultrasonic relaxation studies. J. Chem. Phys. 102 (1995) 6301-6307.

Persson, K.M. and Nilsson, J.L. Fouling resistance models in MF and UF, Desalination 80 (1991) 123-138.

Persson, K.M., Tragardh, G. and Dejmek, P. Fouling behaviour of silica on four different microfiltration membranes, J. Membr. Sci. 76 (1993) 51-60.

Perusich, S.A. and Alkire, R.C. Ultrasonically induced cavitation studies of electrochemical passivity and transport mechanisms. I. Theoretical. J. Electrochem. Soc. 138 (3) (1991) 700-707.

Peterson, R.A.; Greenberg, A.R.; Bond, L.J. and Krantz, W.B. Use of ultrasonic TDR for real-time noninvasive measurement of compressive strain during membrane compaction, Desalination 116 (1998) 115-122.

Pierce, J.R.(ed) The science of musical sound, W.H. Freeman and Company, New York, 1996, p82.

Pontie, M.; Chasseray, X. and Lemordant, D. The streaming potential method for the characterization of ultrafiltration organic membranes and the control of cleaning treatments characterization, J Membr. Sci. 129 (1997) 125-133.

Porter, M.C. Microfiltration, in Bungay, P.M.; Lonsdale, H.K., and de Pinho, M.N., (eds.), Synthetic membranes: Science, Engineering and Application, Nato, ASI Series, Vol. 181, Reidel Publishing Company, 1986, p.225.

Potts, D.E.; Ahlert R.C. and Wang, S.S. A critical review of fouling of reverse osmosis membranes, Desalination 36 (1981) 235-264.

Price, G.J. (Ed.). Current Trends in Sonochemistry, Royal Society of Chemistry, Cambridge, 1992, p1-7.

Rautenbach, R. and Albrecht, R. Membrane Processes, John Wiley & Sons, England, 1989.

Redkar, S.; Kuberkar V. and Davis, R.H. Modeling of concentration polarization and depolarization with high-frequency backpulsing, J Membr. Sci. 121 (1996) 229-242.

Redkar, S.G. and Davis, R.H. Enhancement of crossflow microfiltration performance using high frequency reverse filtration, AIChE J. 41 (1995) 501-508.

Reinsch, V.E.; Greenberg, A.R.; Kelley, S.S.; Peterson, R. and Bond, LJ. A new technique for the simultaneous, real-time measurement of membrane compaction and performance during exposure to high-pressure gas, J. Membr. Sci. 171 (2000) 217-228.

Robertson, B.C. and Zydney, A.L., Protein adsorption in asymmetric ultrafiltration membrane with highly constricted pores, J. Colloid Interf. Sci. 134 (1990) 563-575.

Romero, C. A. and Davis, R.H., Transient model of crossflow microfiltration, Chem. Eng. Sci. 45 (1990) 13-25.

Rowley, L. H. A screening study of 12 biocides for potential use with cellulose acetate reverse osmosis membranes, Desalination 88 (1992) 71-83.

Saad, M. A. Biofouling prevention in RO polymeric membrane systems, Desalination 88 (1992) 85-105.

Schippers, J.C.; Verdouw, J. The modified fouling index: a method of determining the fouling characteristics of water, Desalination 32 (1980) 137-148.

Schippers, J.C.; Hanemaaijer, J.H.; Smolders C.A. and Kostense, A. Predicting flux decline of reverse osmosis membranes, Desalination 38 (1981) 339-348.

Schmidt, E. and Löffeler, F. Preparation of dust cakes for microscopic examination, Power Technol. 60 (1990) 173-177.

Schwinge, J., Wiley D. and Fane, A.G. Flux improvements with a new spacer geometry for ultrafiltration, 6th World Chemical Engineering Congress, Melbourne, Australia 2001.

Scott, K. Overview of the application of synthetic membrane processes, in Scott, K. and Hughes, R. (eds), Industrial membrane separation technology, Blackie Academic & Professional, London, 1996.

Sheppard, J.D.; Thomas, D.G. and Channabasappa, K.C. Membrane fouling part IV. Parallel operation of four tubular hyperfiltration modules at different velocities with feeds of high fouling potential, Desalinaton 11 (1972) 385-398.

Shimichi, W., Japan Patent No. 07,31974, 1995.

Shirato, M.; Sambuishi, M.; Kato, H. and Aragaki, T. Internal flow mechanism in filter cakes, AlChE J. 15 (3) (1969) 405-409.

Sokolov, S., Elek-Nachr-Tek, 6 (1929) 451

Strathmann, H. Membrane separation processes, J Membr. Sci. 9 (1981) 121-189.

Suki, A.; Fane, A.G. and Fell, C.J.D. Flux decline in protein ultrafiltration, J Membr. Sci. 21 (1984) 269-283.

Tanny, G.B.; Hauk D. and Meuin, U. Biotechnical applications of a pleated cross-flow microfiltration module, Desalination 41 (1982) 299-312.

Tarleton, E.S. and Wakeman, R.J. Electro-acoustic crossflow microfiltration, Filtr. & Sep. 29 (9-10) (1992) 425-432.

Tiller, F.M. Formation of filter cakes and precoats, in the scientific basis of filtration, K.J. Ives (ed), Noordhoff, Leyden, 1975.

Tiller, F.M. and Kwon, J. H. Role of porosity in filtration: XIII. Behaviour of highly compactable cakes. AIChE Journal, 44 (1998) 2159-2167.

Tiller, F.M. Formation of filter cakes and precoats, in the scientific basis of filtration, K.J. Ives (ed), Noordhoff, Leyden, 1975.

Tiller, F.M.; Hsyung, N.B. and Cong, D.Z. Role of porosity in filtration: XII filtration with sedimentation, AIChE J. 41 (5) (1995) 1153.

Tiller, F.M. and Li W. Determination of the critical pressure drop for filtration of super-compatible cakes. Water Sci. and Technol. 44 (2001) 171-176.

Tracey, E.M. and Davis, R.H. Protein fouling of track-etched polycarbonate microfiltration membranes, J. Colloid Interf. Sci. 167 (1994) 104-116.

Trägrädh, G. Membrane cleaning, Desalination 71 (1989) 325-335.

Treffry-Goatley, K. and Buchan, M.I.; Renchen, G.E. and Buckley, C.A. The dewatering of sludges using a tubular filter press, Desalination 67 (1987) 467-479.

Tsujimoto, W.; Kimura, H.; Izu, T. and Irie, T. Membrane filtration and pre-treatment by GAC, Desalination 119 (1998) 323-326.

Tung, K.L.; Wang, S.; Lu, W.M. and Pan, C.H. In situ measurement of cake thickness distribution by a photointerrupt sensor, J. Membr. Sci. 190 (2001) 57-67.

van der Horst, H. C.;. Timmer, J. M. K; Robbertsen, T. and Leenders J. Use of nanofiltration for concentration and demineralization in the dairy industry: Model for mass transport, J. Membr. Sci. 104 (1995) 205-218

van Hoof , S.C.J.M.; Minnery, J.G. and Mack, B. Performing a membrane autopsy, Water Sewage and Effluent 22 (2) (2002) 40–46.

Vermeiren, T.I.S., US patent no. 2652,925, 1953.

Vilker, V.L., Colton, C.K. and Smith, K.A. Concentration polarization in protein ultrafiltration, Part 1: An optical shadowgraph technique for measuring concentration profiles near a solution-membrane interface, AIChE. J. 27 (1981) 632-637.

Viswanathan, C. and Aim, R. B. Studies on colloidal membrane fouling mechanisms in crossflow microfiltration, J. Membr. Sci. 45 (1989) 3-15.

Vyas, H.K.; Bennett, R. J. and Marshall, A. D. Cake resistance and force balance mechanism in the crossflow microfiltration of lactalbumin particles, J. Membr. Sci. 192 (2001) 165-176.

Vyas, H.K.; Mawson, A.J.; Bennett, R.J. and Marshall, A.D. A new method for estimating cake height and porosity during crossflow filtration of particulate suspensions, J. Membr. Sci. 176 (2000) 113-119.

Wadley, S. C., Brouckaert, J., Baddock, L. A. D. and Buckley, C. A. Modelling of nanofiltration applied to the recovery of salt from waste brine at a sugar decolourisation plant, J. Membr. Sci. 102 (1995) 163-175.

Wakeman, R. J. and Tarleton, E. S. Membrane fouling prevention in crossflow microfiltration by the use of electric fields, Chemical Engineering Science 42 (1987) 829-842.

Wakeman, R.J. and Tarleton, E.S. An experimental study of electroacoustic crossflow microfiltration, Chem. Eng. Research & Design, 69 (1991) 386-397.

Wakeman, R.J. and Williams, C.J. Additional techniques to improve microfiltration, Separation and Purification Technology 26 (2002) 3-18.

Wakeman, R.J. and Sabri, M.N. Utilizing pulsed electric fields in crossflow microfiltration of titanic suspensions, Tans. IChemE 73 (1995) 455-463 Part A.

Wakeman, R.J. Visualization of cake formation in crossflow microfiltration, Trans. IChemE, Part A 72 (1994) 530-540.

Wandelt, B.; Schmitz, P. and Houi, D. Investigation of transient phenomena in crossflow microfiltation of colloidal suspersions using NMR micro-imaging, in: Proceedings of the 6th World Filtration Congress, Nagoya, Japan, 1992, pp. 601-606.

Weast, Robert C., Handbook of Chemistry and Physics, Chemical Rubber Co., Cleveland, Ohio, 1970.

Wenten, I. G. Mechanisms and control of fouling in crossflow microfiltration, Filtration & Separation 32 (1995) 252-253.

Wijmans, J. G., Nakao, S. and Smolders, C. A. Flux limitation in ultrafiltration: Osmotic pressure model and gel layer model, J. Membr. Sci. 20 (1984) 115-124.

Wijmans, J. G.; Nakao, S.; Van Den Berg, J. W. A.; Troelstra F. R. and Smolders, C. A. Hydrodynamic resistance of concentration polarization boundary layers in ultrafiltration, J. Membr. Sci. 22 (1985) 117-135.

Yacubowicz, J. AlkaSave process for recovery of caustic and acids in diaries, Membrane Technology 67 (1995) 7-9.

Yao, S.; Costello, M.; Fane, A.G. and Pope, J..M. Non-invasive observation of flow profiles and polarization layers in hollow fibre membrane filtration modules using NMR micro-imaging, J. Membr. Sci. 99 (1995) 207-216.

Zhu, C. and Liu, G. Modeling of ultrasonic enhancement on membrane distillation, J Membr. Sci. 176 (2000) 31-34.

Zydney, A.L. and Colton, C.K. A concentration polarization model for the filtrate flux in crossflow microfiltration of particulate suspensions, Chem. Eng. Commun. 47 (1986) 1-21.

PUBLICATIONS AND PRESENTATIONS EMANATING FROM THIS STUDY

1. PUBLICATIONS AND PATENT

1) Jianxin Li, RD Sanderson, EP Jacobs, Ultrasonic cleaning of nylon microfiltration membranes fouled by Kraft paper mill effluent, **J. Membr. Sci. 205 (2002) 247-257.**

2) Jianxin Li, RD Sanderson, EP Jacobs, Non-invasive visualization of the fouling of microfiltration membranes by ultrasonic time-domain reflectometry, **J. Membr. Sci. 201 (2002) 17-29.**

3) RD Sanderson, Jianxin Li LJ Koen, L. Lorenzen, Ultrasonic time-domain reflectometry as a non-destructive visualization technique to monitor fouling and cleaning of reverse osmosis membranes, **J. Membr. Sci. 207 (2002) 105-117**.

4) Jianxin Li, R.D. Sanderson, In situ measurement of particle deposition and its removal in microfiltration by ultrasonic time-domain reflectometry, **Desalination 146 (2002) 169-175.**

5) Jianxin Li, V Yu Hallbauer-Zadorozhnaya, D.K. Hallbauer, R.D. Sanderson, Measurement and modeling of organic fouling during ultrafiltration by Ultrasonic Signal Reflections, **Desalination 146 (2002) 177–185.**

6) Jianxin Li, V Yu Hallbauer-Zadorozhnaya, D.K. Hallbauer, R.D. Sanderson Cake-layer deposition, growth and compressibility during microfiltration, measured and modelled using a non-invasive ultrasonic technique, **Ind. & Eng. Chem. Res**. 41(2002) 4106-4115.

7) Jianxin Li, DK Hallbauer, RD Sanderson, V Yu Hallbauer-Zadorozhnaya, Jianxin Li, V. Y. Hallbauer-Zadorozhnaya, D.K. Hallbauer, R.D. Sanderson, L.J. Koen, Interpretation of calcium sulfate fouling on RO membranes using ultrasonic measurements and simplified model, submitted to **J. Membr. Sci**. 2002.

8) Jianxin Li, DK Hallbauer, RD Sanderson, V Yu Hallbauer-Zadorozhnaya Direct visualization of fouling and cleaning processes during ultrafiltration using ultrasonic time-domain reflectometry, submitted to **J Membr. Sci.** 2002.

9) R.D. Sanderson, D.K. Hallbauer, Jianxin Li, V Yu Hallbauer-Zadorozhnaya, S. Marke, J. Schiller. Flat-bed type slave unit for the detection and monitoring fouling of membranes using liquid separation processes, **SA patent application: 2002/4753**

10) Jianxin Li, G.Y. Chai, D.K. Hallbauer, R.D. Sanderson, Real time detection of protein fouling in tubular ultrafiltration membranes using a new ultrasonic technique, submitted to **J. Membr. Sci**. 2002.

2. PAPERS AND POSTERS PRESENTED

1) R.D. Sanderson, Jianxin Li, EP Jacobs, The use of ultrasonics in membrane visualization and fouling, paper presented at *4th WISA-MTD Symposium-Membranes: Science & Engineering*, Stellenbosch, South Africa, March 26-27, 2001.

2) Jianxin Li, R.D. Sanderson, D.K. Hallbauer, E.P. Jacobs, Visualization of membrane fouling and cleaning in microfiltration and ultrafiltration by ultrasonic time-domain reflectometry, paper presented at *2001 International Conference – Membrane Technology,* Shanghai, China, Sept. 17-21, 2001.

3) Jianxin Li, RD Sanderson, EP Jacobs, Noninvasive in-situ visualization of fouling and cleaning in flat-sheet microfiltration membranes by ultrasonic time-domain reflectometry, paper presented at *WISA 2002*, Durban, South Africa, 19-23 May, 2002.

4) Jianxin Li, R.D. Sanderson, EP Jacobs, Ultrasonic cleaning of membrane fouling in MF fouled by paper mill effluent, poster presented at *4th WISA-MTD Symposium-Membranes: Science & Engineering*, Stellenbosch, South Africa, March 26-27, 2001.

5) Jianxin Li, R.D. Sanderson, Visualization of membrane fouling and its removal during microfiltration and ultrafiltration by ultrasonic time-domain reflectometry, poster presented at *the International Congress on Membranes and Membrane Processes (ICOM2002),* Toulouse, France, July 7-12, 2002.

6) Jianxin Li, D.K. Hallbauer, R.D. Sanderson, V Yu Hallbauer-Zadorozhnaya, Modelling of ultrasonic reflections during the testing of membrane fouling by ultrasonic signal reflections, poster presented at *the International Congress on Membranes and Membrane Processes (ICOM2002)*, Toulouse, France, July 7-12, 2002.